INVESTIGATING THE CHEMICAL RECYCLING OF POLYESTERS AND POLYCARBONATES: THE FACTORS THAT CONTROL THE DEPOLYMERIZATION RATE AND THE FORMATION OF NANOPLASTICS

A Dissertation Presented for the

Doctor of Philosophy

Degree

The University of Tennessee, Knoxville

Shelby Rebecca Watson-Sanders

May 2025

Copyright © 2025 by Shelby Rebecca Watson-Sanders

All rights reserved.

DEDICATION

The journey I have undertaken has been both challenging and incredibly rewarding. None of it would have been possible without the unwavering support of truly remarkable individuals. I extend my heartfelt thanks to the inspiring chemists in my life who encouraged me to research and teach: Prof. Bill Kwochka, Prof. Carmen Huffman, Prof. Jamie Wallen, and Dr. Alison Biery. This dissertation is dedicated to my husband, who has not only been my rock throughout this experience but has also stood by me during my most trying moments. He was always there during my biggest moments of self-doubt and when I mistakenly placed all my worth into my research. I also express my deepest gratitude to my parents, sister, nephew, cats, and in-laws for their unwavering support and patience, as this program took time away from them. I am sincerely grateful to each and every one of you. A special thank you goes to my father for continually pushing me further and shaping me into the person I am today with the following quote:

Good, Better Best,
Never let it rest
Till your good is better
and your better is best
-St. Jerome

ACKNOWLEDGEMENTS

I want to express my gratitude to Professor Mark D. Dadmun for his invaluable mentorship. His guidance has been crucial for my growth as a scientist and individual. He has improved my writing and critical thinking, preventing me from unproductive paths. I am deeply thankful for his belief in me, which has made me an independent scientist, ready to face any challenge.

I am eternally grateful to Dr. Alison Biery for her mentorship and friendship, both inside and outside the lab, which have significantly contributed to my growth. Without her, I would not be the synthetic chemist I am today or possess the confidence I hold now. I will truly miss rushing to her office to share an idea or her willingness to teach me everything I know. I also want to thank Maggie Powell, Brooke Jenkins, Christy Barker, and Susan Kenny for their unwavering friendship and support. Additionally, I want to express my gratitude to my undergrads and friends Kendra Day and Sarah Barber, whom I have seen grow and who have deepened my love for teaching and mentorship!

I want to acknowledge my doctoral committee: Prof. Brian Long, Prof. Shawn Campagana, and Prof. Tominori Saito. Their time, guidance, and critiques have played a vital role in shaping me into the scientist I am today. The support from the National Science Foundation and the University of Tennessee, Knoxville College of Arts and Sciences has been indispensable to my work.

Additionally, I thank Prof. Jamie Wallen, Prof. Bill Kwochka, and Prof. Carmen Huffman from Western Carolina University for their invaluable contributions to my growth and development during my undergraduate education.

I want to express my heartfelt thanks to my husband and family for your unwavering support and for helping to shape me into who I am today.

ABSTRACT

The increasing demand for synthetic polymers is not being met with a corresponding rise in recycling, with only 9% of plastics being recycled annually. Consequently, the management of polymer waste is unsustainable, as most polymers end up in landfills or are incinerated. This research project examines Polyethylene Terephthalate (PET), Polycarbonate (PC), and TritanTM from Eastman Chemical Company, aiming to make recycling processes more sustainable. The focus is on understanding chain structure evolution during depolymerization, the impact of functional groups on depolymerization rates, polymer solvent compatibility, polymer crystal size's influence on depolymerization kinetics, and imaging nanoplastics from environmental samples. It further seeks to utilize telechelics formed during depolymerization for repolymerization or to create value-added products, ultimately advancing sustainable polymer recycling and developing economically viable materials from polymer waste streams.

This project aims to depolymerize polymers into oligomers for next-generation materials. My first project (Chapter II) revealed that annealing PET before depolymerization increased crystallinity and altered crystal structure, enabling the production of desirable dihydroxy-terminated oligomers with limited post-depolymerization reactions. Chapter III demonstrated that diol/polymer compatibility directs the rate of heterogeneous phase depolymerization, although the carbonyl carbon's reactivity also plays a role. Improved solubility (e.g., bisphenol-A) enhances the transition to a homogeneous phase, while poorer solubility (e.g., ethylene glycol) inhibits it. Chapter IV examines how crystallinity and crystal size impact the depolymerization of PET, enabling isolation of telechelic oligomers. The final project discussed (Chapter V) explores visualizing microplastics and nanoplastics using transmission electron microscopes and investigating how solubility affects the shape of formed nanoplastics.

TABLE OF CONTENTS

CHAPTER 1: AN INTRODUCTION TO PLASTIC PRODUCTION, PLASTIC WASTE, AND PLASTIC RECYCLABILITY 1

1.1 Plastic Production and Plastic Waste 2

1.1.1 Plastic Generation 2

1.1.2 Microplastic and Nanoplastic (NPs) Generation 2

1.2 Polymer Recycling 4

1.2.1 Types of Recycling 6

1.2.2 Sovolysis: Homogeneous vs Heterogeneous Catalysis of Depolymerization ... 7

1.2.3 Recent Developments in Organocatalysts 12

1.2.4 Development in Mixed Waste Polymer Depolymerization 14

1.3 Polymer Crystallinity 16

1.4 Generation of value-added products from consumer plastic waste 19

1.5 Conclusions and Outlook 21

CHAPTER 2: MORE EFFICIENT CHEMICAL RECYCLING OF POLY(ETHYLENE TEREPHTHALATE) BY INTERCEPTING INTERMEDIATES 46

2.1 Abstract 47

2.2 Introduction 48

2.3 Methods 52

2.3.1 Materials 52

2.3.2 Catalyst 52

2.3.3 Reaction Conditions 52

2.3.4 Product Workup 53

2.3.5 Repolymerization 53
2.3.6 Depolymerization Product Characterization 54
2.4 Results 57
2.4.1 Evolution of chain molecular weight 57
2.4.2 Crystallinity of reaction products 60
2.4.3 End group evolution during depolymerization 62
2.4.4 Repolymerization of oligomeric intermediates 64
2.5 Discussion 64
2.5 Conclusions 73
2.6 Acknowledgements 74
CHAPTER 3: REACTIVITY OF CARBONATES AND ESTERS IN THE DEPOLYMERIZATION OF PLASTIC WASTE 82
3.1 Abstract 83
3.2 Introduction 85
3.3 Experimental Methods 90
3.3.1 Materials 90
3.3.2 Catalyst 90
3.3.3 Reaction Conditions 90
3.3.4 Depolymerization Product Characterization 93
3.4 Results & Discussion 95
3.4.1 Starting Material Characterization 95
3.4.2 Ethylene Glycol depolymerization of PET, PC, and Tritan™ 97
3.4.3 Depolymerization of PET and PC with Bisphenol-A 109

3.5 Conclusion 118
3.6 Acknowledgements 119
CHAPTER 4: MODIFYING CONSUMER POLYETHYLENE TEREPHTHALATE BEFORE GLYCOLYSIS TO ISOLATE TAILORED TELECHELIC OLIGOMERS 130
4.1 Abstract 131
4.2 Introduction 132
4.3 Methods 135
4.3.1 Materials 135
4.3.2 PET Annealing Procedure 135
4.3.3 Catalyst 135
4.3.4 Reaction Conditions 135
4.3.5 Product Recovery 136
4.3.6 Depolymerization Product Characterization 136
4.4 Results and Discussion 139
4.4.1 Annealing of Polyethylene Terephthalate (PET) 139
4.4.2 Depolymerization of Annealed PET 142
4.4.3 Determination of Average Hydroxyl End Group per PET Chain 142
4.4.4 Reactivity of tie-chains 146
4.5 Conclusions 151
4.6 Acknowledgements 152
CHAPTER 5: VISUALLIZING POLYETHYLENE, POLYETHYLENE TEREPHTHALATE, AND POLYSTYRENE AS MICRO AND NANOPLASTICS UTILIZING TRANSMISSION ELECTRON MICROSCOPY 160

5.1 Abstract 162
5.2 Introduction 163
5.3 Experimental 167
5.3.1 Materials 167
5.3.2 Preparation of polyethylene terephthalate (PET) nanoplastics (NPs) 168
5.3.3 Size Exclusion Chromatography (SEC) 170
5.3.4 Differential Scanning Calorimetry (DSC) 170
5.3.5 Preparation of polyethylene (PE) NPs 170
5.3.6 Raman Spectroscopy and Microscope Imaging 172
5.3.7 Particle Size Analysis 172
5.3.8 Scanning Electron Microscopy (SEM) 173
5.3.9 Transmission Electron Microscopy (TEM) 173
5.4 Results & Discussion 174
5.4.1 Structure of Products of PET Depolymerization 174
5.4.2 Polyethylene micro and nanoparticles 183
5.5 Conclusion 191
5.6 Acknowledgements 193
CHAPTER 6: CONCLUSIONS AND OUTLOOKS 203
6.1 Conclusions 204
6.2 Future Outlook 209
APPENDICES 215
Appendix A: Supporting Information for Chapter III 216
A.1. Methods 217

A.1.1. Differential Scanning Calorimetry (DSC) 217
A.1.2. Fourier Transform Infrared Spectroscopy (FTIR) 217
A.1.3. Normalized Swelling [%] for BPA 217
A.1.4. Glycolysis with Basic Catalyst 218
A.2. Results and Discussion 219
A.2.1. Starting Material Characterization 219
A.2.2. Ethylene Glycol depolymerization of polymers with basic catalyst 221
A.2.3. Bisphenol-A depolymerization of PET and PC 225
Appendix B: Supporting Information for Chapter IV 237
B.1. Methods 238
B.1.1. Differential Scanning Calorimetry (DSC) 238
B.1.2. Normalized Swelling 238
B.2. Results and Discussion 239
B.2.1. Small Angle X-Ray Scattering (SAXS) 239
B.2.2. Analysis of Starting Material (Annealed PET) 241
B.2.3. DSC of PET Annealed or Swelled at Reaction Temperature 245
B.2.4. Change in Crystallinity from Annealing to Depolymerization 247
VITA 254

LIST OF TABLES

Table 5.1 Change in molecular weight, dispersity, and crystallinity of polyethylene terephthalate (PET) after 75 minutes of glycolysis 175

LIST OF FIGURES

Figure 1.1 Million tons of plastic produced since 1960 and predicted to be produced into 2050.[1] 3

Figure 1.2 Pathway of leakage and formation of microplastics into the environment and the formation of nanoplastics (NPs) 5

Figure 1.3 The amount of plastic generated (blue), recycled (red), combusted (green), and landfilled (purple) every year from 1960 to 2018..... 5

Figure 1.4 Depolymerization may occur by two processes: heterogeneously catalyzed (top) and homogeneously catalyzed (bottom). In heterogeneously catalyzed depolymerization, the polymer is initially insoluble in the solvent and progresses through three stages: 1) heterogeneous stage with solvent-insoluble polymer oligomers and solvent-soluble monomers; 2) the coexistence stage with insoluble polymers and oligomers, soluble oligomers, and soluble monomers; and 3) a homogeneous stage with solvent-soluble oligomers, dimers and monomers. The homogeneous phase depolymerization starts with the polymer dissolved in the solvent, quickly producing oligomers, dimers, and monomers, ultimately yielding only monomers and dimers..... 10

Figure 1.5 The effect of annealing temperature on crystal growth of polymers. As polymers are annealed near, but above, the glass transition temperature (T_g), nucleation of new small crystals is dominant. Polymers annealed near, but below, the melting temperature (T_m) dominate in growing existing crystals over nucleation. Below the T_g crystals, neither nucleate nor grow due to the immobility of the polymer chains. Above the T_m the polymer crystals melt. 18

Figure 2.1 General depolymerization process of PET. Depolymerization on top is a heterogeneous surface reaction, and the depolymerization on bottom is a homogeneous reaction..... 50

Figure 2.2 Picture of the PET depolymerization product as a function of reaction time. 58

Figure 2.3 Evolution of PET during glycolysis reaction. M_n from SEC is depicted as green bar graphs, with the y-axis on the left side. The weight percent of recovered EG insoluble depolymerized PET is depicted as the brown line graph, with the y-axis on the right..... 58

Figure 2.4 Evolution of PET during glycolysis reaction. M_n from SEC is depicted as green bar graphs, with the y-axis on the left side. The weight percent of recovered EG insoluble depolymerized PET is depicted as the brown line graph, with the y-axis on the right..... 59

Figure 2.5 Differential Scanning Calorimetry (DSC) first cycle curves of PET depolymerization products for different reaction times. The endothermic transitions in the DSC curves are down..... 61

Figure 2.6 Percent crystallinity of PET annealed at 180 °C (pink) and PET depolymerization products as a function of reaction time at 180 °C (green). 61

Figure 2.7 M_n of the depolymerization products for specific reaction times (lines) as a function of the number of -OH end groups per chain. SEC-derived M_n of the depolymerization products are plotted as green diamonds. The overlap of the green diamond and line denotes the actual number of -OH end groups on each depolymerization reaction product. 63

Figure 2.8 Average number of alcohol end groups per chain on the depolymerization reaction product as a function of reaction time..... 63

Figure 2.9 Change in M_v of PET before depolymerization, after depolymerization, and after repolymerization. 65

Figure 2.10 Changes in DP with Đ of the products of the PET glycolysis reaction and a random chain scission. 67

Figure 2.11 Depiction of slow end group conversion in the amorphous phase by the diffusion of EG into the PET flake in the amorphous phase to depolymerize at the amorphous tie-chains. 71

Figure 3.1 Illustration of the three stages of heterogeneous depolymerization as described in the text: the heterogeneous stage, the coexistence stage, and the homogeneous stage. The heterogeneous stage occurs when the polymer is not dissolved in the solvent. The coexistence stage involves both dissolved polymer and polymer not dissolved in the solvent. The homogeneous stage occurs when all polymers are dissolved in the solvent. 87

Figure 3.2 Picture of the products of polycarbonate (PC) that is depolymerized with BPA for 10 minutes. The BPA insoluble oligomers are noted in green, while the Methanol insoluble oligomers are noted in blue. 94

Figure 3.3 Starting molecular weights of polymers before depolymerization. 96

Figure 3.4 (A) The change in Tritan molecular weight as a function of reaction time: M_n (dark green), M_w (green), and dispersity (Đ) (purple). (B) The change in PET chain length as a function of reaction time: M_n (dark blue), M_w (blue), and Đ (purple). (C) The change in PC chain length as a function of reaction time: M_n (orange), M_w (yellow), and Đ (blue). 98

Figure 3.5 Normalized Swelling per Polymer Flake of PET (blue), PC (orange), and Tritan^{TM} (green) with EG at 180 °C as a function of the square root of time. 101

Figure 3.6 Change in molecular weight during depolymerization via glycolysis as a function of reaction time. Data for Tritan^{TM}: M_n (dark green) and M_w (green); Data for PET: M_n (dark blue) and M_w (blue) Data for PC: M_n (orange) and M_w (yellow). 103

Figure 3.7 Activation Energies of nucleophilic acyl/acyl-type substitution (or the tetrahedral intermediate pathway) and Sn2 substitution at the alkyl oxygen of ester and carbonate-containing polymers..... 105

Figure 3.8 Depolymerization of PET and PC in EG and BPA. Light purple: PET flakes in EG before and after workup (1.75 reaction hours). Dark purple: PC flakes in EG before and after workup (5 reaction hours). Blue: PC flakes in BPA before and after workup (0.75 reaction hours). 110

Figure 3.9 Yield of PET and PC depolymerized with BPA: Change in percent yield of PET and PC as a function of depolymerization time with BPA, including the change in BPA insoluble yield for PET (dark blue) and PC (dark purple). The change in the total yield of BPA soluble and BPA insoluble material as a function of reaction time for PET (blue-green) and PC (light purple) is also shown. 113

Figure 3.10 Change in percent molecular weight for PET and PC with reaction time. It shows the change in molecular weight as a percentage of PET $_{Mn}$ (blue-green), PET M_w (dark blue), PC M_n (dark orange), and PC M_w (orange) with reaction time. 115

Figure 4.1 PET glycolysis work up to isolate ethylene glycol (EG) insoluble PET flakes. 137

Figure 4.2 How annealing affects PET crystallinity and molecular weight. a) Change in percent crystallinity from DSC as a function of annealing time. b) Change in Long period (orange) and crystal phase (blue) of PET as a function of annealing time determined by SAXS. C) Change in M_n (red) and M_w (purple) of PET as a function of annealing time determined from SEC. 141

Figure 4.3 Changes in molecular weight and yield of PET annealed for varying times (0-hour green, 3-hour purple, 6-hour blue, 13-hour red, 24-hour yellow) as a function of

depolymerization reaction time. A) The percent change of the PET M_w for PET annealed at 240 °C for different times. b) Change in the yield of the EG insoluble PET at specific reaction times for PET flakes annealed at 240 °C. 143

Figure 4.4 The average number of hydroxyl end groups per chain changes with glycolysis time to annealed PET. (annealing time: 0-hour dark blue, 3-hour yellow, 6-hour pink, 13-hour green, and 24-hour blue) (a) Shows the number of hydroxyl end groups per chain determined by comparing M_n from NMR and SEC-GPC. The statistical significance of variation was assessed using a one-tailed chi-square test for standard deviation, assuming an expected $\sigma = 0.15$ ($n = 3$). Asterisks indicate the degree of significance in a more significant deviation that is larger than the expected variance: $P < 0.5$ (*), $P < 0.1$ (**), and $P < 0.001$ (***). (b) shows a set of PET flakes that were annealed for varying times and then depolymerized for 75 minutes. 145

Figure 4.5 What occurs during PET annealing at 240 °C: fold dislocation during lamella thickening and subsequent ester interchange to remove stress on tie chains..... 147

Figure 4.6 Visual representation of chain scission occurring at the tie-chains in PET. The PET flakes break into powder once all the tie chains are cut. 150

Figure 5.1 Formation of nanoplastics (NPs) by microplastic fragmentation. Said NPs move up the food chain as they are ingested by aquatic life and eventually humans. 164

Figure 5.2 Scanning Electron Microscopy (SEM) of depolymerized PET. Scale bars in images vary. 177

Figure 5.3 TEM images of depolymerized PET at a range of length scales. Note that the scale bar is different in each image. 177

Figure 5.4 Transmission Electron Microscopy (TEM) images of depolymerized polyethylene terephthalate (PET) from glycolysis. (a) A scale bar of 200 nm reveals a cluster of small particles. (b) A scale bar of 100 nm shows a zoomed-in view of part (a), providing a more detailed representation of the particles. (c) A scale bar of 100 nm depicts a zoomed-in portion of part (a), offering a clearer depiction and size measurement of the particles, which are approximately 10 nm. (d) A scale bar of 20 nm displays a zoomed-in view of part (c) to enhance visualization of the 10 nm particles. 179

Figure 5.5 TEM images and electron diffraction patterns of depolymerized PET (a) Edge of blank TEM grid. (b) TEM of depolymerized PET particles (c) TEM image of depolymerized PET (d) Diffraction pattern of c. (e) TEM image of depolymerized PET microplastic (f) Diffraction pattern of e. (g) TEM image of pulverized virgin PET. (h) Diffraction pattern of g. 181

Figure 5.6 A potential demonstration of nanoplastic formation, where PE sM&NP particles prepared in water/n-dodecane mixtures break from pre-existing microplastics. From left to right, the TEM images zoom in on areas of interest (the middle image is the green area of interest, and the far-right image is the orange area of interest) to show smaller and smaller fragments of PE..... 186

Figure 5.7 TEM images of a PE microplastics fragmented into small micro and nanoplastics (sM&NP) in varying conditions. (a) empty TEM grid with side of grid captured, (b-d) PE sM&NP particles suspended in water for 3 years (aged sample), (e) PE sM&NP prepared in a water/n-dodecane mixture (1000:1), and (f-h) PE sM&NP freshly prepared in water (non-aged sample). 186

Figure 5.8 Energy-dispersive X-ray Spectroscopy (EDS) of polyethylene (PE) aged in water (scale bar: 1 μm). Top row (left to right): EDS overlay showing the distribution of the HAADF image (white), oxygen (green), and lanthanum (yellow); the HAADF image; the oxygen map; and the lanthanum map. Bottom row (left to right): the carbon map (red), the gadolinium map (blue), the phosphorus map (green), and the silicon map (pink). 188

Figure 5.9 TEM images of PS microplastics fragmented into small micro and nanoplastics (sM&NP) (a) PS sM&NP particles prepared in water:dodecane (1000:1) mixture. (b) and (c) zoomed in images of the PS sM&NP particles in the TEM image (a)..... 190

Figure A.1 Differential Scanning Calorimetry of polyethylene terephthalate (PET, blue) and Tritan™ (green) vs. temperature..... 220

Figure A.2 Heterogeneous depolymerization of PET, Tritan™, and PC via glycolysis catalyzed by TBD. (a) Pictures PET, Tritan™, and PC solubilized in EG:TBD 4 minutes into the reaction. (b) shows the percent yield of EG insoluble Tritan™ (orange) and PC (blue) with reaction time. (c) Depicts the percent change in molecular weight for Tritan™ (M_n blue, M_w orange) and PC (M_n grey, M_w yellow) of both the EG soluble and insoluble fraction with reaction time. (d) Shows the molecular weight of for Tritan™ (M_n blue, M_w orange) and PC (M_n grey, M_w yellow) EG insoluble fraction with reaction time. 222

Figure A.3 H^1 NMR spectrum in $CDCl_3$ of PC (green), BPA (blue), PC depolymerized with EG catalyzed with TBD: MSA for 2 hours (purple), and PC depolymerized with EG catalyzed with TBD for 2 minutes (red). This spectrum also depicts impurities like THF (3.75 and 1.88 ppm, dark blue circle), HFIP (4.3 and 4.0-3.5 ppm, red circle) and acetone (3.28 ppm, orange circle). (Left) Shows the whole NMR spectrum. (Right) Shows NMR spectrum in the ppm range where phenol groups are expected to be present..... 224

Figure A.4 Demonstrates the diffusion of the solvent into the polymer flakes. (a) It is a visual signal of solvent (EG or BPA) slowly diffusing into the polymer flake. (b) It shows a visual change in PC flakes with depolymerization time in BPA. (c) shows a graph of PC flake thickness vs reaction time in EG (orange) and BPA (purple)..... 226

Figure A.5 PET and PC depolymerized in BPA. (a) shows the change in molecular weight of the insoluble (M_n dark orange, M_w orange) and soluble (M_n dark green, M_w green) fractions of PET with reaction time and the change in dispersity of the insoluble (purple) and soluble fraction (blue). (b) shows the change in molecular weight of the insoluble (M_n dark purple, M_w purple) and soluble (M_n dark blue, M_w blue) fractions of PC with reaction time and the change in dispersity of the insoluble (orange) and soluble fraction (green)..... 228

Figure A.6 demonstrates the normalized swelling of BPA into PET (green) and PC (pink) ... 230

Figure A.7 shows the change in percent crystallinity of PET under different conditions (Depolymerized with EG (dark blue), swelled with EG (light blue), annealed at reaction temperature (pink), depolymerized with BPA (red), swelled with BPA (orange) with time. 230

Figure A.8 shows the FTIR spectra for BPA, PET, and PC. The top left in red shows the FTIR of BPA with the alcohol peak highlighted in a purple square. The Middle FTIR spectra show the PC powder in red and the flake in pink. The bottom spectra show FTIR of PET powder in red and PET flakes in green. The right side of the image also shows the visual difference in the polymer flakes and the polymer powder..... 232

Figure B.1 SAXS of annealed PET before and after depolymerization. (a) compares PET annealed for 0-24 hours. (b) shows scattering of pre-depolymerization annealed PET for 0-

24 hours depolymerized for 15 minutes (c) shows scattering of pre-depolymerization annealed PET for 0-24 hours depolymerized for 90 minutes. 240
Figure B.2 DSC Q2000 curves of PET with changing Annealing time (0 hours green (unannealed), 3 hours purple, 6 hours blue, 13 hours red, and 24 hours yellow). Exo up . 242
Figure B.3 Average number of hydroxyl end groups per chain changes with annealing time. The number of hydroxyl end groups per chain was determined by comparing M_n from NMR and SEC-GPC. 244
Figure B.4 Swelling of EG into PET that is annealed for varying amounts of time (0 hour green, 3 hour purple, 6 hour blue, 13 hour red, and 24 hour yellow). 244
Figure B.5 Differential Scanning Calorimetry of PET annealed at 180 °C for varying times ... 246
Figure B.6 Differential Scanning Calorimetry of PET swelled at 180 °C for varying times 246
Figure B.7 Crystallinity of annealed and non-annealed PET are changing with glycolysis. PET was annealed for 0 hours (green; unannealed), 3 hours (purple), 6 hours (blue), 13 hours (red), and 24 hours (yellow) before depolymerization. (A) Percent Crystallinity from DSC vs reaction time. (B) Crystalline phase from SAXS vs reaction time. (C) Long phase from SAXS vs reaction time. 249

LIST OF SCHEMES

Scheme 2.1 Heterogenous PET glycolysis reaction catalyzed by TBD:MSA to create BHET ... 53

Scheme 2.2 PET glycolysis conversion of carboxylic acid end groups into alcohol end groups. 68

Scheme 3.1 Ester and Carbonate containing polymers PET and PC respectively..... 89

Scheme 3.2 Heterogenous glycolysis reaction of Tritan™, PET, and PC catalyzed by TBD:MSA to create oligomers. 91

Scheme 3.3 Heterogenous PC and PET reaction with Bisphenol-A catalyzed by TBD:MSA to create new monomers 92

Scheme 4.1 Heterogenous PET glycolysis reaction catalyzed by TBD:MSA to create BHET . 136

Scheme 5.1 Depolymerization of PET via glycolysis 169

Scheme A.1 Heterogenous glycolysis reaction of Tritan™, PET, and PC catalyzed by TBD:MSA to create oligomers. 219

CHAPTER 1: AN INTRODUCTION TO PLASTIC PRODUCTION, PLASTIC WASTE, AND PLASTIC RECYCLABILITY

1.1 Plastic Production and Plastic Waste

1.1.1 Plastic Generation

Around 300 million tons of plastic are produced annually, and an expected 900 million tons will be produced annually within 30 years.[1-3] **Figure 1.1** illustrates the increasing demand for plastic every year as the production of plastics has grown exponentially since the mid-20th century, reaching over 400 million metric tons annually in recent years.[4-6] Despite efforts to improve waste management and recycling systems, approximately 10-15 million metric tons of plastic are estimated to leak into the environment each year, with much of this entering marine ecosystems.[7-12] The leakage occurs through various pathways, including improper waste disposal, stormwater runoff, and industrial discharge.[8] The persistence and ubiquity of plastic pollution has led to severe environmental impacts, ranging from ecosystem disruption to the ingestion of microplastics by marine and terrestrial species.[9-12] Current studies emphasize that without significant intervention, both plastic production and environmental leakage are projected to increase dramatically by mid-century, further exacerbating the global plastic crisis.[5-13]

1.1.2 Microplastic and Nanoplastic (NPs) Generation

An increasing amount of nano and micro-sized plastics in the environment may create pathogens and hazardous chemicals, creating a greater threat to the environment.[14] The ingestion of these micro and nano-sized particles is harmful to aquatic invertebrates and fish, they have been linked to commonly used consumer products, and may be ingested by humans.[15-19] Micro to nanosized plastics can enter the human body through inhalation, direct dermal exposure, and the food chain, causing severe health effects.[19-22] Nanoplastics (NPs) have been defined as plastic with maximal lateral dimensions <1 micrometer. It is estimated that up to 51 trillion microplastic fragments accumulate in the ocean and form NPs upon further fragmentation of the microplastic.

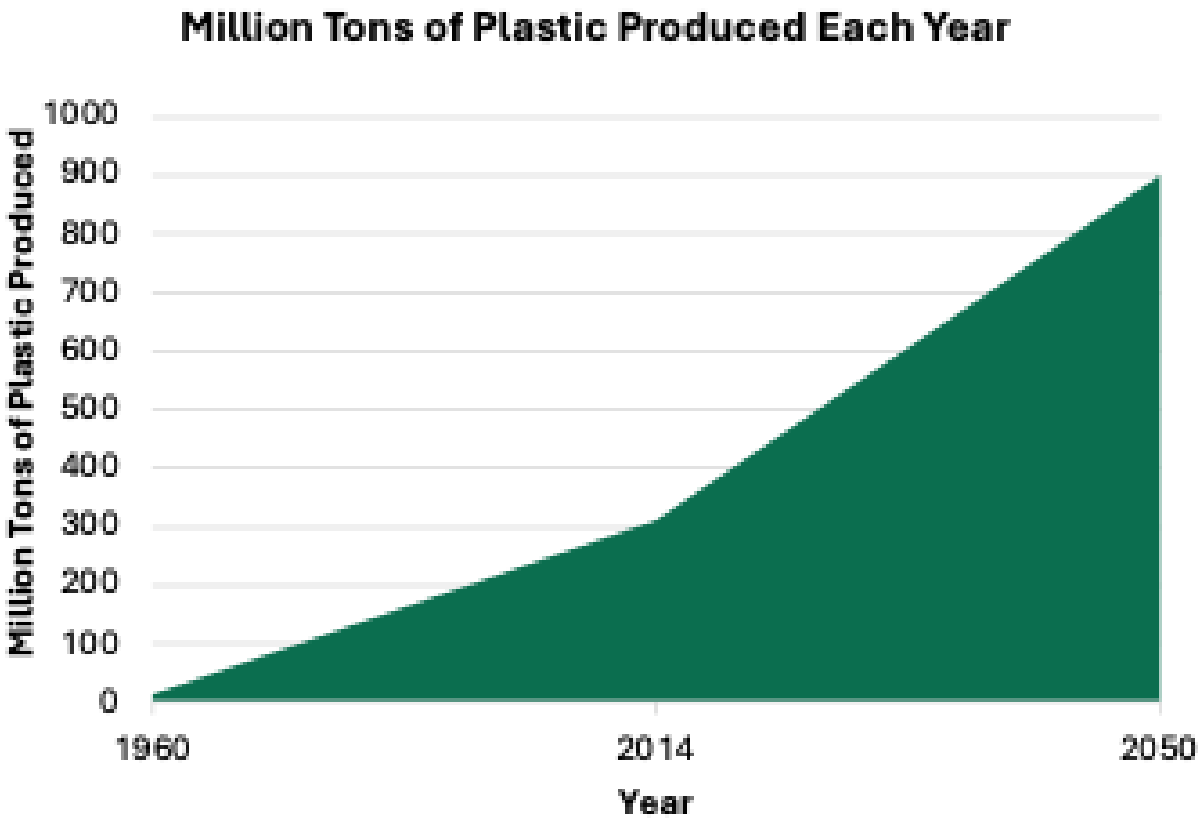

Figure 1.1 Million tons of plastic produced since 1960 and predicted to be produced into 2050.[1]

Figure 1.2 illustrates pathways of microplastic and nanoplastic leakage into the environment.[8, 9, 23, 24] For instance, microplastics end up in the environment through industrial leakage and fragmentation of leaked consumer waste.[8, 9, 11, 12, 23, 24] Our current understanding shows that all NPs come from microplastic fragmentation.[10-12, 18, 22, 24-26] As well, there are very few techniques that are able to isolate and identify sub-100 nm particles in water, and this is a large obstacle in the study of NPs in aqueous enviroments.[20, 22]

1.2 Polymer Recycling

To address the current plastic waste and environmental leakage scenario, an eco-friendly and economical mitigation route is needed, as defined by the United Nations Commission on Environment and Development (Brundtland Commission) in 1987. The report of this commission states that sustainable development and green chemistry are the developments and promotion of innovative technologies that reduce or eliminate the use or generation of hazardous substances that would affect the ability of future generations to meet their own needs.[1, 27] The increasing demand for polymer production in the absence of sustainable manufacturing and recycling processes will make the goals of the Brundtland Commission challenging to achieve. Without sustainable manufacturing and recycling processes, the amount of polymer in global solid waste will only increase since most polymers do not readily degrade in nature.[27-29] The history of the end-of-life destinations for commercial polymers is documented in **Figure 1.3** where the total abundance of plastic generated (blue), and that which is recycled (red), combusted (green), or disposed of in a landfill (purple) is plotted as a function of time since 1960. Of all the plastic produced annually, 76% is disposed of in a landfill, 16% is combusted, and only 9% is recycled.[3, 4] Ongoing research aims to increase the percentage of plastic recycled by simplifying recycling methods.

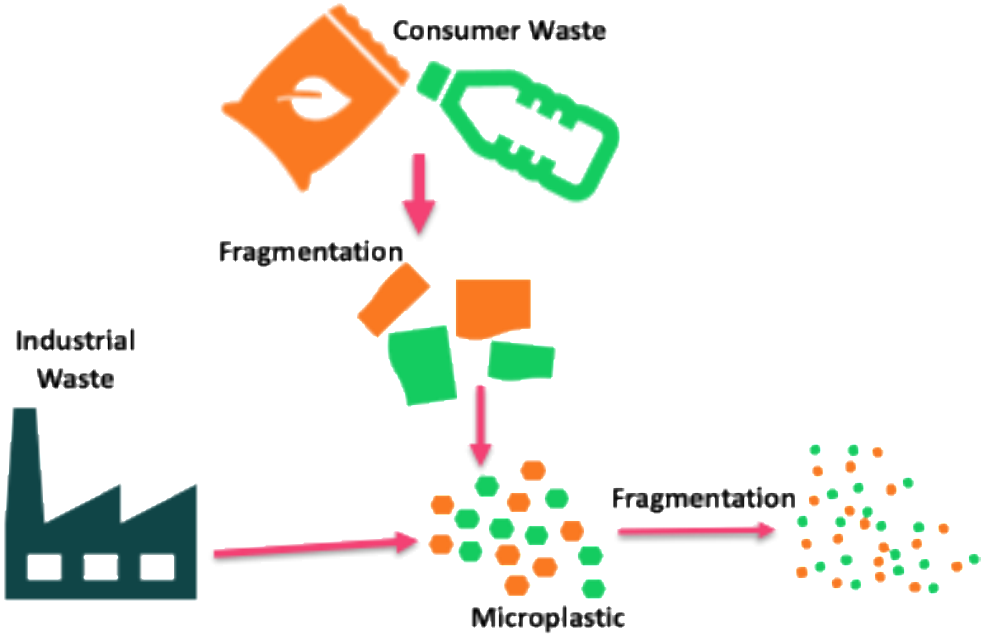

Figure 1.2 Pathway of leakage and formation of microplastics into the environment and the formation of nanoplastics (NPs)

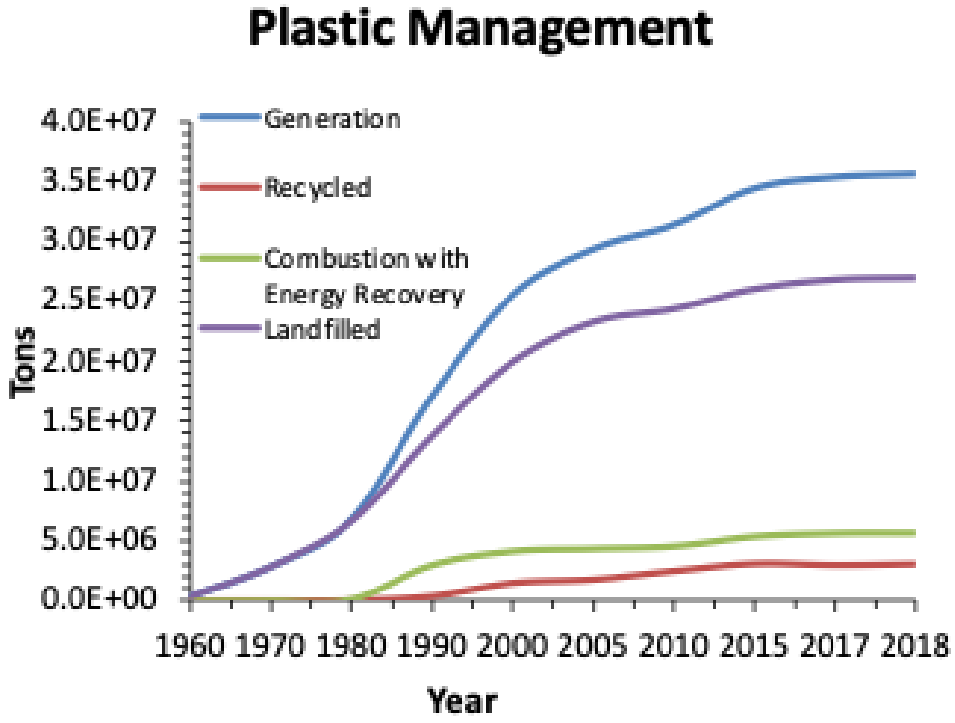

Figure 1.3 The amount of plastic generated (blue), recycled (red), combusted (green), and landfilled (purple) every year from 1960 to 2018

1.2.1 Types of Recycling

Polymers can be recycled through different methods, including primary recycling/physical recycling, mechanical recycling, energy recovery, and chemical recycling. Primary or physical recycling involves reprocessing materials without altering their chemical composition.[30, 31] Primary recycling focuses on maintaining the quality of the materials for re-use while physical recycling includes reprocessing without affecting the polymer structure. A subsection of physical recycling is mechanical recycling, which involves mixing plastic waste with virgin plastic material and then subjecting it to a grinding and melting process to produce new material.[1, 30-33]However, the re-pelletizing process might degrade the polymer, adversely affecting its properties, resulting in structural deterioration and reducing the properties of the recycled product relative to those of the virgin material.[31, 34] Mechanical recycling is relatively simple, requires low investment, and has little adverse environmental impact compared to other methods.[1, 31] However, recycled polymers from this process exhibit relatively low and diverse intrinsic viscosities, preventing their direct use in producing high-quality polymer films, materials, and industrial fibers.[1, 30-32] Additionally, there are several challenges, such as high costs of collection, sorting, and separation of mixed waste, as well as the complexity of separating multilayer films and issues related to the presence of paper labels, adhesives, and residual moisture in creating a homogeneous waste stream for mechanical recycling.[1]

Energy recovery entails incineration, pyrolysis and gasification, or anaerobic digestion.[35-37] However, these processes can generate emissions linked to greenhouse gases, such as CO_2, and toxic byproducts, including bottom ash and fly ash.[37, 38] These processes are also low in energy efficiency and result in a loss of material that could be utilized in other recycling efforts.[39-43] Energy recovery encounters initial high investment costs related to facility

infrastructure and maintenance, along with a limited waste stream, since efficient recovery necessitates clean and sorted waste materials.[44-47]

Chemical recycling offers an alternative to mechanical recycling and energy recovery, as it involves depolymerizing polymers into monomers or oligomer fragments that can be used as value added materials or re-polymerized into the polymer.[1, 31, 32] While current industrial methods to depolymerize plastic waste, such as glycolysis of polyethylene terephthalate (PET), are acceptable to address the principles of sustainable development, there remain issues. For example, chemically recycled PET is more expensive to produce than virgin PET, and there are challenges related to the kinetics of the glycolysis reaction, which can result in the presence of low molecular weight cyclic oligomers in the product, inhibiting repolymerization.[1, 2, 30] Overall, each recycling method has its advantages and challenges, and the choice of recycling method for a given waste stream depends on various factors such as cost, product quality, and targeted environmental impact.

1.2.2 Sovolysis: Homogeneous vs Heterogeneous Catalysis of Depolymerization

Depolymerization is the process of breaking down large polymers into smaller units. Several methods for depolymerization exist, including thermal depolymerization, catalytic depolymerization including enzymatic depolymerization, and solvolysis depolymerization, which, may also be catalyzed.[48-51] However, solvolysis is typically used in an industrial setting because it has lower reaction temperatures than thermal and some catalytic depolymerizations, leading to significant energy savings. By implementing more selective and controlled depolymerization, random degradation of the polymer backbone is reduced, leading to products that are more consistent and of higher quality. Solvolysis is beneficial in this context, as it allows for the selection of different solvents/reactants for the reaction process.[51-53] In solvolysis, the

solvent acts as the reactant and the medium for the polymer chain scission.[51] This process includes glycolysis, hydrolysis, acidolysis, and alcoholysis.[32, 54-62]

Solvolysis, particularly glycolysis, has been extensively studied for recycling polyethylene terephthalate (PET) to isolate monomers for repolymerization.[51, 63-65] Solvolysis can be conducted in two ways: homogeneously catalyzed depolymerization (where the polymer is in the same phase as the catalyst) and heterogeneously catalyzed depolymerization (where the polymer is in a different phase than the catalyst). Generally, in glycolysis depolymerization of PET, the polymer remains insoluble in the glycol, which is most often ethylene glycol (EG). At the same time, the catalyst may be soluble or insoluble in EG; however, both conditions are categorized as heterogeneously catalyzed depolymerizations as the catalyst remains in a separate phase from the polymer in both conditions.[31, 66-69] Homogenously catalyzed depolymerization reactions utilize specific catalysts, pressurized systems, or cosolvents to dissolve the polymer so that the polymer, catalyst, and solvolysis reactant are in the same phase.[62, 70-73] Each method has distinct characteristics, advantages, and limitations, making them suitable for different polymers and applications.

Homogeneously catalyzed depolymerization allows uniform interaction and reaction between the polymer chains, catalyst, and solvolysis agent.[74-76] The system is a one phase mixture throughout the reaction, resulting in a reaction rate that depends on the feeding rate, reaction temperature, and amount of catalyst used. However, this method requires the polymer to be soluble in the chosen solvent, which limits the types of polymers that can be processed or requires specific, often harsh, reaction conditions.[71-73, 77-79]

In contrast, heterogeneously catalyzed depolymerization reaction occurs at the solid-liquid interface, where the solvent and catalyst may be miscible and swell the insoluble

polymer.[78, 80] This method is advantageous when complete dissolution of the polymer into the solvent and catalyst mixture is impractical. However, the penetration of the reactant and catalyst into the polymer inhibits the reaction rate relative to that of a homogeneously catalyzed reaction.[78, 80] The depolymerization reactant and catalyst must penetrate the solid polymer, which can slow down the reaction and result in incomplete depolymerization. Additionally, the reaction rate of heterogeneously catalyzed depolymerization is restricted to the surface of the undissolved polymer, which affects the access of the solvent to the reaction site.[28, 31]

Overall, heterogeneously catalyzed solvolysis reactions are typically dependent on the macroscopic size of the polymer sample. Homogenously catalyzed depolymerizations generally occur more rapidly than heterogeneously catalyzed depolymerizations, as the polymer chain is individually dispersed and, therefore, access of the reactants is straightforward on the molecular scale. In contrast, heterogeneously catalyzed depolymerizations involve solid polymeric materials, which result in inhibited access of polymer and reactant and, consequently, a slower reaction rate.[28, 31]

Figure 1.4 illustrates the variation in the accessibility of polymer chain by the glycol/reactant during heterogeneously catalyzed (top) and homogeneously catalyzed (bottom) depolymerizations, showing the three stages of heterogeneously catalyzed depolymerization and the single stage of homogeneously catalyzed depolymerization.[28] The heterogeneously catalyzed process begins with the minimal dissolution of chains, progresses to a coexistence stage (where oligomers are both dissolved and undissolved in the solvent), and may finally reach a homogeneous process where all chains are dissolved. While heterogeneously catalyzed depolymerizations allow limited access to polymer chains early in the reaction, homogeneously

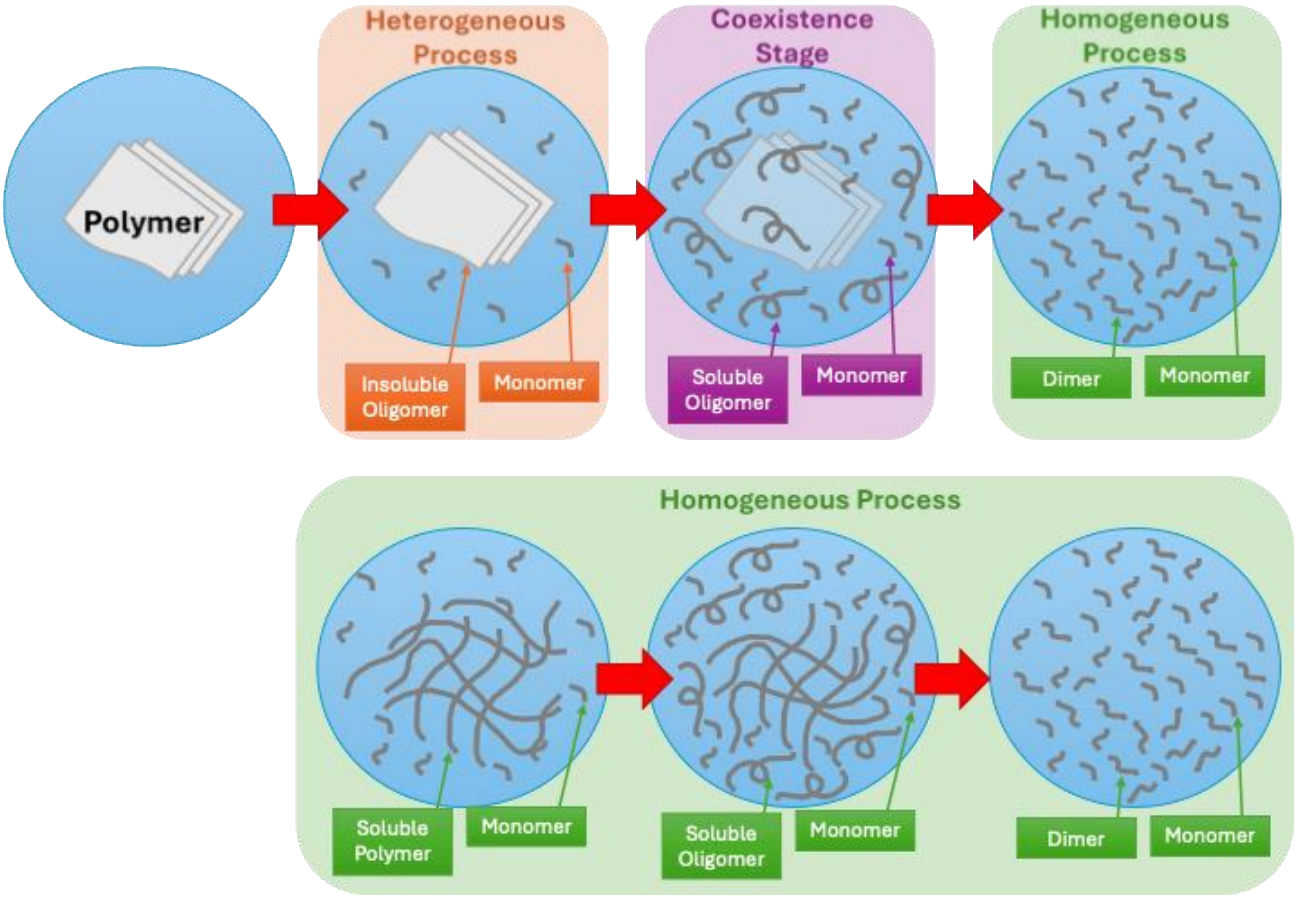

Figure 1.4 Depolymerization may occur by two processes: heterogeneously catalyzed (top) and homogeneously catalyzed (bottom). In heterogeneously catalyzed depolymerization, the polymer is initially insoluble in the solvent and progresses through three stages: 1) heterogeneous stage with solvent-insoluble polymer oligomers and solvent-soluble monomers; 2) the coexistence stage with insoluble polymers and oligomers, soluble oligomers, and soluble monomers; and 3) a homogeneous stage with solvent-soluble oligomers, dimers and monomers. The homogeneous phase depolymerization starts with the polymer dissolved in the solvent, quickly producing oligomers, dimers, and monomers, ultimately yielding only monomers and dimers.

catalyzed depolymerization offers access to all polymer chains for the reactants throughout the reaction.[28]

1.2.2.1 Polymer Solubility and Dissolution

As mentioned above, polymer solubility in a solvent plays an essential role in whether a reaction is homogeneous or heterogeneous. The solubility of a polymer in a given solvent depends on the polymer's chemical structure, the solvent's chemical structure, temperature, and pressure. Dissolving a polymer in a solvent usually involves two stages: first, swelling, where the solvent penetrates the polymer, causing it to swell, and dissolution, where polymer chains disentangle and molecularly disperse into the solvent, leading to complete dissolution.[78] The Hildebrand Solubility Parameter (δ) can be used to predict the solubility of materials, particularly polymers, in various solvents and is based on the cohesive energy density of the material and solvent. The cohesive energy density is a measure of the intermolecular forces holding the material together.[81] The solubility of a polymer in a solvent can be estimated by examining the difference between their solubility parameters, which reflect their cohesive energy densities.[79] When the difference in the solubility parameters of the polymer and the solvent is less than 1-2 $MPa^{1/2}$, the polymer is likely to dissolve in the solvent due to favorable interactions.[82-86] This quantifies the fundamental concept that "like dissolves like", which refers to the idea that materials with similar polarity and structure are more likely to mutually mix or dissolve due to their comparable intermolecular forces. Over time, this idea has evolved into 'like seeks like,' implying that substances actively seek out and interact with similar counterparts during dissolution and adhesion and wetting. This expanded perspective recognizes that materials with similar characteristics tend to form more favorable interactions in solutions and at interfaces.[78, 83-85, 87, 88]

The concept of solubility parameters is based on the energy required to vaporize a liquid, which reflects the cohesive energy holding the liquid molecules together.[87] This concept is particularly relevant when assessing surface phenomena, where the interaction between a polymeric layer and a surface can be optimized by matching their solubility parameters. However, the Hildebrand solubility parameter is a single-parameter model and does not consider specific interactions such as hydrogen bonding or polarity. For more complex systems, the Hansen Solubility Parameters (HSP) provide a more detailed representation of potential interaction mechanisms by dividing δ into three distinct components: δ_d, (dispersion force solubility parameter), δ_p, (polar interaction solubility parameter), and δ_h, (hydrogen bonding solubility parameter), as shown in **Equation 1.1**. These solubility parameters collectively describe the total solubility parameter, enabling a comprehensive understanding of the role of molecular interactions in determining solubility.[87, 89] HSPs are widely used, particularly in the coatings industry, to aid in solvent selection and predict the compatibility of polymers and solvents, chemical resistance, and permeation rates.[79, 87]

Equation 1.1
$$\delta = \sqrt{{\delta_d}^2 + {\delta_p}^2 + {\delta_h}^2}$$

1.2.3 Recent Developments in Organocatalysts

The reaction rate of the depolymerization of a given polymer also depends on catalyst loading and type.[1, 34] While homogenously catalyzed reactions have the fastest reaction rate, the reaction rate of heterogeneously catalyzed reactions is influenced if the catalyst is soluble or insoluble in the reaction medium.[69, 90, 91] Depolymerization utilizing solid acid catalysts (insoluble) like zeolites and metal oxides is advantageous for catalyst recyclability but can be a relatively slow reaction as the limited interaction of the reactants at the surface of the solid catalyst limits the reaction, whereas soluble catalysts do not face this limitation.[69, 91]

Homogenously catalyzed depolymerizations often utilize metal-organic complexes, ionic liquids, and acid/base catalysts (organocatalysts); these catalysts, reactants, and polymers are dissolved in a solvent, which allows for more readily formed interactions between the polymer, reactant and catalyst, leading to more efficient depolymerization.[69, 91]

There is a demand for greener chemistries that utilize catalysts without metals, such as metal acetates, as they are not biodegradable or are quite toxic.[1, 30, 33] This demand requires a change in catalyst structure, where enzyme catalysts, heterogeneous catalysts, and organocatalysts are promising substitutes. As previously mentioned, heterogenous catalysis is quite slow compared to homogeneous catalysis, so recent research has focused on designing highly specific organocatalysts to enhance the depolymerization of polymers but retain sustainability.[66, 68] These catalysts are tailored to target specific functional groups within the polymer chains, allowing for more efficient depolymerization at lower temperatures.[92] For instance, catalysts based on nitrogen heterocycles and thiourea-based catalysts have been shown to enhance the rate of PET glycolysis at relatively low temperatures.[4] Additionally, there have been advancements in developing organocatalysts that can function effectively at room temperature, reducing the energy requirements of the depolymerization process.[93]

Furthermore, organocatalysts have enabled the depolymerization of more complex and mixed plastic waste streams, selectively breaking down one type of polymer in the presence of others.[62, 67, 94] Progress has also been made in creating organocatalysts that can be easily recovered and reused, addressing a significant challenge in the practical application of these catalysts in industrial processes.[66, 94, 95] Lastly, research has been moving towards more biocompatible and environmentally friendly organocatalysts, reducing the overall environmental

impact of the depolymerization process.[66] These organocatalysts help decrease the reaction time of otherwise sluggish depolymerizations.[1]

1.2.4 Development in Mixed Waste Polymer Depolymerization

Recent advancements in the depolymerization of mixed waste polymers have focused on improving the efficiency of recycling processes, as well as their environmental impact and economic viability.[4, 94] Traditional depolymerization methods often necessitate harsh conditions, such as high temperatures and strong acids or bases as catalysts, which result in substantial energy consumption and adverse environmental implications.[30, 32, 92, 96-101] However, recent research has made noteworthy breakthroughs in addressing these challenges.

A key advancement involves developing a catalytic process that breaks down various polymers individually in mixtures of plastic waste into their monomers. This process employs custom synthetic organocatalysts that can efficiently break down different plastics, including PET, polyamides, polyurethanes, and polycarbonates, at specific temperatures tailored to each polymer.[4, 94] This innovation offers the potential for a substantial reduction in energy consumption of up to 94% and a decrease in greenhouse gas emissions by 95% compared to conventional methods.[4] Additionally, this process enables the recycling of complex plastic mixtures that typically end up in landfills due to the challenges of separating and recycling different polymers.[31] These advancements represent significant progress towards more sustainable and efficient recycling processes and have the potential to transform how we manage plastic waste on a global scale.

1.2.4.1 Reactivity of Carbonyl Carbon

Many polymers that are in the waste stream and the focus of depolymerization studies, including the mixed waste studies discussed above, contain a carbonyl carbon.[4, 94] The reactivity

plays an important role in determining the efficiency of their depolymerization as the carbonyl carbon is reasonably reactive due to the polarization of the carbon-oxygen double bond (C=O).[102-106] The electronegativity difference between carbon and oxygen results in a partial positive charge on the carbon atom and a partial negative charge on the oxygen atom, making the carbonyl carbon an electrophilic center, susceptible to nucleophile attack.[102-106] Various factors influence the reactivity of carbonyl compounds, including the electrophilicity of the carbonyl carbon, steric effects, the specific type of carbonyl compound (such as aldehydes, esters, amines, and carboxylic acids), as well as inductive and resonance effects, conjugation and aromaticity, the acidity of alpha hydrogens, influence of solvent, and the nature of the catalyst used.[102-107] Aldehydes are generally more reactive than ketones due to the hydrogen atom attached to the carbonyl carbon, making it more accessible to nucleophiles.[102-104, 106] Ketones, with two alkyl groups connected to the carbonyl, experience steric hindrance and electron-donating effects that decrease the carbonyl carbon's electrophilicity.[102-104, 106]

Carboxylic acids and their derivatives play a significant role in organic chemistry. The carbonyl group of carboxylic acids has a certain level of electrophilicity; however, their electrophilicity is somewhat reduced compared to their derivatives because of resonance stabilization from the hydroxyl group (-OH) and potential hydrogen bonding.[102-104, 106] In the reactivity hierarchy of carbonyl-containing compounds, acid chlorides and anhydrides are more reactive than carboxylic acids due to electron-withdrawing groups that enhance the electrophilicity of the carbonyl carbon. Esters are less reactive than carboxylic acids and derivatives like acid chlorides and anhydrides. The reduced reactivity in esters is due to electron donation through resonance from the alkoxy group (-OR).[102-104, 106] Amides are even less reactive

than esters because the lone pair of electrons on the nitrogen atom can delocalize into the carbonyl group, further reducing the electrophilicity of the carbonyl carbon.[102-106]

The effect of substituents on the carbonyl on its reactivity is also notable. Electron-withdrawing groups such as nitro ($-NO_2$), cyanide (-CN), or halogens increase the reactivity of the carbonyl carbon, while electron-donating groups including alkyl chains, ethers (-OR) and amines ($-NR_2$) decrease the carbonyl reactivity by donating electron density to the carbonyl carbon, making it less susceptible to nucleophilic attack.[102-104, 106]

The reactivity of the carbonyl in a polymer backbone is central to directing the depolymerization pathways in the chemical recycling of such polymers. Many synthetic polymers contain carbonyl functionalities that are electrophilic centers are ideal for chain scission. As discussed earlier, the reactivity of the carbonyl carbon is affected by various factors. Moreover, electron-withdrawing or electron-donating substituents can also influence its further reactivity.[102-107] In recycling, understanding the relationship between molecular structure and carbonyl reactivity is crucial to developing effective depolymerization strategies targeting carbonyl-containing polymers, facilitating their breakdown into valuable monomers, and enabling more sustainable material management.

1.3 Polymer Crystallinity

Many polymers are amorphous. However, a significant percentage of polymers in the waste stream are semi-crystalline, with many studies showing that depolymerization occurs first in the amorphous region of the polymer before depolymerization occurs in the crystalline regions. [56, 58, 108-111] The crystalline regions in polymers consist of areas where polymer chains are atomically arranged in an ordered, repeating lattice.[112, 113] The assembly of the polymer on a crystal lattice can also be facilitated by thermal treatments that promote chain mobility[114] and

mechanical stretching, which enhances orientation.[115] On the other hand, amorphous regions are areas where the polymer chains are randomly assembled and do not form a regular structure; these conformations contribute to the flexibility and impact resistance of the polymer.[116-121] Some common semi-crystalline polymers include polyethylene (PE), polypropylene (PP), polyethylene terephthalate (PET), and nylon.[116-121]

A way to control the size, number, and perfection of crystals is through the annealing of the semi-crystalline polymer between its glass transition temperature and its melting point. Annealing is a thermal process that involves heating a material to a specific temperature, holding it there for some time, and then cooling it. When semicrystalline polymers are annealed between their glass transition temperature (T_g) and melting temperature (T_m), the polymer chains can assemble to alter the size, number, and perfection of the crystals in the polymer.[122-127] Annealing a polymer close to its glass transition temperature (T_g) enhances molecular mobility in the amorphous areas. This allows polymer chains to shift into more stable, lower-energy conformations on a crystal lattice without melting the crystalline sections. This results in secondary crystallization, forming new, small, imperfect crystals primarily in the amorphous regions. Nucleation dominates at these temperatures because the thermodynamic driving forces for crystallization are high, while chain mobility is limited, favoring the formation of new crystalline nuclei over significant crystal growth.[122-127]

In contrast, annealing near T_m increases molecular mobility to a level where polymer chains can readily integrate into existing crystalline structures. This enhanced mobility facilitates significant growth of existing crystals while minimizing nucleation, as the thermodynamic driving force for creating new nuclei diminishes closer to T_m.[128-131] As shown in **Figure 1.5**, annealing below T_g does not lead to crystal nucleation or growth due to polymer chain

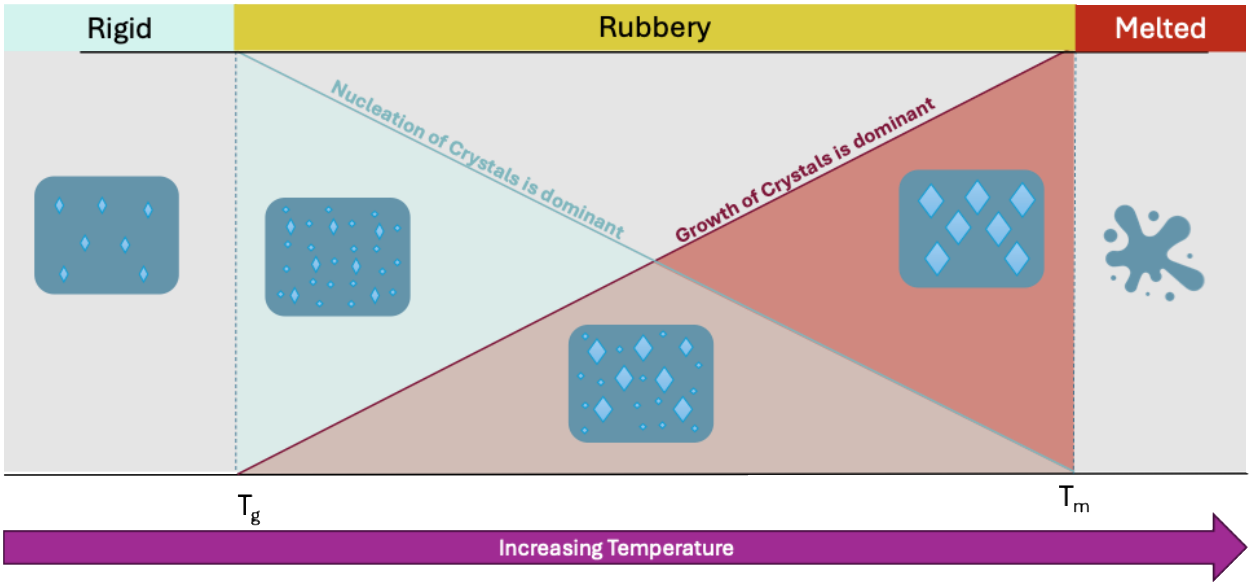

Figure 1.5 The effect of annealing temperature on crystal growth of polymers. As polymers are annealed near, but above, the glass transition temperature (T_g), nucleation of new small crystals is dominant. Polymers annealed near, but below, the melting temperature (T_m) dominate in growing existing crystals over nucleation. Below the T_g crystals, neither nucleate nor grow due to the immobility of the polymer chains. Above the T_m the polymer crystals melt.

immobility, while annealing just above T_g results in nucleation dominating over crystal growth. Conversely, annealing near T_m shifts the balance toward crystal growth over nucleation. The relative contributions of nucleation and growth depend on the annealing temperature's proximity to T_g or T_m, where the specific crystal structure that forms will influence the polymer's resulting crystallinity and mechanical properties.

Recrystallization may also occur when annealing near T_m, as there is sufficient thermal energy to melt smaller imperfect crystals. This results in an improvement of crystal perfection and size by healing defects in existing crystals. Improving crystal perfection has been previously linked to increased T_m and a subtle decrease in the crystalline domain size as the polymer chains become more efficiently packed and occupy less space. These modifications to the crystal can also alter the immediate/rigid amorphous phase, which is the portion of the amorphous phase that is immediately neighboring the crystal. The rigid amorphous phase melts with lower a lower entropy than the bulk amorphous phase and thus improving crystal perfection results in a smaller entropy of melting, increasing the T_m. Unlike bulk amorphous polymers, the conformation of the rigid amorphous chains is influenced by the neighboring crystalline phase. These changes in physical properties can impact recycling due to sorting challenges and recrystallization during processing.[132, 133] In recycling, understanding the relationship between polymer crystallinity and degradation behavior is crucial for developing effective recycling strategies that target semi-crystalline polymers, facilitating their breakdown into reusable components and enabling more sustainable material management.

1.4 Generation of value-added products from consumer plastic waste

Rather than focusing solely on repolymerizing waste plastics, upcycling opens opportunities to engineer entirely new materials from waste plastics with enhanced mechanical,

thermal, or chemical properties tailored for specialized applications. In recent years, significant advancements have been made in exploring innovative techniques to convert waste plastics into valuable materials, chemicals, and fuels. Chemical recycling processes, like depolymerization, are being developed to break down polymer chains into smaller molecules that can be used as feedstocks to create new materials or chemicals.[134-137] Additionally, catalytic methods, such as heterogeneous catalysts, have been explored to enhance the efficiency of plastic conversion processes, producing high-value products like alkanes, olefins, and aromatics.[138-140] Biological techniques involving enzymes and microbes are also being investigated to break down plastics, offering environmentally friendly alternatives to traditional recycling methods.[141, 142] Moreover, upcycling techniques aim to convert low-value waste plastics into high-performance materials, including advanced composites, construction materials, and specialty chemicals, often by modifying the chemical structure of the plastic to enhance its properties. This shift toward upcycling represents a new frontier in polymer waste management, where the focus is not just on recovering materials but on unlocking their potential to create entirely novel, high-value applications. By reimagining waste plastics as building blocks for innovation, upcycling is transforming the lifecycle of polymers into an opportunity for advanced materials engineering. Innovative strategies, such as integrating functional additives or crosslinking agents during upcycling, could lead to the development of high-performance composites, coatings, or even innovative materials that surpass the properties of the original plastic.[134-147] Finally, recent research has also delved into electrocatalysis as a sustainable approach to plastic recycling, utilizing electricity to drive chemical reactions to convert plastic waste into valuable chemicals.[144-147] In this context, approaches that leverage intermediates from depolymerization reactions as macromers or building blocks for new polymers embody the cutting edge of this

emerging field. By tailoring these intermediates for specific applications, researchers can develop entirely new classes of polymers with advanced functionalities, marking a departure from traditional recycling methods and embracing the future of polymer science. This approach bridges the gap between traditional recycling methods and upcycling, leveraging depolymerized fragments not just for repolymerization but also as foundational units for entirely novel polymer classes. By tailoring these intermediates for specific applications, this strategy could expand the value-added potential of plastic waste, transforming it into high-performance materials or specialized chemical products. By addressing the challenge of polymer waste in this transformative way, we are paving the way toward sustainable solutions that redefine the value of plastics in society.

1.5 Conclusions and Outlook

The rising demand for synthetic polymers contrasts with the growing rate of recycling, as only 9% of plastics are currently recycled yearly.[4, 148] The current management of polymer waste is unsustainable, with most polymers being sent to 'end-of-life destinations' such as landfills or incineration.[1, 34, 148-150] This research project, conducted in the face of this urgent need, investigates the depolymerization of polyethylene terephthalate (PET), polycarbonate (PC), and Tritan™ from Eastman Chemical Company, and explores methods to make recycling processes more efficient and sustainable. This research seeks to create a comprehensive understanding of the factors that affect the depolymerization of polyesters and polycarbonates. The main goals include clarifying how chain structures change during depolymerization, assessing the influence of functional groups on reaction rates, and investigating the impact of polymer solvent compatibility and crystal size on depolymerization kinetics. Furthermore, the study explores how telechelic intermediates produced during these processes can be reused for

repolymerization or converted into value-added products. An essential aspect of this research also involves developing advanced imaging techniques for detecting and analyzing nanoplastics in environmental samples, targeting an urgent need to quantify and reduce their impact. Collectively, these initiatives aim to improve sustainable recycling practices and promote the conversion of polymer waste into high-value materials.

In Chapter II, the polymer chain evolution of PET during depolymerization by glycolysis was revealed. Many previous studies that examine the depolymerization of PET via glycolysis or hydrolysis focus on the yield of monomer isolated as the primary metric to characterize the success of PET depolymerization. However, few studies have examined how PET chains are scissioned and elucidate the evolution of chain molecular weight and dispersity of the chains that emerge as the depolymerization proceeds. This study focuses on understanding the evolution of chain structure as the PET degrades so that oligomers may be captured and used as potential feedstocks to produce economically viable materials. This includes repolymerization of the oligomers, where they are used as macromonomers. By monitoring the dispersity, molecular weight, end groups, and crystallinity of intermediates as a function of the progress of the heterogeneous depolymerization of PET, insight into how polymer chains evolve throughout the reaction is gained. This analysis indicates a mechanism in which chain scission initially targets the amorphous tie chains connecting crystalline phases. These findings also indicate that the oligomeric intermediates that can be recovered from the depolymerization can be easily repolymerized, presenting new avenues for more effective and efficient PET chemical recycling from energy and purification perspectives.

In Chapter III, the study explores the impact of various controllable factors on the progression of the depolymerization of polyesters and polycarbonates. These factors include

polymer crystallinity, solvent-polymer compatibility, and carbonyl reactivity. The influence of these factors on the rate of heterogeneous solvolysis depolymerization as it transitions through the heterogeneous, coexistence, and homogeneous stages is also examined. Polymers that contain carbonyl-carbons are readily chemically recycled due to the reactivity of the carbonyl. However, more research is needed to provide insight into the molecular-level processes that control the rate of their depolymerization processes. For instance, an important and understudied aspect of the depolymerization process is the importance of the transport of the diol to the carbonyl in the depolymerization mechanism. The chemical reaction that results in chain cleavage at the carbonyl carbon requires the transport of the hydroxyl-containing reactant to the carbonyl, which may be a potential rate-limiting step. This study examines the depolymerization of Tritan™, an amorphous polyester, consumer waste polyethylene terephthalate (PET), a standard semi-crystalline polyester, and consumer waste bisphenol polycarbonate (PC), an amorphous carbonate. These polymers are depolymerized by reacting with one of two diols, ethylene glycol EG or bisphenol-A BPA, where these two hydroxy-containing reactants have distinctly different chemical structures. This variation in structure enables the study of the importance of polymer-solvent compatibility on the transport of the diol to the carbonyl group, which is quantified by monitoring the swelling of the polymers with the diols. The polymers used in this study also provide insight into the role of polymer crystallinity and carbonyl reactivity on the rate of the depolymerization reaction by monitoring the time evolution of the molecular weight and dispersity of the ester-containing semicrystalline and amorphous polymer (PET and Tritan™, respectively) and the amorphous carbonate-containing polymer (PC). These findings provide fundamental insight that can be used to tune depolymerization reactions, advance sustainable polymer recycling processes, and create economically viable materials from polymer waste

streams. This study also underscores that low compatibility between polymers and solvents can hinder the complete dissolution of the polymer, resulting in fragmentation into micro- and nanoplastics. Since most plastics have poor compatibility with water, their interaction with aqueous environments frequently leads to the formation of nanoplastic particles. This highlights the importance of understanding and tackling these mechanisms when developing sustainable recycling and waste management strategies.

Chapter IV presents the results of a study that examines the impact of crystallinity and crystal size on the evolution of chain structure in the PET depolymerization process and their impact on the emergence of telechelic oligomers, which are advantageous for polymerization or further reactions. Chapter II illustrated that chain scission of PET via glycolysis initially targets amorphous tie chains between crystalline phases. Chain scission of tie chains and isolating highly crystalline PET lowers the dispersity ((Đ)) of the polymer chains, as the crystalline lamellae's size guides the depolymerized oligomers' molecular weight. Annealing the PET alters the lamellar structure before depolymerization and impacts the tie chain reactivity, which alters the evolution of dihydroxy-terminated oligomers during the depolymerization process. These results provide fundamental information that can be used to tailor the chemical structure of the depolymerization reaction of consumer waste to isolate telechelic oligomers. Access to these telechelic products eliminates the need for post-depolymerization functionalization, creating a more economically and environmentally friendly process. Therefore, this insight offers pathways to simplify the isolation of macromonomers that can be repolymerized or as reactants in further reactions for new materials.

The final project discussed in Chapter V explores the visualization of microplastics and nanoplastics utilizing transmission electron microscopes (TEM) to provide insight into how

polymer solubility impacts the size and shape of the nanoplastics formed. The study analyzes the fragmentation of microplastics into nanoplastics (NPs) in water-suspended polymers by Transmission Electron Microscopy (TEM). Providing a method to examining NPs in water addresses key challenges in NP research, including small size, low concentrations, and difficulty distinguishing them from natural particles. Advances such as asymmetrical flow field-flow fractionation (AF4) and TEM enable better isolation and analysis of NPs, enhancing our understanding of their behavior in natural systems and overcoming past research barriers.[151] Examining the micron and nanoscale structure of the depolymerized PET powder that emerges in the reactions discussed in Chapter II provides insight into the fragmentation processes that occur during the depolymerization process. These studies reveal that more crystalline domains detach from microplastics to form NPs. Analysis of the structures that emerge during polyethylene (PE) degradation under varying conditions highlights the influence of polymer solvent compatibility on the shapes of the resulting NP. Despite the low compatibility of PE and water as a solvent, the study demonstrates that NPs form from PE in water given sufficient time, providing foundational knowledge that may explain the prevalence of microplastics and nanoplastics in the oceans.

References

(1) George, N.; Kurian, T. Recent Developments in the Chemical Recycling of Postconsumer Poly(ethylene terephthalate) Waste. *Industrial & Engineering Chemistry Research* **2014**, *53* (37), 14185-14198. DOI: 10.1021/ie501995m.

(2) Fox, B.; Moad, G.; Van Diepen, G.; Willing, I.; Cook, W. D. Characterization of poly(ethylene terephthalate) and poly(ethylene terephthalate) blends. *Polymer* **1997**, *38* (12), 3035-3043. DOI: 10.1016/s0032-3861(96)00872-5.

(3) Agency, U. S. E. P. Facts and Figures about Materials, Waste and Recycling. Agency, U. S. E. P., Ed.; 2023.

(4) Arifuzzaman, M.; Sumpter, B. G.; Demchuk, Z.; Do, C.; Arnould, M. A.; Rahman, M. A.; Cao, P.-F.; Popovs, I.; Davis, R. J.; Dai, S.; et al. Selective deconstruction of mixed plastics by a tailored organocatalyst. *Materials Horizons* **2023**, *10* (9), 3360-3368. DOI: 10.1039/d3mh00801k.

(5) Nayanathara Thathsarani Pilapitiya, P. G. C.; Ratnayake, A. S. The world of plastic waste: A review. *Cleaner Materials* **2024**, *11*, 100220. DOI: 10.1016/j.clema.2024.100220.

(6) Lebreton, L.; Andrady, A. Future scenarios of global plastic waste generation and disposal. *Palgrave Communications* **2019**, *5* (1). DOI: 10.1057/s41599-018-0212-7.

(7) Kibria, M. G.; Masuk, N. I.; Safayet, R.; Nguyen, H. Q.; Mourshed, M. Plastic Waste: Challenges and Opportunities to Mitigate Pollution and Effective Management. *International Journal of Environmental Research* **2023**, *17* (1). DOI: 10.1007/s41742-023-00507-z.

(8) Schwarz, A. E.; Lensen, S. M. C.; Langeveld, E.; Parker, L. A.; Urbanus, J. H. Plastics in the global environment assessed through material flow analysis, degradation and environmental transportation. *Sci. Total Environ.* **2023**, *875*, 162644. DOI: 10.1016/j.scitotenv.2023.162644.

(9) Gómez-Sanabria, A.; Lindl, F. The crucial role of circular waste management systems in cutting waste leakage into aquatic environments. *Nature Communications* **2024**, *15* (1). DOI: 10.1038/s41467-024-49555-9.

(10) Su, L.; Xiong, X.; Zhang, Y.; Wu, C.; Xu, X.; Sun, C.; Shi, H. Global transportation of plastics and microplastics: A critical review of pathways and influences. *Sci. Total Environ.* **2022**, *831*, 154884. DOI: 10.1016/j.scitotenv.2022.154884.

(11) Ziani, K.; Ioniță-Mîndrican, C.-B.; Mititelu, M.; Neacșu, S. M.; Negrei, C.; Moroșan, E.; Drăgănescu, D.; Preda, O.-T. Microplastics: A Real Global Threat for Environment and Food Safety: A State of the Art Review. *Nutrients* **2023**, *15* (3), 617. DOI: 10.3390/nu15030617.

(12) Allen, S.; Allen, D.; Karbalaei, S.; Maselli, V.; Walker, T. R. Micro(nano)plastics sources, fate, and effects: What we know after ten years of research. *Journal of Hazardous Materials Advances* **2022**, *6*, 100057. DOI: 10.1016/j.hazadv.2022.100057.

(13) Stegmann, P.; Daioglou, V.; Londo, M.; Van Vuuren, D. P.; Junginger, M. Plastic futures and their CO2 emissions. *Nature* **2022**, *612* (7939), 272-276. DOI: 10.1038/s41586-022-05422-5.

(14) Tiwari, N.; Santhiya, D.; Sharma, J. G. Biodegradation of micro sized nylon 6, 6 using Brevibacillus brevis a soil isolate for cleaner ecosystem. *Journal of Cleaner Production* **2022**, *378*, 134457. DOI: https://doi.org/10.1016/j.jclepro.2022.134457.

(15) Vethaak, A. D.; Leslie, H. A. Plastic Debris Is a Human Health Issue. *Environmental Science & Technology* **2016**, *50* (13), 6825-6826. DOI: 10.1021/acs.est.6b02569.

(16) Cox, K. D.; Covernton, G. A.; Davies, H. L.; Dower, J. F.; Juanes, F.; Dudas, S. E. Human Consumption of Microplastics. *Environmental Science & Technology* **2019**, *53* (12), 7068-7074. DOI: 10.1021/acs.est.9b01517.

(17) Mason, S. A.; Welch, V. G.; Neratko, J. Synthetic Polymer Contamination in Bottled Water. *Frontiers in Chemistry* **2018**, *6*. DOI: 10.3389/fchem.2018.00407.

(18) Xu, M.; Halimu, G.; Zhang, Q.; Song, Y.; Fu, X.; Li, Y.; Li, Y.; Zhang, H. Internalization and toxicity: A preliminary study of effects of nanoplastic particles on human lung epithelial cell. *Sci. Total Environ.* **2019**, *694*, 133794. DOI: 10.1016/j.scitotenv.2019.133794 From NLM.

(19) Goodman, K. E.; Hare, J. T.; Khamis, Z. I.; Hua, T.; Sang, Q.-X. A. Exposure of Human Lung Cells to Polystyrene Microplastics Significantly Retards Cell Proliferation and Triggers Morphological Changes. *Chem. Res. Toxicol.* **2021**, *34* (4), 1069-1081. DOI: 10.1021/acs.chemrestox.0c00486.

(20) Al-Sid-Cheikh, M.; Rowland, S. J.; Stevenson, K.; Rouleau, C.; Henry, T. B.; Thompson, R. C. Uptake, Whole-Body Distribution, and Depuration of Nanoplastics by the Scallop Pecten maximus at Environmentally Realistic Concentrations. *Environmental Science & Technology* **2018**, *52* (24), 14480-14486. DOI: 10.1021/acs.est.8b05266.

(21) Jenner, L. C.; Rotchell, J. M.; Bennett, R. T.; Cowen, M.; Tentzeris, V.; Sadofsky, L. R. Detection of microplastics in human lung tissue using μFTIR spectroscopy. *Sci. Total Environ.* **2022**, *831*, 154907. DOI: https://doi.org/10.1016/j.scitotenv.2022.154907.

(22) Zangmeister, C. D.; Radney, J. G.; Benkstein, K. D.; Kalanyan, B. Common Single-Use Consumer Plastic Products Release Trillions of Sub-100 nm Nanoparticles per Liter into Water during Normal Use. *Environmental Science & Technology* **2022**, *56* (9), 5448-5455. DOI: 10.1021/acs.est.1c06768.

(23) McCormick, A.; Hoellein, T. J.; Mason, S. A.; Schluep, J.; Kelly, J. J. Microplastic is an Abundant and Distinct Microbial Habitat in an Urban River. *Environmental Science & Technology* **2014**, *48* (20), 11863-11871. DOI: 10.1021/es503610r.

(24) Presence of microplastics and nanoplastics in food, with particular focus on seafood. *EFSA Journal* **2016**, *14* (6), e04501. DOI: 10.2903/j.efsa.2016.4501.

(25) Lu, Y.-Y.; Li, H.; Ren, H.; Zhang, X.; Huang, F.; Zhang, D.; Huang, Q.; Zhang, X. Size-dependent effects of polystyrene nanoplastics on autophagy response in human umbilical vein endothelial cells. *J. Hazard. Mater.* **2022**, *421*, 126770. DOI: https://doi.org/10.1016/j.jhazmat.2021.126770.

(26) Materić, D.; Kjær, H. A.; Vallelonga, P.; Tison, J.-L.; Röckmann, T.; Holzinger, R. Nanoplastics measurements in Northern and Southern polar ice. *Environ. Res.* **2022**, *208*, 112741. DOI: https://doi.org/10.1016/j.envres.2022.112741.

(27) Shaikh, I. R. Organocatalysis: Key Trends in Green Synthetic Chemistry, Challenges, Scope towards Heterogenization, and Importance from Research and Industrial Point of View. *Journal of Catalysts* **2014**, *2014*, 1-35. DOI: 10.1155/2014/402860.

(28) Xin, J.; Zhang, Q.; Huang, J.; Huang, R.; Jaffery, Q. Z.; Yan, D.; Zhou, Q.; Xu, J.; Lu, X. Progress in the catalytic glycolysis of polyethylene terephthalate. *Journal of Environmental Management* **2021**, *296*, 113267. DOI: 10.1016/j.jenvman.2021.113267.

(29) Cowger, W.; Willis, K. A.; Bullock, S.; Conlon, K.; Emmanuel, J.; Erdle, L. M.; Eriksen, M.; Farrelly, T. A.; Hardesty, B. D.; Kerge, K.; et al. Global producer responsibility for plastic pollution. *Science Advances* **2024**, *10* (17). DOI: 10.1126/sciadv.adj8275.

(30) Sinha, V.; Patel, M. R.; Patel, J. V. PET waste management by chemical recycling: a review. *J. Polym. Environ.* **2010**, *18* (1), 8-25.

(31) Jehanno, C.; Flores, I.; Dove, A. P.; Müller, A. J.; Ruipérez, F.; Sardon, H. Organocatalysed depolymerisation of PET in a fully sustainable cycle using thermally stable protic ionic salt. *Green Chemistry* **2018**, *20* (6), 1205-1212. DOI: 10.1039/c7gc03396f.

(32) Carta, D.; Cao, G.; D'Angeli, C. Chemical recycling of poly(ethylene terephthalate) (pet) by hydrolysis and glycolysis. *Environmental Science and Pollution Research* **2003**, *10* (6), 390-394. DOI: 10.1065/espr2001.12.104.8.

(33) Clark, J. H.; Alonso, J. A.; Villalba, J. A.; Aguado, J.; Serrano, D. P.; Serrano, D. *Feedstock recycling of plastic wastes*; Royal society of chemistry, 1999.

(34) Nikles, D. E.; Farahat, M. S. New Motivation for the Depolymerization Products Derived from Poly(Ethylene Terephthalate) (PET) Waste: a Review. *Macromolecular Materials and Engineering* **2005**, *290* (1), 13-30. DOI: 10.1002/mame.200400186.

(35) Al-Salem, S. M.; Lettieri, P.; Baeyens, J. Recycling and recovery routes of plastic solid waste (PSW): A review. *Waste Manage. (Oxford)* **2009**, *29* (10), 2625-2643. DOI: 10.1016/j.wasman.2009.06.004.

(36) Mata-Alvarez, J.; Macé, S.; Llabrés, P. Anaerobic digestion of organic solid wastes. An overview of research achievements and perspectives. *Bioresour. Technol.* **2000**, *74* (1), 3-16. DOI: 10.1016/s0960-8524(00)00023-7.

(37) Karmakar, A.; Daftari, T.; K, S.; Chandan, M. R.; Shaik, A. H.; Kiran, B.; Chakraborty, S. A comprehensive insight into Waste to Energy conversion strategies in India and its associated air pollution hazard. *Environmental Technology & Innovation* **2023**, *29*, 103017. DOI: 10.1016/j.eti.2023.103017.

(38) Beikmohammadi, M.; Yaghmaeian, K.; Nabizadeh, R.; Mahvi, A. H. Analysis of heavy metal, rare, precious, and metallic element content in bottom ash from municipal solid waste incineration in Tehran based on particle size. *Scientific Reports* **2023**, *13* (1). DOI: 10.1038/s41598-023-43139-1.

(39) Astrup, T. F.; Tonini, D.; Turconi, R.; Boldrin, A. Life cycle assessment of thermal Waste-to-Energy technologies: Review and recommendations. *Waste Manage. (Oxford)* **2015**, *37*, 104-115. DOI: 10.1016/j.wasman.2014.06.011.

(40) Dong, J.; Tang, Y.; Nzihou, A.; Chi, Y.; Weiss-Hortala, E.; Ni, M.; Zhou, Z. Comparison of waste-to-energy technologies of gasification and incineration using life cycle assessment: Case studies in Finland, France and China. *Journal of Cleaner Production* **2018**, *203*, 287-300. DOI: 10.1016/j.jclepro.2018.08.139.

(41) Psomopoulos, C. S.; Bourka, A.; Themelis, N. J. Waste-to-energy: A review of the status and benefits in USA. *Waste Manage. (Oxford)* **2009**, *29* (5), 1718-1724. DOI: 10.1016/j.wasman.2008.11.020.

(42) Antonopoulos, I. S.; Perkoulidis, G.; Logothetis, D.; Karkanias, C. Ranking municipal solid waste treatment alternatives considering sustainability criteria using the analytical hierarchical process tool. *Resources, Conservation and Recycling* **2014**, *86*, 149-159. DOI: 10.1016/j.resconrec.2014.03.002.

(43) Vuppaladadiyam, S. S. V.; Vuppaladadiyam, A. K.; Sahoo, A.; Urgunde, A.; Murugavelh, S.; Šrámek, V.; Pohořelý, M.; Trakal, L.; Bhattacharya, S.; Sarmah, A. K.; et al. Waste to energy: Trending key challenges and current technologies in waste plastic management. *Sci. Total Environ.* **2024**, *913*, 169436. DOI: 10.1016/j.scitotenv.2023.169436.

(44) Eboh, F. C.; Andersson, B.-Å.; Richards, T. Economic evaluation of improvements in a waste-to-energy combined heat and power plant. *Waste Manage. (Oxford)* **2019**, *100*, 75-83. DOI: 10.1016/j.wasman.2019.09.008.

(45) Yang, M.; Chen, L.; Wang, J.; Msigwa, G.; Osman, A. I.; Fawzy, S.; Rooney, D. W.; Yap, P.-S. Circular economy strategies for combating climate change and other environmental issues. *Environmental Chemistry Letters* **2023**, *21* (1), 55-80. DOI: 10.1007/s10311-022-01499-6.

(46) Rezania, S.; Oryani, B.; Nasrollahi, V. R.; Darajeh, N.; Lotfi Ghahroud, M.; Mehranzamir, K. Review on Waste-to-Energy Approaches toward a Circular Economy in Developed and Developing Countries. *Processes* **2023**, *11* (9), 2566. DOI: 10.3390/pr11092566.

(47) Lombardi, L.; Carnevale, E. A. Evaluation of the environmental sustainability of different waste-to-energy plant configurations. *Waste Manage. (Oxford)* **2018**, *73*, 232-246. DOI: 10.1016/j.wasman.2017.07.006.

(48) Čabalová, I.; Ház, A.; Krilek, J.; Bubeníková, T.; Melicherčík, J.; Kuvik, T. Recycling of Wastes Plastics and Tires from Automotive Industry. *Polymers* **2021**, *13* (13), 2210. DOI: 10.3390/polym13132210.

(49) Wei, T.; Zhou, P.; Liu, W.; Liu, X.; Kuang, T. Catalytic recycling of plastics into value-added products. *Nano Research* **2024**. DOI: 10.1007/s12274-024-6955-0.

(50) Tournier, V.; Topham, C. M.; Gilles, A.; David, B.; Folgoas, C.; Moya-Leclair, E.; Kamionka, E.; Desrousseaux, M. L.; Texier, H.; Gavalda, S.; et al. An engineered PET depolymerase to break down and recycle plastic bottles. *Nature* **2020**, *580* (7802), 216-219. DOI: 10.1038/s41586-020-2149-4.

(51) Shukla, S. R.; Harad, A. M. Glycolysis of polyethylene terephthalate waste fibers. *J. Appl. Polym. Sci.* **2005**, *97* (2), 513-517. DOI: 10.1002/app.21769.

(52) Garcia, J. M.; Robertson, M. L. The future of plastics recycling. *Science* **2017**, *358* (6365), 870-872. DOI: 10.1126/science.aaq0324.

(53) Brette, M. M.; Holm, A. H.; Drozdov, A. D.; Christiansen, J. D. C. Pure Hydrolysis of Polyamides: A Comparative Study. *Chemistry* **2023**, *6* (1), 13-50. DOI: 10.3390/chemistry6010002.

(54) Bulak, E.; Acar, I. The use of aminolysis, aminoglycolysis, and simultaneous aminolysis–hydrolysis products of waste PET for production of paint binder. *Polymer Engineering & Science* **2014**, *54* (10), 2272-2281. DOI: 10.1002/pen.23773.

(55) Mancini, S. D.; Zanin, M. Optimization of Neutral Hydrolysis Reaction of Post-consumer PET for Chemical Recycling. *Progress in Rubber, Plastics and Recycling Technology* **2004**, *20* (2), 117-132. DOI: 10.1177/147776060402000202 (acccessed 2024/01/14).

(56) Mancini, S. D.; Zanin, M. Post Consumer Pet Depolymerization by Acid Hydrolysis. *Polymer-Plastics Technology and Engineering* **2007**, *46* (2), 135-144. DOI: 10.1080/03602550601152945.

(57) Yoshioka, T.; Sato, T.; Okuwaki, A. Hydrolysis of waste PET by sulfuric acid at 150°C for a chemical recycling. *J. Appl. Polym. Sci.* **1994**, *52* (9), 1353-1355. DOI: 10.1002/app.1994.070520919.

(58) Yoshioka, T.; Okayama, N.; Okuwaki, A. Kinetics of Hydrolysis of PET Powder in Nitric Acid by a Modified Shrinking-Core Model. *Industrial & Engineering Chemistry Research* **1998**, *37* (2), 336-340. DOI: 10.1021/ie970459a.

(59) Yoshioka, T.; Motoki, T.; Okuwaki, A. Kinetics of Hydrolysis of Poly(ethylene terephthalate) Powder in Sulfuric Acid by a Modified Shrinking-Core Model. *Industrial & Engineering Chemistry Research* **2001**, *40* (1), 75-79. DOI: 10.1021/ie000592u.

(60) Gama, N.; Godinho, B.; Marques, G.; Silva, R.; Barros-Timmons, A.; Ferreira, A. Recycling of polyurethane by acidolysis: The effect of reaction conditions on the properties of

the recovered polyol. *Polymer* **2021**, *219*, 123561. DOI: https://doi.org/10.1016/j.polymer.2021.123561.

(61) Gama, N.; Godinho, B.; Marques, G.; Silva, R.; Barros-Timmons, A.; Ferreira, A. Recycling of polyurethane scraps via acidolysis. *Chem. Eng. J.* **2020**, *395*, 125102. DOI: https://doi.org/10.1016/j.cej.2020.125102.

(62) Muangmeesri, S.; Baddigam, K. R.; Navare, K.; Apostolopoulou-Kalkavoura, V.; Witthayolankowit, K.; Håkansson, H.; Mathew, A. P.; Acker, K. V.; Samec, J. S. M. Recycling of Polyesters by Organocatalyzed Methanolysis Depolymerization: Environmental Sustainability Evaluated by Life Cycle Assessment. *ACS Sustainable Chemistry & Engineering* **2024**, *12* (10), 4114-4120. DOI: 10.1021/acssuschemeng.3c07435.

(63) Yue, Q.; Wang, C.; Zhang, L.; Ni, Y.; Jin, Y. Glycolysis of poly (ethylene terephthalate)(PET) using basic ionic liquids as catalysts. *Polym. Degrad. Stab.* **2011**, *96* (4), 399-403.

(64) Pardal, F.; Tersac, G. Comparative reactivity of glycols in PET glycolysis. *Polym. Degrad. Stab.* **2006**, *91* (11), 2567-2578. DOI: 10.1016/j.polymdegradstab.2006.05.016.

(65) Colomines, G.; Robin, J.-J.; Tersac, G. Study of the glycolysis of PET by oligoesters. *Polymer* **2005**, *46* (10), 3230-3247. DOI: https://doi.org/10.1016/j.polymer.2005.02.047.

(66) Jehanno, C.; Pérez-Madrigal, M. M.; Demarteau, J.; Sardon, H.; Dove, A. P. Organocatalysis for depolymerisation. *Polymer Chemistry* **2019**, *10* (2), 172-186. DOI: 10.1039/c8py01284a.

(67) Spicer, A. J.; Brandolese, A.; Dove, A. P. Selective and Sequential Catalytic Chemical Depolymerization and Upcycling of Mixed Plastics. *ACS Macro Letters* **2024**, 189-194. DOI: 10.1021/acsmacrolett.3c00751.

(68) Kaiho, S.; Hmayed, A. A. R.; Delle Chiaie, K. R.; Worch, J. C.; Dove, A. P. Designing Thermally Stable Organocatalysts for Poly(ethylene terephthalate) Synthesis: Toward a One-Pot, Closed-Loop Chemical Recycling System for PET. *Macromolecules* **2022**, *55* (23), 10628-10639. DOI: 10.1021/acs.macromol.2c01410.

(69) Miao, Y.; Von Jouanne, A.; Yokochi, A. Current Technologies in Depolymerization Process and the Road Ahead. *Polymers* **2021**, *13* (3), 449. DOI: 10.3390/polym13030449.

(70) Wanmolee, W.; Daorattanachai, P.; Laosiripojana, N. Depolymerization of Organosolv Lignin to Valuable Chemicals over Homogeneous and Heterogeneous Acid Catalysts. *Energy Procedia* **2016**, *100*, 173-177. DOI: 10.1016/j.egypro.2016.10.161.

(71) Osei, D.; Gurrala, L.; Sheldon, A.; Mayuga, J.; Lincoln, C.; Rorrer, N. A.; Morais, A. R. C. Subcritical CO₂–H₂O hydrolysis of polyethylene terephthalate as a sustainable chemical recycling platform. *Green Chemistry* **2024**, *26* (11), 6436-6445. DOI: 10.1039/d3gc04576e.

(72) Luna, E.; Olazabal, I.; Roosen, M.; Müller, A.; Jehanno, C.; Ximenis, M.; De Meester, S.; Sardon, H. Towards a better understanding of the cosolvent effect on the low-temperature glycolysis of Polyethylene Terephthalate (PET). *Chem. Eng. J.* **2024**, *482*, 148861. DOI: 10.1016/j.cej.2024.148861.

(73) Christoff-Tempesta, T.; Epps, T. H. Ionic-Liquid-Mediated Deconstruction of Polymers for Advanced Recycling and Upcycling. *ACS Macro Letters* **2023**, *12* (8), 1058-1070. DOI: 10.1021/acsmacrolett.3c00276.

(74) Clark, R. A.; Shaver, M. P. Depolymerization within a Circular Plastics System. *Chem. Rev.* **2024**, *124* (5), 2617-2650. DOI: 10.1021/acs.chemrev.3c00739.

(75) Sun, J.; Liu, D.; Young, R. P.; Cruz, A. G.; Isern, N. G.; Schuerg, T.; Cort, J. R.; Simmons, B. A.; Singh, S. Solubilization and Upgrading of High Polyethylene Terephthalate Loadings in a Low-Costing Bifunctional Ionic Liquid. *ChemSusChem* **2018**, *11* (4), 781-792. DOI: 10.1002/cssc.201701798.

(76) Ovejero-Pérez, A.; Rigual, V.; Domínguez, J. C.; Alonso, M. V.; Oliet, M.; Rodriguez, F. Acidic depolymerization vs ionic liquid solubilization in lignin extraction from eucalyptus wood using the protic ionic liquid 1-methylimidazolium chloride. *Int. J. Biol. Macromol.* **2020**, *157*, 461-469. DOI: https://doi.org/10.1016/j.ijbiomac.2020.04.194.

(77) Ghasemi, M.; Singapati, A. Y.; Tsianou, M.; Alexandridis, P. Dissolution of semicrystalline polymer fibers: Numerical modeling and parametric analysis. *AlChE J.* **2017**, *63* (4), 1368-1383. DOI: 10.1002/aic.15615.

(78) Miller-Chou, B. A.; Koenig, J. L. A review of polymer dissolution. *Prog. Polym. Sci.* **2003**, *28* (8), 1223-1270. DOI: 10.1016/s0079-6700(03)00045-5.

(79) *Polymer Handbook*; John Wiley & sons, Inc, 1999.

(80) Najmi, S.; Vance, B. C.; Selvam, E.; Huang, D.; Vlachos, D. G. Controlling PET oligomers vs monomers via microwave-induced heating and swelling. *Chem. Eng. J.* **2023**, *471*, 144712. DOI: https://doi.org/10.1016/j.cej.2023.144712.

(81) Teraoka, I. Polymer Solutions. **2002**. DOI: 10.1002/0471224510.

(82) McBee, E. T. The Solubility of Nonelectrolytes. *Science* **1951**, *113* (2938), 450-450. DOI: 10.1126/science.113.2938.450-a.

(83) Hansen, C. M. Hansen Solubility Parameters. **2007**. DOI: 10.1201/9781420006834.

(84) D. W. Van Krevelen, K. T. N. *Properties of Polymers: Their Correlation with Chemical Structures; Their Numerical Estimation and Prediction from Additive Group Contributions*; Elsevier B.V. , 2009.

(85) Barton, A. F. M. CRC Handbook of Solubility Parameters and Other Cohesion Parameters. **2017**. DOI: 10.1201/9781315140575.

(86) Porter, J. D. The Solubility of Nonelectrolytes . 3rd ed. Joel H. Hildebrand and Robert L. Scott. New York: Reinhold, 1950. 488 pp. $10.00. *Science* **1951**, *113* (2938), 450-451. DOI: 10.1126/science.113.2938.450.b.

(87) Hansen, C. M. The three dimensional solubility parameter - key to paint component affinities: I. Solvents, plasticizers, polymers, and resins. 1967.

(88) Wu, S. Polar and Nonpolar Interactions in Adhesion. *The Journal of Adhesion* **1973**, *5* (1), 39-55. DOI: 10.1080/00218467308078437.

(89) Wall, F. T. Principles of Polymer Chemistry. Paul J. Flory. Cornell Univ. Press, Ithaca, New York, 1953. 688 pp. Illus. $8.50. *Science* **1954**, *119* (3095), 555-556. DOI: 10.1126/science.119.3095.555-a.

(90) Wu, Y.; Hu, Q.; Che, Y.; Niu, Z. Opportunities and challenges for plastic depolymerization by biomimetic catalysis. *Chemical Science* **2024**, *15* (17), 6200-6217. DOI: 10.1039/d4sc00070f.

(91) Farnetti, E.; Monte, R. D.; Kašpar, J. Encyclopedia of Life Support Systems (EOLSS) HOMOGENEOUS AND HETEROGENEOUS CATALYSIS.

(92) Olazabal, I.; Luna Barrios, E. J.; De Meester, S.; Jehanno, C.; Sardon, H. Overcoming the Limitations of Organocatalyzed Glycolysis of Poly(ethylene terephthalate) to Facilitate the Recycling of Complex Waste Under Mild Conditions. *ACS Applied Polymer Materials* **2024**, *6* (7), 4226-4232. DOI: 10.1021/acsapm.4c00326.

(93) Feghali, E.; Cantat, T. Room Temperature Organocatalyzed Reductive Depolymerization of Waste Polyethers, Polyesters, and Polycarbonates. *ChemSusChem* **2015**, *8* (6), 980-984. DOI: 10.1002/cssc.201500054.

(94) Jehanno, C.; Demarteau, J.; Mantione, D.; Arno, M. C.; Ruipérez, F.; Hedrick, J. L.; Dove, A. P.; Sardon, H. Selective Chemical Upcycling of Mixed Plastics Guided by a Thermally Stable Organocatalyst. *Angew. Chem. Int. Ed.* **2021**, *60* (12), 6710-6717. DOI: 10.1002/anie.202014860.

(95) Basterretxea, A.; Jehanno, C.; Mecerreyes, D.; Sardon, H. Dual Organocatalysts Based on Ionic Mixtures of Acids and Bases: A Step Toward High Temperature Polymerizations. *ACS Macro Letters* **2019**, *8* (8), 1055-1062. DOI: 10.1021/acsmacrolett.9b00481.

(96) Gadhave, R. V.; Srivastava, S.; Mahanwar, P. A.; Gadekar, P. T. Recycling and Disposal Methods for Polyurethane Wastes: A Review. *Open Journal of Polymer Chemistry* **2019**, *09* (02), 39-51. DOI: 10.4236/ojpchem.2019.92004.

(97) Raheem, A. B.; Noor, Z. Z.; Hassan, A.; Abd Hamid, M. K.; Samsudin, S. A.; Sabeen, A. H. Current developments in chemical recycling of post-consumer polyethylene terephthalate wastes for new materials production: A review. *Journal of Cleaner Production* **2019**, *225*, 1052-1064. DOI: https://doi.org/10.1016/j.jclepro.2019.04.019.

(98) Schyns, Z. O. G.; Shaver, M. P. Mechanical Recycling of Packaging Plastics: A Review. *Macromol. Rapid Commun.* **2021**, *42* (3), 2000415. DOI: 10.1002/marc.202000415.

(99) Rabiei, N.; Kish, M. H. Aminolysis of polyesters for cracking and structure clarifying: A review. *Polym. Adv. Technol.* **2022**, *33* (12), 3903-3919. DOI: 10.1002/pat.5837.

(100) Zhou, N.; Thilakarathna, W. P. D. W.; He, Q. S.; Rupasinghe, H. P. V. A Review: Depolymerization of Lignin to Generate High-Value Bio-Products: Opportunities, Challenges, and Prospects. *Frontiers in Energy Research* **2022**, *9*. DOI: 10.3389/fenrg.2021.758744.

(101) Kwon, T.; Jeong, H.; Kim, M.; Jung, S.; Ro, I. Catalytic Approaches to Tackle Mixed Plastic Waste Challenges: A Review. *Langmuir* **2024**. DOI: 10.1021/acs.langmuir.4c01303.

(102) Smith, M. B. *March's Advanced Organic Chemistry: Reactions, Mechanisms, and Structure*; Wiley, 2019.

(103) Francic A Carey, R. J. S. *Advanced Organic Chemistry*; Springer Science+Business Media, LLC, 2007.

(104) Clayden, J., Greeves, N., Warren, S., & Wothers, P. . *Organic Chemistry*; Oxford University Press, 2001.

(105) Woittiez, W. J. A. Advanced Organic chemistry. Reactions, mechanisms, and structure. 4th Ed. J. March, John Wiley, Chichester, 1992 1268 + 227 pp., £228,00 ISBN 0-471-58148-8. *Recl. Trav. Chim. Pays-Bas* **1993**, *112* (7-8), 468-468. DOI: 10.1002/recl.19931120711.

(106) March, J. *Advanced Organic Chemistry: Reactions, Mechanisms, and Structure*; Wiley, 1992.

(107) Vollhardt, K. P. C.; Shore, E. N. *Organic Chemistry; Structure and Functions*; Freeman and Company, 2007.

(108) Castilla-Cortázar, I.; Más-Estellés, J.; Meseguer-Dueñas, J. M.; Escobar Ivirico, J. L.; Marí, B.; Vidaurre, A. Hydrolytic and enzymatic degradation of a poly(ε-caprolactone) network. *Polymer Degradation and Stability* **2012**, *97* (8), 1241-1248. DOI: 10.1016/j.polymdegradstab.2012.05.038.

(109) Filiciotto, L.; Rothenberg, G. Biodegradable Plastics: Standards, Policies, and Impacts. *ChemSusChem* **2021**, *14* (1), 56-72. DOI: 10.1002/cssc.202002044.

(110) Asri, N. A.; Sezali, N. A. A.; Ong, H. L.; Mohd Pisal, M. H.; Lim, Y. H.; Fang, J. Review on Biodegradable Aliphatic Polyesters: Development and Challenges. *Macromolecular Rapid Communications* **2024**. DOI: 10.1002/marc.202400475.

(111) Aharoni, S. M.; Harget, P. J. On the location of chain-ends in rapidly crystallized poly(ethylene terephthalate). *Journal of Polymer Science: Polymer Physics Edition* **1978**, *16* (1), 159-169. DOI: 10.1002/pol.1978.180160114.

(112) Zhang, M.; Guo, B.-H.; Xu, J. A Review on Polymer Crystallization Theories. *Crystals* **2016**, *7* (1), 4. DOI: 10.3390/cryst7010004.

(113) Bicerano, J. *Prediction of Polymer Properties*; Marcel Dekker, INC. New York Basel, 2009.

(114) Polaskova, M.; Peer, P.; Cermak, R.; Ponizil, P. Effect of Thermal Treatment on Crystallinity of Poly(ethylene oxide) Electrospun Fibers. *Polymers* **2019**, *11* (9), 1384. DOI: 10.3390/polym11091384.

(115) Nie, Y.; Gao, H.; Wu, Y.; Hu, W. Thermodynamics of strain-induced crystallization of random copolymers. *Soft Matter* **2014**, *10* (2), 343-347. DOI: 10.1039/c3sm52465e.

(116) Polymer Crystallization II. *Adv. Polym. Sci.* **2017**. DOI: 10.1007/978-3-319-50684-5.

(117) Song, F.; Wang, Q.; Wang, T. The effects of crystallinity on the mechanical properties and the limiting PV (pressure×velocity) value of PTFE. *Tribology International* **2016**, *93*, 1-10. DOI: 10.1016/j.triboint.2015.09.017.

(118) Kong, Y.; Hay, J. N. The measurement of the crystallinity of polymers by DSC. *Polymer* **2002**, *43* (14), 3873-3878. DOI: 10.1016/s0032-3861(02)00235-5.

(119) Rungswang, W.; Jarumaneeroj, C.; Patthamasang, S.; Phiriyawirut, P.; Jirasukho, P.; Soontaranon, S.; Rugmai, S.; Hsiao, B. S. Influences of tacticity and molecular weight on crystallization kinetic and crystal morphology under isothermal crystallization: Evidence of tapering in lamellar width. *Polymer* **2019**, *172*, 41-51. DOI: 10.1016/j.polymer.2019.03.052.

(120) Godovsky, Y. K.; Slonimsky, G. L.; Garbar, N. M. Effect of molecular weight on the crystallization and morphology of poly (ethylene oxide) fractions. *Journal of Polymer Science Part C: Polymer Symposia* **1972**, *38* (1), 1-21. DOI: 10.1002/polc.5070380103.

(121) Molnár, J.; Zuba, Z.; Sepsi, Ö.; Ujhelyi, F.; Erdei, G.; Lenk, S.; Menyhárd, A. Structural investigation of semicrystalline polymers. *Polym. Test.* **2021**, *95*, 107098. DOI: 10.1016/j.polymertesting.2021.107098.

(122) Abhari, R. E.; Mouthuy, P.-A.; Zargar, N.; Brown, C.; Carr, A. Effect of annealing on the mechanical properties and the degradation of electrospun polydioxanone filaments. *Journal of the Mechanical Behavior of Biomedical Materials* **2017**, *67*, 127-134. DOI: 10.1016/j.jmbbm.2016.11.023.

(123) Chen, B.; Yang, H.; Shen, K.; Fu, Q.; Gao, X. The effect of high-temperature annealing on thermal properties and morphology of polyethylene pipes prepared by rotational shear. *Polymer* **2020**, *204*, 122770. DOI: 10.1016/j.polymer.2020.122770.

(124) Yu, W.; Wang, X.; Yin, X.; Ferraris, E.; Zhang, J. The effects of thermal annealing on the performance of material extrusion 3D printed polymer parts. *Materials & Design* **2023**, *226*, 111687. DOI: 10.1016/j.matdes.2023.111687.

(125) Hu, Y.; Liao, Y.; Zheng, Y.; Ikeda, K.; Okabe, R.; Wu, R.; Ozaki, R.; Xu, J.; Xu, Q. Influence of Cooling Rate on Crystallization Behavior of Semi-Crystalline Polypropylene:

Experiments and Mathematical Modeling. *Polymers* **2022**, *14* (17), 3646. DOI: 10.3390/polym14173646.

(126) Alaneme, K. K.; Okotete, E. A. Recrystallization mechanisms and microstructure development in emerging metallic materials: A review. *Journal of Science: Advanced Materials and Devices* **2019**, *4* (1), 19-33. DOI: 10.1016/j.jsamd.2018.12.007.

(127) Zennaki, A.; Zair, L.; Arabeche, K.; Benkraled, L.; Maschke, U.; Berrayah, A. Effect of annealing on thermal and dynamic mechanical properties of poly(lactic acid). *J. Appl. Polym. Sci.* **2022**, *139* (44). DOI: 10.1002/app.53095.

(128) Holdsworth, P. J.; Turner-Jones, A. The melting behaviour of heat crystallized poly(ethylene terephthalate). *Polymer* **1971**, *12* (3), 195-208. DOI: https://doi.org/10.1016/0032-3861(71)90045-0.

(129) Alfonso, G. C.; Pedemonte, E.; Ponzetti, L. Mechanism of densification and crystal perfection of poly(ethylene terephthalate). *Polymer* **1979**, *20* (1), 104-112. DOI: https://doi.org/10.1016/0032-3861(79)90052-1.

(130) Wang, Z. G.; Hsiao, B. S.; Sauer, B. B.; Kampert, W. G. The nature of secondary crystallization in poly(ethylene terephthalate). *Polymer* **1999**, *40* (16), 4615-4627. DOI: https://doi.org/10.1016/S0032-3861(99)00067-1.

(131) Groeninckx, G.; Reynaers, H. Morphology and melting behavior of semicrystalline poly(ethylene terephthalate). II. Annealed PET. *Journal of Polymer Science: Polymer Physics Edition* **1980**, *18* (6), 1325-1341. DOI: https://doi.org/10.1002/pol.1980.180180613 (acccessed 2023/11/20).

(132) Li, H.; Aguirre-Villegas, H. A.; Allen, R. D.; Bai, X.; Benson, C. H.; Beckham, G. T.; Bradshaw, S. L.; Brown, J. L.; Brown, R. C.; Cecon, V. S.; et al. Expanding plastics recycling

technologies: chemical aspects, technology status and challenges. *Green Chemistry* **2022**, *24* (23), 8899-9002. DOI: 10.1039/d2gc02588d.

(133) Lubongo, C.; Bin Daej, M. A. A.; Alexandridis, P. Recent Developments in Technology for Sorting Plastic for Recycling: The Emergence of Artificial Intelligence and the Rise of the Robots. *Recycling* **2024**, *9* (4), 59. DOI: 10.3390/recycling9040059.

(134) Peng, Y.; Wang, Y.; Ke, L.; Dai, L.; Wu, Q.; Cobb, K.; Zeng, Y.; Zou, R.; Liu, Y.; Ruan, R. A review on catalytic pyrolysis of plastic wastes to high-value products. *Energy Convers. Manage.* **2022**, *254*, 115243. DOI: 10.1016/j.enconman.2022.115243.

(135) Guselnikova, O.; Semyonov, O.; Sviridova, E.; Gulyaev, R.; Gorbunova, A.; Kogolev, D.; Trelin, A.; Yamauchi, Y.; Boukherroub, R.; Postnikov, P. "Functional upcycling" of polymer waste towards the design of new materials. *Chem. Soc. Rev.* **2023**, *52* (14), 4755-4832. DOI: 10.1039/d2cs00689h.

(136) Balu, R.; Dutta, N. K.; Roy Choudhury, N. Plastic Waste Upcycling: A Sustainable Solution for Waste Management, Product Development, and Circular Economy. *Polymers* **2022**, *14* (22), 4788. DOI: 10.3390/polym14224788.

(137) Fu, L.; Xiong, Q.; Wang, Q.; Cai, L.; Chen, Z.; Zhou, Y. Catalytic Pyrolysis of Waste Polyethylene Using Combined CaO and Ga/ZSM-5 Catalysts for High Value-Added Aromatics Production. *ACS Sustainable Chemistry & Engineering* **2022**, *10* (29), 9612-9623. DOI: 10.1021/acssuschemeng.2c02881.

(138) Wang, X.; Xu, J.; Zhao, M.; Cui, W.; Mu, X.; Wang, X.; Song, S.; Zhang, H. Recent progress of waste plastic upcycling based on multifunctional zeolite catalysts. *Chemical Synthesis* **2024**, *4* (2). DOI: 10.20517/cs.2023.67.

(139) Chu, M.; Kang, Q.; Hu, P.; Zhang, Q.; Chen, J. Unlocking opportunities: Supported metal catalysts for the chemical upcycling of waste plastics. *Chem. Eng. J.* **2024**, *496*, 154375. DOI: 10.1016/j.cej.2024.154375.

(140) Zhang, X.; Yang, H.; Chen, Z.; Wang, X.; Feng, H.; Zhang, J.; Yu, J.; Gao, S.; Lai, D. Sustainable production of aromatics via catalytic pyrolysis of polyolefins towards the carbon cycle for plastics. *Fuel* **2024**, *357*, 129897. DOI: 10.1016/j.fuel.2023.129897.

(141) Zimmermann, W. Biocatalytic recycling of polyethylene terephthalate plastic. *Philosophical Transactions of the Royal Society A: Mathematical, Physical and Engineering Sciences* **2020**, *378* (2176), 20190273. DOI: 10.1098/rsta.2019.0273.

(142) Mudondo, J.; Lee, H.-S.; Jeong, Y.; Kim, T. H.; Kim, S.; Sung, B. H.; Park, S.-H.; Park, K.; Cha, H. G.; Yeon, Y. J.; et al. Recent Advances in the Chemobiological Upcycling of Polyethylene Terephthalate (PET) into Value-Added Chemicals. *J. Microbiol. Biotechnol.* **2023**, *33* (1), 1-14. DOI: 10.4014/jmb.2208.08048.

(143) Jia, Z.; Gao, L.; Qin, L.; Yin, J. Chemical recycling of PET to value-added products. *RSC Sustainability* **2023**, *1* (9), 2135-2147. DOI: 10.1039/d3su00311f.

(144) Sajwan, D.; Sharma, A.; Sharma, M.; Krishnan, V. Upcycling of Plastic Waste Using Photo-, Electro-, and Photoelectrocatalytic Approaches: A Way toward Circular Economy. *ACS Catalysis* **2024**, *14* (7), 4865-4926. DOI: 10.1021/acscatal.4c00290.

(145) Sun, S.; Huang, W. Chemical Upcycling of Polyolefin Plastics Using Structurally Well-defined Catalysts. *JACS Au* **2024**, *4* (6), 2081-2098. DOI: 10.1021/jacsau.4c00289.

(146) Kim, S.; Kong, D.; Zheng, X.; Park, J. H. Upcycling plastic wastes into value-added products via electrocatalysis and photoelectrocatalysis. *Journal of Energy Chemistry* **2024**, *91*, 522-541. DOI: 10.1016/j.jechem.2024.01.010.

(147) Jiang, M.; Wang, X.; Xi, W.; Yang, P.; Zhou, H.; Duan, J.; Ratova, M.; Wu, D. Chemical catalytic upgrading of polyethylene terephthalate plastic waste into value-added materials, fuels and chemicals. *Sci. Total Environ.* **2024**, *912*, 169342. DOI: 10.1016/j.scitotenv.2023.169342.

(148) Hong, M.; Chen, E. Y. X. Chemically recyclable polymers: a circular economy approach to sustainability. *Green Chemistry* **2017**, *19* (16), 3692-3706. DOI: 10.1039/c7gc01496a.

(149) Kenwright, A. M.; Peace, S. K.; Richards, R. W.; Bunn, A.; Macdonald, W. A. End group modification in poly(ethylene terephthalate). *Polymer* **1999**, *40* (8), 2035-2040. DOI: 10.1016/s0032-3861(98)00433-9.

(150) Ma, Y.; Agarwal, U. S.; Vekemans, J. A. J. M.; Sikkema, D. J. NMR based determination of minute acid functionality: end-groups in PET. *Polymer* **2003**, *44* (16), 4429-4434. DOI: 10.1016/s0032-3861(03)00402-6.

(151) Valsesia, A.; Parot, J.; Ponti, J.; Mehn, D.; Marino, R.; Melillo, D.; Muramoto, S.; Verkouteren, M.; Hackley, V. A.; Colpo, P. Detection, counting and characterization of nanoplastics in marine bioindicators: a proof of principle study. *Microplastics and Nanoplastics* **2021**, *1* (1). DOI: 10.1186/s43591-021-00005-z.

CHAPTER 2: MORE EFFICIENT CHEMICAL RECYCLING OF POLY(ETHYLENE TEREPHTHALATE) BY INTERCEPTING INTERMEDIATES

A version of this chapter was originally submitted by Shelby Watson-Sanders:

Watson-Sanders, S.; Dadmun, M. “More Efficient Chemical Recycling of Poly(Ethylene Terephthalate) by Intercepting Intermediates.” *ChemSusChem* **2024**, *17* (23). DOI: 10.1002/cssc.202301698. Department of Chemistry, University of Tennessee Knoxville

In this article, I was responsible for depolymerizing all polymers studied. I also performed all polymer characterization. Dr. Mark Dadmun organized this project and facilitated the writing of the manuscript.

2.1 Abstract

The research presented in this paper offers insight into the availability of intermediates in the depolymerization of polyethylene terephthalate (PET) to be used as feedstock to create value-added products. Monitoring the dispersity, molecular weight, end groups, and crystallinity of reaction intermediates during the heterogeneous depolymerization of PET offers insight into the mechanism by which the polymer chains evolve during the reaction. Our results show dispersity decreases and crystallinity increases while the yield of insoluble PET remains high early in the reaction. Our interpretation of this data depicts a mechanism where chain scission targets amorphous tie chains between crystalline phases. Targeting the tie-chains lowers the M_n of the polymer without changing the amount of recovered polymer flake. Chain scission of tie-chains and isolating highly crystalline PET lowers the dispersity ((Đ)) of the polymer chains, as the size of the crystalline lamellae guides the molecular weight of the depolymerized oligomers. When sufficient end groups of PET chains are converted to alcohol groups, the PET flakes break apart into highly crystalline and less disperse polymer. Our results also demonstrate that the oligomeric depolymerization intermediates are readily repolymerized, offering new opportunities

to chemically recycle PET more effectively and efficiently, from both an energy and purification standpoint.

2.2 Introduction

While there is an increasing demand for synthetic polymers, the amount of polymers that are recycled is not sufficient, as only 9% of plastics are recycled annually.[1] The current methods of managing polymer waste are not sustainable; where most polymers are buried in a landfill, burned, or mechanically recycled.[1-4] The need for more sustainable manufacturing and recycling processes is essential with decreasing petroleum resources and increasing volume of polymer waste.[4-6] Since 2017, China no longer imports plastic waste for recycling, forcing major export countries like the United States, Japan, and parts of Europe to improve/expand their domestic polymer recycling systems, including polyethylene terephthalate (PET). [6, 7]

Polyethylene terephthalate (PET) is one of the most regularly used plastic among the general population for its lightweight and mechanical properties.[3, 7-9] Like most plastics, PET does not readily degrade in nature and can accumulate in living organisms.[6, 7, 10] Currently, PET accounts for 13% of the world's polymer production and takes up 8% by weight and 12% by volume of the global solid waste.[11, 12,13] In 2014, 5% of the 13 million tons of PET produced was used for packaging, with the global PET production reaching 27.8 million tons in 2015.[3, 13] Of the 9% of plastic that is recycled, PET is one of the most recycled types of plastic, where 29% of all recycled plastic is PET.[14-16] There are different methods for recycling plastic, including mechanical or chemical recycling. However, chemical recycling is preferred since mechanical recycling degrades the polymer and prevents it from attaining properties similar to the original polymer, such as food contact compliance, which is necessary for recycled PET to begin to replace virgin PET in the marketplace.[3, 4] Yet chemical recycling has not replaced the need to

synthesize new PET since the production of chemically recycled PET is more expensive than the production of virgin PET.[3] Most industrial-scale chemical recycling of PET involves heterogeneous depolymerization via glycolysis. In this glycolysis reaction, the polymer swells with ethylene glycol, and the heterogenous reaction occurs between the ethylene glycol and the dispersed (but not dissolved) PET flake.[3, 9, 17] Previous work has demonstrated that ethylene glycol swells the PET flakes, which could potentially be a rate limiting step in the depolymerization of some forms of PET.[18] **Figure 2.1** illustrates the difference in accessibility of the polymer chain to the reaction in a heterogeneous reaction (top) and a homogeneous reaction (bottom) and how these differences will affect the structural evolution of the products during the depolymerization reaction. **Figure 2.1** demonstrates that the initial state of the PET in the heterogeneous reaction is a dispersed solid but is molecularly dispersed in a homogeneous reaction. There are three stages in a heterogenous PET depolymerization reaction: early in the reaction, a heterogeneous state exists that mainly contains insoluble PET and some soluble dimer/monomers that are the initial products of the depolymerization reaction; later in the reaction, a mixture of insoluble PET and soluble PET oligomers that emerge from the depolymerization exists; finally towards the end of the reaction the system consists of soluble PET oligomers, dimers, and monomers that form a homogeneous solution. The reaction of the ethylene glycol with the PET occurs between the solid PET flake and the glycol, where the accessibility of the ethylene glycol to the PET segments controls the reaction. In a homogeneous reaction, the PET and ethylene glycol are molecularly dispersed in solution, and thus, the reaction collisions of PET and ethylene glycol occur more readily on a molecular level. Thus, the collisions of reactants in a homogeneous reaction depend on concentration and temperature.[7]

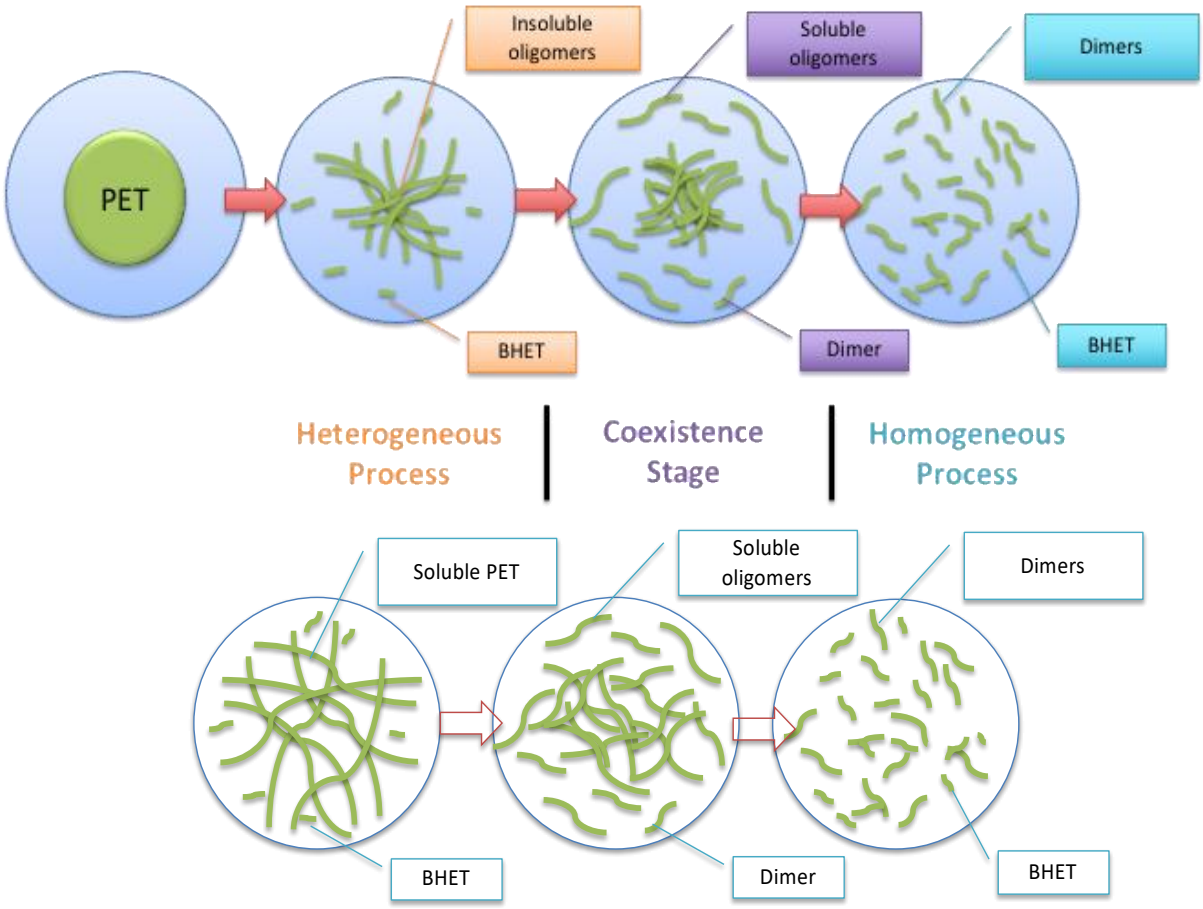

Figure 2.1 General depolymerization process of PET. Depolymerization on top is a heterogeneous surface reaction, and the depolymerization on bottom is a homogeneous reaction

Additionally, the glycolysis depolymerization of PET often requires harsh reaction conditions and long reaction times to reach 100% polymer conversion to monomer. The equilibrium between the formation of monomer, bis(2-hydroxyethyl) terephthalate (BHET), and the formation of small chain oligomers significantly contribute to the long reaction times needed to depolymerize to monomer.[9] But is reaching 100% conversion of polymer to monomer necessary? For instance, intermediates can be intercepted from the depolymerization process and used as reactants in further reactions. The repolymerization of such oligomers to re-form PET may be possible and more time and energy-efficient than depolymerization to monomer. Or the oligomeric intermediates may be used as reactants to form other polymer products, which would simplify the recycling process of PET. For instance, these oligomers could be modified into telechelic oligomers by functionalizing both ends of the modest size polymer chains,[13] to serve as feedstocks for further reactions generating new value added products.

Breaking down PET into oligomers requires less energy compared to breaking it down to monomers, as it requires breaking fewer bonds. More quantitatively, each chain scission transesterification reaction requires approximately 150 kJ/mol of energy.[19-24] By producing oligomers, the number of bond cleavages is reduced, resulting in an overall decrease in energy consumption during the depolymerization process. For instance, for one gram of PET with a molecular weight of 20 kDa, approximately 1.56 kilojoules (or 4.35 x 10-3 kilowatt hours) would be needed to cleave each ester bond to isolate monomers during the depolymerization process. Depolymerizing to oligomers decreases the required energy proportionally to the number of bonds cleaved.

Therefore, this investigation seeks to develop fundamental insight into the evolution of polymer chain structure during the heterogeneous depolymerization of PET, with the goal of

intercepting intermediates from the depolymerization process that can be used as reactants in the repolymerization of PET or to form further value-added products. The evolution of chain structure will be monitored by documenting the variation of molecular weight and dispersity of the depolymerization products. Understanding the evolution of the depolymerization products in a heterogeneous reaction will, therefore, offer pathways to optimize and simplify the recycling process of PET.

2.3 Methods

2.3.1 Materials

PET was sourced from commercial Coca-Cola bottles, which were washed and cut into 8x5mm squares. 1,5,7-Triazabicyclo[4.4.0]dec-5-ene (TBD, 98.0+%, TCI America™), Methanesulfonic Acid (MSA, 99%), Ethylene glycol, (EG, 99.8%, anhydrous, AcroSeal™, Thermo Scientific Chemicals), 20 mL vials, and 12.7x8mm stir bars were sourced from Fischer Scientific. 1,1,1,3,3,3-Hexafluoro-2-propanol (HFIP) was sourced from Oakwood Chemical. All chemicals were used as received.

2.3.2 Catalyst

This investigation uses an organocatalyst previously reported by Jehanno et al. to efficiently depolymerize PET via glycolysis.[17] The salt catalyst was prepared by mixing Triazabicyclodecene (TBD) and Methanesulfonic acid (MSA) at molar ratios of acid to base of 1:1 at 80 °C for 30 minutes. The product obtained was a transparent and homogenous solid.

2.3.3 Reaction Conditions

Ethylene Glycol (EG), TBD:MSA catalyst, PET (20:0.5:1 molar ratio), and stir bar were all placed in a 20 mL reaction vial inside a glovebox, sealed with a septa, and transferred outside the glovebox into a 180 °C oil bath. Previous studies indicate that this reaction takes under 2 hours at

180 °C to reach completion,[17] as illustrated in **Scheme 2.1**. To analyze the evolution of the polymer chains during PET depolymerization, the reaction was stopped at various reaction times, and the products were recovered and characterized as described below.[17]

2.3.4 Product Workup

After the reaction was allowed to run for a set time, the reaction vials were taken from the oil bath, and the mixture of ethylene glycol (EG) and depolymerization products that were soluble in EG were decanted from the reaction vials. The remaining solid PET that is insoluble in EG was washed with water three times by suspending it in 20 mL of water and stirring with a stir bar for 15 minutes. After the third wash and decant, the reaction vial containing the EG insoluble materials was set on a 70 °C hotplate overnight to evaporate off any remaining water.

Scheme 2.1 Heterogenous PET glycolysis reaction catalyzed by TBD:MSA to create BHET

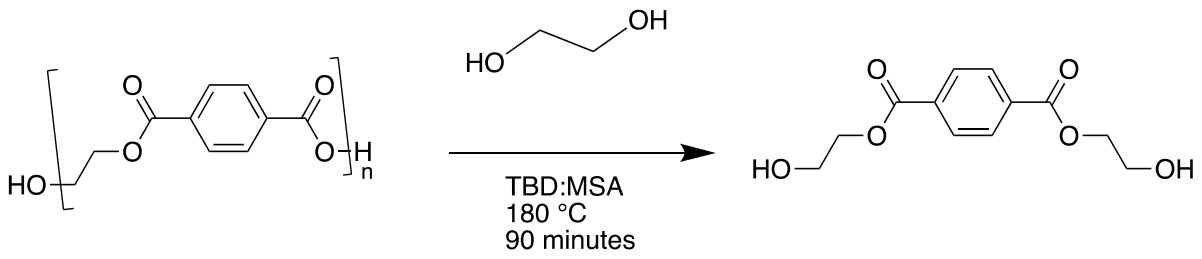

2.3.5 Repolymerization

The repolymerization of the insoluble PET intermediates that were obtained during the depolymerization process was attempted. In this reaction, the partially depolymerized PET was placed in a vacuum oven at 70 °C for 24 hours to ensure thorough drying of the PET flakes. The vacuum oven temperature was then increased to 240 °C for 6 hours to repolymerize the partially depolymerized PET flakes.

2.3.6 Depolymerization Product Characterization

2.3.6.1 Nuclear Magnetic Resonance (NMR)

In the NMR analysis, the EG insoluble products of the PET depolymerization (30 mg) were dissolved in HFIP (1 mL). The PET:HFIP mixture was agitated for five days before 50 microliters of the mixture were mixed with 800 microliters of $CDCl_3$. The NMR data was obtained using a Jeol 400 YH NMR at 35 ºC for 160 scans to ensure the PET did not precipitate out of the solution. The number average molecular weights (M_n) of the depolymerization products were determined using the analysis outlined by Falkenstein.[25]

Equation 2.1-Equation 2.4 elucidate the relationships between the number average molecular weight of the chain and the number of end groups present in the sample, which is determined from the NMR spectra. The peak of the methylene protons on the alpha carbon to the hydroxyl end group, found at 4.01 ppm, is analyzed to document the presence of end groups, where "A" is the integral of a peak in the following analysis. In

Equation 2.1-Equation 2.4, "H" denotes the number of protons associated with a given peak, while "n" represents the number of repeat units in the polymer that contain the functionality associated with that peak. The integral of the terephthalic peak found at 8.0 ppm or of the methylene peak found at 4.65 ppm (denoted by variables Ax, Hx, nx) is divided by the integral of the end group peak at 4.01 ppm (denoted by variables Ay, Hy, ny), providing a ratio of the main chain functional groups to the number of end groups.

Equation 2.2 is rearranged to **Equation 2.3** to provide the number of repeat units per chain, *nx*. The number of repeat units, *nx*, is multiplied by M_o (the repeat unit molecular weight), which is 192 g/mol for PET, to obtain the M_n of the polymer, as shown in **Equation 2.4**.

Equation 2.1 $\boldsymbol{Ax = Hx * nx}$

Equation 2.2 $$\frac{Ax}{Ay} = \frac{Hx*nx}{Hy*ny}$$

Equation 2.3 $$\frac{\left(\frac{Ax}{Ay}\right)*Hy*ny}{Hx} = nx$$

Equation 2.4 $$M_n = nx * M_o$$

2.3.6.2 Intrinsic Viscosity molecular weight, M_v

The viscosity average molecular weight of the depolymerization products is monitored using a Schott instrument Kapillarviskosimetr 531-10. In this experiment, the PET samples (90-100 mg) were dissolved in HFIP (15 mL) for five days before their intrinsic viscosity (IV) was measured. The samples were equilibrated in the viscometer at 25 ºC for 5 minutes before the viscosity was measured. The concentration dependence of the flow times of the PET solution through the viscometer was measured in quadruplicate at each concentration. After four trial times were gathered, the sample was diluted, equilibrated, and run again to obtain the concentration dependence of the flow times. The reduced and inherent viscosities of the PET solutions at each concentration were determined from the measured flow times using

Equation 2.5-Equation 2.9. Intrinsic viscosity was determined by finding the y-intercept of the plots of reduced and inherent viscosity as a function of concentration. The viscosity average molecular weight (M_v) of the PET was then determined using the Mark Houwink equation (**Equation 2.10**) with k and α values, 0.00052 dL/g and 0.695, respectively.[26, 27]

Equation 2.5 Relative Viscosity $$n_{rel} = \frac{t}{t_0}$$

Equation 2.6 Specific Viscosity $$n_{sp} = \frac{t-t_0}{t_0} = n_{rel} - 1$$

Equation 2.7 Reduced Viscosity $$n_{sp} = \frac{t-t_0}{t_0*c} = \frac{n_{sp}}{c}$$

Equation 2.8 Inherent Viscosity $$n_{sp} = \ln\frac{\frac{t}{t_0}}{c} = \left(\frac{\ln(n_{rel})}{c}\right)$$

Equation 2.9 Intrinsic Viscosity $[\boldsymbol{n}] = \lim_{c \to 0} \left(\frac{n_{sp}}{c}\right) = \lim_{c \to 0} \left(\frac{\ln(n_{rel})}{c}\right)$

Equation 2.10 Mark-Houwink $\boldsymbol{\eta = kM_v{}^{\alpha}}$

2.3.6.3 Size Exclusion Chromatography (SEC)

The molecular weight of some of the depolymerization products were also determined by Size exclusion Chromatography to verify the NMR and intrinsic viscosity analyses. The SEC analyses were completed at PolyAnalytik using a Triple Detection GPC/SEC. This analysis used a Viscotek TDA302 and GPCmax instrument with Refractive Index, Light Scattering, and Viscometer detectors using a poly(methyl methacrylate) in HFIP standard. A dn/dc of 0.257 mL/g for PET in HFIP was used in the light scattering detector. The SEC/GPC Columns used are PA-HFIP 603, 604, and 606. The samples were run with a Flow Rate of 0.7 mL/min and an analysis temperature of 35 °C.

2.3.6.4 Dispersity (Đ)

The dispersity of the samples is reported as the ratio of the viscosity average molecular weight, and the number average molecular weight, where M_n is derived from the NMR experiments, and M_v is the result of the viscosity experiments. M_v is used in the calculation of the molecular weight dispersity rather than the weight average molecular weight (M_w), as it is difficult to determine M_w of PET due to its limited solubility and because M_v is similar to M_w.[26]

2.3.6.5 Differential Scanning Calorimetry (DSC)

The Differential Scanning Calorimetry (DSC) Q200 curves of the depolymerization product (3-7 mg) were measured in a Hematic aluminum pan. In the DSC run, the sample was equilibrated at 50 °C before being heated to 280 °C with a ramp of 10 °C/min. Enthalpies of melting of the PET samples were determined by measuring the heat flow associated with the melting of PET from

the first cycle.[28] The percent crystallinity of each sample was calculated by dividing the enthalpy of the melting of a PET sample by the enthalpy of 100% crystalline PET (140 J/g).[29]

2.4 Results

2.4.1 Evolution of chain molecular weight

Figure 2.2 shows a picture of the PET flakes that emerge from the heterogeneous glycolysis reaction as a function of reaction time. Inspection of the PET through the course of the reaction also shows that the PET flakes swell with EG and become increasingly brittle with reaction time. Examination of **Figure 2.2** shows that the PET flakes retain their shape up to 75 minutes into the reaction, though the PET flakes begin to swell and become opaque at 30 minutes. At 75 minutes of reaction time, the PET flakes convert into a powder. **Figure 2.3** plots the yield of the depolymerized insoluble PET (brown line) and the M_n of the recovered PET as a function of reaction time. This plot shows a continuous decrease in M_n, but the insoluble yield of the reaction remains very high (> 95%) for the first 60 minutes of the reaction, with the yield only decreasing after 75 minutes of the depolymerization reaction. From 60 to 75 minutes of reaction time, the M_n does not significantly change (from 3.5 kDa to 3.0 kDa), yet there is a large change in the yield of EG insoluble PET (from > 95% to 50%).

While M_n decreases with reaction time, so does dispersity. **Figure 2.4** shows the dispersity of the EG insoluble PET chains (green diamond) with reaction time, as determined by SEC. The EG insoluble samples demonstrate a gradual decrease in the dispersity of PET chains (from 2.6 to 1.4). There is a drop in $Đ$ within the first 15 minutes (from 2.6 to 1.7), but $Đ$ stabilizes from 30 minutes to 60 minutes. The dispersity of PET chains only decreases further to 1.4 at 75 minutes into the reaction, when the PET flakes have converted into a powder, and the yield of the PET decreases significantly.



Figure 2.2 Picture of the PET depolymerization product as a function of reaction time.

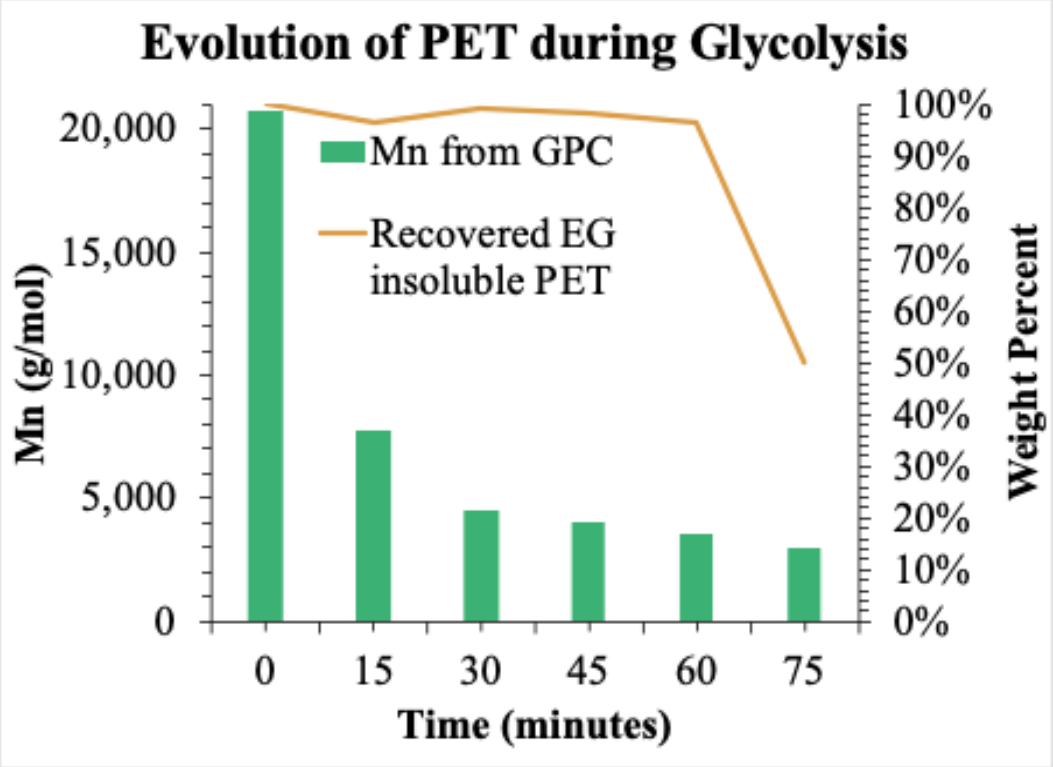

Figure 2.3 Evolution of PET during glycolysis reaction. M_n from SEC is depicted as green bar graphs, with the y-axis on the left side. The weight percent of recovered EG insoluble depolymerized PET is depicted as the brown line graph, with the y-axis on the right.

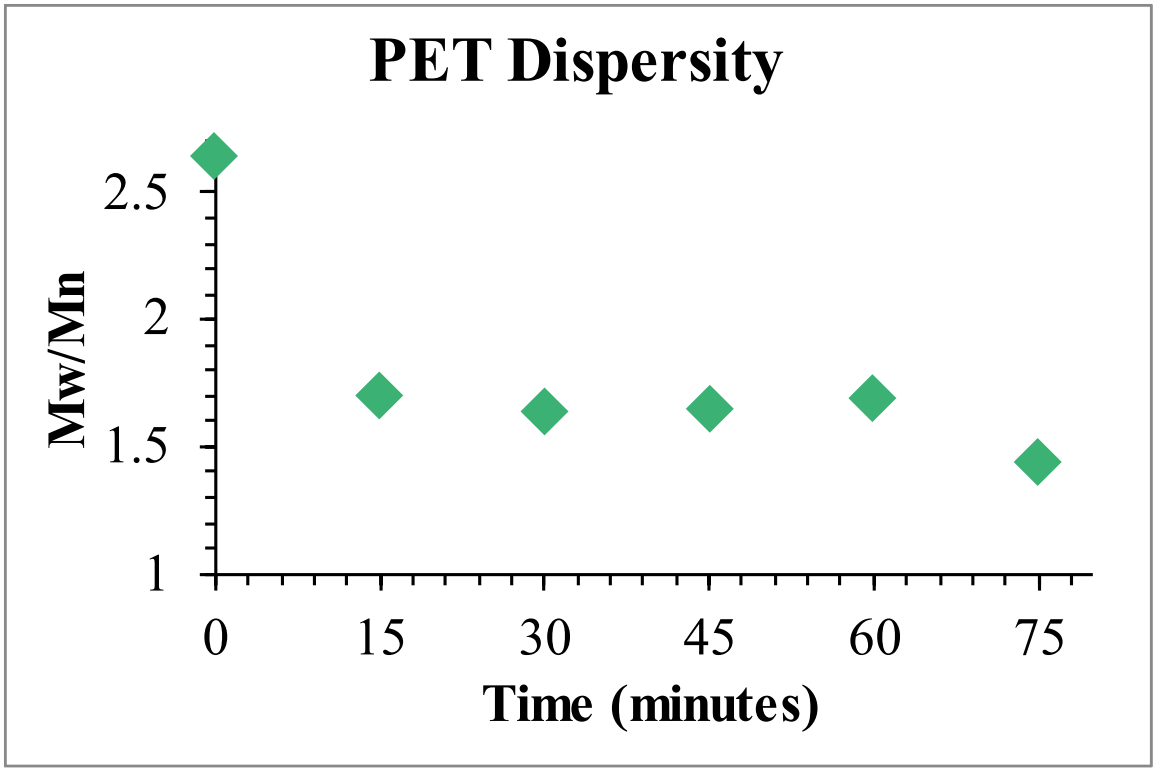

Figure 2.4 Evolution of PET during glycolysis reaction. M_n from SEC is depicted as green bar graphs, with the y-axis on the left side. The weight percent of recovered EG insoluble depolymerized PET is depicted as the brown line graph, with the y-axis on the right.

2.4.2 Crystallinity of reaction products

Inspection of **Figure 2.2** shows that the product of the depolymerization reaction becomes increasingly opaque as the reaction proceeds. Though not the only explanation, this suggests that the crystallinity of the product is increasing, so the percent crystallinity of the depolymerization products was determined by DSC. **Figure 2.5** shows the DSC of the EG insoluble PET depolymerization product as a function of reaction time. **Figure 2.5** shows that there is a broadened melting peak for all depolymerization products compared to that of the unreacted PET (0 minute-pink curve). The melting peaks of the products for the first 60 minutes of reaction time show that the melting peak starts at a lower temperature than the initial PET, which suggests the formation of crystals that are more easily melted in the depolymerization product, such as smaller crystals. The DSC curves were analyzed to determine the percent crystallinity of the depolymerization products as a function of reaction time.[28] **Figure 2.6** shows the percent crystallinity of the reaction product as a function of reaction time (green curve) as well as the crystallinity of PET that was annealed at 180 °C (pink curve). The crystallinity of the annealed sample was determined to account for any changes to PET crystallinity by merely keeping the temperature at 180 °C, between T_g (~80 °C) and T_m (260 °C). A comparison of the green and pink curves shows that the percent crystallinity of the depolymerization products is significantly higher than that of the annealed sample, where the crystallinity of the reaction products increases from 27% to 93% over the 75-minute reaction. Understanding the basis for this increased percent crystallinity will provide significant insight into the mechanism of the depolymerization reaction.

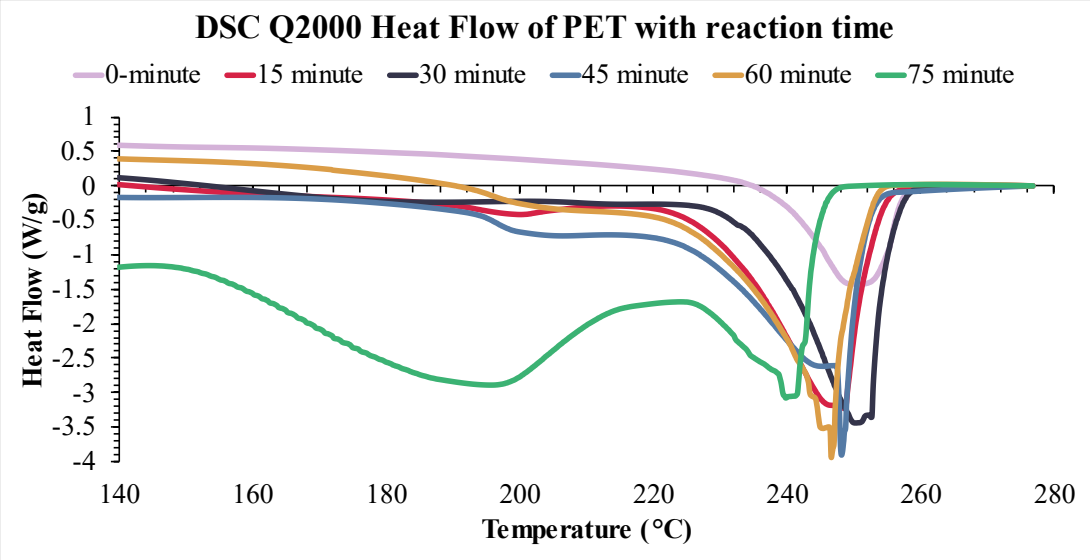

Figure 2.5 Differential Scanning Calorimetry (DSC) first cycle curves of PET depolymerization products for different reaction times. The endothermic transitions in the DSC curves are down.

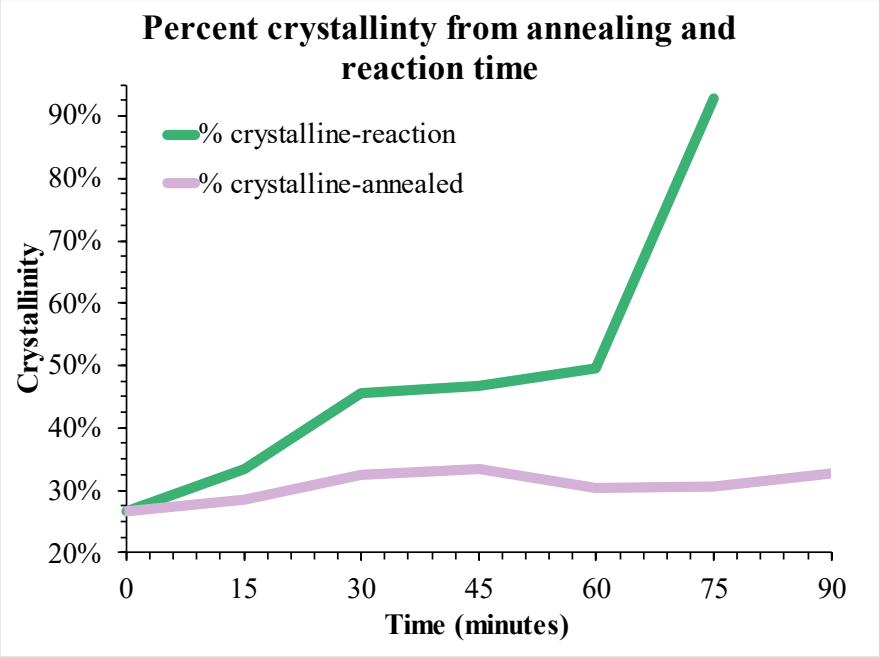

Figure 2.6 Percent crystallinity of PET annealed at 180 °C (pink) and PET depolymerization products as a function of reaction time at 180 °C (green).

2.4.3 End group evolution during depolymerization

NMR was used as the primary technique to determine the number average molecular weight of the depolymerization products. However, the molecular weight characteristics of a few sets of reaction products were also determined by SEC using a commercial vendor. Comparing the SEC and viscosity analyses, M_w and M_v of a given sample are similar. However, a comparison of the M_n as determined by NMR to that derived from SEC showed similar values for the starting PET, verifying that the initial PET contains one hydroxyl end group per chain, but these M_n values diverge for the products of the depolymerization. Upon reflection, the source of this discrepancy is obvious – the analysis of the M_n from the NMR requires knowledge of the number of -OH end groups per chain, which is one hydroxyl group (-OH) for the original PET. Our analysis of the NMR results to determine M_n assume one -OH for the reaction products as well, but the difference between NMR and SEC-derived M_n values clearly shows that this assumption is incorrect for the products of the depolymerization reaction.

However, knowledge of the true M_n of the depolymerization products from SEC provides a route to determine the change in the number of –OH end groups per chain as a function of reaction time. For a given NMR curve, the M_n of the polymer chain can be calculated as a function of the number of –OH end groups per chain. These data are the lines plotted in **Figure 2.7** for the products of the depolymerization at different reaction times. The M_n of the depolymerization products, as determined by SEC, are then plotted as the diamonds on each line, providing the number of –OH end groups of each depolymerization product. In this analysis, we only monitor the change in -OH end groups, while the exact structure of the remaining end groups is not determined. We expect that they are primarily -COOH but may also be vinylic.[30, 31] **Figure 2.8** then plots the average number of alcohol end groups on the depolymerization

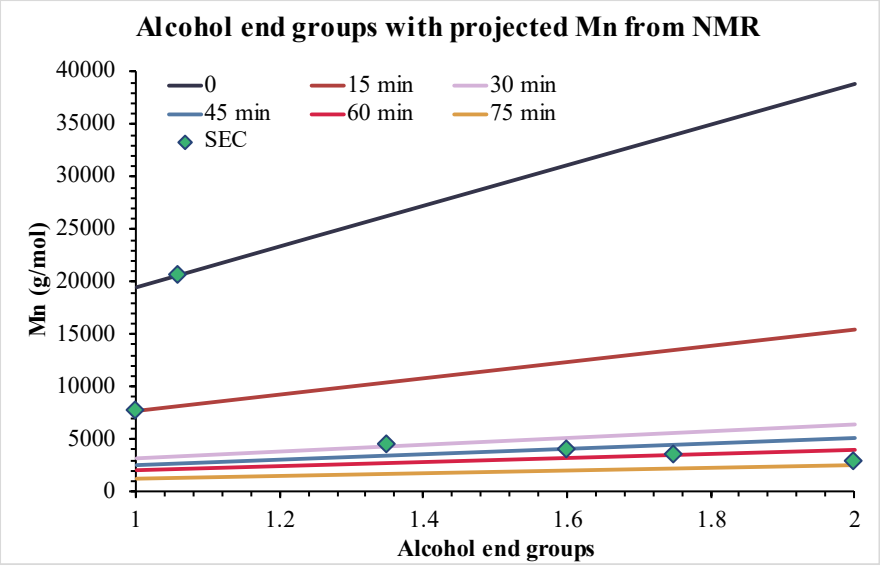

Figure 2.7 M_n of the depolymerization products for specific reaction times (lines) as a function of the number of -OH end groups per chain. SEC-derived M_n of the depolymerization products are plotted as green diamonds. The overlap of the green diamond and line denotes the actual number of -OH end groups on each depolymerization reaction product.

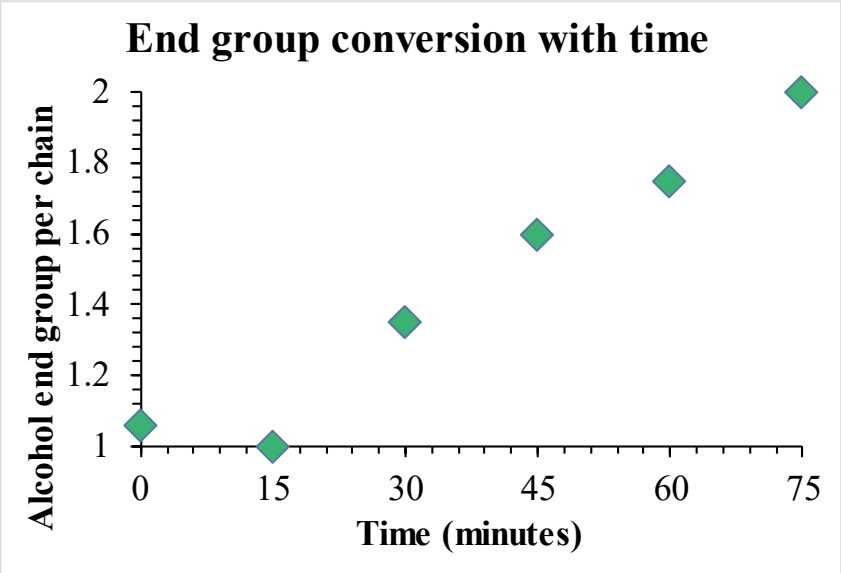

Figure 2.8 Average number of alcohol end groups per chain on the depolymerization reaction product as a function of reaction time.

products as a function of reaction time. This plot shows that there is a slow and steady conversion from one to two alcohol end groups in the course of the reaction. From 15 to 75 minutes reaction time, the conversion of alcohol end groups is nearly linear with reaction time.

2.4.4 Repolymerization of oligomeric intermediates

A goal of this project is to intercept intermediates of the depolymerization process to use as reactants to create value-added products. To test this, we attempted to repolymerize the oligomers that emerge from the depolymerization products as described above as one possible reaction. **Figure 2.9** plots the viscosity average molecular weight of two samples (depolymerization reaction times of 15 and 60 minutes) as they go from the original PET sample to the depolymerization product and are then repolymerized. In the repolymerization reaction, the depolymerization products were dried below their T_g for 24 hours and then repolymerized at 240 °C for 6 hours to form repolymerized PET flakes with a tan hue. Inspection of **Figure 2.9** shows that the depolymerization product, after 15 minutes of reaction time, regained 66% of its initial chain length, while the PET that was depolymerized for 60 minutes regained 90% of their initial chain length with the repolymerization.

2.5 Discussion

The chain evolution that occurs during the heterogenous depolymerization of PET via glycolysis is not well understood. In this study, we have monitored the evolution of molecular weight, dispersity, crystallinity, and end-group conversion to address this shortcoming**. Figure 2.3** and **Figure 2.4** show a steady decrease in M_n and Đ of the product of the depolymerization reaction with reaction time. Moreover, the yield of the depolymerization reaction remains nearly 100% for the first hour of the reaction, even while the molecular weight of the oligomeric products decreases by approximately a factor of 5. **Figure 2.2** further verifies that the PET flakes

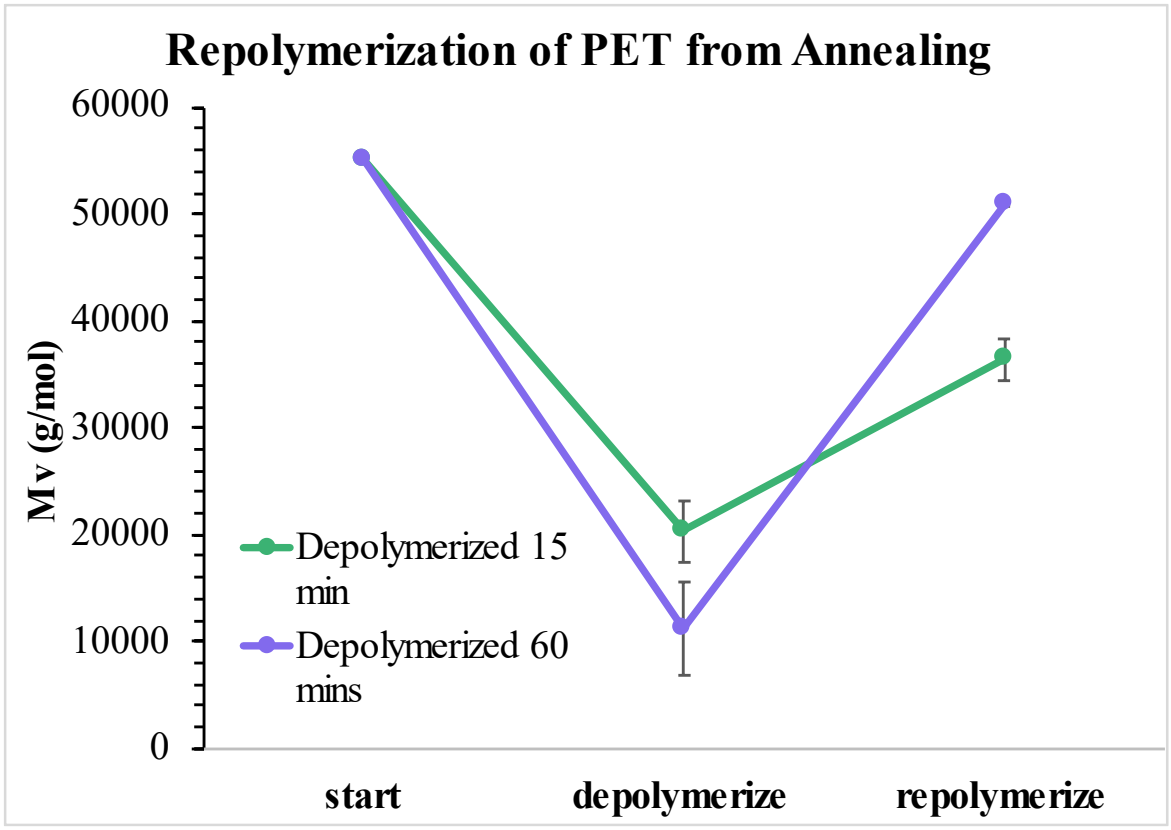

Figure 2.9 Change in M_v of PET before depolymerization, after depolymerization, and after repolymerization.

remain in flake form over this reaction time period. These initial observations indicate that a complex chain scission process must be occurring during the depolymerization.

The change in dispersity with depolymerization progress can provide insight into whether chain scission is random or not. If chain scission is random, the chain length and dispersity should follow Carothers equation, which correlates the degree of polymerization (DP) and conversion, p, (**Equation 2.11**), as well as the relationship between conversion and dispersity, Đ, shown in Equation 2.12. [26] Rearrangement of **Equation 2.12** to **Equation 2.13**, followed by replacement of p by (Đ – 1) in **Equation 2.11**, gives **Equation 2.14**, which can be simplified to **Equation 2.15**. Thus, if chain scission is random in the depolymerization of PET, a plot of DP as a function of Đ should follow **Equation 2.15**. **Figure 2.10** shows the results of a plot of DP as a function of Đ for the PET depolymerization.

Equation 2.11 $$\boldsymbol{Dp = \frac{M}{M_0} = \frac{1}{1-p}}$$

Equation 2.12 $$Đ = \mathbf{1 + p}$$

Equation 2.13 $$\boldsymbol{p = Đ - 1}$$

Equation 2.14 $$\boldsymbol{Dp = \frac{1}{1-(Đ-1)}}$$

Equation 2.15 $$\boldsymbol{Dp = \frac{1}{2-Đ}}$$

Inspection of **Figure 2.10** shows that the products of the PET depolymerization do not follow the same statistics of a random chain scission process, verifying that the chain scission that occurs in the depolymerization is not random.

The rate of conversion of end groups to -OH during the depolymerization also provides insight into the evolution of chain structure. By comparison of the M_n as determined by SEC to that determined by NMR, the average number of hydroxyl end groups per chain is revealed and plotted in **Figure 2.8**. Inspection of **Figure 2.8** shows that end-group conversion is slow, where

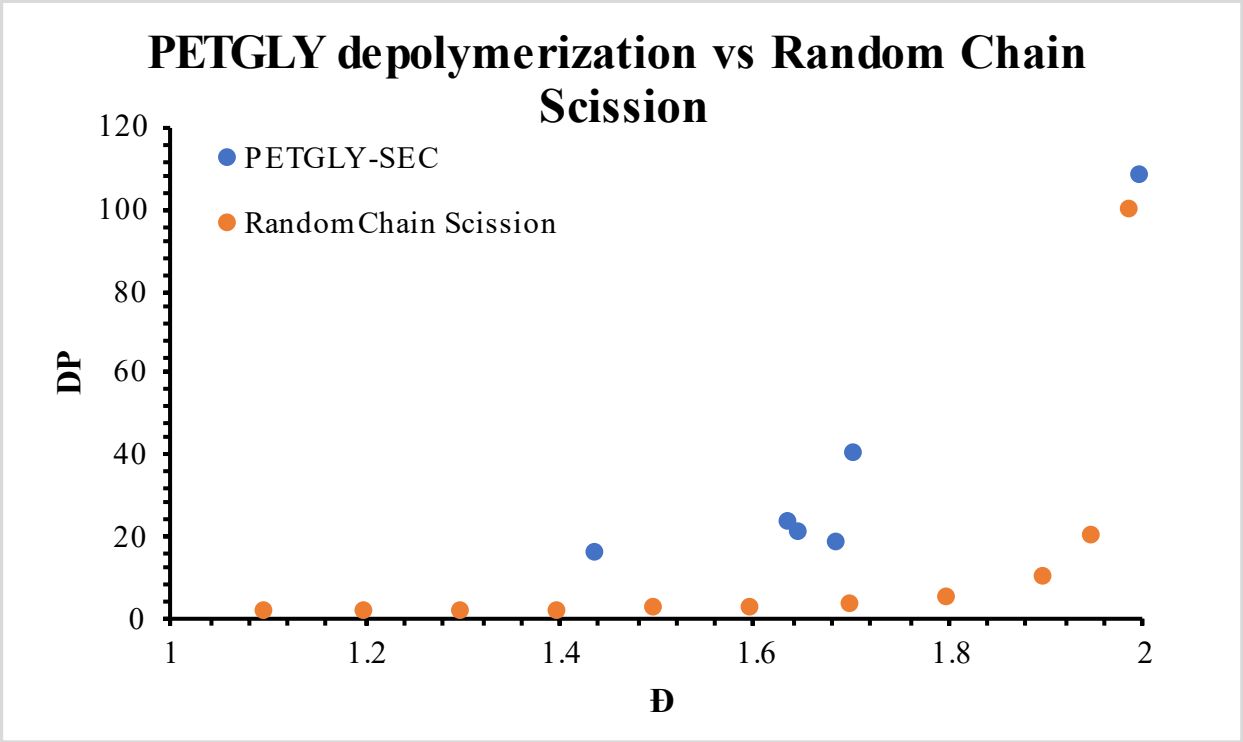

Figure 2.10 Changes in DP with Đ of the products of the PET glycolysis reaction and a random chain scission.

it steadily increases from 1 -OH per chain to 2 -OH per chain at 75 minutes of reaction time. The initial PET has, on average, 1 -OH group per chain. After each PET chain reacts with one ethylene glycol molecule, the resultant products have, on average, 1.5 -OH end groups per chain, as illustrated in **Scheme 2.2**. At this stage, the molecular weight of the depolymerization products decreases by a factor of two, which occurs within the first 15 minutes of the depolymerization reaction, according to **Figure 2.7**. However, the average number of -OH end groups does not increase to 1.5 until after 30 minutes of reaction. This contradiction indicates that only some chains are accessible to the scission reaction in this heterogeneous depolymerization. [7] This also emphasizes that the diffusion of ethylene glycol into the PET flake could be a rate limiting step for this reaction, as semicrystalline polymers are known to swell less than amorphous ones. [18, 32] Further studies are ongoing to more precisely define the importance of the diffusion of the ethylene glycol into the PET on the rate of depolymerization.

Scheme 2.2 PET glycolysis conversion of carboxylic acid end groups into alcohol end groups

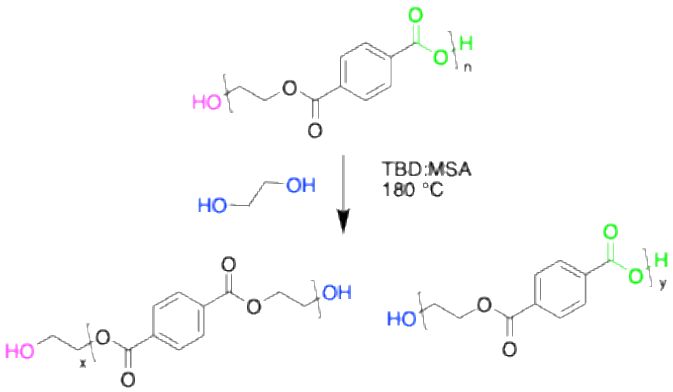

Further insight into the reaction process can derive from the interpretation of the change in polymer crystallinity with reaction time. **Figure 2.6** shows the change in polymer crystallinity during the depolymerization reaction and for a PET sample that has been annealed at 180 °C. At the same time, **Figure 2.2** shows that the flakes remain intact and become more opaque over the

first 60 minutes of depolymerization, consistent with an increase in crystallinity.[33] The crystallinity of a polymer sample can increase by the growth of the number of polymer chains that are packed on the crystalline lattice or by a systematic decrease in the amount of amorphous polymer in the sample while retaining the crystalline portion. We interpret this increase in crystallinity as the result of the fact that the primary reaction of the ethylene glycol is with the amorphous PET in the depolymerization process, thus decreasing the amount of amorphous PET in the depolymerization product. This leaves the PET crystals intact, resulting in an increase in the percent of the depolymerization reaction product that is crystalline, in agreement with **Figure 2.6**.

Moreover, the slow end group conversion and change in dispersity are also consistent with the mechanism that includes the reaction of the ethylene glycol primarily with the amorphous PET, leaving the crystalline lamellae as the products of the reaction. In this case, the average size of the lamellae guides the molecular weight of the depolymerization products, leading to the observed decrease in the dispersity of the depolymerization products. We therefore posit that the ethylene glycol diffuses into the PET flake, [3, 9, 17] penetrating the amorphous phase, where it reacts with tie chains and other amorphous accessible PET. The crystalline portion of the PET flake is so tightly packed that these ordered chains are inaccessible to reaction. [34] Moreover, in this process, the diffusion of ethylene glycol into the PET amorphous phase will impact the rate of the reaction. If this proposed mechanism is correct, a more slowly moving (i.e., larger) glycol would result in a slower depolymerization reaction and access to a broader range of intermediates. Similarly, reacting the PET with a less soluble glycol will also provide a pathway to further control the reaction progress.

This mechanism, depicted in **Figure 2.11**, is also consistent with the steady decrease in oligomer product molecular weight while retaining the yield of depolymerized polymer that is greater than 90%. **Figure 2.11** depicts two crystalline phases that are connected by amorphous tie chains. New alcohol end groups are generated by the scission of the amorphous chain between the crystals to form new alcohol end groups. However, because not all chains are accessible to reaction, the *average* number of -OH end groups per chain increases slowly. Once a majority of the tie-chains are cut, the crystalline portions can disperse to create powders, which appears to occur at 75 minutes reaction time in the studies reported here. We interpret the data to indicate that the insoluble yield finally decreases at 75 minutes of reaction time when the flakes turn into a powder exposing more amorphous polymer to EG, allowing the depolymerization reaction to proceed more quickly. This mechanism has some similarity to other reactions that rely on the access of a reactant to only the amorphous phase in crystalline polymers to form blocky copolymers, including the suspension chlorination of polyethylene[35,36,37] the bromination of syndiotactic polystyrene[38,39,40], and the sulfonation of PEEK[41,42,43]. The success of these reactions lends further support to the validity of the proposed mechanism.

Additionally, our results provide some insight into literature reports that the rate of the depolymerization reaction of PET in different form factors, such as fibers, bottles, and lower crystalline thermoforms, will vary even though the reaction conditions are the same.[44-50] Our results show that the swelling of PET by ethylene glycol is a crucial step in the depolymerization process. Moreover, the rate of this process will vary with the form factor and percent crystallinity of the PET. Thus, the rate of the depolymerization of PET will depend on the form factor and % crystallinity, however, the reaction process (and access to oligomers, which is the focus of this study) will remain the same. Moreover, these results provide foundational

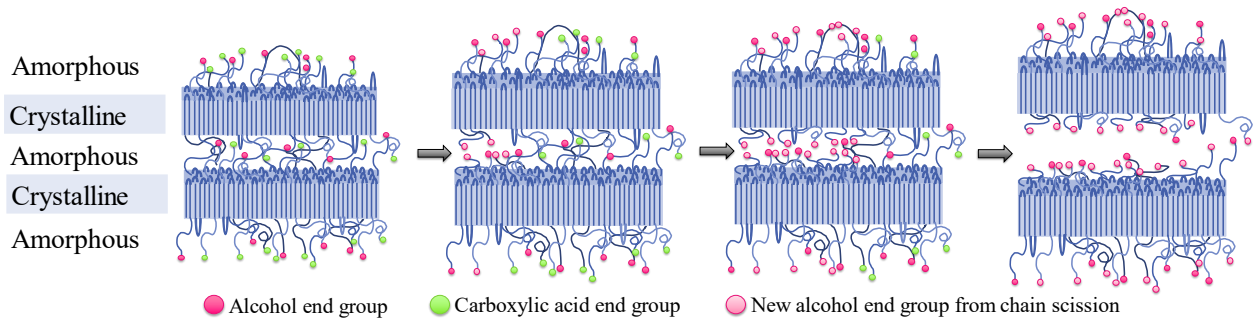

Figure 2.11 Depiction of slow end group conversion in the amorphous phase by the diffusion of EG into the PET flake in the amorphous phase to depolymerize at the amorphous tie-chains.

information to understand the underlying processes that control these variations in rate. In fact, further studies to extend this work to systematically monitor the swelling behavior of distinct forms of PET are underway, with the goal to gain more quantitative, foundational insight into the influence of PET form factor on the depolymerization process.

This additional insight into the process by which the EG diffuses into the amorphous phase and reacts to break the PET chains offers us access to oligomeric intermediates that can serve as reactants to create value-added products. Thus, we have attempted to isolate and repolymerize the depolymerized oligomers. Figure 9 shows the evolution of the chain structure of two intermediates, one that was depolymerized for 15 minutes and another that was depolymerized for 60 minutes**. Figure 2.9** shows that the repolymerization of the isolated oligomers reforms the polymer to a polymer with an M_v near that of the original PET. This proof-of-concept experiment exemplifies that it is not necessary to depolymerize PET all the way to monomer to reform polymer. This concept of repolymerizing oligomers rather than pushing the equilibrium depolymerization reaction to monomer, therefore, offers new pathways to more effectively and efficiently chemically recycle PET.

This method of repolymerizing oligomers rather than of monomers is less energy intensive and involves and easier separation processes. The decreased energy consumption in the depolymerization and further repolymerization of PET by isolating oligomers instead of monomers stems from the need to break or reform fewer polymer backbone bonds. Moreover, the process of separating oligomers requires rinsing the PET flakes with water and then allowing them to dry. This approach eliminates the need for additional purification, which simplifies the process by removing the extra steps required to isolate BHET monomer crystals when

depolymerizing to monomer. Additionally, the process isolates nearly 100% yield of oligomers, whereas previous studies show isolation of 90% of feedstock in the form of monomers.[17]

2.5 Conclusions

This work provides a clear mechanism that elucidates the evolution of chain structure in the depolymerization of PET by heterogeneous catalysis and offers opportunities to intercept oligomeric intermediates in the depolymerization process. The dispersity, molecular weight, end groups, and crystallinity of the products of the heterogeneous depolymerization of PET via glycolysis are monitored to provide insight into the mechanism by which the polymer chain evolves during depolymerization. Our results show that the crystallinity of the depolymerized polymer increases, the dispersity decreases, while the yield remains high during the first hour of the depolymerization process. Our holistic interpretation of these results leads to a mechanism that involves the selective diffusion of EG into the amorphous PET, where it reacts by glycolysis to scission tie chains. This decreases the amount of amorphous material in the sample, leading to a dramatic increase in PET crystallinity in the depolymerization products. This interpretation is also consistent with the slow conversion of the end groups to two alcohol end groups per chain since many chains are inaccessible to the depolymerization process.

This mechanism provides a clear pathway to recover a significant portion of the original polymer as an oligomer that can then be used as reactants to create value-added materials. To this end, our results show that the repolymerization of oligomers to reform polymers is achievable, opening new opportunities to more effectively and efficiently chemically recycle PET.

2.6 Acknowledgements

This work was supported by the National Science Foundation, Polymers program, Division of Materials Research (DMR- 2104982). We also thank Prof. Sanat Kumar (Columbia) for invaluable discussion.

References

(1) Hong, M.; Chen, E. Y. X. Chemically recyclable polymers: a circular economy approach to sustainability. *Green Chemistry* **2017**, *19* (16), 3692-3706. DOI: 10.1039/c7gc01496a.

(2) Kenwright, A. M.; Peace, S. K.; Richards, R. W.; Bunn, A.; Macdonald, W. A. End group modification in poly(ethylene terephthalate). *Polymer* **1999**, *40* (8), 2035-2040. DOI: 10.1016/s0032-3861(98)00433-9.

(3) George, N.; Kurian, T. Recent Developments in the Chemical Recycling of Postconsumer Poly(ethylene terephthalate) Waste. *Industrial & Engineering Chemistry Research* **2014**, *53* (37), 14185-14198. DOI: 10.1021/ie501995m.

(4) Nikles, D. E.; Farahat, M. S. New Motivation for the Depolymerization Products Derived from Poly(Ethylene Terephthalate) (PET) Waste: a Review. *Macromolecular Materials and Engineering* **2005**, *290* (1), 13-30. DOI: 10.1002/mame.200400186.

(5) Ma, Y.; Agarwal, U. S.; Vekemans, J. A. J. M.; Sikkema, D. J. NMR based determination of minute acid functionality: end-groups in PET. *Polymer* **2003**, *44* (16), 4429-4434. DOI: 10.1016/s0032-3861(03)00402-6.

(6) Shaikh, I. R. Organocatalysis: Key Trends in Green Synthetic Chemistry, Challenges, Scope towards Heterogenization, and Importance from Research and Industrial Point of View. *Journal of Catalysts* **2014**, *2014*, 1-35. DOI: 10.1155/2014/402860.

(7) Xin, J.; Zhang, Q.; Huang, J.; Huang, R.; Jaffery, Q. Z.; Yan, D.; Zhou, Q.; Xu, J.; Lu, X. Progress in the catalytic glycolysis of polyethylene terephthalate. *Journal of Environmental Management* **2021**, *296*, 113267. DOI: 10.1016/j.jenvman.2021.113267.

(8) Fox, B.; Moad, G.; Van Diepen, G.; Willing, I.; Cook, W. D. Characterization of poly(ethylene terephthalate) and poly(ethylene terephthalate) blends. *Polymer* **1997**, *38* (12), 3035-3043. DOI: 10.1016/s0032-3861(96)00872-5.

(9) Carta, D.; Cao, G.; D'Angeli, C. Chemical recycling of poly(ethylene terephthalate) (pet) by hydrolysis and glycolysis. *Environmental Science and Pollution Research* **2003**, *10* (6), 390-394. DOI: 10.1065/espr2001.12.104.8.

(10) Cowger, W.; Willis, K. A.; Bullock, S.; Conlon, K.; Emmanuel, J.; Erdle, L. M.; Eriksen, M.; Farrelly, T. A.; Hardesty, B. D.; Kerge, K.; et al. Global producer responsibility for plastic pollution. *Science Advances* **2024**, *10* (17). DOI: 10.1126/sciadv.adj8275.

(11) Todd, A. D.; McEneany, R. J.; Topolkaraev, V. A.; Macosko, C. W.; Hillmyer, M. A. Reactive Compatibilization of Poly(ethylene terephthalate) and High-Density Polyethylene Using Amino-Telechelic Polyethylene. *Macromolecules* **2016**, *49* (23), 8988-8994. DOI: 10.1021/acs.macromol.6b02080.

(12) Ashcraft, E.; Ji, H.; Mays, J.; Dadmun, M. A Novel Reactive Processing Technique: Using Telechelic Polymers To Reactively Compatibilize Polymer Blends. *ACS Applied Materials & Interfaces* **2009**, *1* (10), 2163-2173. DOI: 10.1021/am900333y.

(13) Flores, I.; Demarteau, J.; Müller, A. J.; Etxeberria, A.; Irusta, L.; Bergman, F.; Koning, C.; Sardon, H. Screening of different organocatalysts for the sustainable synthesis of PET. *Eur. Polym. J.* **2018**, *104*, 170-176. DOI: 10.1016/j.eurpolymj.2018.04.040.

(14) Agency, U. S. E. P. *Plastics: Material-Specific Data*. 2024. https://www.epa.gov/facts-and-figures-about-materials-waste-and-recycling/plastics-material-specific-data (accessed 2024 07/31/24).

(15) Resources, N. A. f. P. C. *NAPCOR'S 2022 PET RECYCLING REPORT DEMONSTRATES BOTTLE-TO-BOTTLE CIRCULARITY CONTINUES ON THE RISE*. 2023. https://napcor.com/news/2022-pet-recycling-report/ (accessed 2024 07/31/2024).

(16) Laboratory, N. R. E. *A Low-Emission, Cost-Competitive Enzymatic Platform for Recycling and Upcycling Mixed PET (Text Version)*. 2023. https://www.nrel.gov/news/video/a-low-emission-cost-competitive-enzymatic-platform-for-recycling-and-upcycling-mixed-pet-text.html#:~:text=Chances%20are%20it%20will%20never,with%20other%20kinds%20of%20plastics. (accessed 2024 07/31/2024).

(17) Jehanno, C.; Flores, I.; Dove, A. P.; Müller, A. J.; Ruipérez, F.; Sardon, H. Organocatalysed depolymerisation of PET in a fully sustainable cycle using thermally stable protic ionic salt. *Green Chemistry* **2018**, *20* (6), 1205-1212. DOI: 10.1039/c7gc03396f.

(18) Najmi, S.; Vance, B. C.; Selvam, E.; Huang, D.; Vlachos, D. G. Controlling PET oligomers vs monomers via microwave-induced heating and swelling. *Chem. Eng. J.* **2023**, *471*, 144712. DOI: https://doi.org/10.1016/j.cej.2023.144712.

(19) Chen, F.; Wang, G.; Shi, C.; Zhang, Y.; Zhang, L.; Li, W.; Yang, F. Kinetics of glycolysis of poly(ethylene terephthalate) under microwave irradiation. *Journal of applied polymer science.* **2013**, *127* (4), 2809-2815. DOI: 10.1002/app.37608.

(20) Petrov, A. A.; Repina, L. P.; Aizenshtein, M. Kinetics of the formation of linear oligomers in the glycocysis of polyethylene terephthalate. *Fibre Chemistry* **1985**, *16* (5), 297-300. DOI: 10.1007/bf00551369.

(21) Wu Klingler, W.; Bifulco, A.; Polisi, C.; Huang, Z.; Gaan, S. Recyclable inherently flame-retardant thermosets: Chemistry, properties and applications. *Composites Part B: Engineering* **2023**, *258*, 110667. DOI: https://doi.org/10.1016/j.compositesb.2023.110667.

(22) Bender, M. L.; Ginger, R. D.; Unik, J. P. Activation Energies of the Hydrolysis of Esters and Amides Involving Carbonyl Oxygen Exchange1. *Journal of the American Chemical Society* **1958**, *80* (5), 1044-1048. DOI: 10.1021/ja01538a006.

(23) Gaurav, A.; Dumas, S.; Mai, C. T. Q.; Ng, F. T. T. A kinetic model for a single step biodiesel production from a high free fatty acid (FFA) biodiesel feedstock over a solid heteropolyacid catalyst. *Green Energy & Environment* **2019**, *4* (3), 328-341. DOI: https://doi.org/10.1016/j.gee.2019.03.004.

(24) Roy, T.; Sahani, S.; Chandra Sharma, Y. Study on kinetics-thermodynamics and environmental parameter of biodiesel production from waste cooking oil and castor oil using potassium modified ceria oxide catalyst. *Journal of Cleaner Production* **2020**, *247*, 119166. DOI: https://doi.org/10.1016/j.jclepro.2019.119166.

(25) Falkenstein, P.; Gräsing, D.; Bielytskyi, P.; Zimmermann, W.; Matysik, J.; Wei, R.; Song, C. UV Pretreatment Impairs the Enzymatic Degradation of Polyethylene Terephthalate. *Frontiers in microbiology*. **2020**, *11*. DOI: 10.3389/fmicb.2020.00689.

(26) Paul C. Hiemenz, T. P. L. *Polymer Chemistry*; CRC Press, 2007.

(27) Roovers, J.; Toporowski, P. M. Hydrodynamic studies on model branched polystyrenes. *Journal of Polymer Science: Polymer Physics Edition* **1980**, *18* (9), 1907-1917. DOI: https://doi.org/10.1002/pol.1980.180180904.

(28) Blaine, R. L. *Determination of Polymer Crystallinity by DSC*; TA Instruments, https://www.tainstruments.com/pdf/literature/TA123new.pdf.

(29) Blaine, R. L. *THERMAL APPLICATIONS NOTE*; TA Instrument, https://www.tainstruments.com/pdf/literature/TN048.pdf.

(30) Jang, J. Y.; Sadeghi, K.; Seo, J. Chain-Extending Modification for Value-Added Recycled PET: A Review. *Polymer Reviews* **2022**, *62* (4), 860-889. DOI: 10.1080/15583724.2022.2033765.

(31) Venkatachalam, S.; Nayak, S. G.; Labde, J. V.; Gharal, P. R.; Rao, K.; Kelkar, A. K. *Degradation and recyclability of poly (ethylene terephthalate)*; InTech Rijeka, Croatia, 2012.

(32) Miller-Chou, B. A.; Koenig, J. L. A review of polymer dissolution. *Prog. Polym. Sci.* **2003**, *28* (8), 1223-1270. DOI: 10.1016/s0079-6700(03)00045-5.

(33) Lin, Y.; Bilotti, E.; Bastiaansen, C. W. M.; Peijs, T. Transparent semi-crystalline polymeric materials and their nanocomposites: A review. *Polymer Engineering & Science* **2020**, *60* (10), 2351-2376. DOI: 10.1002/pen.25489.

(34) Aharoni, S. M.; Harget, P. J. On the location of chain-ends in rapidly crystallized poly(ethylene terephthalate). *Journal of Polymer Science: Polymer Physics Edition* **1978**, *16* (1), 159-169. DOI: 10.1002/pol.1978.180160114.

(35) Chang, B. H.; Zeigler, R.; Hiltner, A. Chlorinated high density polyethylene. I. Chain characterization. *Polymer Engineering & Science* **1988**, *28* (18), 1167-1172. DOI: https://doi.org/10.1002/pen.760281806 (acccessed 2023/08/21).

(36) Chang, B. H.; Dai, J. W.; Siegmann, A.; Hiltner, A. Chlorinated high density polyethylene. II. Solid state structure. *Polymer Engineering & Science* **1988**, *28* (18), 1173-1181. DOI: https://doi.org/10.1002/pen.760281807 (acccessed 2023/08/21).

(37) Stoeva, S. Structural and conformational changes in solid-phase chlorinated polyethylene. *J. Appl. Polym. Sci.* **2004**, *94* (1), 189-196. DOI: https://doi.org/10.1002/app.20854 (acccessed 2023/08/21).

(38) Fahs, G. B.; Benson, S. D.; Moore, R. B. Blocky Sulfonation of Syndiotactic Polystyrene: A Facile Route toward Tailored Ionomer Architecture via Postpolymerization Functionalization in the Gel State. *Macromolecules* **2017**, *50* (6), 2387-2396. DOI: 10.1021/acs.macromol.7b00408.

(39) Orler, E. B.; Yontz, D. J.; Moore, R. B. Sulfonation of syndiotactic polystyrene for model semicrystalline ionomer investigations. *Macromolecules* **1993**, *26* (19), 5157-5160. DOI: 10.1021/ma00071a027.

(40) Noble, K. F.; Troya, D.; Talley, S. J.; Ilavsky, J.; Moore, R. B. High-Resolution Comonomer Sequencing of Blocky Brominated Syndiotactic Polystyrene Copolymers Using 13C NMR Spectroscopy and Computer Simulations. *Macromolecules* **2020**, *53* (21), 9539-9552. DOI: 10.1021/acs.macromol.0c01630.

(41) Anderson, L. J.; Yuan, X.; Fahs, G. B.; Moore, R. B. Blocky Ionomers via Sulfonation of Poly(ether ether ketone) in the Semicrystalline Gel State. *Macromolecules* **2018**, *51* (16), 6226-6237. DOI: 10.1021/acs.macromol.8b01152.

(42) Kasprzak, C. R.; Anderson, L. J.; Moore, R. B. Tailored sequencing of highly brominated Poly(ether ether ketone) as a means to preserve crystallizability and enhance Tg. *Polymer* **2022**, *251*, 124918. DOI: https://doi.org/10.1016/j.polymer.2022.124918.

(43) Anderson, L. J.; Moore, R. B. Sulfonation of blocky brominated PEEK to prepare hydrophilic-hydrophobic blocky copolymers for efficient proton conduction. *Solid State Ionics* **2019**, *336*, 47-56. DOI: https://doi.org/10.1016/j.ssi.2019.03.006.

(44) Chen, Z.; Jenkins, M. J.; Hay, J. N. Annealing of poly (ethylene terephthalate). *Eur. Polym. J.* **2014**, *50*, 235-242. DOI: 10.1016/j.eurpolymj.2013.11.004.

(45) Liu, Y.; Yin, L.; Zhao, H.; Song, G.; Tang, F.; Wang, L.; Shao, H.; Zhang, Y. Lamellar and fibrillar structure evolution of poly(ethylene terephthalate) fiber in thermal annealing. *Polymer* **2016**, *105*, 157-166. DOI: https://doi.org/10.1016/j.polymer.2016.10.031.

(46) Wang, Z. G.; Hsiao, B. S.; Sauer, B. B.; Kampert, W. G. The nature of secondary crystallization in poly(ethylene terephthalate). *Polymer* **1999**, *40* (16), 4615-4627. DOI: https://doi.org/10.1016/S0032-3861(99)00067-1.

(47) Zhu, J.-B.; Watson, E. M.; Tang, J.; Chen, E. Y. X. A synthetic polymer system with repeatable chemical recyclability. *Science* **2018**, *360* (6387), 398-403. DOI: 10.1126/science.aar5498 (acccessed 2024/04/08).

(48) Colomines, G.; Robin, J.-J.; Tersac, G. Study of the glycolysis of PET by oligoesters. *Polymer* **2005**, *46* (10), 3230-3247. DOI: https://doi.org/10.1016/j.polymer.2005.02.047.

(49) Jehanno, C.; Demarteau, J.; Mantione, D.; Arno, M. C.; Ruipérez, F.; Hedrick, J. L.; Dove, A. P.; Sardon, H. Selective Chemical Upcycling of Mixed Plastics Guided by a Thermally Stable Organocatalyst. *Angew. Chem. Int. Ed.* **2021**, *60* (12), 6710-6717. DOI: 10.1002/anie.202014860.

(50) Arifuzzaman, M.; Sumpter, B. G.; Demchuk, Z.; Do, C.; Arnould, M. A.; Rahman, M. A.; Cao, P.-F.; Popovs, I.; Davis, R. J.; Dai, S.; et al. Selective deconstruction of mixed plastics by a tailored organocatalyst. *Materials Horizons* **2023**, *10* (9), 3360-3368. DOI: 10.1039/d3mh00801k.

CHAPTER 3: REACTIVITY OF CARBONATES AND ESTERS IN THE DEPOLYMERIZATION OF PLASTIC WASTE

Shelby Watson-Sanders,[1] Kendra Day,[1] Sarah Barber,[1] Landri Wilcox,[1] Clarissa Thompson,[2] Gregg Beckham,[2] Nick Galan,[3] Jackie Zheng,[3] Tomonori Saito,[3] Mark Dadmun[1,*]

[1]Chemistry Department, University of Tennessee, Knoxville, TN 37996

[2]National Renewable Energy Laboratory, Golden, CO

[3]Oak Ridge National Laboratory, Oak Ridge, TN

* Corresponding Author (Dad@utk.edu)

In this article, I was responsible for designing polymer depolymerization with bisphenol-A and characterization of all polymers. Sarah Barber and Landri Wilcox performed all of the swelling studies together. Dr. Saito's and Dr. Beckham's students performed molecular weight analysis of PET and Tritan$^{TM.}$ Dr. Mark Dadmun organized this project and facilitated the writing of the manuscript.

3.1 Abstract

This research investigates how polymer crystallinity, solvent-polymer compatibility, catalyst type, and carbonyl reactivity influence the rate of the heterogeneous depolymerization of carbonyl containing polymers. Carbonyl-containing polymers are more easily chemically recycled than chain-polymerized polymers due to the reactivity of the carbonyl group. However, limited research exists to elucidate the molecular-level processes that control the depolymerization rate of these polymers. In this study, the depolymerization of Tritan™ (an amorphous polyester), polyethylene terephthalate (PET, a semi-crystalline polyester), and bisphenol polycarbonate (PC, an amorphous carbonate) by glycolysis at 180 °C using an organo-salt catalyst was monitored. The diol reactants, ethylene glycol (EG) and bisphenol-A (BPA), were selected for their similarity of structure to the repeat units of PET and PC, respectively. These results show that polymer-diol affinity significantly impacts the depolymerization rate,

compatible with the reaction between polymer-diol pairs transitioning from an initial heterogeneous reaction to a homogeneous reaction more quickly, which increases the depolymerization rate. Initial reactions were catalyzed using TBD:MSA, which facilitated glycolysis through moderate basicity. To further investigate the influence of catalyst strength, TBD, a stronger base, was employed. Unlike TBD:MSA, TBD rapidly dissolved all polymers within 4 minutes, potentially due to the lone pair on its amine group acting as a Lewis base. This lone pair likely interacts with polar groups, such as carbonyl or hydroxyl functionalities, disrupting intermolecular forces and enhancing polymer compatibility with solvents. These interactions accelerate the transition from heterogeneous to homogeneous depolymerization, significantly increasing reaction rates. Surprisingly, polymer crystallinity does not significantly affect the depolymerization rate, despite the inhibition of glycol transport by polymer crystals. Additionally, these results utilizing TBD:MSA show that ester-containing polymers (Tritan™ and PET) are more easily chemically recycled than carbonate-containing polymers (PC), even when solvent-polymer compatibility is low. These results show that the rate of depolymerization varies with polymer structure, with Tritan™ and PET showing similar rates, while PC depolymerizes more slowly. This slower depolymerization of PC is attributed to the higher activation energy required for acyl cleavage of the carbonate relative to that of the ester. However, with TBD as the catalyst, PC depolymerizes more rapidly due to a mechanism involving deprotonated phenol groups forming phenoxide ions, which act as highly nucleophilic species to promote efficient chain scission of the carbonate linkages. This contrasts with the slower depolymerization of PC observed with weaker catalysts due to the higher activation energy required for acyl cleavage of the carbonate relative to the ester. Overall, these findings indicate that solvent-polymer compatibility and catalyst type significantly impact the reaction

rate by governing the transition between the heterogeneous and homogeneous stages. At the same time, the reactivity of the carbonyl group and nucleophile dominates the overall depolymerization rate. Additionally, these results suggest that polymers with poor solubility in water, such as crystalline polymers, may not transition from the heterogeneous reaction during environmental degradation, potentially contributing to the formation of nanoplastics in the environment.

3.2 Introduction

An increasing amount of virgin plastic is produced yearly, with 400 million metric tons produced in 2021.[1] After reaching their end-of-life cycle, the destination of these plastics must be more environmentally friendly, as 79% of plastic is discarded in landfills and 12% is incinerated.[1-5] Only 9% of plastic is recycled, mainly through mechanical recycling, which is only feasible for a number of cycles, as it has been shown to degrade the polymer.[1-5] More sustainable manufacturing and recycling processes, including chemical recycling, are essential to decrease reliance on petroleum resources and the volume of polymer waste.[6-8] The design of efficiently recyclable polymers[9-12] will move society towards this goal, however in parallel, there must be efforts to understand the chemical processes that occur during chemical recycling of current commercially available polymers to develop processes to remediate current waste, as well as provide insight into how to create tomorrow's polymers that are more sustainable.

There is extensive interest in understanding and optimizing the chemical recycling of polyesters and polycarbonates, as the carbonyl group within the polymer chain is reasonably reactive and susceptible to nucleophilic attack.[13, 14] For example, investigations have examined the depolymerization of consumer waste polycarbonate (PC), polyethylene terephthalate (PET), polyamide (PA), and polyurethane (PU) via glycolysis in the same reaction vial.[1, 15] Specifically,

in these studies, the reaction temperature selectivity controlled the polymer that depolymerizes by chain scission. In these studies, PC depolymerizes to monomer at 130 °C, while all other polymers remain intact. Increasing the temperature to 180 °C depolymerizes PET.[1, 15] While utilizing reaction temperature to control chain scission of specific polymer chains and their carbonyl groups is impressive and novel, a more thorough understanding of the important parameters that control the rate of depolymerization of polycarbonate and polyesters will offer foundational insight that will guide future design of more readily depolymerized polymers and depolymerization processes. Our previous studies show that the depolymerization of PET by glycolysis involves consecutive steps that include the swelling of the PET flake with ethylene glycol (EG), followed by the catalyzed reaction of the hydroxyl group on the EG with the PET ester group in the amorphous part of the semi-crystalline PET. In this view, the penetration of the hydroxyl containing reactant (ethylene glycol in this case) into the PET solid, and the reaction of the hydroxyl and carbonyl are important consecutive steps in the process.

An additional important aspect of this research program revolves around the progress of the nature of the heterogeneous reaction as the reaction progresses. At the beginning of the reaction, the reaction is heterogeneously catalyzed as the polymer flake remains as a solid. As the reaction progresses, some depolymerized polymer product becomes soluble in the diol, while some polymer remains insoluble. Thus, at this stage, there are coexisting homogeneously catalyzed reactions of the soluble species and heterogeneously catalyzed reactions of the insoluble polymer. Finally, at the latest stages of the depolymerization, the polymer may be sufficiently depolymerized to be completely soluble in the diol, and thus the reaction is homogeneously catalyzed. These three stages are illustrated in **Figure 3.1** and are labeled as the heterogeneous stage, coexistence stage, and homogeneous stage. Clearly, the crystallinity of the

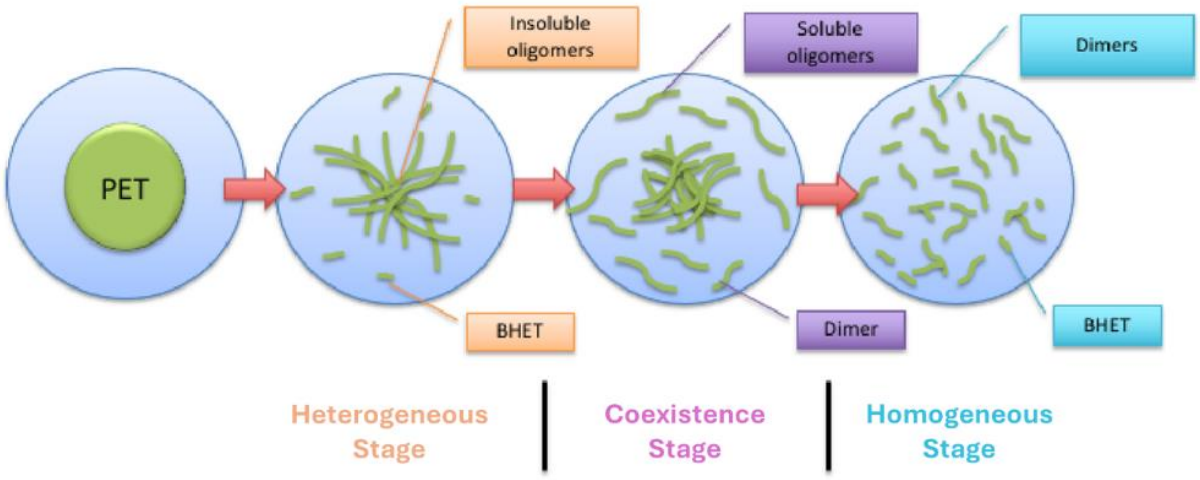

Figure 3.1 Illustration of the three stages of heterogeneous depolymerization as described in the text: the heterogeneous stage, the coexistence stage, and the homogeneous stage. The heterogeneous stage occurs when the polymer is not dissolved in the solvent. The coexistence stage involves both dissolved polymer and polymer not dissolved in the solvent. The homogeneous stage occurs when all polymers are dissolved in the solvent.

polymer and the relative solubility of the diol and polymer will impact the progression of the reaction through these three stages. In fact, the reaction may not reach the homogeneous stage if the depolymerized product is not sufficiently soluble in the diol.

Given this perspective, this study has focused on providing insight into the relative importance of the transport of the glycol (reactant) to the carbonyl and the reactivity of the carbonyl on the observed depolymerization rate. As the transport of the diol to the carbonyl will depend on polymer crystallinity and polymer/diol compatibility, this research program will evaluate the impact of polymer crystallinity, diol-polymer compatibility and carbonyl reactivity on the rate of heterogenous depolymerizations in order to tease out the relative importance of each parameter on the reaction progress.

Many studies have monitored the depolymerization of polyethylene terephthalate (PET) or polycarbonate (PC). PET is a regularly used plastic among the general public and has ~30 million tons produced in the United States annually.[4-6, 8, 16-27] Aromatic PC is a widely used plastic to form safety glasses, airplane windows, helmets, etc., with 3 million tons produced annually.[28, 29] Tritan™ copolyester is a newer, innovative thermoplastic developed within the last 20 years.[4, 5, 30] Moreover, Tritan™ has a PET-like molecular structure yet is amorphous, in contrast to the semi-crystalline PET.[30, 31] As amorphous polymers are more easy to dissolve than crystalline polymers, one might expect that the diols may penetrate and swell Tritan™ and PC more readily than PET.[4, 23, 32, 33] Yet, the relative importance of this swelling and the inherent reactivity of the chemical structures on the depolymerization rate is not well understood. Moreover, literature reports that the acyl cleavage of an ester is more favorable than the acyl cleavage of a carbonate,[34] where **the** acyl cleavage of carbonate groups as transesterification.

Scheme 3.1 illustrates the ester and carbonate functional groups of PET and PC. The literature often refers to the acyl cleavage of carbonate groups as transesterification and transcarbonation.[28, 29, 35, 36] For simplicity, in this study we will refer to the acyl cleavage of carbonate groups as transesterification.

Scheme 3.1 Ester and Carbonate containing polymers PET and PC respectively.

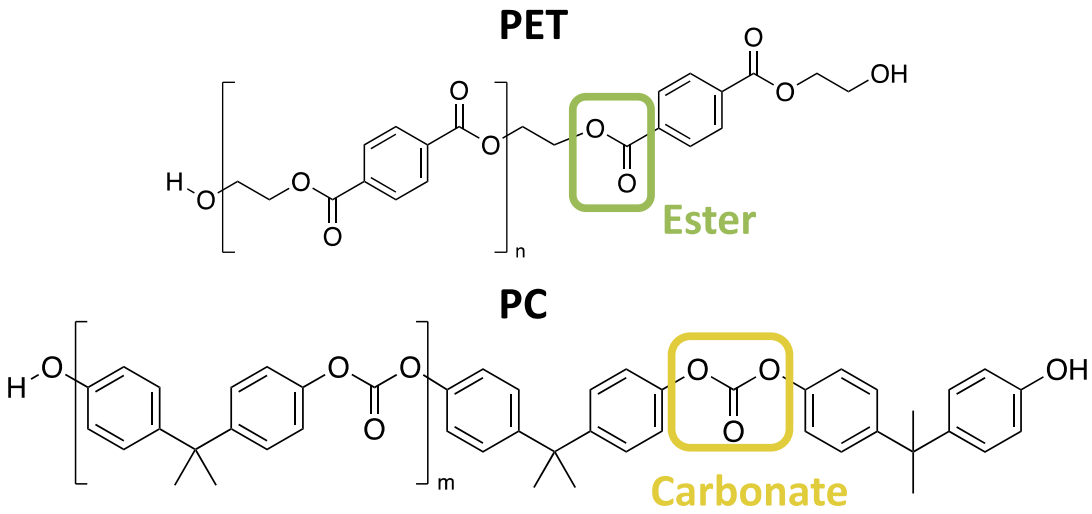

Thus, the depolymerization of polyethylene terephthalate (PET), aromatic polycarbonate (PC), and Tritan™ is examined in this study to provide insight into the impact of polymer crystallinity, polymer/diol solubility and carbonyl reactivity on the rate of depolymerization. These experiments will monitor the depolymerization of these polymers under the same conditions – at 180 °C using Triazabicyclodecene (TBD) and Methanesulfonic acid (MSA) as the organo-salt catalyst,[37, 38] using either ethylene glycol (EG) or bisphenol-a (BPA) as reactants. EG and BPA were the diols of choice as EG has a similar chemical structure to part of the polyesters, while the chemical structure of BPA mimics part of the repeat unit of the PC. The swelling of each polymer by ethylene glycol is also monitored to provide insight into the relative transport rate of the glycol into the solid polymer.

3.3 Experimental Methods

3.3.1 Materials

PET was sourced from commercial Coca-Cola bottles, which were washed and cut into squares (8 mm x 5 mm x 0.3 mm). Polycarbonate (PC) was sourced from a PC sheet from Home Depot, which was cut into squares with a Dremel (8 mm x 6 mm x 2.65 mm). Tritan™ LV copolyester pellets (2.91 mm x 2.72 mm x 1.92 mm) were sourced from Eastman Chemical Company and used as received. 1,5,7-Triazabicyclo[4.4.0]dec-5-ene (98.0+%, TCI America™), Methanesulfonic Acid (99%), Ethylene glycol, (99.8%, anhydrous, AcroSeal™, Thermo Scientific Chemicals), bisphenol-A (BPA), Tetrahydrofuran (THF), methanol, 20 mL vials, 100 mL round bottom flasks, 12.7x8mm stir bars, and 12x4.5mm stir bars were sourced from Fischer Scientific. All chemicals were used as received.

3.3.2 Catalyst

A 1:1 mixture of Triazabicyclodecene (TBD) and Methanesulfonic acid (MSA) is used as the organocatalyst to depolymerize the polymers, as has been previously reported.[37, 39] The salt catalyst was prepared by mixing TBD and MSA at 1:1molar ratios of acid to base at 80 °C until solidified. The product obtained was a transparent and homogenous solid.[37]

3.3.3 Reaction Conditions

3.3.3.1 Ethylene Glycol (EG) reactions

Ethylene Glycol (EG), TBD:MSA catalyst, carbonyl-containing polymer (PC, PET or Trian™) (20:0.5:1 molar ratio), and stir bar were all placed in a 20 mL reaction vial inside a glovebox, sealed with a septum, and transferred outside the glovebox into a 180 °C oil bath. Previous studies indicate that the glycolysis of PET and PC takes 2 hours and 4 hours, respectively, at 180 °C to reach completion.[15, 37] To analyze the evolution of the polymer chains during

depolymerization, the reaction was stopped at various reaction times, and the products were recovered and characterized as described below.[37] **Scheme 3.2** illustrates the glycolysis of the 3 polymers to isolate oligomers.

Scheme 3.2 Heterogenous glycolysis reaction of Tritan™, PET, and PC catalyzed by TBD:MSA to create oligomers.

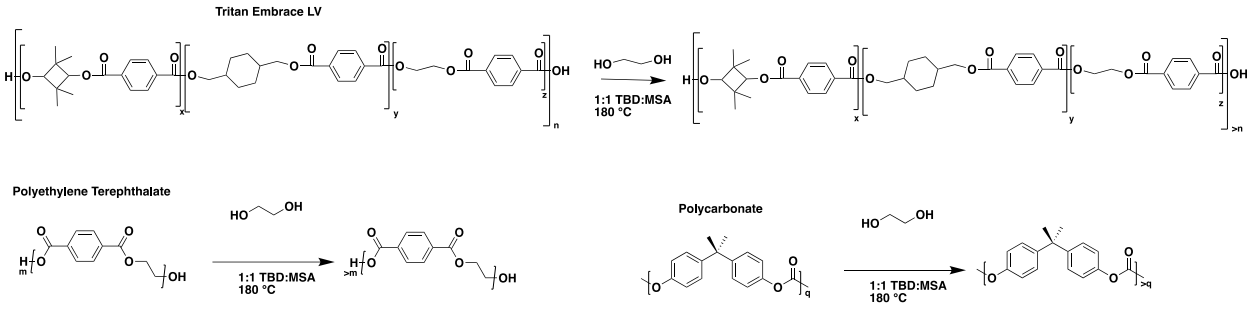

3.3.3.2 Product Workup

After the reaction was allowed to run for a set time, the reaction vials were removed from the oil bath. The ethylene glycol (EG) and depolymerization products that are soluble in EG were decanted from the reaction vials. The remaining solid PC that is insoluble in EG was washed with methanol three times by suspending it in 20 mL of methanol and stirring with a stir bar for 15 minutes. The remaining solid PET or Tritan™ that is insoluble in EG was washed with water three times. After the third wash and decant, the reaction vial containing the EG insoluble materials was set on a 70 °C hotplate overnight to evaporate any remaining methanol or water.

3.3.3.3 Bisphenol-A (BPA) reactions

TBD:MSA catalyst, BPA, polymer (0.5:20:1 molar ratios), and stir bar were all placed in a 100 mL round bottom flask inside a glovebox, sealed with a septa, and transferred outside the glovebox into a 180 °C oil bath. To analyze the evolution of the polymer chains during PC and PET depolymerization, the reaction was stopped at various reaction times, and the products were

recovered and characterized as described below. **Scheme 3.3** illustrates the depolymerization of the 2 polymers to isolate oligomers.

Scheme 3.3 Heterogenous PC and PET reaction with Bisphenol-A catalyzed by TBD:MSA to create new monomers

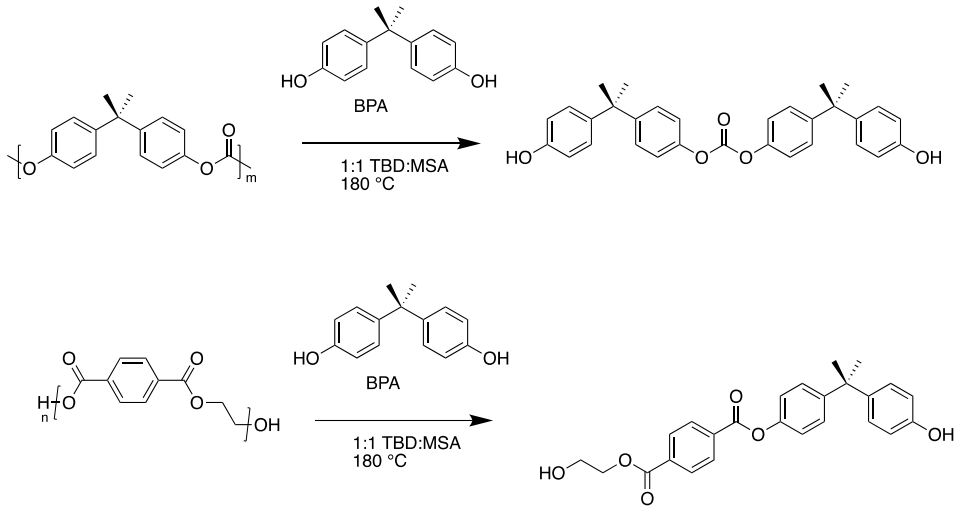

3.3.3.4 Product Workup

After the reaction was allowed to run for a set time, the round bottom flasks were taken from the oil bath. The BPA and polymer mixture were decanted into 200 mL of methanol, as BPA is soluble in methanol, and PC and PET are not. The methanol mixture was vacuum filtered to isolate BPA and methanol insoluble oligomers. After the vacuum filtration, the BPA and methanol insoluble oligomers were set on a 70 °C hotplate overnight to evaporate any remaining methanol. Then, BPA insoluble polymer flakes were separated from the methanol insoluble oligomers. These two oligomers can be separated as the remaining BPA insoluble polymer flakes in the reaction vessel are visible, while the BPA soluble oligomers are not. Upon crashing this reaction mixture into methanol, the BPA soluble oligomers precipitate as powder, as seen in **Figure 3.2**. In **Figure 3.2**, the BPA insoluble oligomers are the remaining polymer flakes

highlighted in green, and the methanol insoluble oligomers are the polymer powder highlighted in blue.

3.3.4 Depolymerization Product Characterization

3.3.4.1 Size Exclusion Chromatography (SEC)

Size-exclusion Chromatography determined the molecular weight characteristics of the depolymerization products as a function of reaction time. The SEC analyses for PC were completed at the Institute of Advanced Materials and Manufacturing (IAMM) using a THF Gel permeation Chromatograph/Size Exclusion Chromatograph (GPC/SEC). This analysis used a Tosoh EcoSEC GPC system and a refractive index (RI) detector calibrated to polystyrene (PS) standards ranging from 600 Da to 2230 kDa. The column set in the instrument include the following: 2 Tosoh TSKgel SuperMultiporeHZ-M (4.6x150 mm and 4 μm) and a TSKgel SuperMultiporeHZ-M guard. The samples were run with a Flow Rate of 0.35 mL/min and an analysis temperature of 40 °C. PC samples were dissolved in THF overnight at a 1.5 mg/mL concentration before being filtered (0.2 μm PTFE filter) and placed in the autosampler.
The SEC analyses for PET and Tritan^{TM} depolymerized with EG were completed in 1,1,1,3,3,3-hexafluoroisopropanol (HFIP). This analysis used an Agilent 1260 Infinity II HPLC stack connected with a Wyatt miniDAWN TREOS (MALS) and Wyatt Optilab T-rEX (dRI) detector. A poly(methyl methacrylate) (PMMA) standard and commercial PET substrate were used to verify system performance. Molar mass values were calculated assuming a dn/dc of 0.191 and 0.257 mL/g for PMMA and PET, respectively. The mobile phase and sample prep used HFIP amended with 20 mM of sodium trifluoroacetate (NaTFAc). The HPLC used 3 Agilent PL HFIPgel 250 x 4.6 mm columns attached in series with a matching guard column. PET and Tritan^{TM} samples were dissolved in HFIP for five days at a ~5 mg/mL concentration before

being filtered (0.2 µm) and placed in the autosampler. The samples were run with a flow rate of 0.35 mL/min and a column temperature of 40 °C.

The SEC analyses of the depolymerization of PET with BPA were completed at the Oak Ridge National Lab using GPC/SEC. PET samples were dissolved in HFIP for five days. Samples were then filtered through a 0.2 µm syringe filter into an autosampler vial. This analysis was performed on an Agilent 1260 Infinity II LC system equipped with an Agilent MiniMIX-C Guard column (PL Gel 5 µM, 50 x 4.6 mm) and two Agilent PL HFIPgel (250 x 4.6 mm, 9 µm). The mobile phase was HFIP at a flow rate of 0.3 mL/min (an Agilent EasiVial PMMA standard, containing four discrete molecular weights, was used for calibration). Detection was conducted using a differential refractive index (RI) detector, a light scattering detector with two angles at 90º and 15º. Number-average molecular weights (M_n), weight-average molecular weights (M_w), and dispersities ($Đ = M_w / M_n$) were calculated based on the system calibration and by assuming 100% mass elution from the columns using the Agilent GPC/SEC software.

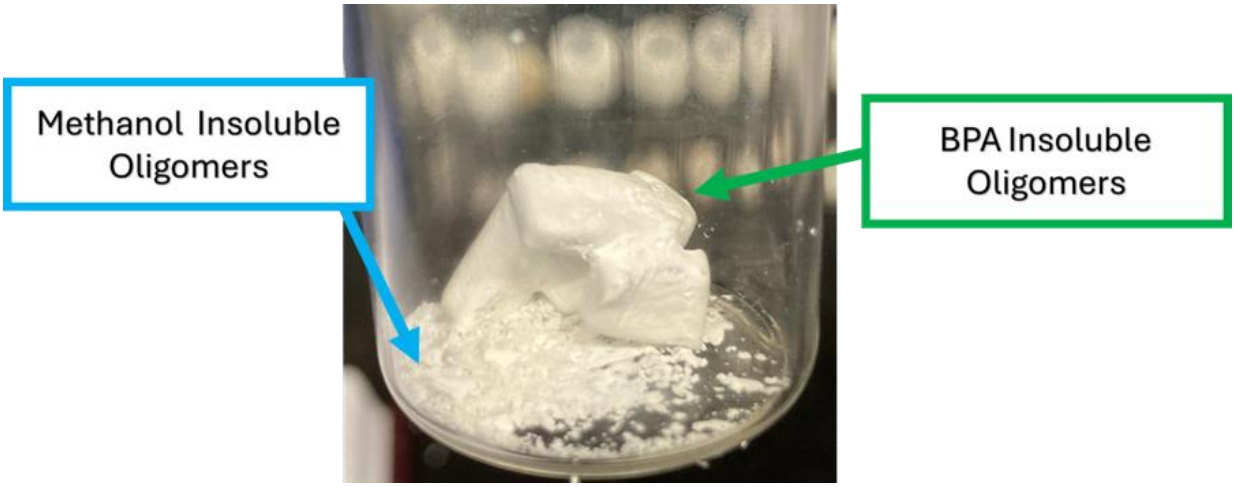

Figure 3.2 Picture of the products of polycarbonate (PC) that is depolymerized with BPA for 10 minutes. The BPA insoluble oligomers are noted in green, while the Methanol insoluble oligomers are noted in blue.

3.3.4.2 Normalized Swelling [%] of Polymers by EG

Half a gram of polymer (PET, Tritan, or PC) was placed in a 20 mL vial with EG and a stir bar in a 1:35 molar ratio of polymer to solvent, where the vial was sealed with a septa. Samples were mixed and heated in a 180 °C oil bath for various times (30, 60, 90, and 135 minutes) following the swelling procedure from Najmi.[23] Swelling times were limited to these times to prevent the dissolution of the polymer into the solvent. After a specific time, the solvent was decanted hot from the vial and rinsed with DI water for 15 minutes. Then, the water was decanted, rinsed again for another 15 minutes, and repeated. The samples were heated at 75 °C for 72 hours to evaporate off the remaining water before being weighed. The mass of the sample was then determined and used to calculate the normalized swelling using **Equation 3.1**, where m_f is the final mass, m_i is the initial mass and n_{flakes} is the number of flakes in the sample. **Equation 3.1** combines the variable swelling ratio of different flakes to obtain the normalized swelling per polymer flake, as the dimensions of the flakes vary between the three polymers of interest.[23, 40] Measurements were stopped when the polymer started to dissolve, as demonstrated by a significant decrease in the normalized swelling.

Equation 3.1
$$\boldsymbol{Normalized\ Swelling}\ [\%] = \frac{\frac{m_f - m_i}{m_i}}{n_{flakes}} * \mathbf{100}$$

3.4 Results & Discussion

3.4.1 Starting Material Characterization

Since Tritan™, Polyethylene Terephthalate (PET), and Polycarbonate (PC) originate from different sources—Tritan™ from Eastman Chemical Company and PET and PC from consumer waste—the starting molecular weights and crystallinities of the polymers were characterized. The results are presented in **Figure 3.3** and **Figure A.1**. **Figure 3.3** displays the

initial polymer molecular weights for all three polymers, while **Figure A.1** presents the DSC curves for PET and Tritan™ before the depolymerization reaction begins.

According to **Figure 3.3**, PC and PET have similar weight average molecular weights (M_w), represented in light purple, whereas Tritan™ has a lower M_w than both. PET also has the largest number-average molecular weight (M_n), indicated in dark purple, followed by Tritan™ and PC. This indicates that the consumer waste-derived PC exhibits the largest dispersity (Đ) among the three starting materials. PET and Tritan™ have comparable dispersities of 1.5 and 1.4, respectively, although they differ in crystallinity. **Figure A.1** demonstrates that PET has a crystalline melting peak starting at 240 °C, while Tritan™ does not exhibit a crystalline melting peak, indicating that it is amorphous.

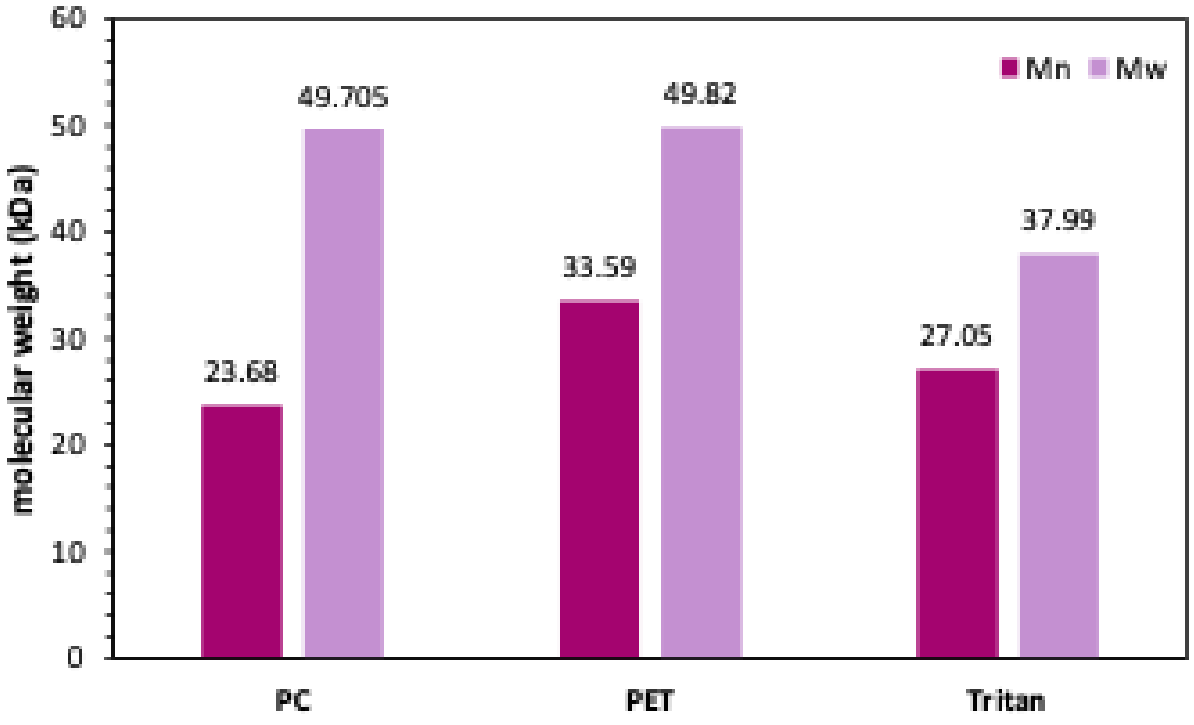

Figure 3.3 Starting molecular weights of polymers before depolymerization.

3.4.2 Ethylene Glycol depolymerization of PET, PC, and Tritan™

Both the ester-containing polymers (Tritan™ and PET) and the carbonate-containing polymer (PC) were depolymerized under the same reaction conditions provide insight into the importance of carbonyl reactivity on the rate of depolymerization. **Figure 3.4** shows the changes in the number-average molecular weight (M_n), weight-average molecular weight (M_w), and dispersity (Đ) for the EG insoluble fraction of all three polymers as a function of glycolysis reaction time. In **Figure 3.4 (a)**, the M_n (dark green), M_w (light green), and Đ (black line) of Tritan™ decrease from 27 kDa, 37 kDa, and 1.4 to 6 kDa, 7 kDa, and 1.2, respectively, over a 75-minute reaction period. Meanwhile, **Figure 3.4 (b)** reveals that the M_n (dark blue), M_w (light blue), and Đ (purple line) of PET decline from 33 kDa, 49 kDa, and 1.5 to 8 kDa, 10 kDa, and 1.2, respectively, over a 105-minute reaction period.

Interestingly, despite Tritan™ and PET having slightly different initial molecular weights and the fact that Tritan™ is amorphous while PET is semi-crystalline, the depolymerization of both ester-containing polymers occurs at similar rates, resulting in comparable molecular weight oligomers at similar reaction times. These two polymers have similar chemical structures, chain lengths, and dispersities, yet PET is semi-crystalline while Tritan™ is amorphous.[30, 31] The similarity of chain evolution during their depolymerization serves as an initial indication that crystallinity of the polyester does not significantly influence the rate of depolymerization by glycolysis. Furthermore, our previous studies[39] and others have demonstrated that PET depolymerization occurs via the reaction of glycol with the ester groups in the amorphous phase, necessitating the transport of glycol throughout the flake.[41, 42] As crystalline polymers are more difficult to dissolve than amorphous polymers,[33, 43] one might expect the transport of ethylene glycol (EG) into the amorphous phase of PET to be slower than that in Tritan™. However, given

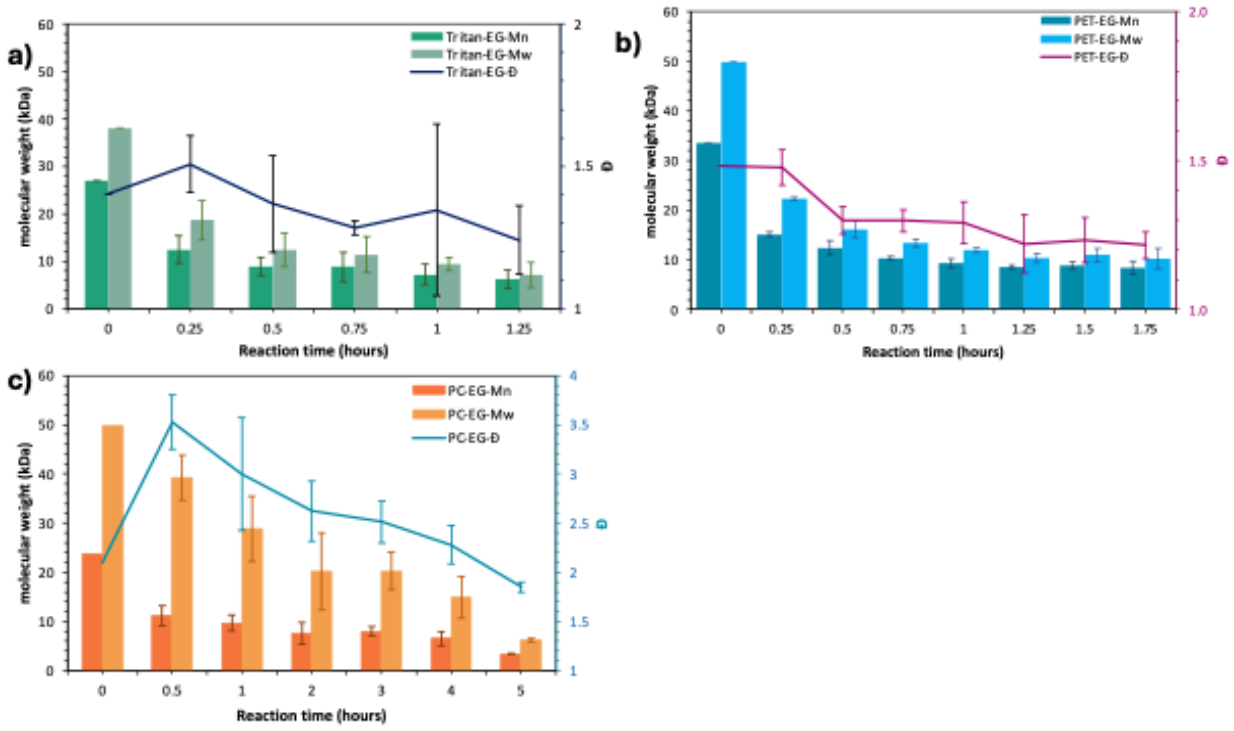

Figure 3.4 (A) The change in Tritan molecular weight as a function of reaction time: M_n (dark green), M_w (green), and dispersity (Đ) (purple). **(B)** The change in PET chain length as a function of reaction time: M_n (dark blue), M_w (blue), and Đ (purple). **(C)** The change in PC chain length as a function of reaction time: M_n (orange), M_w (yellow), and Đ (blue).

that the rate of depolymerization via glycolysis is comparable for both polymers, this data indicates that the transport of glycol to the carbonyl does not control the rate of this depolymerization reaction.

Figure 3.4 (c) displays the evolution of molecular weight of PC during depolymerization, plotting M_n (dark orange), M_w (light orange), and Đ (blue line) of PC as a function of reaction time. The data indicates a decrease in M_n and M_w with increased depolymerization time; however, it takes almost four to five times longer to depolymerize PC into oligomers compared to the depolymerization of PET or Tritan™. Notably, the Đ of the PC oligomers that emerge from the depolymerization initially increases during the first half-hour of the reaction before decreasing at later times, with Đ falling slightly below 2 after five hours, contrasting the behavior observed in the polyesters. Overall, **Figure 3.4** clearly demonstrates that PC depolymerizes more slowly than PET or Tritan™ under identical reaction conditions.

To evaluate the importance of the transport of ethylene glycol (EG) to the carbonyl group in the solid polymer on the rate of depolymerization, swelling experiments were conducted. This swelling process is the initial step in polymer dissolution, so discussing this process can provide valuable insights into the importance of glycol transport in the depolymerization process. Polymer dissolution is known to be a multistep process,[9, 11-13, 43] where the solvent first diffuses into the polymer, causing it to swell. In amorphous polymers, the chains then begin to disentangle and dissolve into the bulk solution. In contrast, the diffusion of the solvent is hindered in crystalline polymers due to confinement by the crystals, which adds an additional step—polymer decrystallization—to the dissolution process.[33] Thus, understanding the rate of swelling in the polymers, and consequently the transport of EG into the polymer during

depolymerization, will provide quantitative evidence of the importance of this process on the rate of depolymerization.

Figure 3.5 shows the percent swelling per polymer flake as a function of the square root of swelling time. Tritan™ (green) and polycarbonate (PC) (orange) absorb ethylene glycol more quickly than polyethylene terephthalate (PET) (blue), where the normalized swelling amounts and rates being quite similar for both amorphous polymers. PET swells to a lesser extent per flake, which we attribute to the inhibition of glycol diffusion into the polymer flake by the PET crystallinity.[33] Interestingly, despite Tritan™ and PET having similar chemical structures and therefore comparable affinities for EG, their swelling behaviors differ. The rate at which glycol diffuses into Tritan™ is more similar to that of EG diffusing into PC, even though these two have very different chemical structures. Importantly, both PC and Tritan™ are amorphous. Clearly, in these systems, the transport of glycol into the polymer flake is influenced more by the presence or absence of polymer crystals than by the specific affinity between the polymer and glycol. Moreover, both amorphous polymers begin to dissolve at later times in the swelling tests, whereas the semicrystalline polymer (PET) does not. We interpret this to indicate that EG does not disrupt the crystalline structure of PET but merely swells the amorphous phase, as shown in previous studies.[44] The data in **Figure 3.5** clearly demonstrate that the swelling of the polymer flake by EG is primarily governed by polymer crystallinity and is largely independent of the chemical structure of the polymer in these studies.

Figure 3.5 reveals that the amorphous polymers, Tritan™ and PC, swell similarly and more quickly with more glycol than PET. However, Tritan™ and PC do not depolymerize at the same rates. Likewise, while Tritan™ absorbs glycol faster than PET, both polymers depolymerize at comparable rates. Put another way, despite the more rapid transport of glycol

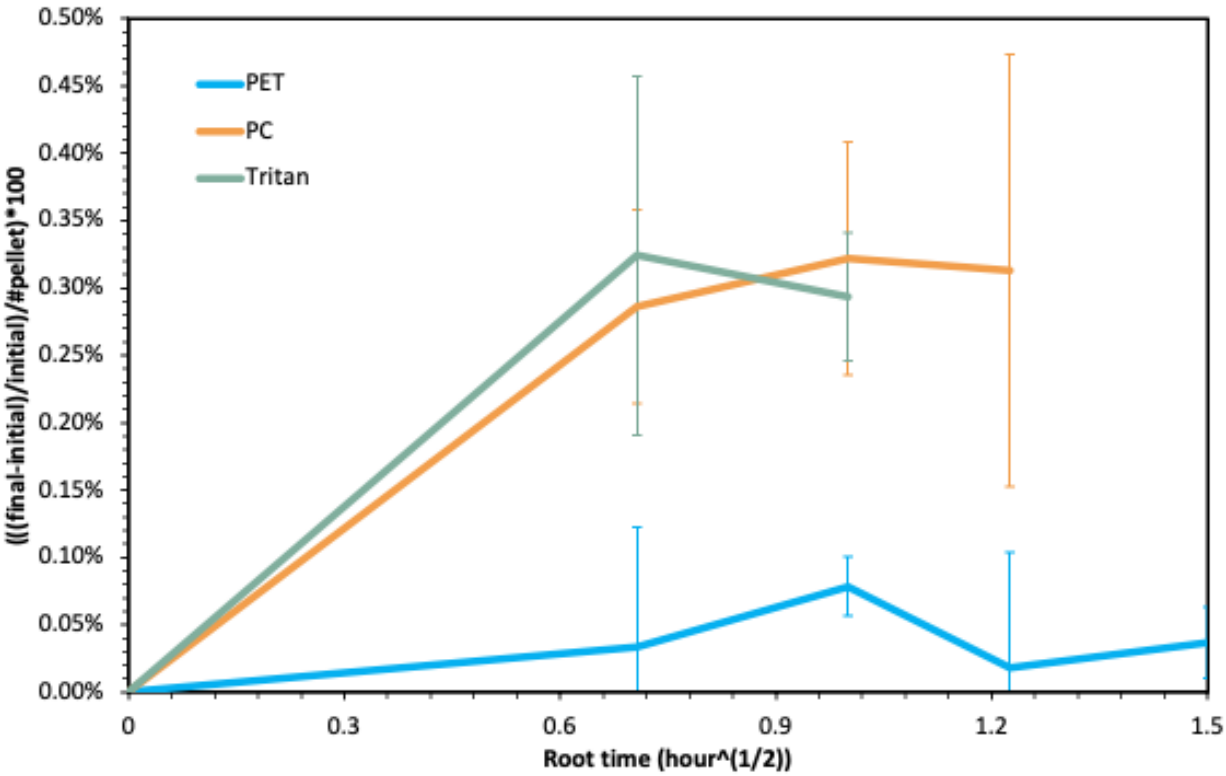

Figure 3.5 Normalized Swelling per Polymer Flake of PET (blue), PC (orange), and Tritan™ (green) with EG at 180 °C as a function of the square root of time.

into Tritan than in PET, Tritan™ does not depolymerize more quickly than PET. These results therefore demonstrate that the depolymerization by glycolysis reaction of these polymers is not limited by the diffusion of the glycol to the carbonyl. We interpret the fact that both ester-containing polymers depolymerize faster than the carbonate-containing polymers despite the observed differences in swelling to demonstrate the importance of the reactivity of the carbonyl carbon on the depolymerization reaction.

To provide more insight into the importance of carbonyl reactivity on depolymerization rates, **Figure 3.6** plots the percent decrease in M_n and M_w of all three polymers over the course of the depolymerization reaction. Given their different starting molecular weights, this figure provides a clear quantitative overview of the variation in chain length with reaction time for the EG-insoluble depolymerization product. The data in **Figure 3.6** emphasizes that PET and Tritan™ depolymerize at similar rates, as evidenced by the similar decrease in $\%M_w$ (light blue for PET and light green for Tritan™) and $\%M_n$ (dark blue for PET and dark green for Tritan™). Interestingly, both PET and Tritan™ show a more rapid decrease in $\%M_w$ relative to $\%M_n$. Since M_w correlates with higher molecular weight polymers in the sample, this suggests that the glycolysis reactions more readily break larger polyester chains than smaller ones.

Figure 3.6 also shows that the M_n (dark orange) and M_w (light orange) of PC decrease by 50% within the first hour of the reaction, only reaching 20% of the original molecular weight after 5 hours. In contrast, a similar reduction in chain length for PET and Tritan™ takes approximately 75 minutes of reaction time. Thus, **Figure 3.6** demonstrates that polymers containing esters depolymerize at a similar rate, regardless of crystallinity, while the polymer with carbonate functionality depolymerizes more slowly than those with ester groups. Interestingly, PC shows a more rapid decrease in $\%M_n$ relative to $\%M_w$ until 5 hours into the

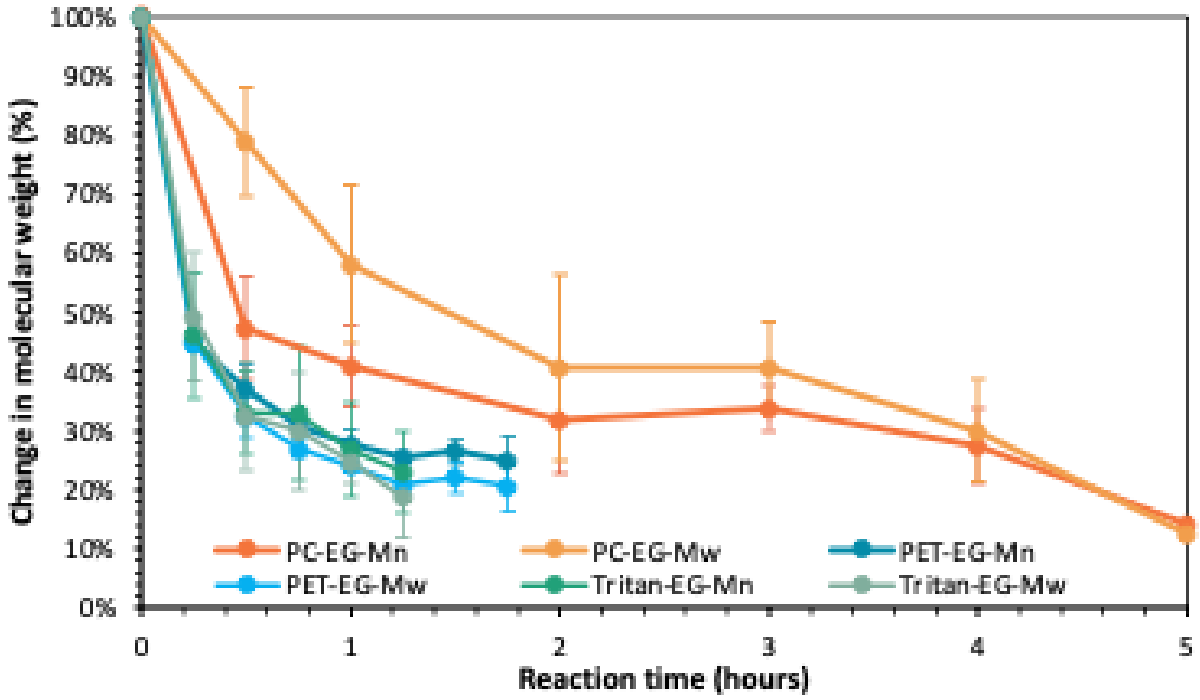

Figure 3.6 Change in molecular weight during depolymerization via glycolysis as a function of reaction time. Data for Tritan^{TM}: M_n (dark green) and M_w (green); Data for PET: M_n (dark blue) and M_w (blue) Data for PC: M_n (orange) and M_w (yellow).

reaction when the Đ falls slightly below 2. Since M_w correlates with higher molecular weight polymers in the sample, this suggests that glycolysis reactions more readily break shorter polycarbonate chains than larger ones.

A review of the relative reactivity of the carbonate carbonyl and ester carbonyl provides further fundamental insight to these observations. Literature reports that esters react via acyl cleavage, while carbonates react via alkyl cleavage, where acyl cleavage refers to the process that breaks the bond between a carbonyl group (C=O) and the adjacent atom, typically resulting in the release of an acyl group. In contrast, alkyl cleavage involves breaking the bond between two alkyl (carbon-hydrogen) groups, often necessitating harsher conditions. These distinct mechanisms influence the reactivity of organic molecules such as esters, amides, and ethers under specific circumstances.[34, 45-47]

Figure 3.7 shows the relative activation energies of esters (left) and carbonates (right) undergoing nucleophilic acyl/acyl-type substitution and Sn2 substitution at the alkyl oxygen.[34, 45-47] Nucleophilic acyl/acyl-type substitution is a reaction pathway that proceeds through a tetrahedral intermediate and is referred to as 'nucleophilic acyl substitution' in the case of esters. This study has adopted 'nucleophilic acyl-type substitution' as the nomenclature to encompass the analogous reaction occurring with carbonates. Sn2 substitution refers to an unimolecular substitution that occurs at the alkyl oxygen, which has been previously observed in ester hydrolysis.[48] In this figure, nucleophilic acyl/acyl-type substitution of esters and carbonates is shown in light blue and pink, respectively, and Sn2 substitution at the alkyl oxygen of esters and carbonates is shown in blue and red, respectively. Esters tend to undergo substitution at the sp^3 carbonyl carbon (nucleophilic acyl substitution) because the activation energy for Sn2 substitution at the alkyl oxygen of the ester is considerably higher.[34, 45-47] Carbonates tend to

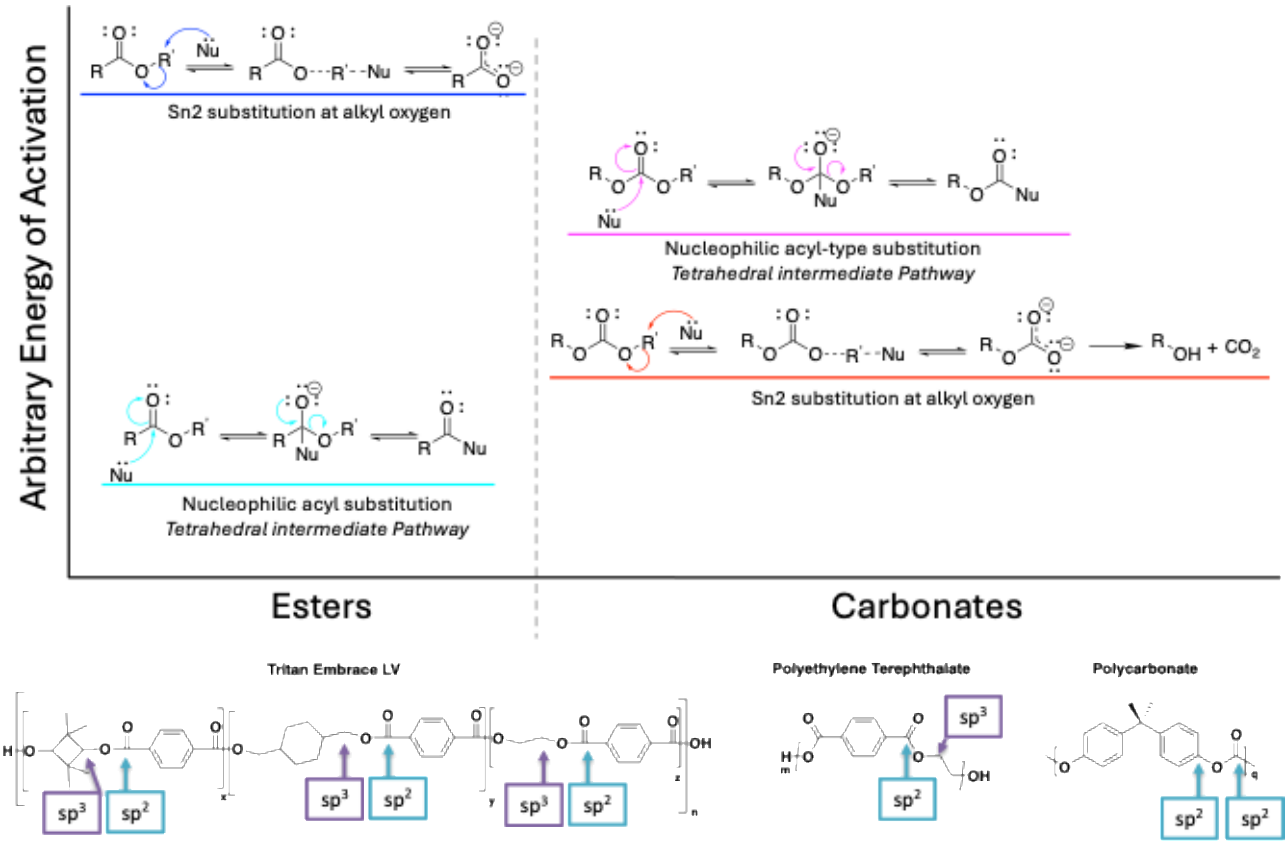

Figure 3.7 Activation Energies of nucleophilic acyl/acyl-type substitution (or the tetrahedral intermediate pathway) and Sn2 substitution at the alkyl oxygen of ester and carbonate-containing polymers

undergo Sn2 substitution at the alkyl oxygen on an sp^2 carbon.[28, 29, 35, 36] Carbonates can undergo nucleophilic acyl-type substitution; however, this reaction has a higher activation energy than Sn2 substitution at the alkyl oxgyen and a higher activation energy than the nucleophilic acyl substitution of an ester. [34]

Figure 3.7 also documents the hybridization of the three polymers examined in this study at and around the carbonyl carbon, highlighting the processes of sp^2 nucleophilic acyl/acyl-type substitution (light blue) and sp^3 Sn2 substitution at the alkyl oxygen (purple). Both Tritan™ and PET possess sp^2 and sp^3 carbon atoms that can undergo cleavage. However, existing literature indicates that nucleophilic acyl substitution at the sp^2 carbon is favored, facilitating transesterification during the depolymerization of these polymers.[34, 49] As demonstrated in **Figure 3.6**, the rates of of nucleophilic acyl substitution of an ester by PET and Tritan™ are comparable despite the differing alkyl groups present (i.e., secondary and tertiary alkyl groups) that influence the reactivity of Sn2 substitution at the alkyl oxygen.[50-52] The TBD:MSA catalyst mixture used in our experiments likely creates an amphoteric or "buffered" environment**,** which combines both acidic and basic sites to stabilize proton transfer and promote selective activation at the acyl carbon.[38, 53] This balanced catalytic environment facilitates nucleophilic attack on the ester carbonyl carbon while moderating the basicity or acidity, helping to avoid excessive cleavage reactions at sensitive sites.[53-57]

Notably, the literature supports that Sn2 substitution at the alkyl oxygen at an sp^3 carbon is preferred for carbonates, as basic or neutral conditions tend to favor this pathway over nucleophilic acyl-type substitution.[34, 46, 47] However, aromatic polycarbonate (PC) lacks sp^3 carbons at/near the carbonate group, necessitating a less favorable nucleophilic acyl-type substitution at the sp^2 carbonyl carbon. **Figure 3.6** further illustrates this, showing that the

slower depolymerization rate of PC compared to ester-containing polymers correlates with the reduced favorability of nucleophilic acyl-type substitution. The TBD:MSA mixture creates an environment that enables selective cleavage, enhancing depolymerization. While both ester and carbonate groups undergo nucleophilic acyl/acyl-type substitution, the ester bonds break down more readily due to their lower activation energy than those of the carbonate bonds.

To investigate the claim that the nucleophilic acyl substitution of an ester is favored over the nucleophilic acyl-type substitution of carbonate in both basic and neutral conditions, TBD, a very strong base, was used to catalyze the glycolysis instead of TBD:MSA, an amphoteric catalyst. Remarkably, all three polymers dissolved in ethylene glycol (EG) within 4 minutes of the reaction, shown in **Figure A.2 (a)**, demonstrating the potential change in solubility and catalytic mechanism achieved with TBD. This strong base used as a catalyst accelerates the depolymerization of Tritan™ and polycarbonate (PC) by increasing polymer solubility and enhancing reaction rates, as seen in **Figure A.2 (b-d)**. The unshared electron pairs on TBD could enhance solubility by disrupting the intermolecular forces between the polymer chains, aiding in dissolution.[58-61] This solubilization effect could allow for a more efficient reaction, as shown by the faster decrease in molecular weight and percent yield of EG-insoluble polymers when glycolysis is catalyzed with TBD compared to TBD-MSA. The elevated temperature of the reaction could also promote the deprotonation of the hydroxyl and phenol end groups, a change in the catalytic mechanism. For PC, the end-group deprotonation forms phenoxide ions, which can act as good nucleophiles and cause further chain scission.[15, 28, 62-65] Because of the higher acidity of the phenol groups compared to the hydroxyl groups, it can be inferred that the phenol end groups will be deprotonated alongside the hydroxyl groups. Thus, the use of a strong base in creating a basic environment potentially altered the solubility and catalytic mechanism of the

reaction, introducing a level of uncertainty compared to the more controlled conditions of a buffered solution, such as with TBD-MSA.

The depolymerization rates of PET, PC, and Tritan™ catalyzed with TBD:MSA in 'buffered' environments align with this analysis of the activation energies of the various reaction processes and reaction rates. Consequently, our data suggest that PC exhibits a slower depolymerization rate than PET and Tritan™ due to the higher activation energy required for the nucleophilic acyl-type substitution of the carbonate group in PC compared to the nucleophilic acyl-type substitution of the ester groups in PET and Tritan™. Interestingly, **Figure 3.2** and **Figure 3.4** demonstrate that when transesterification is favorable, M_w decreases more rapidly than M_n, resulting in a lowered Đ. In contrast, unfavorable transesterification leads to a rapid decrease in M_n relative to M_w, causing an increase in Đ. This implies that unfavorable transesterification favors the scission of shorter polymer chains, while favorable transesterification does not show this preference. However, under strongly basic conditions catalyzed by TBD, this difference narrows as phenolic nucleophiles generated from BPA based PC enhance depolymerization rates.

Overall, these results indicate that transporting glycols into a polymer is a key step in the depolymerization of carbonyl-containing polymers via glycolysis, and that the presence or absence of polymer crystallinity controls the rate and extent of swelling of the polymer by the glycol. Simultaneously, the rate of polymer depolymerization does not depend on the amount and rate of glycol transport, as both amorphous (Tritan^{TM}) and semi-crystalline (PET) polyesters demonstrate very similar depolymerization rates. This variation in depolymerization rate is attributed to the activation energies (and consequently rates) of the depolymerization reactions that occur between the polymer and the EG during glycolysis — specifically, the nucleophilic

acyl-type substitution of polycarbonate, which has a higher activation energy than the nucleophilic acyl substitution of the ester. Additionally, the type of catalyst used and the resulting end groups influence nucleophilic acyl/acyl-type substitution, as stronger bases like TBD enhance the deprotonation of end groups, generating reactive species such as phenoxide ions that facilitate cleavage reactions.

Therefore, the transport of glycol to the carbonyl carbon, which relies on glycol/polymer interactions and polymer crystallinity, is a necessary step in the glycolysis depolymerization of polymers, but it is not the rate-limiting step. Instead, the reactivity (and reaction rate) of the carbonyl group on the polymer backbone with the glycol governs the observed depolymerization rate. The use of TBD further emphasizes how catalyst selection and the resulting chemical environment influence polymer dissolution, nucleophilic activation, and depolymerization efficiency.

3.4.3 Depolymerization of PET and PC with Bisphenol-A

Both an ester-containing polymer (PET) and the carbonate-containing polymer (PC) were also depolymerized with the same reaction conditions, except for using a distinctly different diol, BPA. The depolymerization with BPA was examined to provide additional insight into the importance of the diol-polymer compatibility in the depolymerization process. The results reported above show that the swelling of the polymer flake, inhibited by polymer crystallinity, does not impact the rate of chain scission, thus the semicrystalline PET continued to be the ester-containing polymer used in this section of the study.

When depolymerizing PET, PC, and Tritan^{TM} in EG, all of the polymer oligomers remained in the heterogeneous stage, where the polymer remains largely insoluble in the ethylene glycol throughout the reaction and is described in **Figure 3.1. Figure 3.8** pictorially

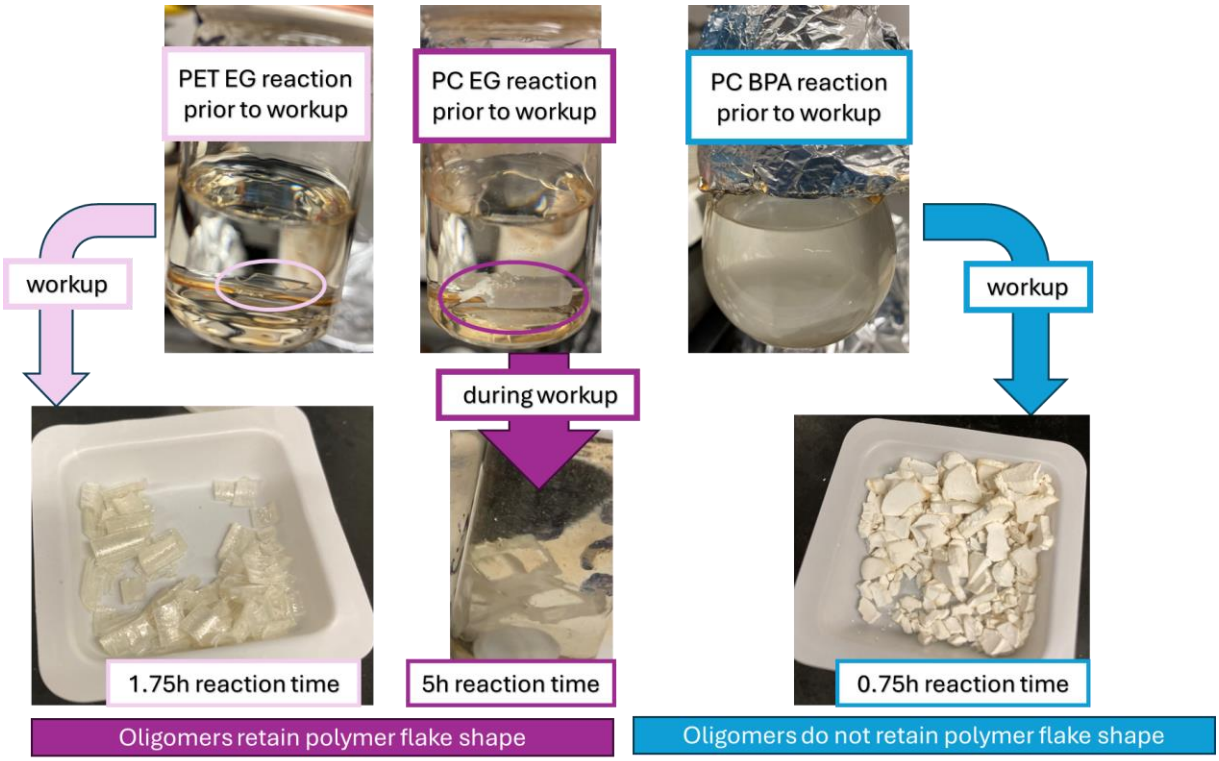

Figure 3.8 Depolymerization of PET and PC in EG and BPA. Light purple: PET flakes in EG before and after workup (1.75 reaction hours). Dark purple: PC flakes in EG before and after workup (5 reaction hours). Blue: PC flakes in BPA before and after workup (0.75 reaction hours).

documents the macroscopic changes in the PC or PET flake during the depolymerization with ethylene glycol or bisphenol-A. This figure shows that at the longest reaction times the PET and PC product retain their flake shape when depolymerized with EG, but product of the PC depolymerization with BPA is dispersed in the BPA, and thus has transitioned into the coexistence or homogeneous stages of the depolymerization. In this figure the light purple highlights the state of the PET flakes before and after the workup when depolymerized with EG. These polymers remain a solid with their distinct flake shape even after 1.75 hours of reaction time. Similarly, the dark purple highlight shows that the PC flakes that are depolymerized with EG also retain the flake shape before and during the workup process after 5 hours of reaction time. Finally, the blue highlighted portion in **Figure 3.8** shows that the PC that is depolymerized with BPA quickly loses all of its undissolved polymer flakes, where the product loses their flake structure after only 0.75 hours of reaction time. These observations lead to the conclusion that the depolymerization of PET and PC with BPA does not remain in the heterogeneous stage as it does when the reaction occurs with ethylene glycol, rather, the reactions quickly transition to the coexistence stage, where some of the product/oligomers are dispersed in the diol, while some are not. Thus, the product of the PC or PET depolymerization in EG retain their solid behavior and flake shape, while those that are depolymerized in BPA do not. To further illustrate the transition from the heterogeneous stage for polymers depolymerized with BPA, **Figure A.4** shows the visual changes in PC flakes that are depolymerized with either EG or BPA, including the flake thickness of both. These pictures show that the thickness of PC flakes depolymerized with EG increases as reaction time increases, where a similar swelling effect is observed in **Figure 3.5.** Furthermore, **Figure A.4** reveals that the PC flakes that are depolymerized with BPA become thinner, indicating polymer dissolution. This further suggests that PC depolymerized in BPA

does not remain in the heterogeneous stage throughout the reaction, but transitions to the coexistence stage partially through the reaction.

Thus, the choice of diol for the depolymerization appears to play an important role in the transition of the depolymerization reaction from the heterogeneously to homogeneously catalyzed reactions. The choice of BPA as the diol modifies the reaction such that the depolymerized oligomeric product becomes dispersed in the BPA, transitioning the reaction from heterogeneous stage to a coexistence stage and then to a homogeneous stage. This, in turn, significantly impacts the yield of the product, where **Figure 3.9** shows the percent yield as a function of reaction time for the depolymerization of both PET and PC with BPA as diol. **Figure 3.9** shows the total yield of the depolymerization product oligomers that are both of soluble and insoluble BPA oligomers for both PET (blue-green) and PC (dark purple), as well as the yield of the produced oligomers that are insoluble in BPA for both PET (dark blue) and PC (dark purple).

The total yield of recovered product for both polymers remains high (~100%) throughout the reaction. As the oligomers dissolve into BPA, the yield of BPA insoluble oligomers decreases. Hence, the transition of the reaction from the heterogeneous stage to the coexistence stage and the homogeneous stage decreases the yield of BPA insoluble oligomers with reaction time. A small decrease in the total yield for PC at later reaction times is due to the solubility of smaller PC oligomers and monomer in the methanol used during the workup.

To provide insight into the evolution of chain structure of the PET and PC depolymerization product that are in the coexistence or homogeneous stage of the reaction, SEC provided the molecular weight distribution of the BPA soluble and BPA insoluble products. **Figure A.5** presents the weight and number average molecular weight of the BPA soluble and BPA insoluble product oligomers for the depolymerization of PET and PC as a function of

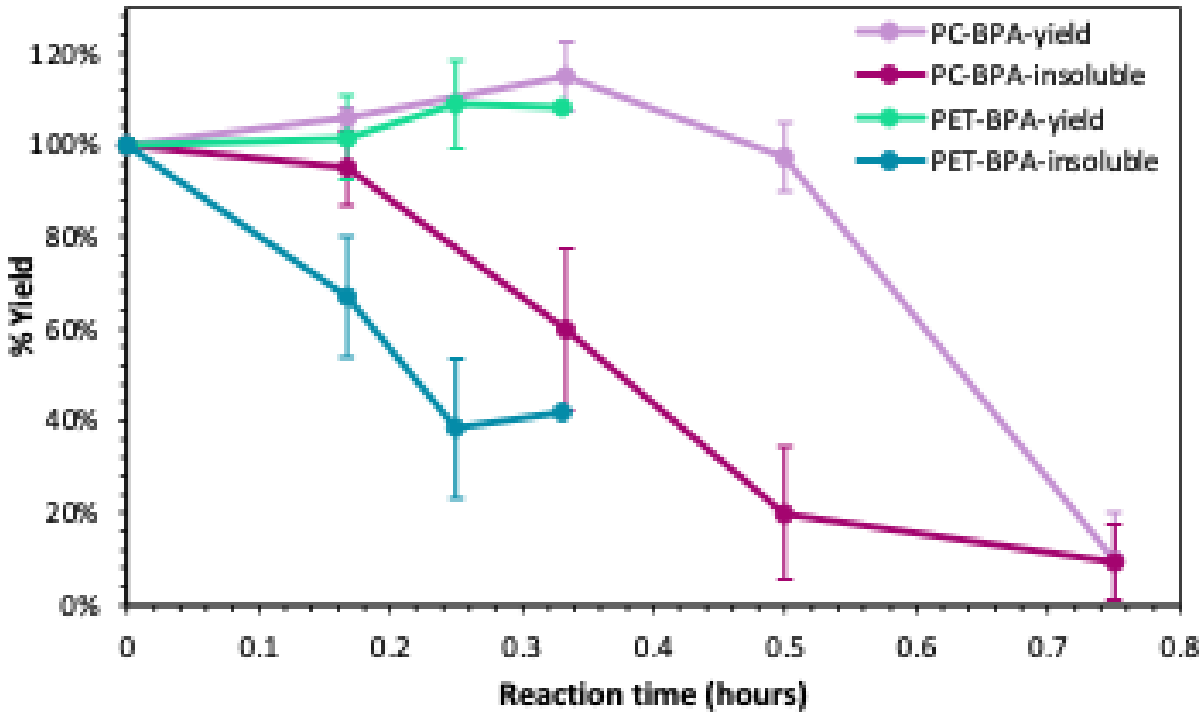

Figure 3.9 Yield of PET and PC depolymerized with BPA: Change in percent yield of PET and PC as a function of depolymerization time with BPA, including the change in BPA insoluble yield for PET (dark blue) and PC (dark purple). The change in the total yield of BPA soluble and BPA insoluble material as a function of reaction time for PET (blue-green) and PC (light purple) is also shown.

reaction time. Inspection of this figure shows that these products are of substantial chain length. The BPA soluble fraction of the oligomeric products decreases in molecular weight faster than the BPA insoluble fraction, emphasizing the acceleration of the depolymerization reaction with the transition from the heterogeneous stage.

To further analyze the overall molecular weight of the polymers with reaction time, the average percent change in the weight and number average molecular weight was calculated using

Equation 3.2. In

Equation 3.2, $\Delta MW_{average}$ is the average percent change in molecule weight, $n_{insoluble}$ is the yield of insoluble depolymerization product oligomers, $n_{soluble}$ is the yield of soluble depolymerization product oligomers, $M_{t\ insoluble}$ is the molecular weight of insoluble depolymerization product oligomers at a given reaction time, $M_{t\ soluble}$ is the molecular weight of soluble depolymerization product oligomers at a given reaction time, and M_0 was the original molecular weight of the polymer prior to depolymerization. **Figure 3.10** plots the variation in the average molecular weight of PET M_n (dark blue) and M_w (blue-green), as well as PC M_n (dark orange) and M_w (orange) with reaction time. The overall depolymerization reaction time for both polymers in BPA is shorter than in EG, as PET and PC reach the homogenous stage at 20 minutes and 45 minutes, respectively, respectively when reacting with BPA. As mentioned above, PET depolymerizes faster than PC because the ester group more readily reacts with the diol than the carbonate group in PC. We hypothesized that the depolymerization of PET with BPA as the diol would depolymerize more slowly than the depolymerizations using EG as the diol, because BPA is a poorer nucleophile than EG due to the lower pKa of the phenol of BPA than that of the hydroxyl of EG.[66]

Equation 3.2 $$\Delta \boldsymbol{MW_{average}}\ [\%] = \frac{(\boldsymbol{n_{insoluble} * M_{t\ insouble}}) + (\boldsymbol{n_{soluble} * M_{t\ soluble}})}{\boldsymbol{M_0}} * \mathbf{100}$$

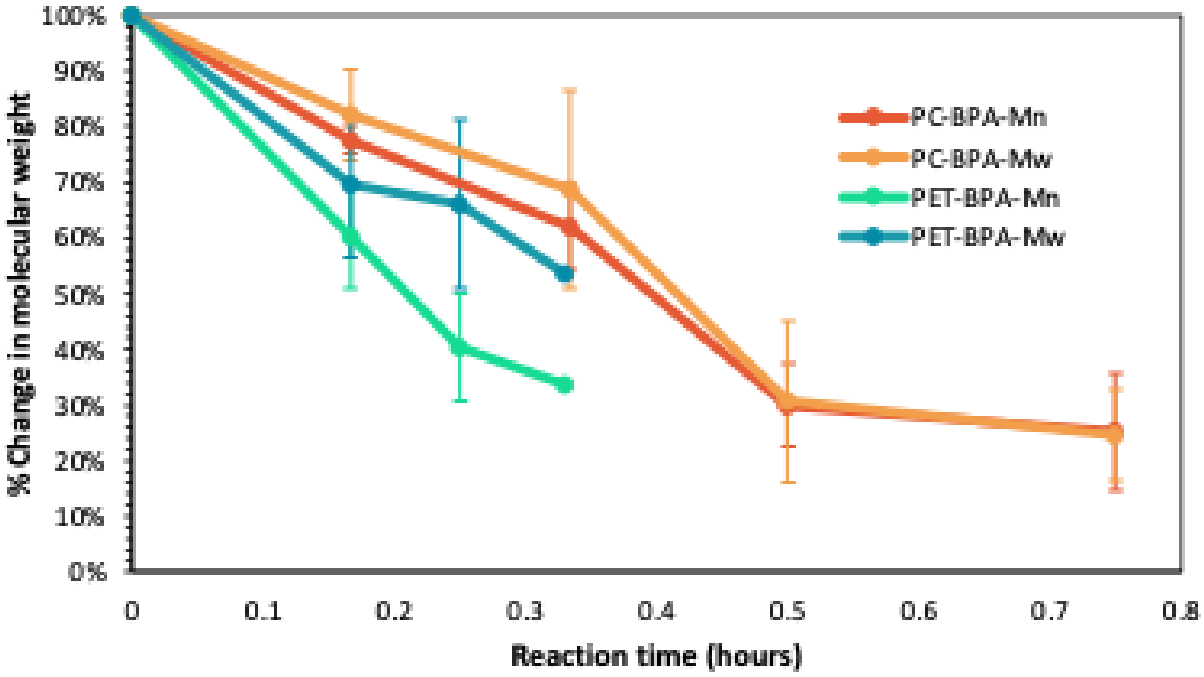

Figure 3.10 Change in percent molecular weight for PET and PC with reaction time. It shows the change in molecular weight as a percentage of PET M_n (blue-green), PET M_w (dark blue), PC M_n (dark orange), and PC M_w (orange) with reaction time.

The data in **Figure 3.10** shows that the depolymerization reactions utilizing BPA as the diol progress faster than the reactions utilizing EG as diol. This is due the more rapid transition of the BPA reactions beyond the heterogeneous stage, where the reaction between the polymer diol is more rapid in the coexistence and homogeneous stages than in the heterogeneous stage. This observation suggests that the BPA more readily dissolves or disperses the PET and PC depolymerization reaction products. To provide qualitative insight into the affinity of the two polymers to the BPA and EG diols, the swelling behavior of PET and PC in BPA was monitored, as swelling is the first step to dissolution.[33] **Figure A.6** plots the normalized swelling per polymer flake in BPA of PET and PC as a function of swelling time. **Figure A.6** indicates that the PET and PC swell more quickly and with more BPA per flake than was observed in their swelling with EG in **Figure 3.5**. Moreover, the PET and PC swell similarly with BPA despite the crystallinity of PET. This is interesting as **Figure 3.5** demonstrated that the PET crystallinity impacted swelling rates of PC and PET with EG.

Moreover, EG does not dissolve PET, and thus, decrystallization does not occur. To verify if decrystallization is occurring for PET with BPA, **Figure A.7** shows the percent crystallinity of PET with time for different environments, including annealed without catalyst at the reaction temperature, depolymerized with EG, swelled with EG at room temperature, depolymerized with BPA, and swelled with BPA at room temperature. This data shows that annealing at the reaction temperature without catalyst or depolymerization/swelling with EG increases the bulk crystallinity of PET. In contrast, the depolymerization/swelling of the PET with BPA decreases the bulk crystallinity, demonstrating that decrystallization of PET occurs with BPA. This variation in solubility can be understood by invoking the Hildebrand solubility parameters of PET, PC, BPA and EG. PET and PC have solubility parameters ($MPa^{1/2}$) (20.85

$MPa^{1/2}$ and 22.25 $MPa^{1/2}$, respectively) that differ from that of BPA (24.37 $MPa^{1/2}$) by less than 4 $MPa^{1/2}$, while the difference in solubility parameters of PET and PET and that of EG (32.98 $MPa^{1/2}$) is much larger ~ 10-12 $MPa^{1/2}$.[67-72] The similarity of the BPA d to that of the polymers indicates that there is a greater affinity of the two polymers to BPA than to EG. Thus, it makes sense that the depolymerization products of both polymers BPA dissolve in BPA more readily, while the depolymerization products do not dissolve in EG. This results in the reactions that occur with EG remain in the heterogeneous stage, due to the insolubility of the polymers in the EG.

Holistically, this data shows that the affinity of the polymer and the diol significantly impacts the rate of the depolymerization reaction. However, it is not the transport of the diol into the polymer flake that controls the reaction; instead, the polymer's solubility in the diol controls the rate at which the reaction passes through the three stages of heterogenous depolymerization. The more soluble polymer-diol pair will transition from the heterogeneous stage to the homogeneous stage more quickly, increasing the rate of the depolymerization reaction. Additionally, this study demonstrates that strong catalysts, such as TBD, can disrupt intermolecular forces and enhance the solubility of polymers in the diol, accelerating the depolymerization process. This effect was evident in all polymers dissolving in EG within 4 minutes of the reaction, showing the critical role of solubility in determining reaction efficiency. This study elucidates the impact of polymer crystallinity, the reactivity of carbonyl functional groups, and solvent-polymer compatibility on the rate of the depolymerization of polyesters and polycarbonates. Surprisingly, crystallinity does not greatly impact the rate of depolymerization despite the inhibition of the transport of the diol into the polymer flake by the presence of the polymer crystals. The rapid dissolution of all three polymers in EG catalyzed with TBD,

observed within the first few minutes of the reaction, highlights the overriding influence of solubility over crystallinity in controlling depolymerization rates. This study also shows that ester-containing polymers are more easily chemically recycled than carbonate-containing polymers, even if solvent-polymer compatibility is low. Finally, this study reveals that the solvent-polymer compatibility has the highest impact on the reaction rate by governing when the heterogeneous reaction transitions through the three stages of a heterogenous depolymerization.

3.5 Conclusion

This study explores the factors that influence the depolymerization rate of carbonyl containing polymers, focusing on diol transport to the carbonyl and the fundamental reactivity of the carbonyl group, to advance recycling methods and inspire the design of more easily recyclable polymers. Ester-containing polymers, such as PET and Tritan™, depolymerize more rapidly than carbonate-containing polymers like PC due to the higher reactivity of the ester functional group. Interestingly, diol transport and polymer-diol compatibility do not govern the depolymerization rate, as PET and Tritan™ exhibit similar depolymerization rates despite Tritan™ absorbing more EG per polymer flake. Rather, the solubility of the polymer in the diol dictates the transition of the initial heterogeneous reaction to a homogeneous reaction. The rapid dissolution of the polymers in EG facilitated by strong bases such as TBD further underscores the role of solubility in accelerating this transition. Due to the limited solubility of all three polymers in EG alone, the depolymerization remains heterogeneously catalyzed with amphoteric TBD-MSA when reacting with EG. However, the depolymerization reaction transitions more readily to a homogeneous reaction with BPA, due to the increased solubility of the diol and the polymers. Improved solubility accelerates the transition to the homogeneously catalyzed depolymerization, whereas poor solubility impedes this transition. This observation also provides

insight into our understanding of nanoplastic formation in the environment: the environmental degradation of crystalline polymers in the waste stream, which have limited solubility in water, will remain heterogeneously catalyzed in amphoteric conditions, potentially hindering their breakdown and contributing to the formation of nanoplastics in plastic pollution.

3.6 Acknowledgements

This work was supported by the National Science Foundation, Polymers program, Division of Materials Research (DMR- 2104982). The SEC analysis and some of mechanistic discussion were supported by the US Department of Energy, Office of Science, Materials Sciences and Engineering Division.

References

(1) Arifuzzaman, M.; Sumpter, B. G.; Demchuk, Z.; Do, C.; Arnould, M. A.; Rahman, M. A.; Cao, P.-F.; Popovs, I.; Davis, R. J.; Dai, S.; et al. Selective deconstruction of mixed plastics by a tailored organocatalyst. *Materials Horizons* **2023**, *10* (9), 3360-3368. DOI: 10.1039/d3mh00801k.

(2) Fox, B.; Moad, G.; Van Diepen, G.; Willing, I.; Cook, W. D. Characterization of poly(ethylene terephthalate) and poly(ethylene terephthalate) blends. *Polymer* **1997**, *38* (12), 3035-3043. DOI: 10.1016/s0032-3861(96)00872-5.

(3) George, N.; Kurian, T. Recent Developments in the Chemical Recycling of Postconsumer Poly(ethylene terephthalate) Waste. *Industrial & Engineering Chemistry Research* **2014**, *53* (37), 14185-14198. DOI: 10.1021/ie501995m.

(4) Company, E. C. *2023 Sustainability Report*; 2024. https://www.eastman.com/content/dam/eastman/corporate/en/media-center/resources/eastman-sustainability-report-2023.pdf (accessed 02/25/24).

(5) Company, E. C. *2022 Sustainability Report*; 2023. https://www.eastman.com/content/dam/eastman/corporate/en/media-center/resources/eastman-sustainability-report-2022.pdf.

(6) Nikles, D. E.; Farahat, M. S. New Motivation for the Depolymerization Products Derived from Poly(Ethylene Terephthalate) (PET) Waste: a Review. *Macromolecular Materials and Engineering* **2005**, *290* (1), 13-30. DOI: 10.1002/mame.200400186.

(7) Shaikh, I. R. Organocatalysis: Key Trends in Green Synthetic Chemistry, Challenges, Scope towards Heterogenization, and Importance from Research and Industrial Point of View. *Journal of Catalysts* **2014**, *2014*, 1-35. DOI: 10.1155/2014/402860.

(8) Xin, J.; Zhang, Q.; Huang, J.; Huang, R.; Jaffery, Q. Z.; Yan, D.; Zhou, Q.; Xu, J.; Lu, X. Progress in the catalytic glycolysis of polyethylene terephthalate. *Journal of Environmental Management* **2021**, *296*, 113267. DOI: 10.1016/j.jenvman.2021.113267.

(9) Hong, M.; Chen, E. Y. X. Towards Truly Sustainable Polymers: A Metal-Free Recyclable Polyester from Biorenewable Non-Strained γ-Butyrolactone. *Angew. Chem.* **2016**, *128* (13), 4260-4265. DOI: 10.1002/ange.201601092.

(10) Hong, M.; Chen, E. Y. X. Completely recyclable biopolymers with linear and cyclic topologies via ring-opening polymerization of γ-butyrolactone. *Nature Chemistry* **2016**, *8* (1), 42-49. DOI: 10.1038/nchem.2391.

(11) Zhu, J.-B.; Watson, E. M.; Tang, J.; Chen, E. Y. X. A synthetic polymer system with repeatable chemical recyclability. *Science* **2018**, *360* (6387), 398-403. DOI: 10.1126/science.aar5498 (acccessed 2024/04/08).

(12) Plummer, C. M.; Li, L.; Chen, Y. Ring-Opening Polymerization for the Goal of Chemically Recyclable Polymers. *Macromolecules* **2023**, *56* (3), 731-750. DOI: 10.1021/acs.macromol.2c01694.

(13) Otera, J. *Modern Carbonyl Chemistry*; WILEY-VCH, 2000.

(14) Vollhardt, K. P. C.; Shore, E. N. *Organic Chemistry; Structure and Functions*; Freeman and Company, 2007.

(15) Jehanno, C.; Demarteau, J.; Mantione, D.; Arno, M. C.; Ruipérez, F.; Hedrick, J. L.; Dove, A. P.; Sardon, H. Selective Chemical Upcycling of Mixed Plastics Guided by a Thermally Stable Organocatalyst. *Angew. Chem. Int. Ed.* **2021**, *60* (12), 6710-6717. DOI: 10.1002/anie.202014860.

(16) Sinha, V.; Patel, M. R.; Patel, J. V. PET waste management by chemical recycling: a review. *J. Polym. Environ.* **2010**, *18* (1), 8-25.

(17) Raheem, A. B.; Noor, Z. Z.; Hassan, A.; Abd Hamid, M. K.; Samsudin, S. A.; Sabeen, A. H. Current developments in chemical recycling of post-consumer polyethylene terephthalate wastes for new materials production: A review. *Journal of Cleaner Production* **2019**, *225*, 1052-1064. DOI: https://doi.org/10.1016/j.jclepro.2019.04.019.

(18) Jang, J. Y.; Sadeghi, K.; Seo, J. Chain-Extending Modification for Value-Added Recycled PET: A Review. *Polymer Reviews* **2022**, *62* (4), 860-889. DOI: 10.1080/15583724.2022.2033765.

(19) Company, C. C. *THE COCA-COLA COMPANY 2022 BUSINESS & SUSTAINABILITY REPORT*; 2022. https://www.coca-colacompany.com/content/dam/company/us/en/reports/coca-cola-business-sustainability-report-2022.pdf#page%3D38.

(20) Aguado, A.; Martínez, L.; Becerra, L.; Arieta-Araunabeña, M.; Arnaiz, S.; Asueta, A.; Robertson, I. Chemical depolymerisation of PET complex waste: hydrolysis vs. glycolysis. *J. Mater. Cycles Waste Manage.* **2014**, *16* (2), 201-210. DOI: 10.1007/s10163-013-0177-y.

(21) Carta, D.; Cao, G.; D'Angeli, C. Chemical recycling of poly(ethylene terephthalate) (pet) by hydrolysis and glycolysis. *Environmental Science and Pollution Research* **2003**, *10* (6), 390-394. DOI: 10.1065/espr2001.12.104.8.

(22) Colomines, G.; Robin, J.-J.; Tersac, G. Study of the glycolysis of PET by oligoesters. *Polymer* **2005**, *46* (10), 3230-3247. DOI: https://doi.org/10.1016/j.polymer.2005.02.047.

(23) Najmi, S.; Vance, B. C.; Selvam, E.; Huang, D.; Vlachos, D. G. Controlling PET oligomers vs monomers via microwave-induced heating and swelling. *Chem. Eng. J.* **2023**, *471*, 144712. DOI: https://doi.org/10.1016/j.cej.2023.144712.

(24) Sheel, A.; Pant, D. Chemical Depolymerization of PET Bottles via Glycolysis. **2019**, 61-84. DOI: 10.1016/B978-0-12-811361-5.00004-3.

(25) Silva, C. V. G.; Silva Filho, E. A. D.; Uliana, F.; Jesus, L. F. R. D.; Melo, C. V. P. D.; Barthus, R. C.; Rodrigues, J. G. A.; Vanini, G. PET glycolysis optimization using ionic liquid [Bmin]ZnCl3 as catalyst and kinetic evaluation. *Polímeros* **2018**, *28* (5), 450-459. DOI: 10.1590/0104-1428.00418.

(26) Wang, L.; Nelson, G. A.; Toland, J.; Holbrey, J. D. Glycolysis of PET Using 1,3-Dimethylimidazolium-2-Carboxylate as an Organocatalyst. *ACS Sustainable Chemistry & Engineering* **2020**, *8* (35), 13362-13368. DOI: 10.1021/acssuschemeng.0c04108.

(27) Yue, Q.; Wang, C.; Zhang, L.; Ni, Y.; Jin, Y. Glycolysis of poly (ethylene terephthalate)(PET) using basic ionic liquids as catalysts. *Polym. Degrad. Stab.* **2011**, *96* (4), 399-403.

(28) Kamps, J. H.; Hoeks, T.; Kung, E.; Lens, J. P.; McCloskey, P. J.; Noordover, B. A. J.; Heuts, J. P. A. Activated carbonates: enabling the synthesis of differentiated polycarbonate resins via melt transcarbonation. *Polymer Chemistry* **2016**, *7* (33), 5294-5303. DOI: 10.1039/c6py00925e.

(29) Snyder, R. L.; Fortman, D. J.; De Hoe, G. X.; Hillmyer, M. A.; Dichtel, W. R. Reprocessable Acid-Degradable Polycarbonate Vitrimers. *Macromolecules* **2018**, *51* (2), 389-397. DOI: 10.1021/acs.macromol.7b02299.

(30) Bhagia, S.; Bornani, K.; Ozcan, S.; Ragauskas, A. J. Terephthalic Acid Copolyesters Containing Tetramethylcyclobutanediol for High-Performance Plastics. *ChemistryOpen* **2021**, *10* (8), 830-841. DOI: 10.1002/open.202100171.

(31) Donald R. Kelsey, B. M. S., Janusz S. Grebowicz, and Hoe H Chuah. High Impact, Amorphous Terephthalate Copolyesters of Rigid2,2,4,4-Tetramethyl-1,3-cyclobutanediol with Flexible Diols. *Macromolecules* **2000**, (33), 5810-5818. DOI: 10.1021/ma000223.

(32) Saxon, D. J.; Gormong, E. A.; Shah, V. M.; Reineke, T. M. Rapid Synthesis of Chemically Recyclable Polycarbonates from Renewable Feedstocks. *ACS Macro Letters* **2021**, *10* (1), 98-103. DOI: 10.1021/acsmacrolett.0c00747.

(33) Miller-Chou, B. A.; Koenig, J. L. A review of polymer dissolution. *Prog. Polym. Sci.* **2003**, *28* (8), 1223-1270. DOI: 10.1016/s0079-6700(03)00045-5.

(34) Tundo, P.; Aricò, F. Reaction Pathways in Carbonates and Esters. *ChemSusChem* **2023**, *16* (23). DOI: 10.1002/cssc.202300748.

(35) Aricò, F.; Bravo, S.; Crisma, M.; Tundo, P. 1,3-Oxazinan-2-ones via carbonate chemistry: a facile, high yielding synthetic approach. *Pure Appl. Chem.* **2016**, *88* (3), 227-237. DOI: 10.1515/pac-2015-1004.

(36) Kim, W. B.; Joshi, U. A.; Lee, J. S. Making Polycarbonates without Employing Phosgene: An Overview on Catalytic Chemistry of Intermediate and Precursor Syntheses for Polycarbonate. *Industrial & Engineering Chemistry Research* **2004**, *43* (9), 1897-1914. DOI: 10.1021/ie034004z.

(37) Jehanno, C.; Flores, I.; Dove, A. P.; Müller, A. J.; Ruipérez, F.; Sardon, H. Organocatalysed depolymerisation of PET in a fully sustainable cycle using thermally stable protic ionic salt. *Green Chemistry* **2018**, *20* (6), 1205-1212. DOI: 10.1039/c7gc03396f.

(38) Jehanno, C.; Pérez-Madrigal, M. M.; Demarteau, J.; Sardon, H.; Dove, A. P. Organocatalysis for depolymerisation. *Polymer Chemistry* **2019**, *10* (2), 172-186. DOI: 10.1039/c8py01284a.

(39) Watson-Sanders, S. D., M. Evolution of Chain Structure during the Glycolysis of Poly(ethylene terephthalate). *Chem Sus Chem* **2023**.

(40) Zhou, X.; Wang, J.; Nie, J.; Du, B. Poly(N-isopropylacrylamide)-based ionic hydrogels: synthesis, swelling properties, interfacial adsorption and release of dyes. *Polym. J.* **2016**, *48* (4), 431-438. DOI: 10.1038/pj.2015.123.

(41) Yoshioka, T.; Okayama, N.; Okuwaki, A. Kinetics of Hydrolysis of PET Powder in Nitric Acid by a Modified Shrinking-Core Model. *Industrial & Engineering Chemistry Research* **1998**, *37* (2), 336-340. DOI: 10.1021/ie970459a.

(42) Mancini, S. D.; Zanin, M. Post Consumer Pet Depolymerization by Acid Hydrolysis. *Polymer-Plastics Technology and Engineering* **2007**, *46* (2), 135-144. DOI: 10.1080/03602550601152945.

(43) Ghasemi, M.; Singapati, A. Y.; Tsianou, M.; Alexandridis, P. Dissolution of semicrystalline polymer fibers: Numerical modeling and parametric analysis. *AlChE J.* **2017**, *63* (4), 1368-1383. DOI: 10.1002/aic.15615.

(44) Li, H.; Aguirre-Villegas, H. A.; Allen, R. D.; Bai, X.; Benson, C. H.; Beckham, G. T.; Bradshaw, S. L.; Brown, J. L.; Brown, R. C.; Cecon, V. S.; et al. Expanding plastics recycling technologies: chemical aspects, technology status and challenges. *Green Chemistry* **2022**, *24* (23), 8899-9002. DOI: 10.1039/d2gc02588d.

(45) Wang, H. An accurate theoretical study of energy barriers of alkaline hydrolysis of carboxylic esters. *Res. Chem. Intermed.* **2012**, *38* (9), 2175-2190. DOI: 10.1007/s11164-012-0535-8.

(46) Tundo, P.; Musolino, M.; Aricò, F. The reactions of dimethyl carbonate and its derivatives. *Green Chemistry* **2018**, *20* (1), 28-85, 10.1039/C7GC01764B. DOI: 10.1039/C7GC01764B.

(47) Tundo, P.; Selva, M. The Chemistry of Dimethyl Carbonate. *Acc. Chem. Res.* **2002**, *35* (9), 706-716. DOI: 10.1021/ar010076f.

(48) Gómez-Bombarelli, R.; Calle, E.; Casado, J. Mechanisms of Lactone Hydrolysis in Neutral and Alkaline Conditions. *The Journal of Organic Chemistry* **2013**, *78* (14), 6868-6879. DOI: 10.1021/jo400258w.

(49) Zhan, C.-G.; Landry, D. W.; Ornstein, R. L. Energy Barriers for Alkaline Hydrolysis of Carboxylic Acid Esters in Aqueous Solution by Reaction Field Calculations. *The Journal of Physical Chemistry A* **2000**, *104* (32), 7672-7678. DOI: 10.1021/jp001459i.

(50) Detar, D. F. Effects of alkyl groups on rates of SN2 reactions. *The Journal of Organic Chemistry* **1980**, *45* (25), 5174-5176. DOI: 10.1021/jo01313a030.

(51) Böhm, S.; Exner, O. Steric effects of the alkyl groups: evaluation on isolated molecules by means of isodesmic reactions. *Org. Biomol. Chem.* **2007**, *5* (13), 2081-2086. DOI: 10.1039/b704459c.

(52) Smith, M. B. *March's Advanced Organic Chemistry: Reactions, Mechanisms, and Structure*; Wiley, 2019.

(53) Liguori, F.; Moreno-Marrodán, C.; Barbaro, P. Valorisation of plastic waste via metal-catalysed depolymerisation. *Beilstein Journal of Organic Chemistry* **2021**, *17*, 589-621. DOI: 10.3762/bjoc.17.53.

(54) Eshaq, G.; Elmetwally, A. E. (Mg–Zn)–Al layered double hydroxide as a regenerable catalyst for the catalytic glycolysis of polyethylene terephthalate. *J. Mol. Liq.* **2016**, *214*, 1-6. DOI: 10.1016/j.molliq.2015.11.049.

(55) Chen, C.-T.; Kuo, J.-H.; Pawar, V. D.; Munot, Y. S.; Weng, S.-S.; Ku, C.-H.; Liu, C.-Y. Nucleophilic Acyl Substitutions of Anhydrides with Protic Nucleophiles Catalyzed by

Amphoteric, Oxomolybdenum Species. *The Journal of Organic Chemistry* **2005**, *70* (4), 1188-1197. DOI: 10.1021/jo048363v.

(56) Chen, C.-T.; Kuo, J.-H.; Li, C.-H.; Barhate, N. B.; Hon, S.-W.; Li, T.-W.; Chao, S.-D.; Liu, C.-C.; Li, Y.-C.; Chang, I. H.; et al. Catalytic Nucleophilic Acyl Substitution of Anhydrides by Amphoteric Vanadyl Triflate. *Org. Lett.* **2001**, *3* (23), 3729-3732. DOI: 10.1021/ol016684c.

(57) Chen, C.-T.; Munot, Y. S. Direct Atom-Efficient Esterification between Carboxylic Acids and Alcohols Catalyzed by Amphoteric, Water-Tolerant TiO(acac)₂. *The Journal of Organic Chemistry* **2005**, *70* (21), 8625-8627. DOI: 10.1021/jo051337s.

(58) Hong, M.; Chen, J.; Chen, E. Y. X. Polymerization of Polar Monomers Mediated by Main-Group Lewis Acid–Base Pairs. *Chem. Rev.* **2018**, *118* (20), 10551-10616. DOI: 10.1021/acs.chemrev.8b00352.

(59) Kaiho, S.; Hmayed, A. A. R.; Delle Chiaie, K. R.; Worch, J. C.; Dove, A. P. Designing Thermally Stable Organocatalysts for Poly(ethylene terephthalate) Synthesis: Toward a One-Pot, Closed-Loop Chemical Recycling System for PET. *Macromolecules* **2022**, *55* (23), 10628-10639. DOI: 10.1021/acs.macromol.2c01410.

(60) Grabowski, S. J. Hydrogen Bond and Other Lewis Acid–Lewis Base Interactions as Preliminary Stages of Chemical Reactions. *Molecules* **2020**, *25* (20), 4668. DOI: 10.3390/molecules25204668.

(61) Olazabal, I.; Luna, E.; De Meester, S.; Jehanno, C.; Sardon, H. Upcycling of BPA-PC into trimethylene carbonate by solvent assisted organocatalysed depolymerisation. *Polymer Chemistry* **2023**, *14* (19), 2299-2307. DOI: 10.1039/d3py00441d.

(62) Tang, X. C.; Pikal, M. J.; Taylor, L. S. *Pharm. Res.* **2002**, *19* (4), 484-490. DOI: 10.1023/a:1015199713635.

(63) Lee, H. Effects of temperature, salt concentration, and the protonation state on the dynamics and hydrogen-bond interactions of polyelectrolyte multilayers on lipid membranes. *Physical Chemistry Chemical Physics* **2016**, *18* (9), 6691-6700. DOI: 10.1039/c5cp08039h.

(64) Gupta, M.; Svendsen, H. F. Theoretical Study of Temperature dependent Enthalpy of Absorption, Heat Capacity, and Entropy changes for Protonation of Amines and Amino Acid Solvents. *Energy Procedia* **2014**, *63*, 1099-1105. DOI: 10.1016/j.egypro.2014.11.118.

(65) Maia, J.; Cruz, J. M.; Sendón, R.; Bustos, J.; Cirugeda, M. E.; Sanchez, J. J.; Paseiro, P. Effect of amines in the release of bisphenol A from polycarbonate baby bottles. *Food Research International* **2010**, *43* (5), 1283-1288. DOI: 10.1016/j.foodres.2010.03.014.

(66) Dave Evans, D. H. R. *pKa's of Inorganic and Oxo-Acids*. ACS Organic Division, 2024. https://organicchemistrydata.org/hansreich/resources/pka/pka_data/evans_pKa_table.pdf (accessed 2024.

(67) TESTS, A. D. *Surface Free Energy Components by Polar/Dispersion and Acid—Base Analyses; and Hansen Solubility Parameters for Various Polymers*. https://www.accudynetest.com/polytable_02.html (accessed.

(68) Kwok, A. Y.; Qiao, G. G.; Solomon, D. H. Synthetic hydrogels 3. Solvent effects on poly(2-hydroxyethyl methacrylate) networks. *Polymer* **2004**, *45* (12), 4017-4027. DOI: https://doi.org/10.1016/j.polymer.2004.03.104.

(69) Sun, J.; Wang, L.; Ding, S.; Sun, X.; Xu, L. Solubility Behavior and Thermodynamic Analysis of Bisphenol A in 14 Different Pure Solvents. *Journal of Chemical & Engineering Data* **2020**, *65* (5), 2846-2858. DOI: 10.1021/acs.jced.0c00166.

(70) Hansen, C. M. Hansen Solubility Parameters. **2007**. DOI: 10.1201/9781420006834.

(71) *Polymer Handbook*; John Wiley & sons, Inc, 1999.

(72) Hansen, C. M. The Universality of the Solubility Parameter. *Product R&D* **1969**, *8* (1), 2-11. DOI: 10.1021/i360029a002.

CHAPTER 4: MODIFYING CONSUMER POLYETHYLENE TEREPHTHALATE BEFORE GLYCOLYSIS TO ISOLATE TAILORED TELECHELIC OLIGOMERS

Shelby Watson-Sanders,[1] Kendra Day,[1] Timothy Taylor,[1] Sarah Barber,[1] Clarissa Thompson,[2] Gregg Beckham,[2] Mark Dadmun[1,*]

[1] Chemistry Department, University of Tennessee, Knoxville TN 37996

2 National Renewable Energy Laboratory, Golden, CO

* Corresponding Author (Dad@utk.edu)

In this article, I was responsible for polymer depolymerization, characterization, and annealing of all polymers. Sarah Barber and Landri Wilcox performed all of the swelling studies together. Timothy Taylor performed all of the small angle x-ray scattering. Dr. Beckham's students performed molecular weight analysis of PET and Tritan$^{TM.}$ Dr. Mark Dadmun organized this project and facilitated the writing of the manuscript.

4.1 Abstract

Polyethylene Terephthalate (PET) is a widely used material in single-use consumer products, with increasing production demands each year. This study examines a new method to upcycle PET to produce telechelic oligomers that can function as macromonomers as reactants in polymerization or to be transformed into value-added products. The research examines the impact of annealing PET near its melting point on the evolution of chain structure during the depolymerization. These results show that this annealing provides a protocol to successfully obtain dihydroxy-terminated oligomers from consumer waste, with varying molecular weights that are guided by the pre-depolymerization annealing time. Dihydroxy-terminated PET oligomers are isolated from the depolymerization process more quickly if the PET is annealed before depolymerization. The molecular weight of the telechelic oligomers is controllable by adjusting the pre-depolymerization annealing time. This is because longer annealing times yield higher molecular weight precursors with enhanced chemically reactive tie chains formed from

stretched amorphous tie chains. However, increased crystallinity prior to depolymerization, as indicated by differential scanning calorimetry (DSC), does not alter the time evolution of the molecular weight of oligomers isolated from depolymerization. The production of the dihydroxy-terminated oligomers also leads to the fragmentation of PET flakes into a powder, providing a visual indication of the isolation of telechelic oligomers via glycolysis. It is hypothesized that the PET flakes fracture when most tie chains are severed. Consequently, dihydroxy-terminated oligomers can be more promptly obtained with pre-depolymerization annealing, thus minimizing the requirement for additional post-depolymerization functionalization reactions to form targeted difunctional oligomers.

4.2 Introduction

Polyethylene terephthalate (PET) is one of the most used consumer plastics, with 30 million tons produced annually and Coca-Cola alone producing 134 billion PET bottles in 2022.[1-5] Currently, PET accounts for 13% of the world's plastic production and takes up 8% by weight and 12% by volume of global solid waste.[6, 7] Moreover, PET does not readily degrade in nature and can accumulate in living organisms, demonstrating a need to increase and simplify methods of recycling PET as only 9% of plastic is recycled.[8-13] The depolymerization of PET to isolate monomers for repolymerization has been developed using many mechanisms, including glycolysis, aminolysis, and hydrolysis; reactions that have been thoroughly investigated over the years.[2, 9, 14-21] However, these methods are designed to isolate monomers, yet do not achieve 100% yield and limit how many cycles that a given sample can undergo the depolymerization-polymerization process.[7]

Additionally, pushing the equilibrium reaction of PET glycolysis to achieve high monomer yield is energy and cost-intensive.[15] This leads to the question of whether

depolymerization to form monomers is necessary. Additional research has also focused on turning PET waste into value-added products such as paint binders and H_2 gas has begun, which will provide alternative pathways to utilize waste PET in the formation of materials to address this question.[22-24] As an additional method to recycle PET more efficiently, we hypothesize that oligomeric polymer chains that emerge from the depolymerization can be used as building blocks to form valuable materials.

Our previous work[25] demonstrates the evolution of chain structure during the glycolysis of PET chains. That work showed that ethylene glycol (EG) diffuses into the amorphous phase of PET, causing swelling, where the EG reacts with the PET ester group to cut the tie-chains, which are the chains connecting crystalline phases. This initial chain scission leaves the macroscopic flake structure intact. This was unexpected, as previous work theorized that PET glycolysis was primarily a surface reaction of the EG with the flake exterior; such a reaction would depend on flake surface area and not on the diffusion of the EG in the amorphous PET.[7, 26] Furthermore, further studies have shown that chain scission occurs first in the amorphous phase in the depolymerization of PET.[27, 28] This previous study also showed the ability to isolate nearly 100% yield of the highly crystalline dispersed oligomers, which have narrower dispersities (Đ) than the original chains.[25] Dihydroxy terminated oligomers that may emerge from the depolymerization process are valuable products of the reaction as they will be useful as macromers in producing next-generation materials without further purification. Unfortunately, the formation of dihydroxy terminated oligomers only occurs at long reaction times in these previous studies, where the yield begins to decrease. At earlier times in the depolymerization reaction, the oligomers that are formed are not functionalized at both ends, and therefore these macromonomers are not optimal for further reactions, like repolymerization.[25] Thus, further functionalization of the chain ends

on these products is required to use them as reactants in further reactions. Difunctional telechelic oligomers are the targeted macromonomer structure as they have a reactive end group on each chain end, which can serve in repolymerization or be utilized in other reactions to form unique macromolecules.[29, 30] Thus, it would be beneficial to control the structure of the intermediate oligomers that emerge from the depolymerization, including the production of difunctionalized oligomers at high yield and with lower dispersities. Could the chain evolution during depolymerization be controlled to create telechelics with lower dispersities and at high yield?

These previous results also suggest that the molecular weight of the oligomers that emerge when chain scission occurs in the amorphous phase is guided by the crystal size. Thus, altering crystal size could guide the molecular weight of oligomers that are formed. Previous studies have shown that annealing PET fibers near the T_m at 240 °C increases the size of the crystal.[31] We hypothesize that annealing PET before depolymerization will result in secondary crystallization that forms larger crystals, which in turn will generate larger intermediate oligomers. This study therefore seeks to understand how annealing PET before depolymerization impacts the structure of oligomers that emerge from the depolymerization of PET by glycolysis. The secondary crystallization is expected to increase the PET bulk crystallinity and potentially increase the crystal size and chemical reactivity of the tie chains.[32, 33] This may offer pathways to control the molecular weight of isolated telechelic oligomers, where controlling the molecular weight can expand the uses of the telechelic oligomers as building blocks and utilized in other research areas, such as repolymerization, and formation of A-B block polymers. Thus, this study will provide insight into the role of PET crystal structure on the evolution of chain structure during the depolymerization of PET by glycolysis, offering opportunities to guide the reactions towards preferred oligomeric structures for their use in further reactions.

4.3 Methods

4.3.1 Materials

PET was sourced from consumer waste Coca-Cola bottles, which were washed and cut into 8 mm x 5 mm squares. 1,5,7-Triazabicyclo[4.4.0]dec-5-ene (98.0+%, TCI America™), Methanesulfonic Acid (99%), Ethylene glycol, (99.8%, anhydrous, AcroSeal™, Thermo Scientific Chemicals), 20 mL vials, and 12.7x8mm stir bars were sourced from Fischer Scientific. 1,1,1,3,3,3-Hexafluoro-2-propanol (HFIP) was sourced from Oakwood Chemical. All chemicals were used as received.

4.3.2 PET Annealing Procedure

PET cut into 8 mm x 5 mm x 0.3 mm squares was placed in a vacuum oven at 240 °C to anneal to allow secondary crystallization. The PET flakes were annealed under vacuum for varied amounts of time: 0 hours (unannealed), 3 hours, 6 hours, 13 hours, 24 hours.

4.3.3 Catalyst

The catalyst was prepared using the same methods previously reported by Jehanno et al.[7] The organo-salt catalyst was prepared by mixing Triazabicyclodecene (TBD) and Methanesulfonic acid (MSA) at acid to base molar ratios of 1:1 at 80 °C for 20 minutes or until solidified. The product obtained was a transparent and homogenous solid.[7]

4.3.4 Reaction Conditions

Ethylene Glycol (EG), TBD:MSA catalyst, PET (20:0.5:1 molar ratio), and stir bar were all placed in a 20 mL reaction vial inside a glovebox, sealed with septa, and transferred outside the glovebox into a 180 °C oil bath. Previous studies indicate that this reaction takes under 2 hours at 180 °C to reach completion.[7] In our hands, non-recycled Coca-Cola bottles were fully depolymerized after 90 minutes. The glycolysis reaction is illustrated in**Scheme 4.1.** To analyze

the evolution of the polymer chains during PET depolymerization, the reaction was stopped at various reaction times, and the products were recovered and characterized as described below.[7]

Scheme 4.1 Heterogenous PET glycolysis reaction catalyzed by TBD:MSA to create BHET

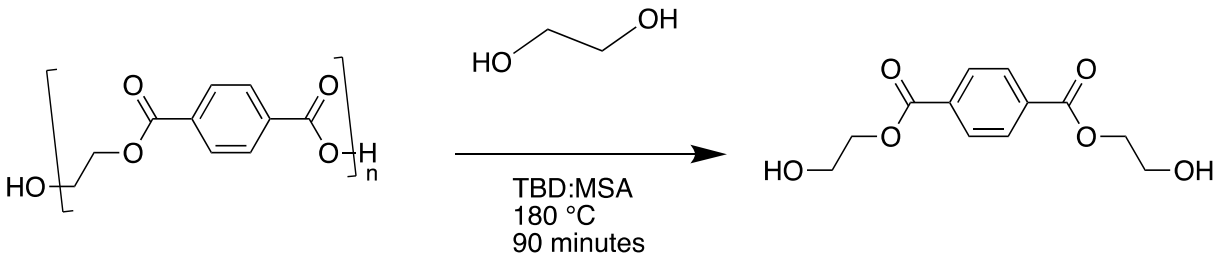

4.3.5 Product Recovery

After the reaction was allowed to run for a set time, the reaction vials were taken from the oil bath. The ethylene glycol (EG) and any depolymerization products that are soluble in EG were immediately decanted hot from the reaction vials, as visually depicted in **Figure 4.1**. The remaining solid PET that is insoluble in EG was washed with water three times by suspending it in 20 mL of water and stirring with a stir bar for 15 minutes. After the third wash and decant, the reaction vial containing this product, termed as EG insoluble, was set on a 70 °C hotplate overnight to evaporate any remaining water.

4.3.6 Depolymerization Product Characterization

4.3.6.1 Nuclear Magnetic Resonance (NMR)

The EG insoluble products of the PET depolymerization (30-60 mg) were dissolved in HFIP (1 mL) for NMR analysis. The PET:HFIP mixture was agitated for five days before 100 microliters of this solution wase mixed with 600 microliters of $CDCl_3$. The NMR spectra of these samples were obtained using a Jeol 400 YH NMR at 35 ºC for 160 scans to ensure the PET did not precipitate out of the solution. The number average molecular weights (M_n) of the depolymerization products were determined using the analysis outlined by Falkenstein[34] and

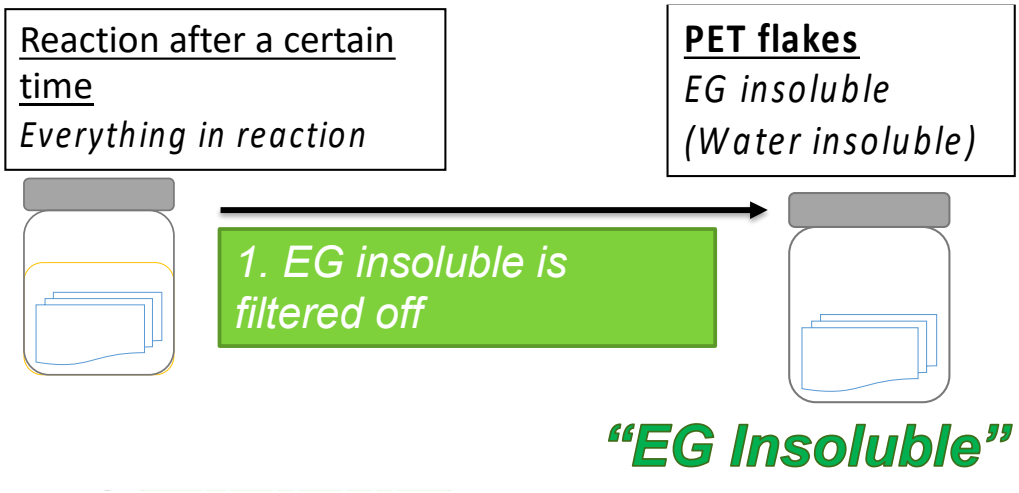

Figure 4.1 PET glycolysis work up to isolate ethylene glycol (EG) insoluble PET flakes.

assuming, on average, one hydroxyl end group per chain.

4.3.6.2 Size Exclusion Chromatography (SEC)

The SEC analyses for PET depolymerized with EG were completed in 1,1,1,3,3,3-hexafluoroisopropanol (HFIP). This analysis used an Agilent 1260 Infinity II HPLC stack connected with a Wyatt miniDAWN TREOS (MALS) and Wyatt Optilab T-rEX (dRI) detector. A poly(methyl methacrylate) (PMMA) standard and commercial PET substrate were used to verify system performance. Molar mass values were calculated assuming a dn/dc of 0.191 and 0.257 mL/g for PMMA and PET, respectively. The mobile phase and sample prep used HFIP amended with 20 mM of sodium trifluoroacetate (NaTFAc). The HPLC used 3 Agilent PL HFIPgel 250 x 4.6 mm columns attached in series with a matching guard column. PET samples were dissolved in HFIP for five days at a ~5 mg/mL concentration before being filtered (0.2 µm) and placed in the autosampler. The samples were run with a flow rate of 0.35 mL/min and a column temperature of 40 °C.

4.3.6.3 Differential Scanning Calorimetry (DSC)

The Differential Scanning Calorimetry (DSC) curves of the depolymerization products (3-7 mg) were measured in a hermetic aluminum pan with a TA Instruments Q200 DSC. In the DSC run, the sample was equilibrated at 50 °C before being heated to 280 °C with a ramp of 10 °C/min. This ramp rate was chosen to inhibit recrystallization during the scanning process.[35] Enthalpies of melting of the PET samples were determined by measuring the heat flow associated with the melting of PET from the first cycle.[36] The percent crystallinity of each sample was calculated by dividing the enthalpy of the melting of a PET sample to the enthalpy of 100% crystalline PET (140 J/g).[37]

4.3.6.4 Small Angle X-ray Scattering (SAXS)

Small Angle X-ray Scattering was collected on a Xenocs Xeuss 2.0 X-ray scattering instrument with a Pilatus3 detector. The wavelength of the X-rays was 1.54 Å. The cut samples from annealed and depolymerized PET flakes were placed on the solids sample stage. The sample-to-detector distance was 0.9m. The scattering was obtained on an absolute intensity scale then normalized by sample thickness. Scattering curves were then analyzed using the 1-dimensional correlation function using the XSact software. This analysis provides the PET lamellar crystal size and the thicknesses of the crystalline and amorphous phases of the lamellae. The long period and crystalline phase sizes were assigned from the correlation function following Holdsworth's methodology.[35]

4.3.6.5 Statistical Analysis of Variance in End-Group Data

To determine whether the variability in the number of hydroxyl end groups per PET chain was statistically significant across conditions, a one-tailed chi-square (χ^2) test for standard deviation was conducted on triplicate datasets (n = 3) for each annealing time point to identify any samples that exhibited a greater variation than our expected standard deviation. The expected standard deviation ($\sigma = 0.15$) served as a threshold above which variability was deemed practically significant, based on the point where increasing numbers of comparisons reached $P < 0.1$. The observed sample standard deviations were evaluated against this threshold, and statistical significance was assigned using $P < 0.5$ (*), $P < 0.1$ (**), and $P < 0.001$ (***) criteria.

4.4 Results and Discussion

4.4.1 Annealing of Polyethylene Terephthalate (PET)

PET was annealed at 240 °C for varying times to increase the crystal size and crystallinity. DSC, SAXS, and SEC were used to understand how the PET flakes change with

annealing, as shown in **Figure 4.2**. Over 24 hours, **Figure 4.2 (a)** shows that the bulk percent crystallinity determined from DSC increased with annealing time. However, the crystallinity increase primarily occurs within the first 3 hours of annealing. **Figure 4.2 (b)** demonstrates how the long period (green) and the crystalline phase (blue) change with annealing time at 240 °C. The long period is the length from one crystal phase to another,[35] while the crystalline phase is the size of the crystal within that lamella.[35] This data shows that the amorphous phase thickens with annealing while the crystal size changes little, which was unexpected as previous studies that annealed PET fibers at the same temperature observed an increase in crystal size.[31] However, other work in the literature has explained similar changes in the crystalline domain, as shown in **Figure 4.2 (b)**, to the perfection of the PET crystal, such as ordering of the amorphous phase that immediately neighbors the crystal, rather than lamella thickening.[38] **Figure B.1** graphs the SAXS data of the PET samples that are annealed for 0-24 hours and demonstrates an increased alignment and order to the crystalline domains with annealing time that is consistent with further crystal perfection. **Figure B.2** shows the DSC curves of the PET annealed for varying times and establishes an increase in the onset melting temperature, which is also consistent with modifications in the immediate amorphous phase.[35, 38, 39] Thus, multiple analytical techniques suggest that the annealing results in perfection of the PET crystals. **Figure 4.2 (c)** shows the change in M_n (red) and M_w (purple) of the PET with annealing time. These results show that the M_n increases slightly with annealing, while M_w more readily increases with annealing time, with the most significant increase in M_w occurring between 6 and 13 annealing hours. **Figure B.3** shows the average number of hydroxyl groups per chain with annealing time, which shows that the average number of hydroxyl end groups decreases with annealing time. We hypothesize transesterification is occurring during annealing at 240 °C, causing the increase in

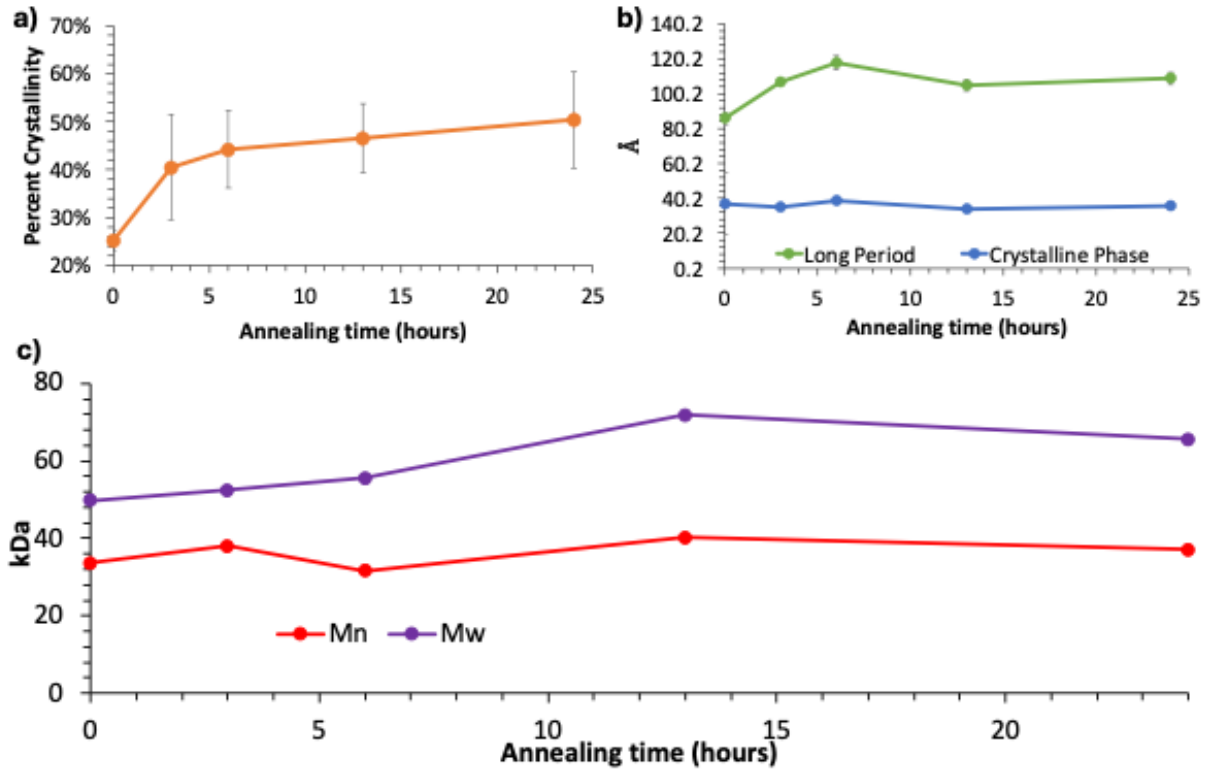

Figure 4.2 How annealing affects PET crystallinity and molecular weight. **a)** Change in percent crystallinity from DSC as a function of annealing time. **b)** Change in Long period (orange) and crystal phase (blue) of PET as a function of annealing time determined by SAXS. **C)** Change in M_n (red) and M_w (purple) of PET as a function of annealing time determined from SEC.

M_w and the decrease in hydroxyl end groups.

4.4.2 Depolymerization of Annealed PET

After the PET flakes were annealed for a time ranging between 0-24 hours, the PET flakes were depolymerized via glycolysis. **Figure 4.3** plots the change in the weight average molecular weight **(a)** and yield of the depolymerization reaction **(b)** as a function of depolymerization time for the PET flakes that are annealed at 240 °C for various times. Inspection of **Figure 4.2 (c)** shows that the M_w of the PET at the beginning of the glycolysis reaction increases with annealing, so to compare the change in M_w during depolymerization for the annealed samples, the percent change in M_w is calculated as the M_w at a specific glycolysis reaction time divided by the initial M_w of the PET after annealing. Generally, the M_w of oligomers that are isolated at particular depolymerization reaction times are similar independent of the pre-depolymerization annealing times. **Figure 4.3 (b)** shows that the yield of the PET that emerges from the reaction is ~100% regardless of annealing or reaction time. Interestingly, the yield of the PET flakes that are annealed for 13 hours at 240 °C before depolymerization decreased after 60 minutes of reaction; at this reaction time, it was visually observed that the PET flakes broke apart into a powder.

4.4.3 Determination of Average Hydroxyl End Group per PET Chain

The average number of hydroxyl groups per chain as a function of glycolysis time was determined to understand how the pre-depolymerization annealing may alter the depolymerization process and impact the isolation of telechelic oligomers from the depolymerization. **Figure 4.4** shows the average number of hydroxyl end groups per PET chain as a function of glycolysis time for each annealing time (0-hour dark blue, 3-hour yellow, 6-hour pink, 13-hour green, and 24-hour blue). **Figure 4.4 (a)** shows the change in the average

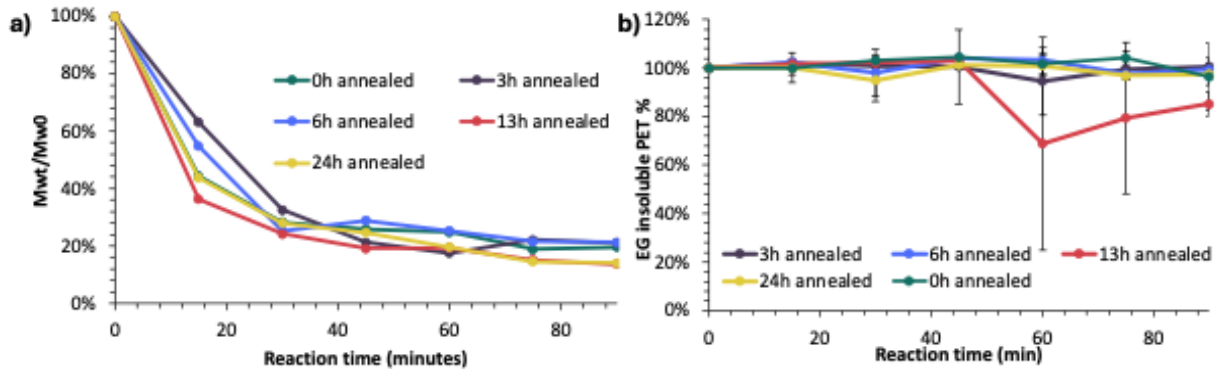

Figure 4.3 Changes in molecular weight and yield of PET annealed for varying times (0-hour green, 3-hour purple, 6-hour blue, 13-hour red, 24-hour yellow) as a function of depolymerization reaction time. **A)** The percent change of the PET M_w for PET annealed at 240 °C for different times. **b)** Change in the yield of the EG insoluble PET at specific reaction times for PET flakes annealed at 240 °C.

hydroxyl end group of the annealed PET with depolymerization time. During depolymerization, the number of hydroxyl end groups varies from one to two hydroxyl groups per chain.[7, 17, 18, 25, 40] Statistical analysis assessed whether the observed variability in hydroxyl end group values was significantly greater than expected based on an assumed standard deviation of 0.15 (see **Figure 4.4** caption). Samples without asterisks demonstrate variability that is not significantly different from the expected threshold ($\sigma = 0.15$), indicating consistent behavior across replicates. In contrast, samples marked with *, **, or *** show increasing levels of significant variation ($P < 0.5$, $P < 0.1$, and $P < 0.001$, respectively), suggesting more significant inconsistency in end-group formation under those conditions. Inspection of **Figure 4.4 (a)** shows that the number of hydroxyl end groups per chain for a given reaction time generally increases with pre-depolymerization annealing time at 240 °C. The oligomers that emerge from the depolymerization of the PET that is annealed for 13 hours before depolymerization have *ca.* two hydroxyl end groups per chain after 75 minutes of reaction. **Figure 4.4 (a)** also demonstrates that the end group conversion of the PET that is annealed for 13 and 24 hours at 240 °C before depolymerization varies with reaction time in a similar way. **Figure 4.4 (b)** shows a picture of the physical condition of the annealed PET flakes after 75 minutes of the glycolysis reaction. The number of hydroxyl groups per chain (at 75-minute glycolysis reaction) is highlighted in the orange box in **Figure 4.4 (a). Figure 4.4 (b)** shows that the PET flakes annealed at 240 °C for more extended periods (13-24 hours) before depolymerization break apart into a powder when depolymerized for 75 minutes, while those that are annealed for shorter times retain their flake-like structure. The data in the orange box in **Figure 4.4 (a)** shows that the samples that have fragmented to powder have become dihydroxy-terminated PET oligomers, while those that retain their flake-like structure have fewer hydroxyl end groups per chain. Generally, the longer the

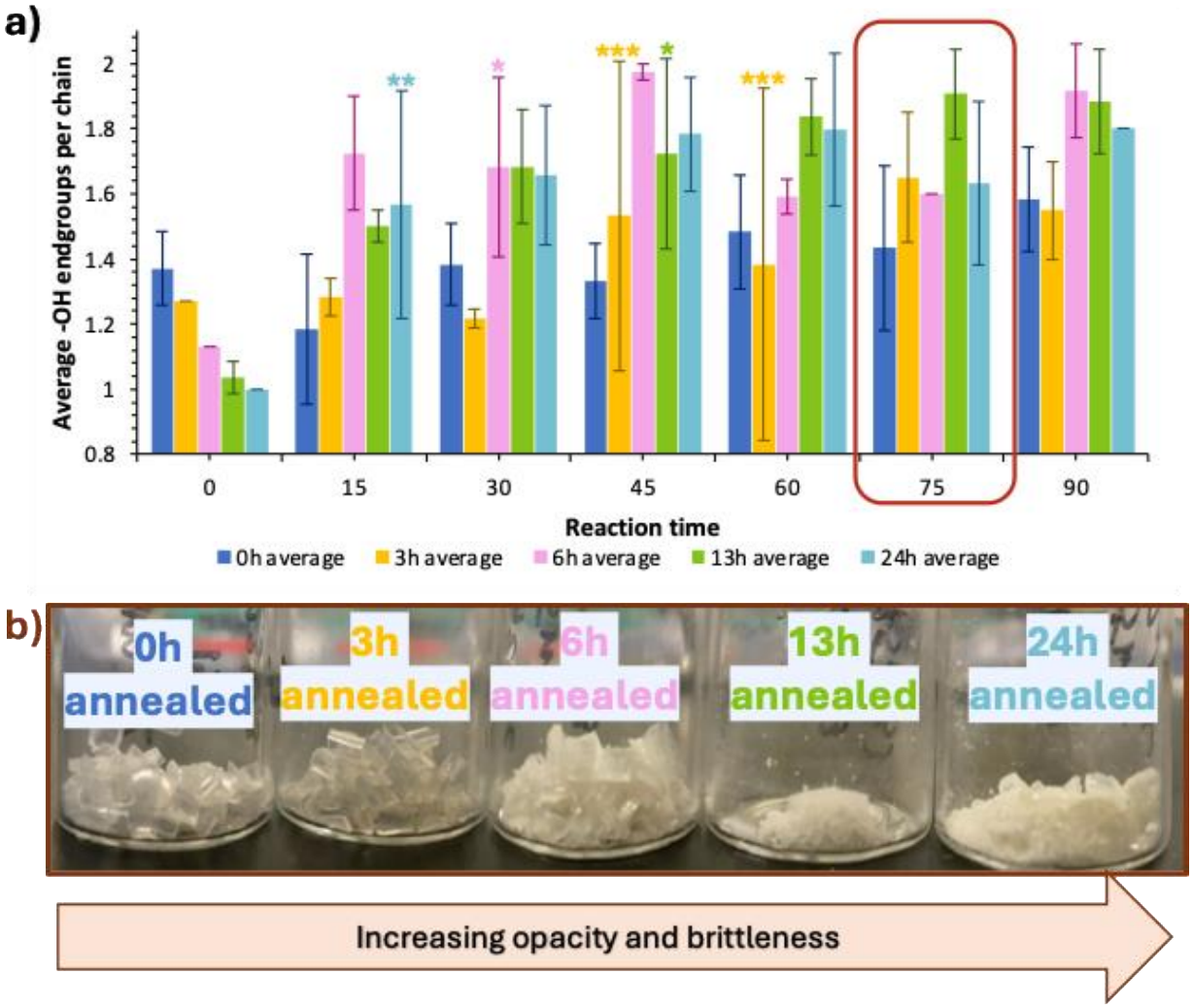

Figure 4.4 The average number of hydroxyl end groups per chain changes with glycolysis time to annealed PET. (annealing time: 0-hour dark blue, 3-hour yellow, 6-hour pink, 13-hour green, and 24-hour blue) (a) Shows the number of hydroxyl end groups per chain determined by comparing M_n from NMR and SEC-GPC. The statistical significance of variation was assessed using a one-tailed chi-square test for standard deviation, assuming an expected $\sigma = 0.15$ ($n = 3$). Asterisks indicate the degree of significance in a more significant deviation that is larger than the expected variance: $P < 0.5$ (*), $P < 0.1$ (**), and $P < 0.001$ (***). (b) shows a set of PET flakes that were annealed for varying times and then depolymerized for 75 minutes.

PET flakes are annealed at 240 °C prior to depolymerization, the more opaque and brittle their flakes become at this longer depolymerization time (75 minutes), which seems to coincide with the presence of two hydroxyl groups per chain on average.

4.4.4 *Reactivity of tie-chains*

We interpret these results to indicate that annealing PET at 240 °C prior to glycolysis alters the depolymerization process, leading to an increased formation of hydroxyl end groups. This effect can be attributed to the impact of the crystal evolution and stress-induced modifications in the amorphous phase on the depolymerization, which has been shown to promote selective cleavage and transesterification of tie chains.[32, 38, 41] As illustrated in **Figure 4.5**, we hypothesize that annealing induces fold dislocations and lamella thickening, resulting in ester interchange reactions that relieve stress on tie chains. These structural reorganizations then enhance the chemical reactivity of PET during glycolysis.

Our interpretation is supported by prior studies that have shown that annealing near the melting temperature of PET can stretch and stress amorphous tie chains, increasing their susceptibility to transesterification.[38, 41] This phenomenon is consistent with our SAXS, DSC, and SEC data (**Figure 4.2**), which indicate that annealing at 240 °C does not significantly thicken the crystalline lamellae but instead promotes reorganization of the amorphous phase. Specifically, **Figure 4.2 (b)** shows that the long period (green) increases while the crystalline phase (blue) remains largely unchanged, supporting the interpretation that the amorphous phase becomes more ordered rather than forming larger crystals. This is further supported by **Figure B.1**, where SAXS data demonstrates increased alignment and ordering of crystalline domains, indicative of crystal perfection.

DSC provides additional evidence of these structural changes. **Figure B.2** shows the

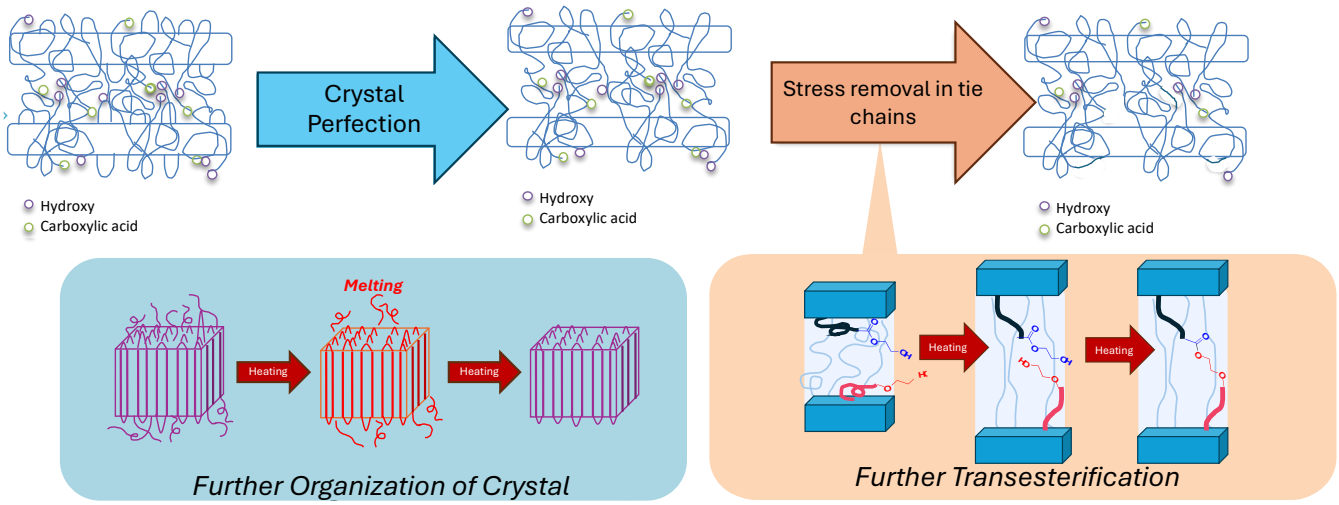

Figure 4.5 What occurs during PET annealing at 240 °C: fold dislocation during lamella thickening and subsequent ester interchange to remove stress on tie chains.

evolution of the melting behavior of PET with annealing time, where a secondary melting peak progressively merges with the initial melting peak with annealing time. The melting curves show that when the sample was annealed at 240 °C for 3 hours, a secondary melting peak appears at 230 °C, which shifts to higher temperatures with prolonged annealing, while the initial peak at 240 °C gradually disappears. This shift is consistent with the perfection and growth of smaller, with annealing time suggests modifications in the amorphous phase rather than lamella thickening, aligning with the slight decrease in crystalline phase size observed in **Figure 4.2 (b)**.[38, 42, 43]

During annealing at 240 °C, transesterification reactions facilitate reorganization of tie chains, leading to an increase in M_w over time, which is observed in our samples as shown in **Figure 4.2 (c).** The most significant M_w increase occurs between 6 and 13 hours of annealing, suggesting that prolonged exposure to elevated temperatures enhances segmental mobility and allows for further ester interchange. Simultaneously, **Figure B.3** demonstrates that the number of hydroxyl end groups on the PET chains decreases with continued annealing past 3 hours. The observed decrease in hydroxyl-terminated PET chains suggests that these chains are involved in transesterification or condensation reactions, which result in the linking of chains into longer molecules. The decrease in hydroxyl end groups implies that these -OH moieties participate in the chain extension reactions. This process is similar to the polymerization of PET from terephthalic acid (TPA) and EG, where the number of hydroxyl end groups in the reaction vessel decreases as the PET chains grow.[44, 45]

Previous studies have demonstrated that further esterification can occur when annealing PET at similar temperatures, but the impact of these reactions on molecular weight has not been previously established.[38] Since M_n is more sensitive to changes in the lower molecular weight

tail of the distribution, the observed increase in M_w with a relatively smaller change in M_n during annealing indicates that higher molecular weight chains more readily participate in these reactions than lower molecular weight ones. Thus, these reactions primarily extend high molecular weight chains leading to a more significant increase in M_w relative to M_n.[46, 47] Thus, the loss of hydroxyl end groups during transesterification is consistent with chain extension reactions, while the increase in M_w rather than M_n indicates that the reactions are more likely to occur among higher molecular weight PET chains rather than uniformly across the entire molecular weight distribution. The increase in M_w is attributed to transesterification occurring specifically among hydroxyl-capped tie chains, as illustrated in **Figure 4.5**.

These structural changes that occur in the amorphous tie chains during pre-glycolysis annealing appear to influence the PET depolymerization reactions that occur during glycolysis. As previously observed in our group,[25] once sufficient tie chains are cleaved, PET flakes lose their structural integrity and fragment into a crystalline powder. **Figure 4.6** visually depicts this phenomenon of cleaving tie chains, which results in products that are primarily telechelic oligomers. This fragmentation from flake to powder increases surface area, facilitating further glycolysis reactions and accelerating the formation of dihydroxy-terminated PET oligomers. The visual signal of powder formation from initial flakes, first noted in our previous studies,[25] remains evident in the depolymerization of annealed PET. This visual observation indicates the loss of amorphous tie chains, the formation of highly crystalline products and the emergence of telechelic oligomers in the reaction product.

Ultimately, the results confirm that pre-depolymerization annealing modifies the structure of the amorphous and crystalline chains within PET, which appears to selectively activate tie chains for glycolysis. This variation in reactivity leads to faster isolation of telechelic PET

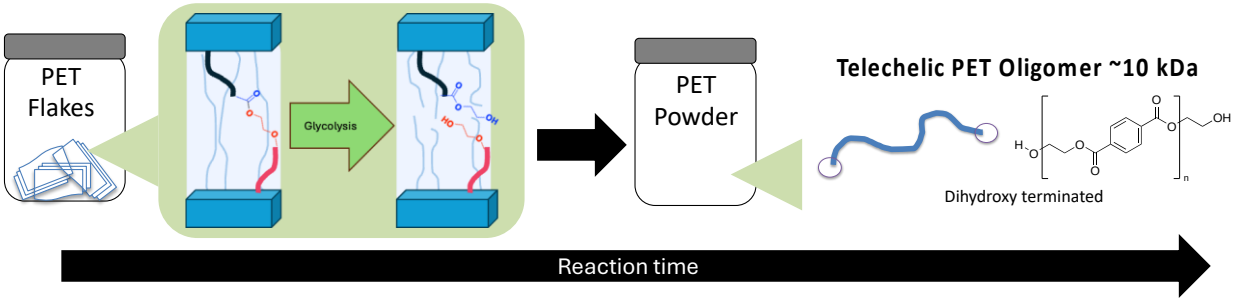

Figure 4.6 Visual representation of chain scission occurring at the tie-chains in PET. The PET flakes break into powder once all the tie chains are cut.

oligomers, with molecular weight tunability depending on annealing time. These findings align with previous literature, which has reported that annealing PET slightly below its melting temperature promotes chain reorganization rather than lamella thickening.[32, 38, 41]

4.5 Conclusions

This research project aims to understand how altering the crystalline structure of PET before depolymerization impacts the depolymerization process and how these changes could be leveraged to simplify recycling or create new value-added products. Annealing PET prior to depolymerization increases bulk crystallinity and modifies lamella structure to stretch tie chains, as demonstrated by DSC and SAXS. However, expanding bulk crystallinity before depolymerization does not influence the time variation of the molecular weight of the oligomer that results from the depolymerization. Annealing enhances the reactivity of tie chains in PET, allowing for quicker production of dihydroxy-terminated oligomers with varying molecular weights based on the duration of pre-depolymerization annealing, thereby reducing the need for post-depolymerization reactions. Through annealing PET before depolymerization, the molecular weight of the telechelic oligomers isolated from post-consumer plastic waste via chemical recycling can be regulated; for instance, telechelic oligomers of approximately 10 kDa were obtained by annealing PET for 13–24 hours before depolymerization, while earlier studies indicated that unannealed PET yields telechelic oligomers of roughly 3 kDa. This study also revealed that the macroscopic fragmentation of PET flakes into a powder coincides with the formation of PET oligomers that are dihydroxy terminated, providing a straightforward visual indication of the reaction progress.

4.6 Acknowledgements

This work was supported by the National Science Foundation, Polymers program, Division of Materials Research (DMR- 2104982). We also acknowledge Dr. Gregg Beckham and Ms. Clarissa Thompson's analysis of the depolymerized and annealed PET samples on the size exclusion chromatography (SEC). We would also like to acknowledge Mr. Timothy Taylor for his contribution by analyzing PET samples via small angle x-ray scattering (SAXS). We would also like to thank Ms. Kendra Day and Ms. Sarah Barber for their assistance on the PET depolymerization and swelling experiments.

References

(1) Sinha, V.; Patel, M. R.; Patel, J. V. PET waste management by chemical recycling: a review. *J. Polym. Environ.* **2010**, *18* (1), 8-25.

(2) Raheem, A. B.; Noor, Z. Z.; Hassan, A.; Abd Hamid, M. K.; Samsudin, S. A.; Sabeen, A. H. Current developments in chemical recycling of post-consumer polyethylene terephthalate wastes for new materials production: A review. *Journal of Cleaner Production* **2019**, *225*, 1052-1064. DOI: https://doi.org/10.1016/j.jclepro.2019.04.019.

(3) Nikles, D. E.; Farahat, M. S. New Motivation for the Depolymerization Products Derived from Poly(Ethylene Terephthalate) (PET) Waste: a Review. *Macromolecular Materials and Engineering* **2005**, *290* (1), 13-30. DOI: 10.1002/mame.200400186.

(4) Jang, J. Y.; Sadeghi, K.; Seo, J. Chain-Extending Modification for Value-Added Recycled PET: A Review. *Polymer Reviews* **2022**, *62* (4), 860-889. DOI: 10.1080/15583724.2022.2033765.

(5) Company, C. C. *THE COCA-COLA COMPANY 2022 BUSINESS & SUSTAINABILITY REPORT*; 2022. https://www.coca-colacompany.com/content/dam/company/us/en/reports/coca-cola-business-sustainability-report-2022.pdf#page%3D38.

(6) Atta, A. M.; Abdel-Raouf, M. E.; Elsaeed, S. M.; Abdel-Azim, A.-A. A. Curable resins based on recycled poly(ethylene terephthalate) for coating applications. *Prog. Org. Coat.* **2006**, *55* (1), 50-59. DOI: 10.1016/j.porgcoat.2005.11.004.

(7) Jehanno, C.; Flores, I.; Dove, A. P.; Müller, A. J.; Ruipérez, F.; Sardon, H. Organocatalysed depolymerisation of PET in a fully sustainable cycle using thermally stable protic ionic salt. *Green Chemistry* **2018**, *20* (6), 1205-1212. DOI: 10.1039/c7gc03396f.

(8) Shaikh, I. R. Organocatalysis: Key Trends in Green Synthetic Chemistry, Challenges, Scope towards Heterogenization, and Importance from Research and Industrial Point of View. *Journal of Catalysts* **2014**, *2014*, 1-35. DOI: 10.1155/2014/402860.

(9) Xin, J.; Zhang, Q.; Huang, J.; Huang, R.; Jaffery, Q. Z.; Yan, D.; Zhou, Q.; Xu, J.; Lu, X. Progress in the catalytic glycolysis of polyethylene terephthalate. *Journal of Environmental Management* **2021**, *296*, 113267. DOI: 10.1016/j.jenvman.2021.113267.

(10) Mason, S. A.; Welch, V. G.; Neratko, J. Synthetic Polymer Contamination in Bottled Water. *Frontiers in Chemistry* **2018**, *6*. DOI: 10.3389/fchem.2018.00407.

(11) McCormick, A.; Hoellein, T. J.; Mason, S. A.; Schluep, J.; Kelly, J. J. Microplastic is an Abundant and Distinct Microbial Habitat in an Urban River. *Environmental Science & Technology* **2014**, *48* (20), 11863-11871. DOI: 10.1021/es503610r.

(12) Qian, N.; Gao, X.; Lang, X.; Deng, H.; Bratu, T. M.; Chen, Q.; Stapleton, P.; Yan, B.; Min, W. Rapid single-particle chemical imaging of nanoplastics by SRS microscopy. *Proceedings of the National Academy of Sciences* **2024**, *121* (3). DOI: 10.1073/pnas.2300582121.

(13) Arifuzzaman, M.; Sumpter, B. G.; Demchuk, Z.; Do, C.; Arnould, M. A.; Rahman, M. A.; Cao, P.-F.; Popovs, I.; Davis, R. J.; Dai, S.; et al. Selective deconstruction of mixed plastics by a tailored organocatalyst. *Materials Horizons* **2023**, *10* (9), 3360-3368. DOI: 10.1039/d3mh00801k.

(14) Aguado, A.; Martínez, L.; Becerra, L.; Arieta-Araunabeña, M.; Arnaiz, S.; Asueta, A.; Robertson, I. Chemical depolymerisation of PET complex waste: hydrolysis vs. glycolysis. *J. Mater. Cycles Waste Manage.* **2014**, *16* (2), 201-210. DOI: 10.1007/s10163-013-0177-y.

(15) Carta, D.; Cao, G.; D'Angeli, C. Chemical recycling of poly(ethylene terephthalate) (pet) by hydrolysis and glycolysis. *Environmental Science and Pollution Research* **2003**, *10* (6), 390-394. DOI: 10.1065/espr2001.12.104.8.

(16) Colomines, G.; Robin, J.-J.; Tersac, G. Study of the glycolysis of PET by oligoesters. *Polymer* **2005**, *46* (10), 3230-3247. DOI: https://doi.org/10.1016/j.polymer.2005.02.047.

(17) Najmi, S.; Vance, B. C.; Selvam, E.; Huang, D.; Vlachos, D. G. Controlling PET oligomers vs monomers via microwave-induced heating and swelling. *Chem. Eng. J.* **2023**, *471*, 144712. DOI: https://doi.org/10.1016/j.cej.2023.144712.

(18) Sheel, A.; Pant, D. Chemical Depolymerization of PET Bottles via Glycolysis. **2019**, 61-84. DOI: 10.1016/B978-0-12-811361-5.00004-3.

(19) Silva, C. V. G.; Silva Filho, E. A. D.; Uliana, F.; Jesus, L. F. R. D.; Melo, C. V. P. D.; Barthus, R. C.; Rodrigues, J. G. A.; Vanini, G. PET glycolysis optimization using ionic liquid [Bmin]ZnCl3 as catalyst and kinetic evaluation. *Polímeros* **2018**, *28* (5), 450-459. DOI: 10.1590/0104-1428.00418.

(20) Wang, L.; Nelson, G. A.; Toland, J.; Holbrey, J. D. Glycolysis of PET Using 1,3-Dimethylimidazolium-2-Carboxylate as an Organocatalyst. *ACS Sustainable Chemistry & Engineering* **2020**, *8* (35), 13362-13368. DOI: 10.1021/acssuschemeng.0c04108.

(21) Yue, Q.; Wang, C.; Zhang, L.; Ni, Y.; Jin, Y. Glycolysis of poly (ethylene terephthalate)(PET) using basic ionic liquids as catalysts. *Polym. Degrad. Stab.* **2011**, *96* (4), 399-403.

(22) Bulak, E.; Acar, I. The use of aminolysis, aminoglycolysis, and simultaneous aminolysis-hydrolysis products of waste PET for production of paint binder. *Polymer Engineering & Science* **2014**, *54* (10), 2272-2281. DOI: 10.1002/pen.23773.

(23) Diao, J.; Hu, Y.; Tian, Y.; Carr, R.; Moon, T. S. Upcycling of poly(ethylene terephthalate) to produce high-value bio-products. *Cell Reports* **2023**, *42* (1), 111908. DOI: 10.1016/j.celrep.2022.111908.

(24) Uekert, T.; Kuehnel, M. F.; Wakerley, D. W.; Reisner, E. Plastic waste as a feedstock for solar-driven H₂ generation. *Energy & Environmental Science* **2018**, *11* (10), 2853-2857. DOI: 10.1039/c8ee01408f.

(25) Watson-Sanders, S.; Dadmun, M. More Efficient Chemical Recycling of Poly(Ethylene Terephthalate) by Intercepting Intermediates. *ChemSusChem* **2024**, *17* (23). DOI: 10.1002/cssc.202301698.

(26) Jehanno, C.; Pérez-Madrigal, M. M.; Demarteau, J.; Sardon, H.; Dove, A. P. Organocatalysis for depolymerisation. *Polymer Chemistry* **2019**, *10* (2), 172-186. DOI: 10.1039/c8py01284a.

(27) Yoshioka, T.; Okayama, N.; Okuwaki, A. Kinetics of Hydrolysis of PET Powder in Nitric Acid by a Modified Shrinking-Core Model. *Industrial & Engineering Chemistry Research* **1998**, *37* (2), 336-340. DOI: 10.1021/ie970459a.

(28) Mancini, S. D.; Zanin, M. Post Consumer Pet Depolymerization by Acid Hydrolysis. *Polymer-Plastics Technology and Engineering* **2007**, *46* (2), 135-144. DOI: 10.1080/03602550601152945.

(29) Ashcraft, E.; Ji, H.; Mays, J.; Dadmun, M. A Novel Reactive Processing Technique: Using Telechelic Polymers To Reactively Compatibilize Polymer Blends. *ACS Applied Materials & Interfaces* **2009**, *1* (10), 2163-2173. DOI: 10.1021/am900333y.

(30) Todd, A. D.; McEneany, R. J.; Topolkaraev, V. A.; Macosko, C. W.; Hillmyer, M. A. Reactive Compatibilization of Poly(ethylene terephthalate) and High-Density Polyethylene

Using Amino-Telechelic Polyethylene. *Macromolecules* **2016**, *49* (23), 8988-8994. DOI: 10.1021/acs.macromol.6b02080.

(31) Liu, Y.; Yin, L.; Zhao, H.; Song, G.; Tang, F.; Wang, L.; Shao, H.; Zhang, Y. Lamellar and fibrillar structure evolution of poly(ethylene terephthalate) fiber in thermal annealing. *Polymer* **2016**, *105*, 157-166. DOI: https://doi.org/10.1016/j.polymer.2016.10.031.

(32) Miyagi, A.; Wunderlich, B. Annealing during polymerization of crystalline poly(ethylene terephthalate). *Journal of Polymer Science: Polymer Physics Edition* **1972**, *10* (10), 2085-2092. DOI: 10.1002/pol.1972.180101019.

(33) Wunderlich, B. The Annealing of Crystals. *Macromolecular Physics* **1976**, 348-435. DOI: 10.1016/B978-0-12-765602-1.50009-4.

(34) Falkenstein, P.; Gräsing, D.; Bielytskyi, P.; Zimmermann, W.; Matysik, J.; Wei, R.; Song, C. UV Pretreatment Impairs the Enzymatic Degradation of Polyethylene Terephthalate. *Frontiers in microbiology*. **2020**, *11*. DOI: 10.3389/fmicb.2020.00689.

(35) Holdsworth, P. J.; Turner-Jones, A. The melting behaviour of heat crystallized poly(ethylene terephthalate). *Polymer* **1971**, *12* (3), 195-208. DOI: https://doi.org/10.1016/0032-3861(71)90045-0.

(36) Blaine, R. L. *Determination of Polymer Crystallinity by DSC*; TA Instruments, https://www.tainstruments.com/pdf/literature/TA123new.pdf.

(37) Blaine, R. L. *THERMAL APPLICATIONS NOTE*; TA Instrument, https://www.tainstruments.com/pdf/literature/TN048.pdf.

(38) Wang, Z. G.; Hsiao, B. S.; Sauer, B. B.; Kampert, W. G. The nature of secondary crystallization in poly(ethylene terephthalate). *Polymer* **1999**, *40* (16), 4615-4627. DOI: https://doi.org/10.1016/S0032-3861(99)00067-1.

(39) Ronkay, F.; Molnár, B.; Nagy, D.; Szarka, G.; Iván, B.; Kristály, F.; Mertinger, V.; Bocz, K. Melting temperature versus crystallinity: new way for identification and analysis of multiple endotherms of poly(ethylene terephthalate). *Journal of Polymer Research* **2020**, *27* (12). DOI: 10.1007/s10965-020-02327-7.

(40) Jehanno, C.; Demarteau, J.; Mantione, D.; Arno, M. C.; Ruipérez, F.; Hedrick, J. L.; Dove, A. P.; Sardon, H. Selective Chemical Upcycling of Mixed Plastics Guided by a Thermally Stable Organocatalyst. *Angew. Chem. Int. Ed.* **2021**, *60* (12), 6710-6717. DOI: 10.1002/anie.202014860.

(41) Wunderlich, B. The Annealing of Crystals. In *Macromolecular Physics: Volume 2 Crystal Nucleation, Growth, Annealing*, Academic Press, 1976; pp 348-435.

(42) Röttele, A.; Thurn-Albrecht, T.; Sommer, J.-U.; Reiter, G. Thermodynamics of Formation, Reorganization, and Melting of Confined Nanometer-Sized Polymer Crystals. *Macromolecules* **2003**, *36* (4), 1257-1260. DOI: 10.1021/ma021434c.

(43) Xu, J.-T.; Zhao, Y.-Q.; Liang, G.-D.; Fan, Z.-Q. Melting–Recrystallization of Block Copolymer Crystals in Confined Environments. *Polym. J.* **2005**, *37* (1), 43-46. DOI: 10.1295/polymj.37.43.

(44) Bardoquillo, E. I. M.; Firman, J. M. B.; Montecastro, D. B.; Basilio, A. M. Chemical recycling of waste polyethylene terephthalate (PET) bottles via recovery and polymerization of terephthalic acid (TPA) and ethylene glycol (EG). *Materials Today: Proceedings* **2023**. DOI: 10.1016/j.matpr.2023.04.160.

(45) Khairul Anuar, N. F. S.; Huyop, F.; Ur-Rehman, G.; Abdullah, F.; Normi, Y. M.; Sabullah, M. K.; Abdul Wahab, R. An Overview into Polyethylene Terephthalate (PET) Hydrolases and

Efforts in Tailoring Enzymes for Improved Plastic Degradation. *International Journal of Molecular Sciences* **2022**, *23* (20), 12644. DOI: 10.3390/ijms232012644.

(46) Stevens, M. P. *Polymer Chemistry: An Introduction*; Oxford University Press: Oxford, 1999.

(47) Odian, G. *Principles of Polymerization*; John Wiley & Sons, Inc., 2004.

CHAPTER 5: VISUALLIZING POLYETHYLENE, POLYETHYLENE TEREPHTHALATE, AND POLYSTYRENE AS MICRO AND NANOPLASTICS UTILIZING TRANSMISSION ELECTRON MICROSCOPY

A portion of this chapter was included in a publication in *Science of the Total Environment* by Dr. Julie R. Peller:

Julie R. Peller; Stephen Mezyk; Mark Dadmun; Juan Medina-Garcia; Julien Tournebise; Shelby Watson; Christina Davis; Abbie Valicevic; Yanni Flaherty; Noah Durlam (2025) "Incognito forms of polyethylene: modified molecular vibrational bands of small micro and nanoplastics in water and other solvent" Science of The Total Environment 2025 Vol. 968 Pages 178923 DOI: 10.1016/j.scitotenv.2025.178923 Department of Chemistry, Valparaiso University

I was responsible for PET depolymerization, characterization, and TEM imaging in this article. Dr. Julie Peller and her students prepared the polyethylene and polystyrene nanoparticle samples. Dr. Mark Dadmun organized this project and facilitated the writing of the manuscript.

A portion of this chapter was included in a publication in *Nature Communications* by Nicholas F. Mendez:

Nicholas F. Mendez, Vivek Sharma, Michele Valsecchi, Vighnesh Pai, Johnny K. Lee, Linda S. Schadler, Alejandro J. Müller, Shelby Watson-Sanders, Mark Dadmun, Guruswamy Kumaraswamy & Sanat K. Kumar; Mechanism of quiescent nanoplastic formation from semicrystalline polymers. *Nature Communications* **2025**, *16* (1). DOI: 10.1038/s41467-025-58233-3. Department of Chemical Engineering, Columbia University, New York, New York 10027, USA

I was responsible for PET depolymerization via glycolysis, characterization, and TEM imaging in this article. Dr. Sanat K. Kumar and his students prepared characterized the PET nanoparticle samples that were fragmented via hydrolysis. Dr. Mark Dadmun organized this project and facilitated the writing of the manuscript.

5.1 Abstract

The formation of small micro and nanoplastic (sM&NP) particles is a critical yet poorly understood aspect of plastic degradation, primarily due to the challenges linked to their detection and characterization. This study explores the fragmentation of polyethylene terephthalate (PET), polyethylene (PE), and polystyrene (PS) into sM&NP, focusing on the roles of polymer-solvent compatibility, glass transition temperature (T_g), and exposure duration. Transmission Electron Microscopy (TEM) effectively captures sM&NP particles suspended in water, providing essential insights into their morphology and crystallinity. TEM images of sM&NP derived from depolymerized PET reveal particles showing heterogeneous contrast, where darker regions in TEM images correlate with higher crystallinity. PE sM&NP appeared as thin films in TEM images, aligning with Raman Spectroscopy results that indicated decreased crystallinity due to solvent-induced swelling. Energy-Dispersive X-ray Spectroscopy (EDS) and High-Angle Annular Dark-Field (HAADF) imaging revealed oxygen-rich areas in PE particles, suggesting oxidation and molecular rearrangement during fragmentation. In contrast, PS sM&NP were larger, more distinct, and darker in shading in TEM, indicating that its higher T_g inhibits solvent penetration and subsequent nanoscale fragmentation. These results underscore the influence of polymer properties on environmental degradation pathways, demonstrating that lower-T_g polymers like PE undergo solvent-assisted fragmentation, while higher-T_g polymers like PS remain more resistant. The findings highlight the need for further research into how solvent interactions and polymer physicochemical properties govern the formation of nanoscale plastic pollutants, shaping their persistence and impact in aquatic environments.

5.2 Introduction

Plastic production has grown significantly since the mid-20th century, with over 400 million metric tons produced annually.[1-3] Despite increased waste management and recycling efforts, an estimated 10 to 15 million metric tons of plastic leak into the environment annually, with a considerable portion entering marine ecosystems.[4-9] This leakage occurs through various pathways, including improper waste disposal, stormwater runoff, and industrial discharge.[5] Plastics are essential materials in modern life, but their accumulation and breakdown into microplastics (MPs, 1 µm to 5 mm) and nanoplastics (NPs, <1 µm) pose environmental and health risks.[1, 10-27] Many recent studies have demonstrated that even biodegradable polymers fragment into millions of MPs, often more abundantly than non-biodegradable plastics.[28-31] The increasing presence of small micro and nanoplastic (sM&NP) particles in the environment poses a significant environmental and ecological threat by generating pathogens and hazardous chemicals.[14] These particles are detrimental to aquatic life and have been associated with potential ingestion by humans through commonly used consumer products.[16, 19-27] Furthermore, sM&NP can enter the human body through inhalation, skin contact, and the food chain, leading to severe health effects.[21, 26, 32-37] **Figure 5.1** illustrates how MPs and NPs may leach into the environment from industrial discharges or fragmentation of discarded consumer waste and may be ingested by aquatic organisms, moving up the food chain. It is estimated that up to 51 trillion microplastic fragments accumulate in the ocean and form NPs through further fragmentation.[5-9, 14-17, 21-23, 35]

Despite the abundance of sM&NP particles, analyzing and characterizing MPs and NPs remains challenging due to their small sizes, heterogeneous morphologies, and diverse chemical compositions, often a result of the degradation of larger plastics.[32, 35] These particles commonly

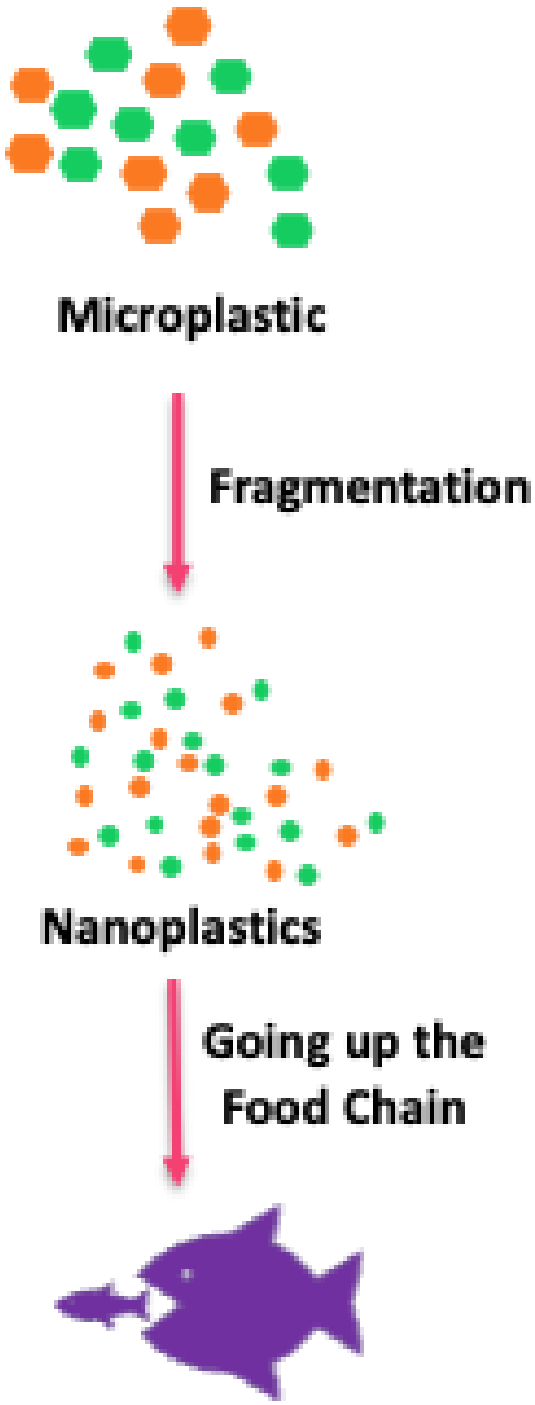

Figure 5.1 Formation of nanoplastics (NPs) by microplastic fragmentation. Said NPs move up the food chain as they are ingested by aquatic life and eventually humans.

.

accumulate environmental contaminants, such as heavy metals and organic pollutants, which can obscure their intrinsic properties and complicate spectroscopic identification.[14] Advanced analytical methods, including Raman spectroscopy, Fourier-transform infrared spectroscopy (FTIR), dynamic light scattering (DLS), and electron microscopy, are necessary to provide the sensitivity and resolution required to identify and characterize these materials. However, these techniques are time-consuming, require extensive sample preparation, and demand highly specialized expertise.[38] Furthermore, differentiating MPs and NPs from natural organic matter, mineral particles, or other anthropogenic debris often results in false positives or mischaracterizations.[39, 40] The lack of universally accepted protocols or standards exacerbates these issues, leading to inconsistencies across studies and limiting the reliability of collected data. A concerted effort to establish standardized methodologies and cross-disciplinary approaches is crucial to effectively address these challenges.

Other challenges in characterizing MPs and NPs lie in their unique physicochemical properties resulting from their small size, which includes behaviors such as Brownian motion and homogeneous dispersion in water and air.[41] Their high surface area-to-volume ratio enhances interfacial interactions with solvents and other substances.[42] In aqueous environments, wettability — the ability of water to interact with these particles — is affected by free-energy factors. These interactions may vary with real-world weathering, as it may introduce polar functional groups and surface roughness to the particles.[43] Similarly, surface hydrophobicity is influenced by intermolecular interactions and micro- to nanoscale roughness. These changes in characteristics, compared to those of the bulk polymer from which these MPs and NPs are derived, complicate their characterization.

This chapter outlines our efforts to develop tools that will facilitate the study of sM&NP

particle fragmentation processes using transmission electron microscopy (TEM). These tools are subsequently employed to examine the significance of solvent-polymer compatibility on polyethylene (PE) and polystyrene (PS) fragmentation processes over time. Previous research within our group has emphasized the importance of solvent-polymer compatibility in regulating the rate of heterogeneous depolymerization. These studies indicate that depolymerizing polyethylene terephthalate (PET) with ethylene glycol (EG), a diol that has low compatibility with PET, leads to the isolation of a highly crystalline and narrowly dispersed PET powder, where the formed powder particles are on the micron and sub-micron length scale. These findings suggest a connection between the depolymerization process and the formation of sM&NP. Consequently, the depolymerized PET powder is analyzed to provide a baseline for TEM's ability to detect and characterize the properties of MPs or NPs. In a parallel investigation, the Peller group at Valparaiso University studied the degradation of PE samples as a function of polymer-solvent compatibility and temperature. The collaborative research with the Peller group sheds light on the significance of solvent compatibility on the evolution of the unique physicochemical properties of MPs and NPs with time. Furthermore, these Raman Spectroscopy and Electron Microscopy studies illustrate that increased exposure of sM&NP to less-compatible solvents modifies their unique physicochemical properties compared to those of the bulk polymer.

In this study, we aim to enhance the understanding of how TEM can be utilized to observe and analyze the structural evolution of MPs and NPs during the fragmentation of microplastics and the subsequent formation of sM&NP. TEM imaging reveals distinct morphological changes that occur over time, highlighting the progressive breakdown of microplastics into smaller fragments and the eventual formation of NPs. These findings were

corroborated by Raman spectroscopy and DLS, which confirm the chemical integrity and characteristic vibrational bands of the polyethylene (PE) particles throughout the fragmentation process, as well as the particle size of sM&NP. These complementary approaches underscore the influence of solvent-polymer interactions on the degradation pathways and the resulting particle size distribution in aqueous environments.[44] By combining high-resolution TEM imaging with Raman spectral analysis, this study contributes to a more comprehensive understanding of the environmental fate of plastic waste and advances the methodologies available for accurately characterizing NPs, particularly in water. [32, 35]

5.3 Experimental

5.3.1 Materials

Before glycolysis or pulverization for TEM imaging, coke bottles (PET source) were cut into 8x5mm flakes. PET was sourced from commercial Coca-Cola bottles, which were washed and cut into 8x5mm squares. 1,5,7-Triazabicyclo[4.4.0]dec-5-ene (TBD, 98.0+%, TCI America™), Methanesulfonic Acid (MSA, 99%), Ethylene glycol, (EG, 99.8%, anhydrous, AcroSeal™, Thermo Scientific Chemicals), 20 mL vials, and 12.7x8mm stir bars were sourced from Fischer Scientific. 1,1,1,3,3,3-Hexafluoro-2-propanol (HFIP) was sourced from Oakwood Chemical. All chemicals were used as received.

Polyethylene (PE) microplastics were purchased from MilliporeSigma (Burlington, MA, USA) with an M_w of ~4,000 g mol^{-1} and M_n ~1700 g mol^{-1}, as determined by gel permeation chromatography (GPC), and a density of 0.92 g/mL at 25 °C. Polystyrene microplastics were also purchased from MilliporeSigma (Burlington, MA, USA) with a particle size of 10-20 µm and density of 1.05 g/cm^3. These microplastics were heat-treated at 70 °C for several days to eliminate volatile and semi-volatile contaminants.[25] Analytical standard grade n-dodecane

(>99.8%), was purchased from MilliporeSigma. Laboratory water mixtures were prepared with Millipore MilliQ deionized water (18.2 MΩ) that was distilled in-house to reduce or eliminate micro and nanoplastics that are contaminants.[26] LCMS grade acetonitrile, acetone and methanol were purchased from MilliporeSigma. Stainless steel slides, μ-RIM slides, were purchased from BioTools (Jupiter, FL, USA).

5.3.2 Preparation of polyethylene terephthalate (PET) nanoplastics (NPs)

Virgin PET flakes and water were mixed in a Nutra Bullet for 45 minutes to pulverize them into a sufficiently small size for the TEM grid. The pulverized virgin PET flakes were then gravity-filtered and air-dried before the preparation of the TEM grids. These samples served as a standard for the micro and nano-sized PET particles that are formed by PET depolymerization.

Depolymerized PET micro- and nanoparticles were formed by glycolysis, the reaction of which is shown in **Scheme 5.1**. This reaction uses an organocatalyst previously reported by Jehanno et al. to efficiently depolymerize PET via glycolysis.[45] The salt catalyst was prepared by mixing Triazabicyclodecene (TBD) and Methanesulfonic acid (MSA) at molar ratios of acid to base of 1:1 at 80 °C for at least 15 minutes. The product obtained was a transparent and homogenous solid. In the depolymerization reaction, Ethylene Glycol (EG), TBD:MSA catalyst, PET (20:0.5:1 molar ratio), and a stir bar were all placed in a 20 mL reaction vial inside a glovebox, sealed with a septa, and transferred outside the glovebox into a 180 °C oil bath. Previous studies indicate that this reaction takes under 2 hours at 180 °C to reach completion.[45, 46] To analyze the evolution of the polymer chains during PET depolymerization, the reaction was stopped at various reaction times, and the products were recovered and characterized as described below.[45, 46]

Scheme 5.1 Depolymerization of PET via glycolysis

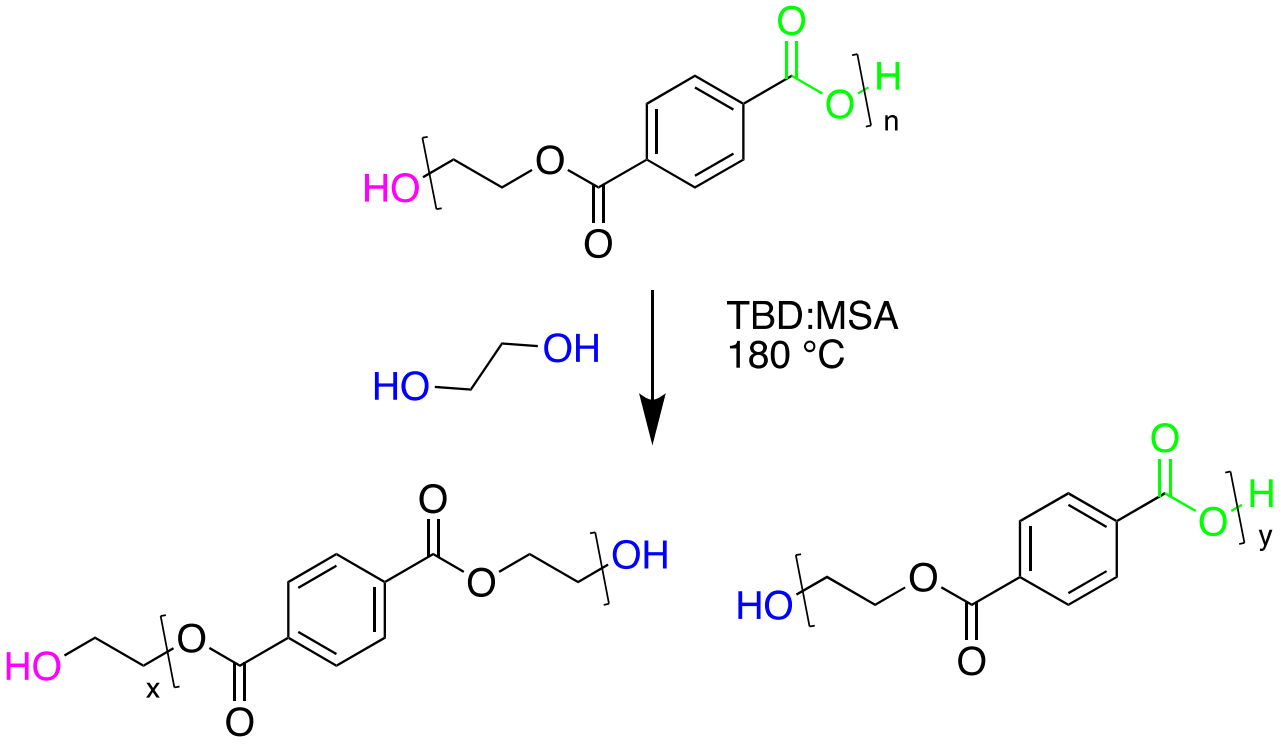

5.3.3 Size Exclusion Chromatography (SEC)

The molecular weight of some of the depolymerized PET products were determined by Size exclusion Chromatography. The SEC analyses were completed at PolyAnalytik using a Triple Detection GPC/SEC. This analysis used a Viscotek TDA302 and GPCmax instrument with Refractive Index, Light Scattering, and Viscometer detectors using a poly(methyl methacrylate) in HFIP standard. A dn/dc of 0.257 mL/g for PET in HFIP was used in the light scattering detector. The SEC/GPC Columns used are PA-HFIP 603, 604, and 606. The samples were run with a Flow Rate of 0.7 mL/min and an analysis temperature of 35 °C.

5.3.4 Differential Scanning Calorimetry (DSC)

The Differential Scanning Calorimetry (DSC) Q200 curves of the depolymerization products (3-7 mg) were measured in a Hematic aluminum pan. In the DSC run, the sample was equilibrated at 50 °C before being heated to 280 °C with a ramp of 10 °C/min. Enthalpies of melting of the PET samples were determined by measuring the heat flow associated with the melting of PET from the first cycle.[47] The percent crystallinity of each sample was calculated by dividing the enthalpy of the melting of a PET sample by the enthalpy of 100% crystalline PET (140 J/g).[48]

5.3.5 Preparation of polyethylene (PE) NPs

Polystyrene (PS) and polyethylene (PE) microplastic particles were purchased and suspended in different solvents to observe how solvent conditions influenced particle formation and potential NP generation. While PE was dispersed in many solvents (acetonitrile, acetone, and methanol, water, water/n-dodecane mixture), PS was only suspended in a water/n-dodecane mixture.

5.3.5.1 PE & PS small micro and nanoplastics (sM&NP) suspended in water/n-dodecane mixture

To create nanoparticles in water/n-dodecane mixtures, PE or PS microplastics (3–10 mg) were

added to 10 mL of DI water in a 20 mL scintillation vial, capped, and shaken vigorously by hand. A syringe was then used to introduce 10–30 µL of n-dodecane as the solubilizer to the mixture. Each vial was shaken for 30–60 seconds, resulting in a cloudy suspension, which was further processed via ultrasound mixing (40 kHz) for 20–120 minutes to optimize dispersion/dissolution. Higher solubilizer-to-plastic ratios (e.g., 500 µL n-dodecane in 500 mL aqueous solution with 20 mg plastic) facilitated the complete dispersion of the polymer. Solvent extraction using diisopropyl ether and/or heat treatment was performed to remove residual solubilizer from the microplastic and NP suspensions. The effectiveness of solubilizer removal was confirmed using headspace solid-phase microextraction (SPME) and gas chromatography-mass spectrometry (GC-MS), following the methodology established in previous work by the Peller group.[49] Transmission electron microscopy (TEM) was used to analyze the PE and PS particles that are formed in the water/n-dodecane solutions.

5.3.5.2 PE sM&NP suspended in water

To create nanoparticles in water dispersions, PE microplastics (3–10 mg) were added to 10 mL of DI water in a 20 mL scintillation vial, capped, and shaken vigorously by hand before undergoing similar ultrasound mixing as PE or PS in water/n-dodecane solutions. Additionally, the PE particles that were prepared in only water were also characterized by TEM. To investigate the effect of aging of PE sMP&NP suspensions on further NP formation, some PE sM&NP suspended in water were freshly mixed prior to shipment for TEM characterization while other PE sM&NP suspended in water had been sealed and stored under standard laboratory lighting for three years prior to shipment for TEM characterization. The structure of particles in the freshly prepared suspensions were compared to the particles that exist in the three-year-old aged suspensions.

5.3.5.3 PE sM&NP suspended in organic solvents

To create nanoparticles in organic solvents, PE microplastics (3–10 mg) were added to 10 mL of organic solvent (acetonitrile, acetone, or methanol) in a 20 mL scintillation vial, capped, and shaken vigorously by hand before undergoing similar ultrasound mixing as PE and PS in water/n-dodecane solutions.

5.3.6 Raman Spectroscopy and Microscope Imaging

A Renishaw inVia Qontor confocal Raman microscope, equipped with a Leica optical microscope with brightfield and darkfield microscopy capabilities, was used to analyze the formed sM&NP. Droplets of sM&NP suspensions were deposited onto stainless-steel slides and heated on a hot plate at 40°C until dry. Using a 532 nm laser, high spatial resolution Raman spectra were collected at a rate of 30 seconds/point using a 100X microscope objective. A 1200 lines/mm grating was used, capturing a spectral window from 700 to 3150 cm^{-1}. Prior to data collection, the instrument was calibrated using an internal silicon (Si) sample, setting the first order silicon band to 520.5 cm^{-1}. All post processing, including baseline subtraction using intelligent polynomials, was performed using the Renishaw WiRE software. Spectral figures were generated from the Renishaw WiRE data files using Igor64 software. Igor64 was also used to produce normalized spectra.

5.3.7 Particle Size Analysis

Particle size distributions and averages, along with zeta potentials, were measured using a Malvern Zetasizer Nano zs90 dynamic light scattering (DLS) analyzer at room temperature. Nanoparticle solutions (2.0 mL) were transferred to Suprasil UV cuvettes using glass Pasteur pipettes and run in triplicate. Average particle sizes were as calculated using the in-built software analyses.

5.3.8 Scanning Electron Microscopy (SEM)

SEM was used to verify the size distribution of the depolymerized PET particles, ensuring that they were of suitable size for TEM use. SEM sample preparation involved preparing the SEM stage by applying double-sided carbon tape before transferring the depolymerized PET powder sample onto it. After transferring the sample, the stage was tapped, and air was blown to remove any excess sample. The SEM stage was then inserted into the brass holder and placed into the SPI-Module™ Sputter Coater, positioned 50 mm away from the Iridium source. The sputter coating was conducted at 20-25 Amps for two intervals of 20 seconds each. This preparation method does not require that the depolymerized PET particles are suspended in water.

5.3.9 Transmission Electron Microscopy (TEM)

To prepare the TEM samples, the micro and nano-plastic PE, PS, or PET particles were suspended in DI water. A copper-coated carbon grid was placed atop a drop of sample (copper side up) for 2 minutes. Excess sample on the carbon grid was removed by touching the edge of the grid to filter paper. The grid was then placed on a drop of DI water for 5 seconds for washing, and again excess DI water from the grid was removed by touching the edge of the grid with filter paper. Washing is essential for removing excess loosely bound particles that could interfere with uniform staining or become detached in the high vacuum environment of the TEM chamber. The grid was then placed copper side up on a drop of UranyLess EM stain solution for 2 minutes to create a coating that will limit charging of the polymer particles during the TEM experiment. The grids were allowed to dry in air for at least 24 hours and then imaged using a JEOL 1440-Flask TEM at 120 kV. [50, 51] The images of the samples that emerge from the TEM exhibit varying darkness that depends on sample thickness. Thicker regions of samples scatter more electrons, resulting in darker areas on the image. Thinner regions allow more electrons to

pass through, appearing brighter. [52, 53] Electron Diffraction was performed with a beam stop and a 20 μm hat aperture condenser.

5.4 Results & Discussion

5.4.1 Structure of Products of PET Depolymerization

Given our insight into the depolymerization process of PET by glycolysis from our previous work,[46] we attempted to use the powder particles resulting from this process as a foundation for elucidating the ability of TEM to visualize the size and shapes of micron and nanoscale polymer particles. This approach also enables us to observe how low-solubility solvent environments influence the fragmentation process, thus affecting the formation of both micro and nanoplastics. The solubility parameters of PET (20.85 $MPa^{1/2}$) and ethylene glycol (32.98 $MPa^{1/2}$), with a difference of over 4 $MPa^{1/2}$, indicate poor solvent compatibility.[54-56] This process provides a foundational understanding of TEM's limitations to characterize MPs and NPs in modest or poor solvents, as most polymers discarded in the environment exhibit low solubility with water, which may impact their fragmentation and analysis under environmental conditions. PET was depolymerized for 75 minutes and then analyzed using SEC and DSC. The molecular weight of the PET oligomers isolated from this reaction was ~20% of that of the virgin PET's; as **Table 5.1** shows, the virgin PET had a number average molecular weight (M_n) of 20 kDa while the M_n of the isolated oligomers was 4.3 kDa. As demonstrated in the group's previous work on PET glycolysis,[46] the dispersity (PDI) of the oligomers decreased with depolymerization, as the virgin material has a dispersity of 2.6, and the dispersity of the isolated oligomers was 1.148. DSC also demonstrated that the percent bulk crystallinity of the depolymerization products increased after glycolysis from 25% to 70%. [57]

Table 5.1 Change in molecular weight, dispersity, and crystallinity of polyethylene terephthalate (PET) after 75 minutes of glycolysis

Reaction Time (min)	M_n (kDa)	Đ	% Crystallinity (DSC)[+]
PETGLY-0m*	20	2.6	25%
PETGLY-75m	4.265	1.148	70%

*non-reacted or virgin PET is included in this table to detail the PET changes due to this glycolysis reaction

[+] 100% crystalline PET is estimated to be 140 J/g

Scanning Electron Microscopy (SEM) was initially used to characterize the size and size distribution of the particles formed in the depolymerized PET. **Figure 5.2** shows SEM images of the PET powder, which reveals a wide range of fragment sizes, from 700 µm to over 100 nm. To better visualize the smaller, nanometer-sized fragments, transmission electron microscopy (TEM) was used. These smaller fragments were predominantly found on the surface of larger particles. Despite efforts to isolate the particles by blowing air to remove excess material not adhered to the carbon tape, some smaller fragments still clung to the larger particles. We interpret this observation to indicate the formation of the smaller particles being driven by the fragmentation of pieces from the larger particles. Since MPs are formed during the chemical recycling of PET, it is assumed that the fragmentation process for PET MPs and NPs in these conditions is primarily a chemical process. The fragmentation process did not occur uniformly across the sample, as the size of the smaller fragments varied, and the various smaller particles did not break apart at the same rate. The irregular fragmentation behavior is likely due to the poor solubility of PET in ethylene glycol, which may hinder the uniform breakdown of the polymer, resulting in uneven fragmentation and the persistence of larger particles that resist further degradation. The limited solvent-polymer compatibility likely hinders the effective breakdown of PET, causing uneven fragmentation and the persistence of larger particles that resist further degradation.

Figure 5.3 presents TEM images of additional PET powder particles. Inspection of this figure reveals that, as seen in **Figure 5.2**, the depolymerized PET powder particles span a range of sizes from the micron to nanometer scale. **Figure 5.3** shows TEM images of the PET powder particles at higher magnification than in Figure 5.2, with sizes ranging from ~100 nm to 5 microns. In **Figure 5.3 (a)**, a non-uniformly shaped microplastic is imaged alongside smaller

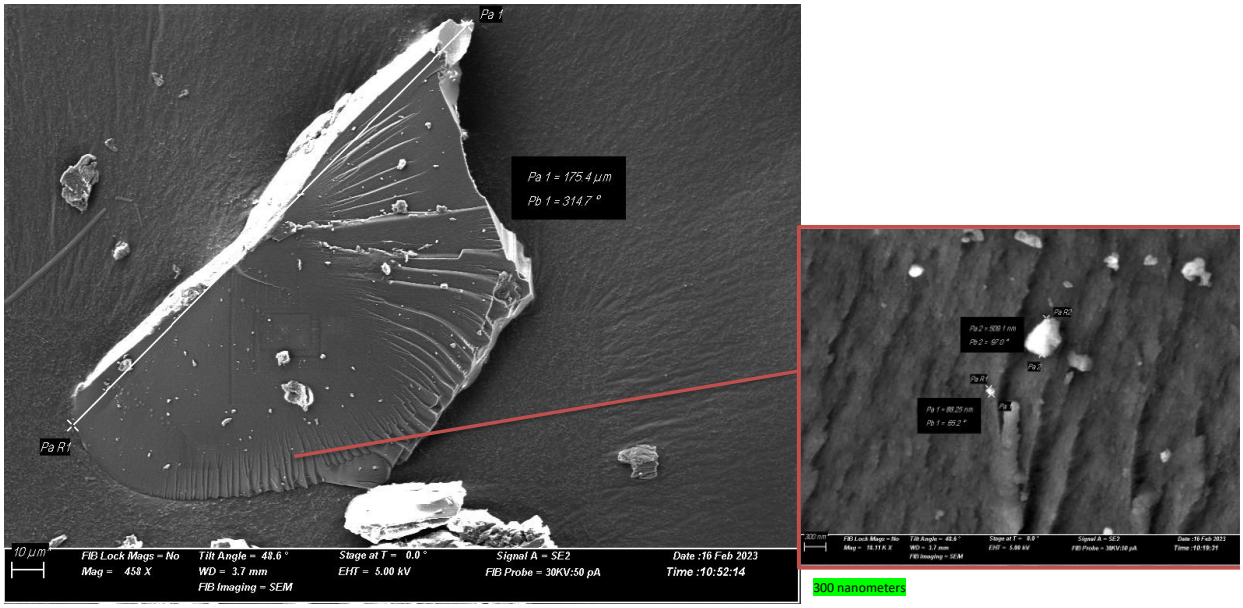

Figure 5.2 Scanning Electron Microscopy (SEM) of depolymerized PET. Scale bars in images vary.

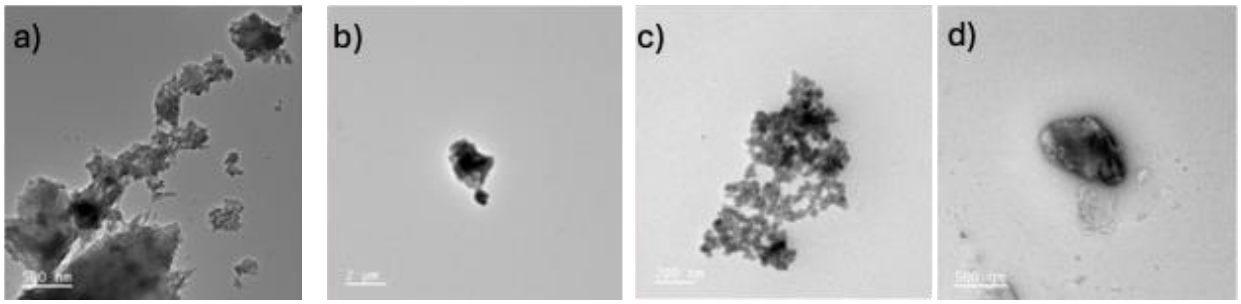

Figure 5.3 TEM images of depolymerized PET at a range of length scales. Note that the scale bar is different in each image.

nanoplastics, possibly demonstrating the fragmentation process from microplastics to nanoplastics in real-time. In **Figure 5.3 (b),** two particles, each hundreds of nanometers in length, display varying shades due to differences in particle thickness and three-dimensional shape. Thicker regions of the samples scatter more electrons, leading to darker images, while thinner regions allow more electrons to pass through, appearing brighter.[52, 53] The thicker regions of the particles, which remain more intact, may indicate the presence of crystalline domains of PET. The fact that these crystalline domains remain suggest they are less accessible to the solvent which hinders their fragmentation. **Figure 5.3 (c)** shows particles ranging from tens to hundreds of nanometers in size, with varying contrast. This figure also reveals the presence of voids within the particles, suggesting that some products of the PET depolymerization dissolved into the ethylene glycol while others were left behind. These voids may result from the degradation of the amorphous phase of the PET, with the remaining crystalline polymer being more resistant to the depolymerization process. The thicker, more crystalline regions likely contribute to the persistence of larger fragments, resisting further fragmentation. Finally, **Figure 5.3 (d)** shows the presence of polymer powder particles on the micron scale, i.e., microplastics, within the TEM samples. These results demonstrate that TEM is suitable to monitor the fragmentation process of polymer powders, from microplastics to NPs.

Additional TEM images were captured to more fully examine the length scales that are accessible by TEM and verify the presence of PET nanoparticles (NPs). **Figure 5.4** provides images of the powder particles that exist in the PET depolymerization product on length scales down to 10 nm. **Figure 5.4** clearly shows that the NPs exist that are as small as 10 nm in size. **Figure 5.4 (a)** shows the assembly of the powder particles in a concentrated area of PET NPs. This image can be further magnified to focus on specific areas within the concentrated NP

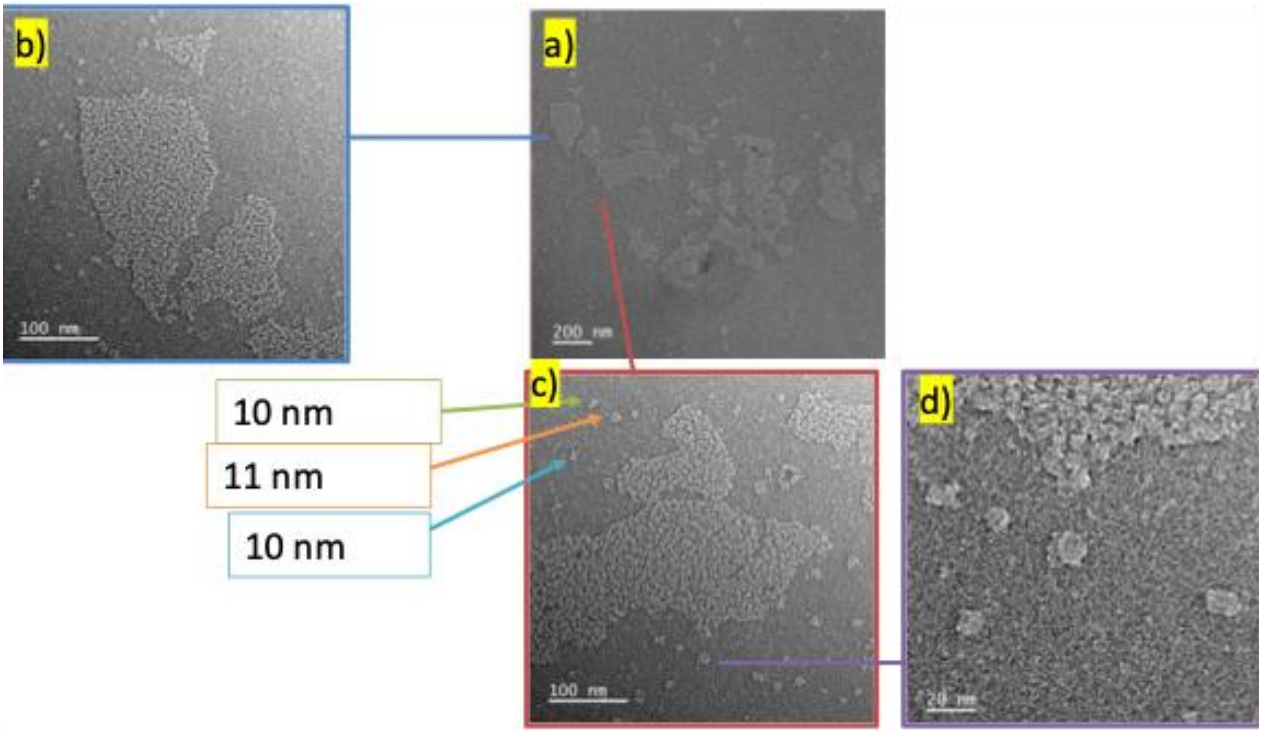

Figure 5.4 Transmission Electron Microscopy (TEM) images of depolymerized polyethylene terephthalate (PET) from glycolysis. **(a)** A scale bar of 200 nm reveals a cluster of small particles. **(b)** A scale bar of 100 nm shows a zoomed-in view of part (a), providing a more detailed representation of the particles. **(c)** A scale bar of 100 nm depicts a zoomed-in portion of part (a), offering a clearer depiction and size measurement of the particles, which are approximately 10 nm. **(d)** A scale bar of 20 nm displays a zoomed-in view of part (c) to enhance visualization of the 10 nm particles.

region, as highlighted in **Figure 5.4 (b-c)**. Further magnification provides **Figure 5.4 (d),** which showcases a closer view of **Figure 5.4 (c).** Inspection of this figure shows that the larger NP or microplastic appear to consist of assemblies of nanoparticles that are around 10 nm in size. The variability in size of the particles that are observed may be influenced by the poor solvent compatibility of PET in ethylene glycol (EG), which likely impacts the fragmentation rate of the polymer and persistence of the NPs. Thus, these results show that TEM is suitable to investigate the size of nano plastic particles that exist down to ~ 10 nm and that the size of the polymer particles formed from the depolymerization of PET by glycolysis ranges from 10's of nm to many microns.

As **Table 5.1** shows, the depolymerized PET particles are highly crystalline (70%). To provide additional information on the crystal structure that may exist in a given nano- or microparticle, electron diffraction of the particles is completed in the electron microscope**.** **Figure 5.5** presents TEM images and electron diffraction patterns of virgin PET and particles that exist in the depolymerized PET sample.

In **Figure 5.5 (a)** and **(b),** the edge of a TEM grid and a thin PET nanoparticle with numerous voids are shown for reference. The edge of the TEM grid illustrates what an empty grid looks like, while the image of the thin PET particle reveals many voids that may indicate a polycrystalline structure. **Figure 5.5 (c)** displays the TEM image of a particle similar to that shown in **Figure 5.5 (b),** which is approximately 100 nm in size and contains voids. **Figure 5.5 (d)** presents the electron diffraction pattern of the sample imaged in **Figure 5.5 (c).** The presence of individual diffraction spots in the electron diffraction pattern is consistent with a sample that is a single crystal.

Figure 5.5 (e) shows the TEM image of a PET microplastic particle that is thicker, as

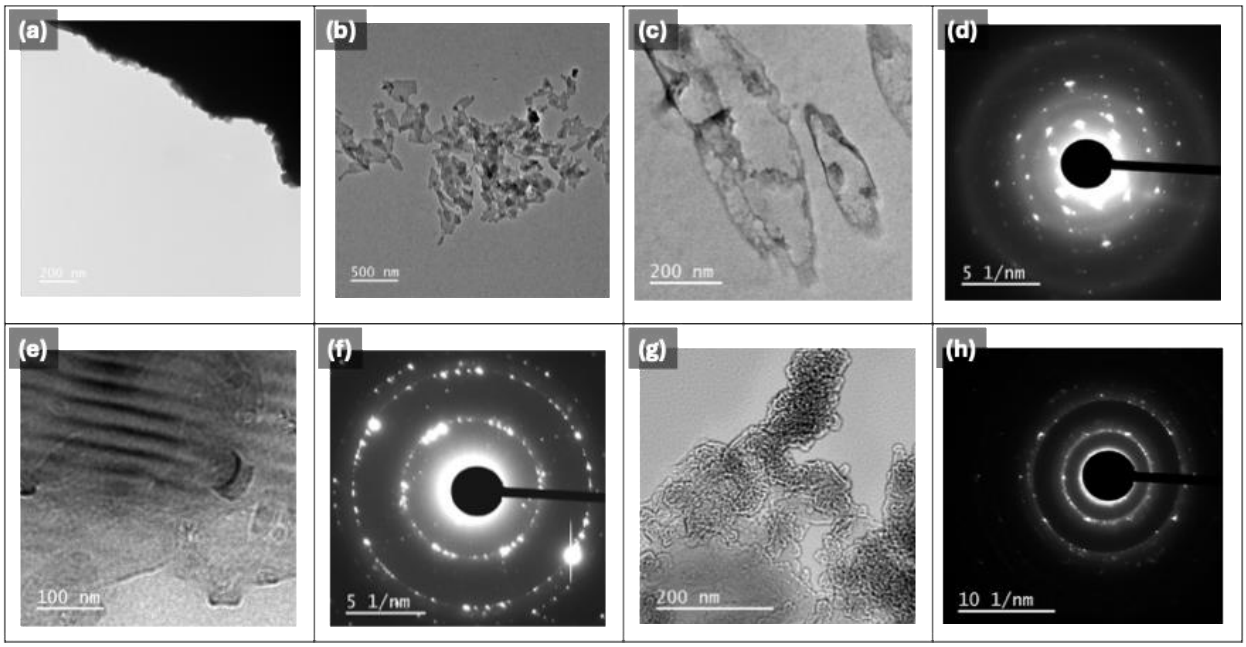

Figure 5.5 TEM images and electron diffraction patterns of depolymerized PET **(a)** Edge of blank TEM grid. **(b)** TEM of depolymerized PET particles **(c)** TEM image of depolymerized PET **(d)** Diffraction pattern of c. **(e)** TEM image of depolymerized PET microplastic **(f)** Diffraction pattern of e. **(g)** TEM image of pulverized virgin PET. **(h)** Diffraction pattern of g.

demonstrated by the darker image, and has no voids, while **Figure 5.5 (f)** shows the electron diffraction pattern of that sample. The electron diffraction of this sample consists of crystalline diffraction rings rather than spots, which is consistent with a polycrystalline sample, where the thicker sample contains multiple crystal domains. These results suggest that the smaller, thinner particles are more likely to be single crystals than thicker particles. To further test this interpretation, **Figure 5.5 (g)** shows the TEM of pulverized virgin PET, while **Figure 5.5 (h)** shows the electron diffraction of these particles. The particles in **Figure 5.5 (g)** are darker, indicating they are thicker particles, while **Figure 5.5 (h)** shows a polycrystalline electron diffraction pattern with very few bright spots. Interestingly, the **Figure 5.5 (h)** polycrystalline diffraction pattern has fewer spots than that of the depolymerized PET in **Figure 5.5 (f).** One interpretation of this variation is that the polycrystalline depolymerized PET sample contains more single crystals than virgin PET – which is consistent with the loss of amorphous PET in the depolymerization process.

The observation of a range of particle sizes with varying crystallinity in the depolymerized PET powder may be explained by the successive fragmentation of micron-sized particles to form nanosized particles by the loss of the amorphous phase. The increased crystalline nature of the smaller particles suggests that the fragmented nanoplastics are primarily the polymer's crystalline domain. The low solvent compatibility between PET and EG likely hinders the dissolution of the crystalline regions, a process that is also known as decrystallization. The limited solubility of PET and EG thus leads to the isolation and preservation of the more crystalline portions of the polymer. These data, therefore, not only provide insight into the micron and nanoscale structure of the particles that emerge from the PET depolymerization by glycolysis, but also provide protocols to examine a range polymer particles

that emerge from polymer degradation. These results confirm that TEM can image nanoplastics previously suspended in water, as the PET particles in this study were suspended during the preparation of the TEM grids.

5.4.2 Polyethylene micro and nanoparticles

Polyethylene (PE) microplastics and nanoplastics were created by sonicating PE granules in a system of deionized water and n-dodecane, where n-dodecane acted as a solubilizer to enhance the dispersion of PE in the aqueous phase. This method, adapted from the previous work of the Peller group[49] improves the solubilization and dispersion of PE in water. PE micro and nanoparticles were prepared in water alone or in a mixture of water and n-dodecane. Additionally, some micro and nanoparticles prepared in water were aged for three years before analysis to evaluate the effects of aging on particle formation. After removing n-dodecane through solvent extraction or heat treatment, the resulting PE micro- and nanoplastics (sM&NPs) were resuspended in water and imaged using transmission electron microscopy (TEM) to assess their morphology in the aqueous phase.

PE sM&NP particles were produced by mechanical mixing (hand-mixing and sonication) in water, water/n-dodecane mixtures or organic solvents. The Peller group completed Raman spectroscopy to illuminate the differences in the crystallinity of the PE sM&NP produced in these different conditions. Raman spectroscopy revealed reduced bands at 1131 cm^{-1} and 1295 cm^{-1} in the particles, which are associated with crystalline PE regions, indicating partial decrystallization.[58-60] This effect was most pronounced when the nanoparticles are formed in the organic solvents and, to a lesser extent, with mechanical mixing in water—especially in aged mixtures. This is interpreted to indicate the swelling of the polymer by solvents, which serves as the first step in the dissolution process, facilitating molecular rearrangements and promoting

decrystallization and fragmentation into sM&NPs.[61, 62] The low T_g of PE, which is well below room temperature, may aid in this swelling process.

Dynamic Light Scattering (DLS) showed that sM&NPs formed in organic solvents are smaller and more narrowly dispersed than those formed in water, with particles created in acetonitrile and acetone exhibiting similar size distributions (200 nm), while particles formed in water displayed a wider size distribution (375-250 nm). The observed difference in particle size based on solvent is consistent with greater swelling and decrystallization occurring in organic solvents compared to in water. The extent of these effects corresponds with solvent compatibility, as indicated by the solubility parameters: PE (17.99 $MPa^{1/2}$), water (47.82 $MPa^{1/2}$), methanol (29.7 $MPa^{1/2}$), acetonitrile (24.1 $MPa^{1/2}$), and acetone (20.3 $MPa^{1/2}$)[54-56] The smaller the difference between the solubility of the solvent and that of PE, the greater the polymer-solvent interaction, which promotes swelling, polymer molecular rearrangement, and ultimately, fragmentation into smaller particles.

In water/*n*-dodecane mixtures (*n*-dodecane: 16.2 $MPa^{1/2}$)[54-56], the Raman crystalline bands of the sM&NPs were reduced less than in the sM&NPs formed in water, suggesting that the presence of the *n*-dodecane initially slows water penetration into the PE by interacting with PE's hydrophobic regions. However, with aging, water appears to gradually infiltrate the polymer, causing delayed decrystallization and fragmentation. Together, these findings indicate that solvent compatibility, coupled with PE's low T_g, drives swelling, decrystallization, and fragmentation, ultimately influencing the formation of sM&NP particles. Understanding these mechanisms is crucial for predicting microplastic degradation and informing sustainable polymer design and plastic remediation strategies.

TEM images visually depict the fragmentation of PE into micro- and nanoplastics, supporting previous findings that nanoplastics form from the breakdown of larger microplastics.[14, 16] **Figure 5.6** shows PE prepared in a water/*n*-dodecane (1:1000) mixture, where *n*-dodecane was expected to solubilize PE and promote fragmentation. Raman analysis by the Peller group indicated that these sM&NP PE particles retained crystallinity, resembling bulk PE. TEM reveals the existence of a ~53 μm PE particle with smaller fragments (1.67 μm and 0.18 μm within the green square) nearby. Further magnification highlights ~100 nm nanoplastic fragments in the orange square. This suggests that nanoplastic formation begins with the fragmentation of larger microplastic particles.

Electron microscopy provides further evidence of the size and shape of PE sM&NP particles to assess how polymer-solvent interactions and aging affect nanoparticle formation and fragmentation. **Figure 5.7** shows TEM images of PE sM&NP particles that have aged in water for three years, that have been freshly formed in a water/n-dodecane mixture, and sM&NP particles that have been freshly formed in water. **Figure 5.7 (a)** shows a blank TEM grid for reference. **Figure 5.7 (b-d)** depict PE sM&NP particles aged in water for three years, revealing particles ranging in size from microns to nanometers. Many appear as thin, film-like structures with lower electron density, suggesting increased amorphous character, which aligns with Raman data showing reduced 1131 cm^{-1} and 1295 cm^{-1} crystallinity bands. These results indicate that prolonged water exposure promotes particle degradation, reducing crystallinity and generating smaller, thinner fragments. DLS data further confirm the broad size distribution of these aged particles. **Figure 5.7 (e)** shows PE sM&NP particles that are freshly formed in a water/n-dodecane mixture, which produces larger, denser particles with more well-defined shapes. This is consistent with preserved PE crystallinity, as previously shown in **Figure 5.6**.

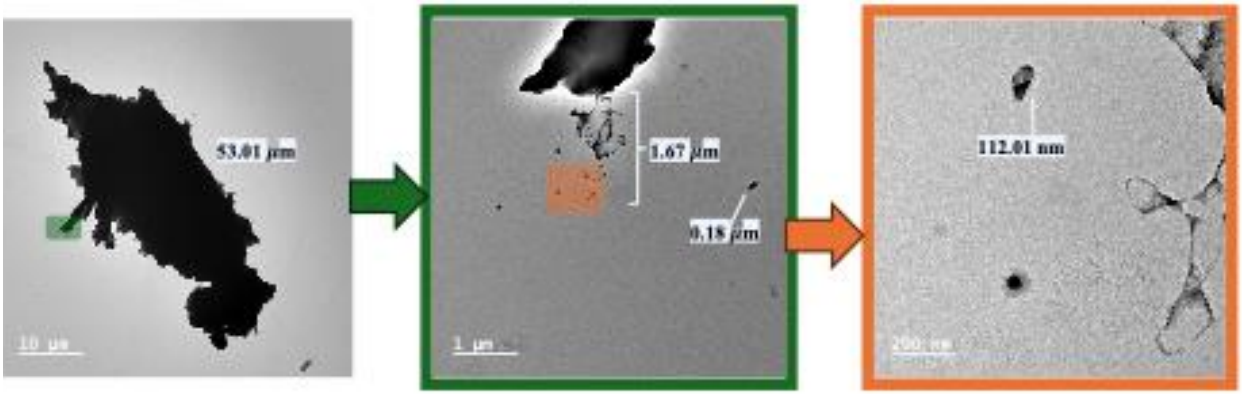

Figure 5.6 A potential demonstration of nanoplastic formation, where PE sM&NP particles prepared in water/n-dodecane mixtures break from pre-existing microplastics. From left to right, the TEM images zoom in on areas of interest (the middle image is the green area of interest, and the far-right image is the orange area of interest) to show smaller and smaller fragments of PE.

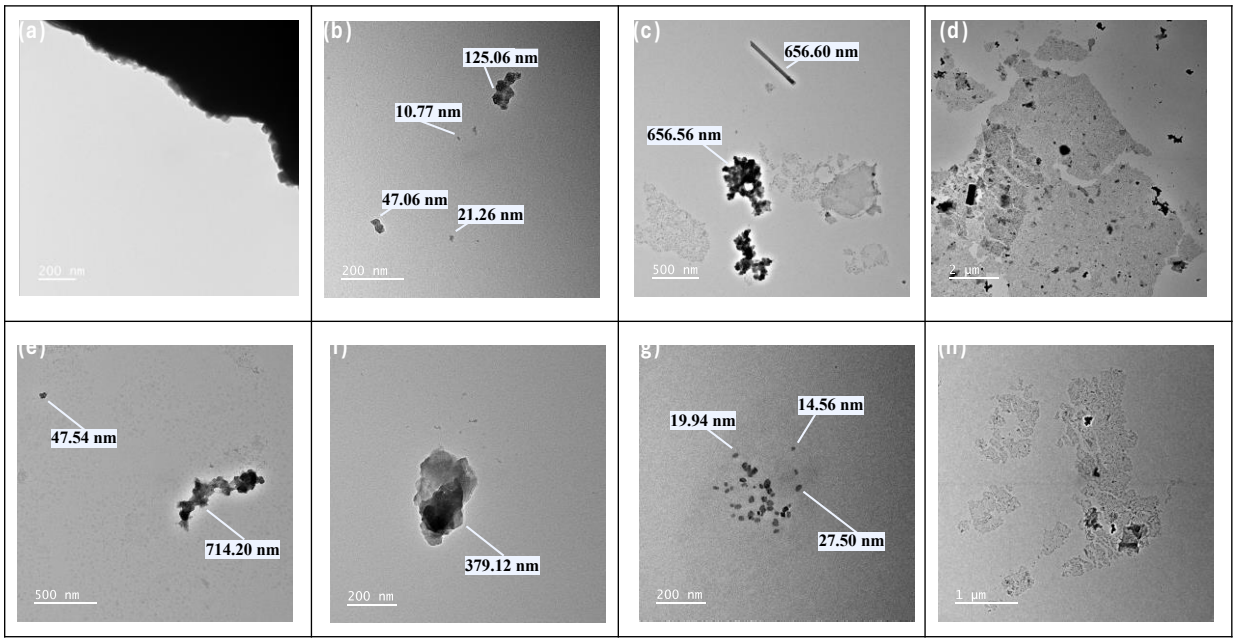

Figure 5.7 TEM images of a PE microplastics fragmented into small micro and nanoplastics (sM&NP) in varying conditions. **(a)** empty TEM grid with side of grid captured, **(b-d)** PE sM&NP particles suspended in water for 3 years (aged sample), **(e)** PE sM&NP prepared in a water/n-dodecane mixture (1000:1), and **(f-h)** PE sM&NP freshly prepared in water (non-aged sample).

This is also consistent with the Raman spectra showing minimal reduction in crystallinity bands, suggesting n-dodecane moderates solubilization and slows decrystallization. **Figure 5.7 (f-h)** present sM&NP particles that are freshly formed in water, which exhibit smaller particles with thin, film-like structures that are similar to the aged samples, though less pronounced. Corresponding Raman spectra reveal only slight reductions in crystallinity bands, indicating the early stages of molecular rearrangement. In contrast, PE in the water/n-dodecane mixture showed larger, denser particles, confirming that n-dodecane slows fragmentation while maintaining crystallinity.

In this study, energy-dispersive X-ray spectroscopy (EDS) and high-angle annular dark-field (HAADF) imaging were employed using the Spectra 300 TEM equipped with a SuperXG2 detector at 60 kV to analyze the elemental composition and structure of sM&NP particles that are freshly formed in water. **Figure 5.8** presents the EDS elemental maps of this analysis, showing the presence of oxygen (green), lanthanum (yellow), carbon (red), gadolinium (blue), phosphorus (green), and silicon (purple). The widespread presence of lanthanum, gadolinium, phosphorus, and silicon results from Uranyless staining, which contains lanthanide elements. HAADF imaging, which is sensitive to atomic number (Z), emphasize regions with heavier atoms as areas of higher white intensity.[63, 64] Notably, only the EDS map of oxygen (green) reveals sections of the polyethylene sample that appeared brighter, indicating the presence of oxygen in these samples. This increased intensity suggests the formation of oxidized areas of the polymer, which correlates with Raman spectroscopy results, that have been interpreted to indicate potential water swelling in the samples. Therefore, the combined EDS, HAADF, and Raman data indicate that oxidation alters the chemical composition of polyethylene and structural integrity, with oxidized areas exhibiting distinct elemental distribution.

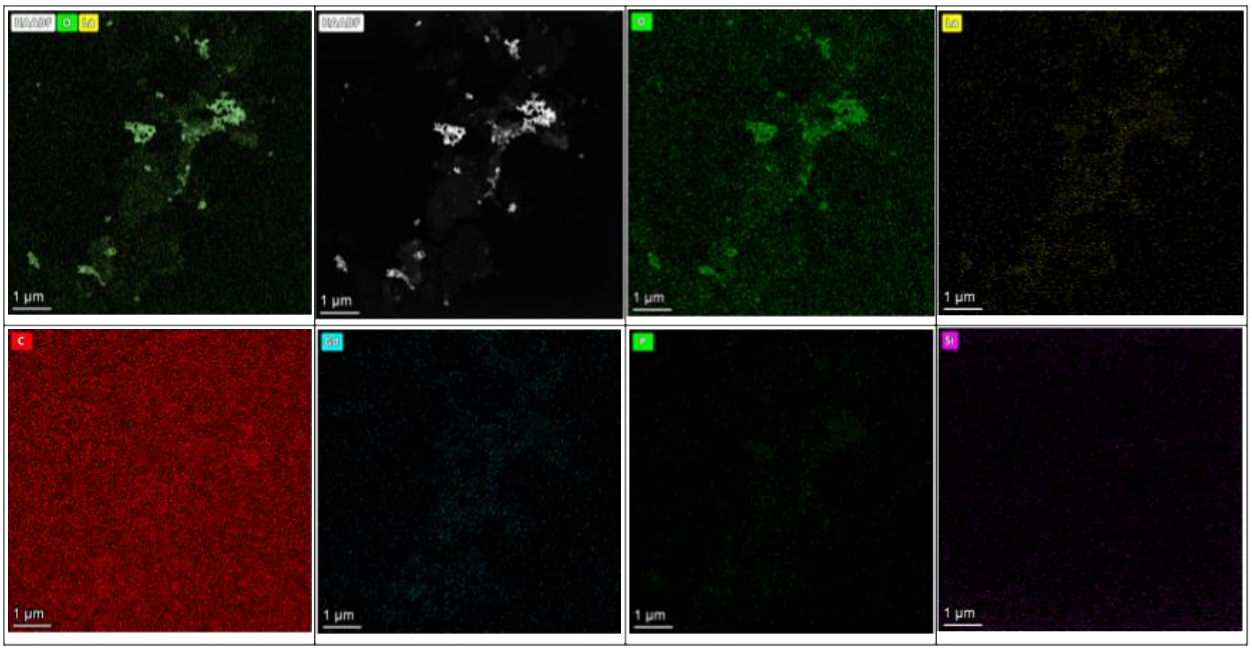

Figure 5.8 Energy-dispersive X-ray Spectroscopy (EDS) of polyethylene (PE) aged in water (scale bar: 1 µm). Top row (left to right): EDS overlay showing the distribution of the HAADF image (white), oxygen (green), and lanthanum (yellow); the HAADF image; the oxygen map; and the lanthanum map. Bottom row (left to right): the carbon map (red), the gadolinium map (blue), the phosphorus map (green), and the silicon map (pink).

Inspection of the TEM images of depolymerized PET shown in **Figure 5.3** provides additional insight into the relationship between crystallinity, particle morphology, and polymer-solvent interactions. The PET particles, which exhibit approximately 70% crystallinity as determined by DSC, appear as denser and darker structures in TEM, consistent with the well-ordered molecular packing of crystalline regions. This observation parallels the findings with PE, where particles that retained crystallinity were larger and more defined. In contrast, those with reduced crystallinity appeared as thinner, less electron-dense films, as shown in **Figure 5.6** and **Figure 5.7**. The Raman spectra further support this correlation, as PE aged in water exhibits a reduction or shift in the crystallinity band, aligning with the thinner films observed in TEM. At the same time, the PE sM&NP particles prepared in water:dodecane retained its crystallinity band and appeared as denser, more well-defined particles. A holistic view of these data suggests that solvent interactions and aging processes directly impact the polymer's molecular structure in the sM&NP, with longer aging time or improved solubility resulting in sM&NP particles with decreased crystallinity leading to more flexible, amorphous regions that are more susceptible to structural changes and fragmentation.

To further explore the role of the thermal properties of the polymer in these fragmentation processes, the structures of polystyrene (PS) sM&NP formed under the same conditions as PE were also monitored by TEM. **Figure 5.9** shows the TEM images of PS sM&NP, with panels **(b)** and **(c)** being zoomed-in sections of the TEM image in **Figure 5.9 (a).** Overall, the PS sM&NP particles observed through TEM were dark and electron-dense across all sizes. Despite PS and PE having similar solubility parameters, the same mechanical procedure results in PS sM&NP particles that are larger, more well-defined, and denser than those formed by PE. One interpretation of this variation is that the higher T_g of the PS inhibits the penetration

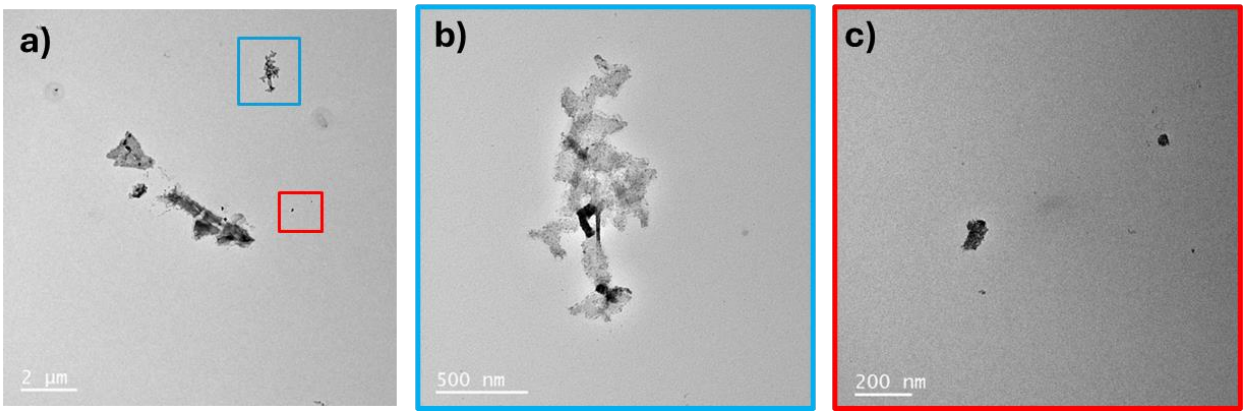

Figure 5.9 TEM images of PS microplastics fragmented into small micro and nanoplastics (sM&NP) **(a)** PS sM&NP particles prepared in water:dodecane (1000:1) mixture. **(b)** and **(c)** zoomed in images of the PS sM&NP particles in the TEM image (a).

of the solvent or solubilizer into the polymer, which helps maintain structural integrity of the PS during fragmentation.

In contrast, the lower T_g of PE increases their amorphous regions' susceptibility to penetration by the solvent or solubilizer, enabling efficient rearrangement and fragmentation into smaller, thinner films. This comparison between PS and PE sM&NP particles highlights how both crystallinity and thermal properties of the polymer may influence not only the morphology of micro- and nanoplastics but also their interactions with solvents and environmental factors. Collectively, these findings suggest that polymers with lower T_g and reduced crystallinity are more prone to molecular rearrangement, oxidation, and fragmentation, which may accelerate their breakdown into smaller particles with altered physical and chemical properties.

A comparison of the structure of the sM&NP particles fabricated under various conditions highlights the balance between solvent-induced decrystallization and fragmentation in the fabrication process. As seen with water, low compatibility between polymer and solvent disrupts polymer packing and promotes fragmentation. As observed with water/dodecane mixtures, partial compatibility helps preserve crystallinity, reducing excessive breakdown. However, excessive compatibility, such as PE dissolved in good solvents leads to decrystallization as indicated by the loss of the crystalline band in the Raman spectra. Thus, solvent-polymer interactions play a key role in controlling both molecular structure and particle morphology of sM&NP particles and their fabrication process. TEM provides visual evidence of how slight changes in the solvent environment impact polymer fragmentation at the nanoscale.

5.5 Conclusion

This research provides critical insights into the nanoscale fragmentation of microplastics (MPs) by effectively capturing images of small micro and nanoplastic (sM&NP) particles in

water using Transmission Electron Microscopy (TEM). By overcoming previous challenges in characterizing aqueous sM&NP, this study reveals key factors influencing their formation, including polymer crystallinity, polymer-solvent interactions, and polymer glass transition temperature (T_g). TEM imaging of polyethylene terephthalate (PET) sM&NP, utilizing both virgin and depolymerized PET, demonstrates that highly crystalline domains persist as distinct, darker-shaded particles, a finding validated by Differential Scanning Calorimetry (DSC). This suggests that the fragmentation of PET is strongly influenced by its crystalline structure, where nanoscale particles form through the cleavage of rigid domains from larger particles rather than uniform degradation.

The study further emphasizes the importance of solvent-polymer compatibility in determining sM&NP morphology. Polyethylene (PE) fragments to smaller particles in water, regardless of its low compatibility with water, as evidenced by thin-film TEM images and supporting Raman Spectroscopy data. High-Angle Annular Dark-Field (HAADF) imaging and Energy-Dispersive X-ray Spectroscopy (EDS) confirm oxidation and molecular rearrangement in PE sM&NP, suggesting that even low-compatibility solvents can drive gradual nanoscale breakdown of polymers through swelling and oxidative processes. In contrast, polystyrene (PS) sM&NP appear larger, more distinct, and resistant to swelling, indicating that its higher T_g inhibits solvent penetration and fragmentation, reinforcing the significance of T_g in determining a polymer's environmental persistence.

These findings underscore the delicate interplay between polymer physicochemical properties and solvent interactions in driving plastic degradation. While higher solvent compatibility can accelerate fragmentation by disrupting polymer crystallinity, low-compatibility solvents such as water still contribute to long-term breakdown, particularly in lower-T_g

polymers. This research highlights the need for further investigation into how these factors influence the environmental fate of plastics, emphasizing that both polymer composition and surrounding conditions dictate their persistence and impact in aquatic ecosystems.

5.6 Acknowledgements

This work was supported by the National Science Foundation, Polymers program, Division of Materials Research (DMR- 2104982). We also acknowledge Dr. Julie R. Peller for providing the polyethylene samples. TEM experiments were completed at the Advanced Microscopy and Imaging Center at the University of Tennessee Knoxville.

References

(1) Arifuzzaman, M.; Sumpter, B. G.; Demchuk, Z.; Do, C.; Arnould, M. A.; Rahman, M. A.; Cao, P.-F.; Popovs, I.; Davis, R. J.; Dai, S.; et al. Selective deconstruction of mixed plastics by a tailored organocatalyst. *Materials Horizons* **2023**, *10* (9), 3360-3368. DOI: 10.1039/d3mh00801k.

(2) Nayanathara Thathsarani Pilapitiya, P. G. C.; Ratnayake, A. S. The world of plastic waste: A review. *Cleaner Materials* **2024**, *11*, 100220. DOI: 10.1016/j.clema.2024.100220.

(3) Lebreton, L.; Andrady, A. Future scenarios of global plastic waste generation and disposal. *Palgrave Communications* **2019**, *5* (1). DOI: 10.1057/s41599-018-0212-7.

(4) Kibria, M. G.; Masuk, N. I.; Safayet, R.; Nguyen, H. Q.; Mourshed, M. Plastic Waste: Challenges and Opportunities to Mitigate Pollution and Effective Management. *International Journal of Environmental Research* **2023**, *17* (1). DOI: 10.1007/s41742-023-00507-z.

(5) Schwarz, A. E.; Lensen, S. M. C.; Langeveld, E.; Parker, L. A.; Urbanus, J. H. Plastics in the global environment assessed through material flow analysis, degradation and environmental transportation. *Sci. Total Environ.* **2023**, *875*, 162644. DOI: 10.1016/j.scitotenv.2023.162644.

(6) Gómez-Sanabria, A.; Lindl, F. The crucial role of circular waste management systems in cutting waste leakage into aquatic environments. *Nature Communications* **2024**, *15* (1). DOI: 10.1038/s41467-024-49555-9.

(7) Su, L.; Xiong, X.; Zhang, Y.; Wu, C.; Xu, X.; Sun, C.; Shi, H. Global transportation of plastics and microplastics: A critical review of pathways and influences. *Sci. Total Environ.* **2022**, *831*, 154884. DOI: 10.1016/j.scitotenv.2022.154884.

(8) Ziani, K.; Ioniță-Mîndrican, C.-B.; Mititelu, M.; Neacșu, S. M.; Negrei, C.; Moroșan, E.; Drăgănescu, D.; Preda, O.-T. Microplastics: A Real Global Threat for Environment and Food Safety: A State of the Art Review. *Nutrients* **2023**, *15* (3), 617. DOI: 10.3390/nu15030617.

(9) Allen, S.; Allen, D.; Karbalaei, S.; Maselli, V.; Walker, T. R. Micro(nano)plastics sources, fate, and effects: What we know after ten years of research. *Journal of Hazardous Materials Advances* **2022**, *6*, 100057. DOI: 10.1016/j.hazadv.2022.100057.

(10) Fox, B.; Moad, G.; Van Diepen, G.; Willing, I.; Cook, W. D. Characterization of poly(ethylene terephthalate) and poly(ethylene terephthalate) blends. *Polymer* **1997**, *38* (12), 3035-3043. DOI: 10.1016/s0032-3861(96)00872-5.

(11) George, N.; Kurian, T. Recent Developments in the Chemical Recycling of Postconsumer Poly(ethylene terephthalate) Waste. *Industrial & Engineering Chemistry Research* **2014**, *53* (37), 14185-14198. DOI: 10.1021/ie501995m.

(12) Agency, U. S. E. P. Facts and Figures about Materials, Waste and Recycling. Agency, U. S. E. P., Ed.; 2023.

(13) Clark, R. A.; Shaver, M. P. Depolymerization within a Circular Plastics System. *Chem. Rev.* **2024**, *124* (5), 2617-2650. DOI: 10.1021/acs.chemrev.3c00739.

(14) Tiwari, N.; Santhiya, D.; Sharma, J. G. Biodegradation of micro sized nylon 6, 6 using Brevibacillus brevis a soil isolate for cleaner ecosystem. *Journal of Cleaner Production* **2022**, *378*, 134457. DOI: https://doi.org/10.1016/j.jclepro.2022.134457.

(15) Materić, D.; Kjær, H. A.; Vallelonga, P.; Tison, J.-L.; Röckmann, T.; Holzinger, R. Nanoplastics measurements in Northern and Southern polar ice. *Environ. Res.* **2022**, *208*, 112741. DOI: https://doi.org/10.1016/j.envres.2022.112741.

(16) Allen, D.; Allen, S.; Le Roux, G.; Simonneau, A.; Galop, D.; Phoenix, V. R. Temporal Archive of Atmospheric Microplastic Deposition Presented in Ombrotrophic Peat. *Environmental Science & Technology Letters* **2021**, *8* (11), 954-960. DOI: 10.1021/acs.estlett.1c00697.

(17) Presence of microplastics and nanoplastics in food, with particular focus on seafood. *EFSA Journal* **2016**, *14* (6), e04501. DOI: 10.2903/j.efsa.2016.4501.

(18) Agarwal, S. Biodegradable Polymers: Present Opportunities and Challenges in Providing a Microplastic-Free Environment. *Macromolecular Chemistry and Physics* **2020**, *221* (6), 2000017. DOI: 10.1002/macp.202000017.

(19) Park, J. H.; Hong, S.; Kim, O.-H.; Kim, C.-H.; Kim, J.; Kim, J.-W.; Hong, S.; Lee, H. J. Polypropylene microplastics promote metastatic features in human breast cancer. *Scientific Reports* **2023**, *13* (1), 6252. DOI: 10.1038/s41598-023-33393-8.

(20) Brahney, J.; Mahowald, N.; Prank, M.; Cornwell, G.; Klimont, Z.; Matsui, H.; Prather, K. A. Constraining the atmospheric limb of the plastic cycle. *Proceedings of the National Academy of Sciences* **2021**, *118* (16), e2020719118. DOI: 10.1073/pnas.2020719118.

(21) Xu, M.; Halimu, G.; Zhang, Q.; Song, Y.; Fu, X.; Li, Y.; Li, Y.; Zhang, H. Internalization and toxicity: A preliminary study of effects of nanoplastic particles on human lung epithelial cell. *Sci. Total Environ.* **2019**, *694*, 133794. DOI: 10.1016/j.scitotenv.2019.133794 From NLM.

(22) Lu, Y.-Y.; Li, H.; Ren, H.; Zhang, X.; Huang, F.; Zhang, D.; Huang, Q.; Zhang, X. Size-dependent effects of polystyrene nanoplastics on autophagy response in human umbilical vein endothelial cells. *J. Hazard. Mater.* **2022**, *421*, 126770. DOI: https://doi.org/10.1016/j.jhazmat.2021.126770.

(23) McCormick, A.; Hoellein, T. J.; Mason, S. A.; Schluep, J.; Kelly, J. J. Microplastic is an Abundant and Distinct Microbial Habitat in an Urban River. *Environmental Science & Technology* **2014**, *48* (20), 11863-11871. DOI: 10.1021/es503610r.

(24) Ali, I.; Cheng, Q.; Ding, T.; Yiguang, Q.; Yuechao, Z.; Sun, H.; Peng, C.; Naz, I.; Li, J.; Liu, J. Micro- and nanoplastics in the environment: Occurrence, detection, characterization and toxicity – A critical review. *Journal of Cleaner Production* **2021**, *313*, 127863. DOI: https://doi.org/10.1016/j.jclepro.2021.127863.

(25) Amato-Lourenço, L. F.; Carvalho-Oliveira, R.; Júnior, G. R.; dos Santos Galvão, L.; Ando, R. A.; Mauad, T. Presence of airborne microplastics in human lung tissue. *J. Hazard. Mater.* **2021**, *416*, 126124. DOI: https://doi.org/10.1016/j.jhazmat.2021.126124.

(26) Cox, K. D.; Covernton, G. A.; Davies, H. L.; Dower, J. F.; Juanes, F.; Dudas, S. E. Human Consumption of Microplastics. *Environmental Science & Technology* **2019**, *53* (12), 7068-7074. DOI: 10.1021/acs.est.9b01517.

(27) Yee, M. S.; Hii, L. W.; Looi, C. K.; Lim, W. M.; Wong, S. F.; Kok, Y. Y.; Tan, B. K.; Wong, C. Y.; Leong, C. O. Impact of Microplastics and Nanoplastics on Human Health. *Nanomaterials (Basel)* **2021**, *11* (2). DOI: 10.3390/nano11020496 From NLM.

(28) Wei, X.-F.; Capezza, A. J.; Cui, Y.; Li, L.; Hakonen, A.; Liu, B.; Hedenqvist, M. S. Millions of microplastics released from a biodegradable polymer during biodegradation/enzymatic hydrolysis. *Water Res.* **2022**, *211*, 118068. DOI: 10.1016/j.watres.2022.118068.

(29) Wei, X.-F.; Bohlén, M.; Lindblad, C.; Hedenqvist, M.; Hakonen, A. Microplastics generated from a biodegradable plastic in freshwater and seawater. *Water Res.* **2021**, *198*, 117123. DOI: 10.1016/j.watres.2021.117123.

(30) Colwell, J.; Pratt, S.; Lant, P.; Laycock, B. Hazardous state lifetimes of biodegradable plastics in natural environments. *Sci. Total Environ.* **2023**, *894*, 165025. DOI: 10.1016/j.scitotenv.2023.165025.

(31) Allemann, M. N.; Tessman, M.; Reindel, J.; Scofield, G. B.; Evans, P.; Pomeroy, R. S.; Burkart, M. D.; Mayfield, S. P.; Simkovsky, R. Rapid biodegradation of microplastics generated from bio-based thermoplastic polyurethane. *Scientific Reports* **2024**, *14* (1). DOI: 10.1038/s41598-024-56492-6.

(32) Al-Sid-Cheikh, M.; Rowland, S. J.; Stevenson, K.; Rouleau, C.; Henry, T. B.; Thompson, R. C. Uptake, Whole-Body Distribution, and Depuration of Nanoplastics by the Scallop Pecten maximus at Environmentally Realistic Concentrations. *Environmental Science & Technology* **2018**, *52* (24), 14480-14486. DOI: 10.1021/acs.est.8b05266.

(33) Goodman, K. E.; Hare, J. T.; Khamis, Z. I.; Hua, T.; Sang, Q.-X. A. Exposure of Human Lung Cells to Polystyrene Microplastics Significantly Retards Cell Proliferation and Triggers Morphological Changes. *Chem. Res. Toxicol.* **2021**, *34* (4), 1069-1081. DOI: 10.1021/acs.chemrestox.0c00486.

(34) Jenner, L. C.; Rotchell, J. M.; Bennett, R. T.; Cowen, M.; Tentzeris, V.; Sadofsky, L. R. Detection of microplastics in human lung tissue using μFTIR spectroscopy. *Sci. Total Environ.* **2022**, *831*, 154907. DOI: https://doi.org/10.1016/j.scitotenv.2022.154907.

(35) Zangmeister, C. D.; Radney, J. G.; Benkstein, K. D.; Kalanyan, B. Common Single-Use Consumer Plastic Products Release Trillions of Sub-100 nm Nanoparticles per Liter into Water during Normal Use. *Environmental Science & Technology* **2022**, *56* (9), 5448-5455. DOI: 10.1021/acs.est.1c06768.

(36) Vethaak, A. D.; Leslie, H. A. Plastic Debris Is a Human Health Issue. *Environmental Science & Technology* **2016**, *50* (13), 6825-6826. DOI: 10.1021/acs.est.6b02569.

(37) Mason, S. A.; Welch, V. G.; Neratko, J. Synthetic Polymer Contamination in Bottled Water. *Frontiers in Chemistry* **2018**, *6*. DOI: 10.3389/fchem.2018.00407.

(38) Ivleva, N. P. Chemical Analysis of Microplastics and Nanoplastics: Challenges, Advanced Methods, and Perspectives. *Chem. Rev.* **2021**, *121* (19), 11886-11936. DOI: 10.1021/acs.chemrev.1c00178.

(39) Kusch, P. Challenges in the Analysis of Micro- and Nanoplastics. Springer International Publishing, 2022; pp 477-501.

(40) Zhang, W.; Wang, Q.; Chen, H. Challenges in characterization of nanoplastics in the environment. *Frontiers of Environmental Science & Engineering* **2022**, *16* (1). DOI: 10.1007/s11783-021-1445-z.

(41) Gigault, J.; Halle, A. T.; Baudrimont, M.; Pascal, P.-Y.; Gauffre, F.; Phi, T.-L.; El Hadri, H.; Grassl, B.; Reynaud, S. Current opinion: What is a nanoplastic? *Environ. Pollut.* **2018**, *235*, 1030-1034. DOI: 10.1016/j.envpol.2018.01.024.

(42) Al Harraq, A.; Bharti, B. Microplastics through the Lens of Colloid Science. *ACS Environmental Au* **2022**, *2* (1), 3-10. DOI: 10.1021/acsenvironau.1c00016.

(43) Benke, A.; Sonnenberg, J.; Oelschlägel, K.; Schneider, M.; Lux, M.; Potthoff, A. Wettability after Artificial and Natural Weathering of Polyethylene Terephthalate. *Environments* **2022**, *9* (11), 134. DOI: 10.3390/environments9110134.

(44) Peller, J. R.; Durlam, N.; Flaherty, Y.; Valicevic, A.; Davis, C. M.; Watson, S.; Tournebise, J. E.; Medina-Garcia, J. A.; Dadmun, M.; Mezyk, S. P. Incognito forms of polyethylene small

micro and nanoplastics in solvents: Changes in molecular vibrations. *Sci. Total Environ.* **2025**, *968*, 178923. DOI: 10.1016/j.scitotenv.2025.178923.

(45) Jehanno, C.; Flores, I.; Dove, A. P.; Müller, A. J.; Ruipérez, F.; Sardon, H. Organocatalysed depolymerisation of PET in a fully sustainable cycle using thermally stable protic ionic salt. *Green Chemistry* **2018**, *20* (6), 1205-1212. DOI: 10.1039/c7gc03396f.

(46) Watson-Sanders, S.; Dadmun, M. More Efficient Chemical Recycling of Poly(Ethylene Terephthalate) by Intercepting Intermediates. *ChemSusChem* **2024**, *17* (23). DOI: 10.1002/cssc.202301698.

(47) Blaine, R. L. *Determination of Polymer Crystallinity by DSC*; TA Instruments, https://www.tainstruments.com/pdf/literature/TA123new.pdf.

(48) Blaine, R. L. *THERMAL APPLICATIONS NOTE*; TA Instrument, https://www.tainstruments.com/pdf/literature/TN048.pdf.

(49) Peller, J. R.; Mezyk, S. P.; Shidler, S.; Castleman, J.; Kaiser, S.; Horne, G. P. The reactivity of polyethylene microplastics in water under low oxygen conditions using radiation chemistry. *Water* **2021**.

(50) Workman, C. E.; Bag, P.; Cawthon, B.; Ali, F. H.; Brady, N. G.; Bruce, B. D.; Long, B. K. Alternatives to Styrene- and Diisobutylene-Based Copolymers for Membrane Protein Solubilization via Nanodisc Formation. *Angew. Chem.* **2023**, *135* (43). DOI: 10.1002/ange.202306572.

(51) Brady, N. G.; Workman, C. E.; Cawthon, B.; Bruce, B. D.; Long, B. K. Protein Extraction Efficiency and Selectivity of Esterified Styrene–Maleic Acid Copolymers in Thylakoid Membranes. *Biomacromolecules* **2021**, *22* (6), 2544-2553. DOI: 10.1021/acs.biomac.1c00274.

(52) Williams, D. B.; Carter, C. B. Imaging in the TEM. Springer US, 1996; pp 349-366.

(53) Reimer, L. Transmission Electron Microscopy. *Springer Series in Optical Sciences* **1997**. DOI: 10.1007/978-3-662-14824-2.

(54) *Polymer Handbook*; John Wiley & sons, Inc, 1999.

(55) Barton, A. F. M. CRC Handbook of Solubility Parameters and Other Cohesion Parameters. **2017**. DOI: 10.1201/9781315140575.

(56) Hansen, C. M. Hansen Solubility Parameters. **2007**. DOI: 10.1201/9781420006834.

(57) Watson-Sanders, S. D., M. Evolution of Chain Structure during the Glycolysis of Poly(ethylene terephthalate). *Chem Sus Chem* **2023**.

(58) Najmi, S.; Vance, B. C.; Selvam, E.; Huang, D.; Vlachos, D. G. Controlling PET oligomers vs monomers via microwave-induced heating and swelling. *Chem. Eng. J.* **2023**, *471*, 144712. DOI: https://doi.org/10.1016/j.cej.2023.144712.

(59) Miller-Chou, B. A.; Koenig, J. L. A review of polymer dissolution. *Prog. Polym. Sci.* **2003**, *28* (8), 1223-1270. DOI: 10.1016/s0079-6700(03)00045-5.

(60) Shimanouchi, T. *Tables of molecular vibrational frequencies. Consolidated volume I*; Washington, D.C. : National Bureau of Standards, 1972., 1972.

(61) Stevens, M. P. *Polymer Chemistry: An Introduction*; Oxford University Press: Oxford, 1999.

(62) Odian, G. *Principles of Polymerization*; John Wiley & Sons, Inc., 2004.

(63) Kübel, C.; Voigt, A.; Schoenmakers, R.; Otten, M.; Su, D.; Lee, T.-C.; Carlsson, A.; Bradley, J. Recent Advances in Electron Tomography: TEM and HAADF-STEM Tomography for Materials Science and Semiconductor Applications. *Microsc. Microanal.* **2005**, *11* (5), 378-400. DOI: 10.1017/s1431927605050361.

(64) He, Q.; Li, A.; Yao, B.; Zhou, W.; Kiely, C. J. STEM High Angle Annular Dark-Field Imaging. Springer International Publishing, 2023; pp 409-448.

CHAPTER 6: CONCLUSIONS AND OUTLOOKS

6.1 Conclusions

The increasing demand for synthetic polymers is not being met with a proportional increase in recycling, as only 9% of plastics are recycled annually.[1, 2] The current management of polymer waste is unsustainable, as most polymers are disposed of in 'end-of-life destinations' such as landfills or incineration.[1, 3-6] This research project is centered on investigating the chemical recycling of Polyethylene Terephthalate (PET), Polycarbonate (PC), and Tritan™ from Eastman Chemical Company. The project involves examining the evolution of chain structure in their depolymerization and exploring methods to enhance the sustainability of these chemical recycling processes. This research aims to improve our understanding of the depolymerization process and the factors that affect it. It seeks to design chemical recycling processes for consumer waste that optimize its use in repolymerization or creating value-added products. This research project examined the influence of functional groups, solvent compatibility, and crystallinity on the development of chain structure during depolymerization. The fragmentation of plastic into microplastics and further into small micro and nanoplastics (sM&NP) was also explored in this project to develop techniques for imaging sM&NP environmental samples. Additionally, the project sought insight into how telechelics formed during the depolymerization process can be utilized for repolymerization or as feedstocks in reactions to generate value-added products. The overarching goal is to advance sustainable polymer recycling processes and create economically viable materials from polymer waste streams.

In the initial project, Chapter II describes the evolution of the PET chain during heterogeneous glycolysis, focusing on molecular weight, dispersity, crystallinity, and average hydroxyl end groups. This facilitated the creation of desired dihydroxy-terminated oligomers with minimal additional reactions needed after breaking down the PET. This research outlines a

clear process that explains how the chain structure evolves during the depolymerization of PET through heterogeneous catalysis and presents opportunities to capture oligomeric intermediates in the process. We closely monitored the dispersity, molecular weight, end groups, and crystallinity of the products obtained from the heterogeneous depolymerization of PET via glycolysis to gain insights into how the polymer chain changes. Our findings show that the crystallinity of the depolymerized polymer increased, dispersity decreased, and yield remained high during the first hour of depolymerization. Our comprehensive analysis of these results led to a mechanism involving the selective diffusion of EG into the amorphous PET, where it reacted through glycolysis to break tie chains. This reduced the amorphous material in the sample, significantly increasing PET crystallinity in the depolymerization products. This interpretation also aligns with the slow conversion of the end groups to two alcohol end groups per chain, as many chains were inaccessible to the depolymerization process. This mechanism offers a straightforward route to recover a substantial portion of the original polymer as oligomers, which can then be used as raw materials to create value-added materials. This study also demonstrated that annealing these oligomers near the melting temperature of PET can yield repolymerized PET with 90% of the original molecular weight. These results indicate that it is feasible to recombine oligomers to regenerate polymers, opening up new possibilities for more effective and efficient chemical recycling of PET.

In Chapter III, the study investigates how crystallinity, solvent-polymer compatibility, and functional group reactivity impact the rate of depolymerization for polyesters (PET and Tritan™) and polycarbonate. This study compares the reaction rates and swelling behaviors of the polyesters (Tritan™ and PET) with PC in Ethylene Glycol (EG) to determine whether diol transport, restricted by the crystallinity in semi-crystalline PET, or the reactivity of the functional

groups is the key factor in the rate of depolymerization. This is assessed by comparing and observing the changes in molecular weight and dispersity of the polymers. PET and PC were also depolymerized in bisphenol-A (BPA) to assess how solvent compatibility affects the heterogeneous depolymerization process and the phases it undergoes. A heterogeneous depolymerization goes through three phases: heterogeneous process (undissolved oligomers), coexistence process (dissolved and undissolved oligomers), and a homogeneous process (dissolved oligomers).

Chapter III observed enhanced solubility, such as using bisphenol-A (BPA), facilitates the transition to a homogeneous phase. In contrast, lower solubility, as observed with ethylene glycol (EG), hinders the shift from the heterogeneous process. These findings are significant for advancing sustainable polymer recycling processes and developing economically viable materials from polymer waste streams. This study investigated diol transport to the carbonyl and the carbonyl's fundamental reactivity to better understand their impact on depolymerization rates, aiming to simplify recycling processes and inspire the design of more easily recyclable polymers. Ester-containing polymers (PET or Tritan^{TM}) depolymerize faster than carbonate-containing polymers in the presence of either diol (BPA or EG) due to the reactivity of the ester functional group. It was found that diol transport and polymer diol compatibility do not regulate the reaction rate. PET and Tritan^{TM} depolymerize at similar rates despite Tritan^{TM} swelling with more EG per polymer flake. The polymer's solubility in the diol controls the transition of heterogeneous reactions through the three stages. Both polymers remain in a heterogeneous process when in contact with EG, where the solubility of the polymer in the diol is low. Still, they transition through the stages to a homogeneous process when reacting with BPA, where the polymer's solubility in the diol is high. Improved solubility promotes the transition to a

homogeneous phase, while poorer solubility impedes the transition from the heterogeneous phase. This could play a role in the formation of nanoplastics in the environment. Crystalline polymers in the waste stream have low solubility in water, and therefore, degradation occurring in the environment will not transition out of the heterogeneous phase.

Chapter IV delves into the influence of crystallinity and crystal size on the depolymerization process for PET and its potential in isolating telechelic oligomers. The research demonstrates that pre-annealing PET before depolymerization enhances tie chains' chemical reactivity, reducing› the required reaction time to sever all tie chains and isolate telechelic oligomers. The primary objective of this research project is to provide insight into how modifying specific PET conditions, such as crystallinity, before depolymerization impacts the depolymerization process and how these modifications could streamline recycling or facilitate the creation of new value-added products. Pre-annealing PET before depolymerization results in increased crystallinity and modified crystal structure, although it does not affect the molecular weight of the oligomer produced during depolymerization for a given time. Annealing generates more reactive tie chains, enabling the rapid production of desired dihydroxy-terminated PET oligomers, thus reducing the necessity for post-depolymerization reactions. By pre-annealing PET before depolymerization, we can control the molecular weight of the telechelic oligomers isolated from post-consumer plastic waste through chemical recycling. For instance, annealing PET for 13–24 hours before depolymerization led to the isolation of telechelic oligomers of approximately 10 kDa, whereas unannealed PET typically isolates telechelic oligomers of around 3 kDa. Furthermore, it was observed that during glycolysis, when PET flakes break down into a powder, the PET flakes become dihydroxy-terminated, providing a simple visual indicator of the progress of the reaction.

The research project in Chapter V delves into the visualization of microplastics and nanoplastics using transmission electron microscopes (TEM). It investigates how polymer-solvent interactions and thermal properties affect the shape and crystallinity of nanoplastics. The study utilized Transmission Electron Microscopy (TEM) to examine the breakdown of microplastics into sM&NP in water samples, representing a significant advancement in analyzing sM&NP suspended in water.[7, 8] The research provides a deeper understanding of the fragmentation process by utilizing depolymerized PET nanoparticle powder, revealing that heterogeneous contrast in TEM images corresponds to differences in crystallinity, with darker regions indicating more crystalline domains breaking off from microplastics to form sM&NPs. Additionally, the study found that the glass transition temperature (T_g) and solvent interactions significantly influence the shape of the NPs formed when studying PE under different conditions. Despite the low compatibility of PE and water as polymer solvents, TEM images revealed PE sM&NPs appearing as thin films, aligning with Raman Spectroscopy results that indicated decreased crystallinity due to solvent-induced swelling. Furthermore, Energy-Dispersive X-ray Spectroscopy (EDS) and High-Angle Annular Dark-Field (HAADF) imaging detected oxygen-rich areas in PE particles, indicating oxidation and molecular rearrangement during fragmentation. These findings indicate that even low-compatibility solvents can contribute to the fragmentation of plastics, potentially leading to microplastics and nanoplastics in oceans.

The research project aimed to address the imbalance between the increasing demand for synthetic polymers and the low recycling rate, with only 9% of plastics being recycled annually. It focuses on the depolymerization processes of Polyethylene Terephthalate (PET), Polycarbonate (PC), and Tritan^{TM} from Eastman Chemical Company, aiming to enhance the sustainability of recycling processes. The project investigated the changes in chain structure

during depolymerization, the impact of functional groups on depolymerization rates, polymer solvent compatibility, and methods for imaging nanoplastics from environmental samples. Additionally, it explored the utilization of telechelics formed during depolymerization for repolymerization or value-added products, aiming to advance sustainable polymer recycling processes and create economically viable materials from polymer waste streams.

6.2 Future Outlook

This project focused on depolymerizing polymers to form oligomers with targeted structures for next-generation materials. These findings contribute to the advancement of sustainable polymer recycling processes and the creation of economically viable materials from polymer waste streams. In recent years, there have been significant advancements in the exploration of innovative techniques for converting waste plastics into valuable materials, chemicals, and fuels.[9-17] Moreover, upcycling techniques aim to convert low-value waste plastics into high-performance materials, including advanced composites, construction materials, and specialty chemicals, often by modifying the chemical structure of the plastic to enhance its properties. [9-22] This project has demonstrated the impact of functional groups on depolymerization rates, studied the influence of polymer solvent compatibility, and explored the role of polymer crystal size on depolymerization kinetics.

Future work will build on these insights by leveraging the ability to isolate telechelic oligomers during depolymerization, enabling their use in repolymerization or the synthesis of multiblock copolymers. This approach can reduce the number of synthetic steps needed to introduce ideal functional groups for copolymer assembly, streamlining the process and improving efficiency. Additionally, designing next-generation polymers with more easily cleavable functional groups will facilitate controlled depolymerization, enhancing recyclability

and sustainability. Another key direction is developing new depolymerization methods that allow for selective functionalization of the resulting oligomers, expanding beyond hydroxyl end groups to include functional groups like phenols. This level of control would enable the tailored synthesis of value-added materials with precise chemical properties.

Additionally, this research opens the door to designing next-generation plastics that resist fragmentation into nanoplastics, addressing environmental concerns related to micro- and nanoplastic pollution. By integrating knowledge of polymer degradation pathways, future materials can be engineered to maintain structural integrity while remaining recyclable, reducing the long-term impact of plastic waste. By understanding all of these components, depolymerization reactions can be further optimized with the isolation of telechelic oligomers in mind, paving the way for more sustainable polymer life cycles and novel high-performance materials.

References

(1) Hong, M.; Chen, E. Y. X. Chemically recyclable polymers: a circular economy approach to sustainability. *Green Chemistry* **2017**, *19* (16), 3692-3706. DOI: 10.1039/c7gc01496a.

(2) Arifuzzaman, M.; Sumpter, B. G.; Demchuk, Z.; Do, C.; Arnould, M. A.; Rahman, M. A.; Cao, P.-F.; Popovs, I.; Davis, R. J.; Dai, S.; et al. Selective deconstruction of mixed plastics by a tailored organocatalyst. *Materials Horizons* **2023**, *10* (9), 3360-3368. DOI: 10.1039/d3mh00801k.

(3) Kenwright, A. M.; Peace, S. K.; Richards, R. W.; Bunn, A.; Macdonald, W. A. End group modification in poly(ethylene terephthalate). *Polymer* **1999**, *40* (8), 2035-2040. DOI: 10.1016/s0032-3861(98)00433-9.

(4) George, N.; Kurian, T. Recent Developments in the Chemical Recycling of Postconsumer Poly(ethylene terephthalate) Waste. *Industrial & Engineering Chemistry Research* **2014**, *53* (37), 14185-14198. DOI: 10.1021/ie501995m.

(5) Nikles, D. E.; Farahat, M. S. New Motivation for the Depolymerization Products Derived from Poly(Ethylene Terephthalate) (PET) Waste: a Review. *Macromolecular Materials and Engineering* **2005**, *290* (1), 13-30. DOI: 10.1002/mame.200400186.

(6) Ma, Y.; Agarwal, U. S.; Vekemans, J. A. J. M.; Sikkema, D. J. NMR based determination of minute acid functionality: end-groups in PET. *Polymer* **2003**, *44* (16), 4429-4434. DOI: 10.1016/s0032-3861(03)00402-6.

(7) Zangmeister, C. D.; Radney, J. G.; Benkstein, K. D.; Kalanyan, B. Common Single-Use Consumer Plastic Products Release Trillions of Sub-100 nm Nanoparticles per Liter into Water during Normal Use. *Environmental Science & Technology* **2022**, *56* (9), 5448-5455. DOI: 10.1021/acs.est.1c06768.

(8) Al-Sid-Cheikh, M.; Rowland, S. J.; Stevenson, K.; Rouleau, C.; Henry, T. B.; Thompson, R. C. Uptake, Whole-Body Distribution, and Depuration of Nanoplastics by the Scallop Pecten maximus at Environmentally Realistic Concentrations. *Environmental Science & Technology* **2018**, *52* (24), 14480-14486. DOI: 10.1021/acs.est.8b05266.

(9) Peng, Y.; Wang, Y.; Ke, L.; Dai, L.; Wu, Q.; Cobb, K.; Zeng, Y.; Zou, R.; Liu, Y.; Ruan, R. A review on catalytic pyrolysis of plastic wastes to high-value products. *Energy Convers. Manage.* **2022**, *254*, 115243. DOI: 10.1016/j.enconman.2022.115243.

(10) Guselnikova, O.; Semyonov, O.; Sviridova, E.; Gulyaev, R.; Gorbunova, A.; Kogolev, D.; Trelin, A.; Yamauchi, Y.; Boukherroub, R.; Postnikov, P. "Functional upcycling" of polymer waste towards the design of new materials. *Chem. Soc. Rev.* **2023**, *52* (14), 4755-4832. DOI: 10.1039/d2cs00689h.

(11) Balu, R.; Dutta, N. K.; Roy Choudhury, N. Plastic Waste Upcycling: A Sustainable Solution for Waste Management, Product Development, and Circular Economy. *Polymers* **2022**, *14* (22), 4788. DOI: 10.3390/polym14224788.

(12) Fu, L.; Xiong, Q.; Wang, Q.; Cai, L.; Chen, Z.; Zhou, Y. Catalytic Pyrolysis of Waste Polyethylene Using Combined CaO and Ga/ZSM-5 Catalysts for High Value-Added Aromatics Production. *ACS Sustainable Chemistry & Engineering* **2022**, *10* (29), 9612-9623. DOI: 10.1021/acssuschemeng.2c02881.

(13) Wang, X.; Xu, J.; Zhao, M.; Cui, W.; Mu, X.; Wang, X.; Song, S.; Zhang, H. Recent progress of waste plastic upcycling based on multifunctional zeolite catalysts. *Chemical Synthesis* **2024**, *4* (2). DOI: 10.20517/cs.2023.67.

(14) Chu, M.; Kang, Q.; Hu, P.; Zhang, Q.; Chen, J. Unlocking opportunities: Supported metal catalysts for the chemical upcycling of waste plastics. *Chem. Eng. J.* **2024**, *496*, 154375. DOI: 10.1016/j.cej.2024.154375.

(15) Zhang, X.; Yang, H.; Chen, Z.; Wang, X.; Feng, H.; Zhang, J.; Yu, J.; Gao, S.; Lai, D. Sustainable production of aromatics via catalytic pyrolysis of polyolefins towards the carbon cycle for plastics. *Fuel* **2024**, *357*, 129897. DOI: 10.1016/j.fuel.2023.129897.

(16) Zimmermann, W. Biocatalytic recycling of polyethylene terephthalate plastic. *Philosophical Transactions of the Royal Society A: Mathematical, Physical and Engineering Sciences* **2020**, *378* (2176), 20190273. DOI: 10.1098/rsta.2019.0273.

(17) Mudondo, J.; Lee, H.-S.; Jeong, Y.; Kim, T. H.; Kim, S.; Sung, B. H.; Park, S.-H.; Park, K.; Cha, H. G.; Yeon, Y. J.; et al. Recent Advances in the Chemobiological Upcycling of Polyethylene Terephthalate (PET) into Value-Added Chemicals. *J. Microbiol. Biotechnol.* **2023**, *33* (1), 1-14. DOI: 10.4014/jmb.2208.08048.

(18) Jia, Z.; Gao, L.; Qin, L.; Yin, J. Chemical recycling of PET to value-added products. *RSC Sustainability* **2023**, *1* (9), 2135-2147. DOI: 10.1039/d3su00311f.

(19) Sajwan, D.; Sharma, A.; Sharma, M.; Krishnan, V. Upcycling of Plastic Waste Using Photo-, Electro-, and Photoelectrocatalytic Approaches: A Way toward Circular Economy. *ACS Catalysis* **2024**, *14* (7), 4865-4926. DOI: 10.1021/acscatal.4c00290.

(20) Sun, S.; Huang, W. Chemical Upcycling of Polyolefin Plastics Using Structurally Well-defined Catalysts. *JACS Au* **2024**, *4* (6), 2081-2098. DOI: 10.1021/jacsau.4c00289.

(21) Kim, S.; Kong, D.; Zheng, X.; Park, J. H. Upcycling plastic wastes into value-added products via electrocatalysis and photoelectrocatalysis. *Journal of Energy Chemistry* **2024**, *91*, 522-541. DOI: 10.1016/j.jechem.2024.01.010.

(22) Jiang, M.; Wang, X.; Xi, W.; Yang, P.; Zhou, H.; Duan, J.; Ratova, M.; Wu, D. Chemical catalytic upgrading of polyethylene terephthalate plastic waste into value-added materials, fuels and chemicals. *Sci. Total Environ.* **2024**, *912*, 169342. DOI: 10.1016/j.scitotenv.2023.169342.

APPENDICES

Appendix A: Supporting Information for Chapter III

A.1. Methods

A.1.1. Differential Scanning Calorimetry (DSC)

The Differential Scanning Calorimetry (DSC) Q200 curves of the depolymerization product (3-7 mg) were measured in a Hermetic aluminum pan. In the DSC run, the sample was equilibrated at 50 °C before being heated to 280 °C for Polyethylene Terephthalate (PET) and 350 °C for Tritan™ with a ramp of 10 °C/min. PET was heated to 280 °C as literature has shown PET melts at 260 °C. [1, 2] Tritan™ was heated to 350 °C to ensure no melting peak past PET's melting curve. However, we didn't expect a melting curve for Tritan™ as it is amorphous. [3] This ramp rate was chosen to inhibit recrystallization during scanning. [4] Enthalpies of melting of the PET samples were determined by measuring the heat flow associated with the melting of PET from the first cycle. [5] The percent crystallinity of each sample was calculated by dividing the enthalpy of the melting of a PET sample by the enthalpy of 100% crystalline PET (140 J/g). [6]

A.1.2. Fourier Transform Infrared Spectroscopy (FTIR)

FTIR was utilized to evaluate the heterogeneous process and confirm the swelling index of the polymer flake. The FTIR was set to 64 scans to acquire smooth spectra of both the flake and powder. As such, the reaction powder and flake were scanned separately in triplicate, with a background measured between every 5 scans. The instrument's sample holder was cleaned and dried with isopropyl to prevent contaminated and inaccurate readings.

A.1.3. Normalized Swelling [%] for BPA

Half a gram of polymer (PET, or PC) was placed in a 100 mL round bottom flask with BPA and stir bar and sealed with septa in a 1:35 molar ratio of polymer to solvent. Samples were mixed and heated in a 180 °C oil bath for various times (10, 15, 20, 30, or 45 minutes, depending on the polymer) following the swelling procedure from Najmi. [7] Swelling times are not as long as

previously reported by Najmi to as dissolution of the polymer started to occur before one hour of swelling. After a specific time, the solvent was decanted hot from the vial and rinsed with methanol for 15 minutes. Then, the methanol was decanted, rinsed again for another 15 minutes, and repeated. The samples were heated at 75 °C for 72 hours to evaporate off the remaining methanol before being weighed. Very quickly, both polymers had a BPA soluble and BPA insoluble fraction, where the BPA soluble polymers dissolute from the polymer flake. This made it more complex to calculate normalized swelling and required us to calculate the amount of BPA diffused into the polymer flake and the amount of insoluble polymer. The amount of BPA gained was calculated using **Equation A.1**, where m_f is the final mass (BPA soluble and insoluble), m_i is the initial mass, and $m_{BPA\ gained}$ is the mass of BPA diffused into the polymer flakes. The amount of polymer remaining that was BPA insoluble ($m_{polymer}$) was calculated using **Equation A.2**, where mfinal pellet is the final mass, not including BPA soluble polymer (powder $m_{BPA\ gained}$ is the mass of BPA diffused into the polymer flakes. **Equation A.3** combines different swelling ratio equations and **Equation A.1** and **Equation A.2** to obtain the normalized swelling per polymer flake, as the dimensions of the flakes vary between the two polymers of interest. [7, 8]

Equation A.1 $$\boldsymbol{m_{BPA\ gained} = (m_f - m_i)}$$

Equation A.2 $$\boldsymbol{m_{polymer} = m_{final\ pellet} - m_{BPA\ gained}}$$

Equation A.3 $$\boldsymbol{Normalized\ Swelling\ [\%]_{BPA} = \frac{\frac{m_{final\ flake} - m_{polymer}}{m_{polymer}}}{\#\ flakes} * 100}$$

A.1.4. Glycolysis with Basic Catalyst

Ethylene Glycol (EG), Triazabicyclodecene (TBD) catalyst, carbonyl-containing polymer (PC, PET or Trian^{TM}) (20:0.5:1 molar ratio), and stir bar were all placed in a 20 mL reaction vial inside a glovebox, sealed with a septum, and transferred outside the glovebox into a 180 °C oil

bath. Previous studies indicate that the glycolysis of PET and PC takes 2 hours and 4 hours, respectively, at 180 °C to reach completion.[9, 10] However, these reactions reached completion within 4 minutes. To analyze the evolution of the polymer chains during depolymerization, the reaction was stopped at various reaction times (i.e. 1, 2, 3, 4 minutes), and the products were recovered and characterized as described for the glycolysis reactions utilizing TBDMSA catalyst.[10] PC and Tritan™ oligomers were analyzed using THF Gel permeation Chromatograph/Size Exclusion Chromatograph (GPC/SEC). Tritan™ and its oligomers were dissolved in THF at 80 °C overnight to ensure dissolution. **Scheme A.1** illustrates the glycolysis of the 3 polymers to isolate oligomers.

Scheme A.1 Heterogenous glycolysis reaction of Tritan™, PET, and PC catalyzed by TBD:MSA to create oligomers.

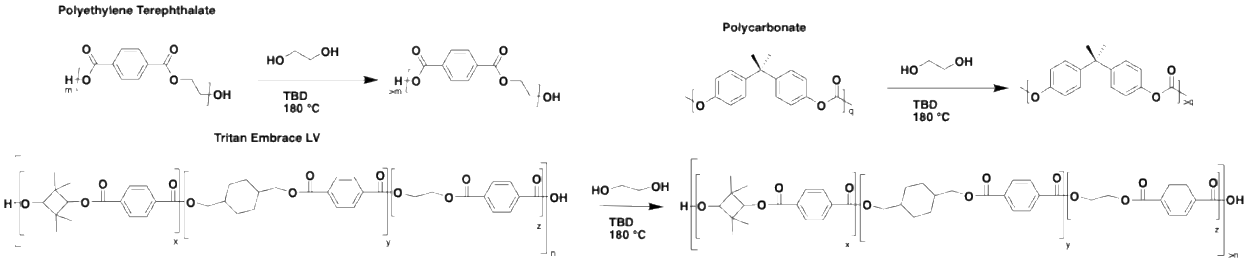

A.2. Results and Discussion

A.2.1. Starting Material Characterization

Since Tritan™, Polyethylene Terephthalate (PET), and Polycarbonate (PC) all come from different sources, Tritan™ from Eastman Chemical Company and PET and PC from consumer waste, we first characterized the starting molecular weights and crystallinity of the polymers, where the results are shown in **Figure 3.3** and **Figure A.1** respectively. **Figure A.1** shows PET (blue) heat flow and Tritan™ (green) vs. reaction time. PET has a distinct melting curve starting at 240 °C, which follows the literature. [1, 2] There is no melting curve for Tritan™, as expected. The multiple T_g's that appear in the DSC curve for Tritan™ (68 °C, 113 °C, and 216 °C) could be from the 10 °C/min ramp rate being too fast for Tritan™. However, 68 °C and 113 °C T_g have

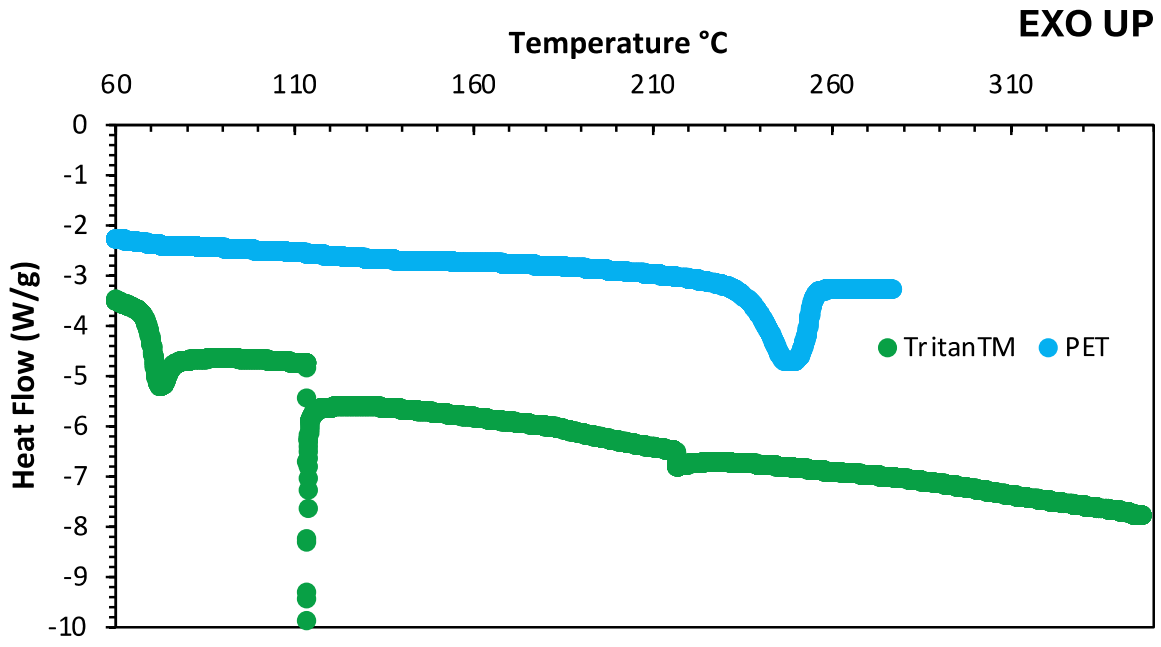

Figure A.1 Differential Scanning Calorimetry of polyethylene terephthalate (PET, blue) and Tritan^{TM} (green) vs. temperature.

been previously shown in the literature and could bring a better insight into the composition of the copolyester, though this is beyond this project's scope.[3] **Figure A.1** has verified that PET is semicrystalline, with a 25% crystallinity, and that Tritan™ is amorphous.

A.2.2. Ethylene Glycol depolymerization of polymers with basic catalyst

Figure A.2 depicts the results of depolymerizing PET, Tritan™, and PC via glycolysis using TBD, a very strong base (pKa=26.2), as a catalyst.[11] **Figure A.2 (a)** shows reaction vials of PET, Tritan™, and PC 4 minutes into this glycolysis reaction. As shown in **Figure 3.8**, PET and PC do not dissolve in EG when the TBD:MSA salt catalyst is used, even after 1.5 and 5 hours, respectively. The lone pair on TBD, not present in TBD:MSA, could enhance the polymer's solubility by acting as a Lewis base, suggesting it may interact with the polymer's polar groups, such as carbonyl or hydroxyl functionalities. These interactions could disrupt intermolecular forces and increase the polymer's compatibility with solvents, potentially aiding in its dissolution.[12-14] **Figure A.2 (b)** shows how the percent yield of EG insoluble Tritan™ (orange) and PC (blue) flakes decreases with reaction time. The carbonate-containing polymer solubilizes faster than the ester-containing polymer, which was not previously shown in the EG and BPA reactions utilizing TBD:MSA catalyst. **Figure A.2 (c)** shows the percent change in molecular weight of Tritan™ and PC from both the EG soluble and insoluble fractions. **Figure A.2 (c)** shows that PC decreases to less than 20% of its original M_n (grey) and M_w (yellow) within 1 minute of the reaction, which takes Tritan™ between 2-3 minutes to reach a similar decrease in M_n (blue) and M_w (orange). **Figure A.2 (d)** better illustrates what is happening to the EG insoluble polymer flake by showing M_n (blue for Tritan™ and grey for PC) and M_w (orange for Tritan and yellow for PC) with reaction time. Based on the rapid decrease in percent yield and molecular weight of the EG insoluble fraction compared to our previous reactions, we infer that

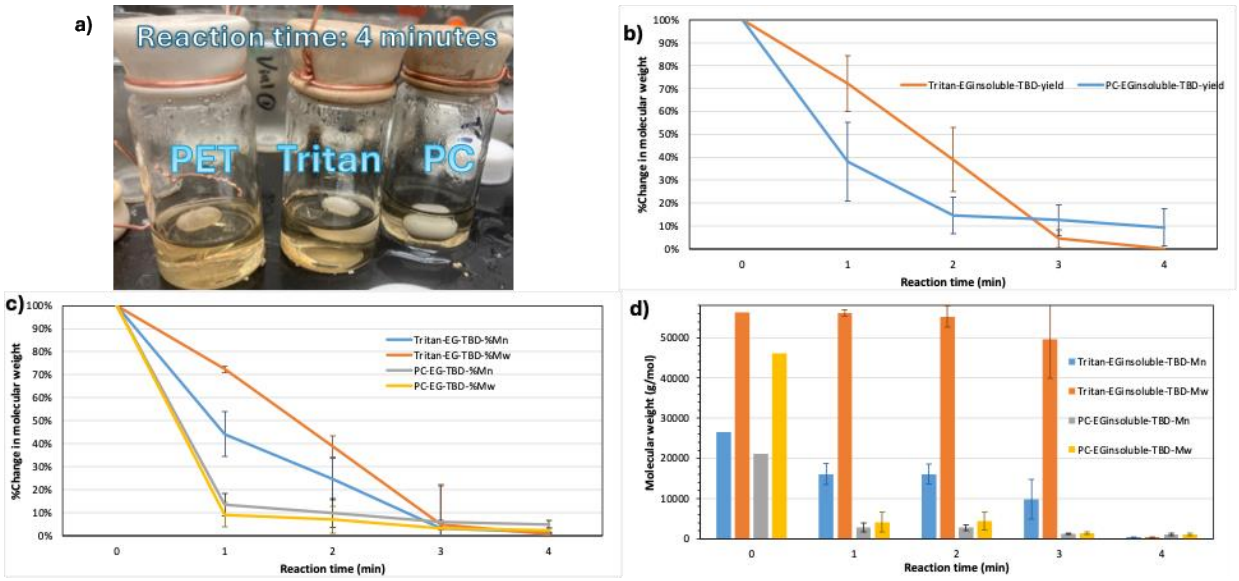

Figure A.2 Heterogeneous depolymerization of PET, Tritan^{TM}, and PC via glycolysis catalyzed by TBD. (a) Pictures PET, Tritan^{TM}, and PC solubilized in EG:TBD 4 minutes into the reaction. (b) shows the percent yield of EG insoluble Tritan^{TM} (orange) and PC (blue) with reaction time. (c) Depicts the percent change in molecular weight for Tritan^{TM} (M_n blue, M_w orange) and PC (M_n grey, M_w yellow) of both the EG soluble and insoluble fraction with reaction time. (d) Shows the molecular weight of for Tritan^{TM} (M_n blue, M_w orange) and PC (M_n grey, M_w yellow) EG insoluble fraction with reaction time.

using a suitable catalyst results in higher polymer solubilization,[12-15] controlling when the heterogeneous reaction transitions through the three stages of a heterogenous depolymerization.

To better understand why, in this case, the carbonate-containing polymer depolymerizes faster than the ester-containing polymer, H^1 NMR was taken. **Figure A.3** depicts H^1 NMR in $CDCl_3$ of PC (green), BPA (blue), PC depolymerized with EG catalyzed with TBD:MSA for 2 hours (purple), and PC depolymerized with EG catalyzed with TBD for 2 minutes (red). **Figure A.3 (left)** shows the whole spectrum from 8 ppm to 1.5 ppm, highlighting aromatic peaks (7.25 to 6.6 ppm, purple circle), methyl groups (1.65 ppm, green circle), and phenol groups (4.86 ppm, blue circle).[16] This spectrum also depicts impurities like THF (3.75 and 1.88 ppm, dark blue circle) and acetone (3.28 ppm, orange circle) used during the workup process of the NMR samples. HFIP (4.3 and 4.0-3.5 ppm, red circle) was added to the depolymerized PC samples to view hydroxyl and phenol groups better.[17] **Figure A.3 (right)** shows the NMR spectrums from 6.6 to 4.6 ppm to highlight a range where phenol groups (highlighted in blue circles) can be displayed. The spectrum indicates that phenol groups are present in BPA, PC depolymerized with EG catalyzed with TBD: MSA for 2 hours, and PC depolymerized with EG catalyzed with TBD for 2 minutes. When chain scission occurs via glycolysis or hydrolysis of BPA-based PC at the carbonyl carbon, phenol end groups are expected to be produced.[9, 18, 19]

Yet, how does catalyzing depolymerization with TBD alone instead of TBDMSA increase the reaction rate? TBD is known to facilitate reactions through four distinct pathways. Path 1 follows a 'fully concerted' mechanism, resembling an SN_2-like O → N acyl-transfer transition state, stabilized by hydrogen bonding interactions with TBD.[11] Path 2 involves a stepwise mechanism where tetrahedral intermediates are formed and stabilized through hydrogen bonding with TBD.[11, 20, 21] Path 3 also proceeds via a stepwise mechanism but includes the

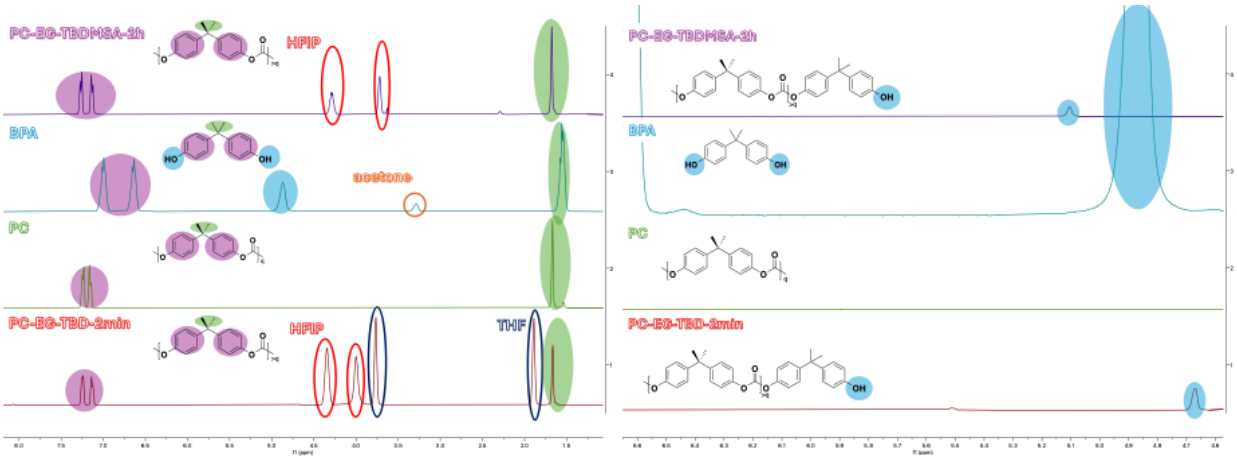

Figure A.3 H^1 NMR spectrum in $CDCl_3$ of PC (green), BPA (blue), PC depolymerized with EG catalyzed with TBD: MSA for 2 hours (purple), and PC depolymerized with EG catalyzed with TBD for 2 minutes (red). This spectrum also depicts impurities like THF (3.75 and 1.88 ppm, dark blue circle), HFIP (4.3 and 4.0-3.5 ppm, red circle) and acetone (3.28 ppm, orange circle). **(Left)** Shows the whole NMR spectrum. **(Right)** Shows NMR spectrum in the ppm range where phenol groups are expected to be present.

nucleophilic attack of TBD on the ester, leading to the formation of a covalent bond with TBD.[11, 22] Path 4 involves TBD's deprotonation of hydroxyl groups or water molecules, generating hydroxide ions, which act as more reactive nucleophiles. [11, 23] These hydroxide ions then attack the carbonate carbon center in the middle of the trimeric chain, promoting efficient chain cleavage.[23] At lower temperatures, hydrogen bonding may be more favorable due to kinetic factors, as the weaker interactions can form more readily. However, at higher temperatures, the increased thermal energy helps overcome the thermodynamic threshold for deprotonation, promoting the formation of hydroxide ions.[24-26] Previous studies have shown that beyond the onset degradation temperature of TBD (around 150 °C), the basicity of TBD remains unaffected,[27] supporting the notion that at temperatures around 180 °C, TBD can effectively deprotonate hydroxyl and phenol end groups, enhancing reactivity and polymer cleavage. Due to the elevated temperatures, we believe the depolymerization of Tritan™ and PC occurs more rapidly because the hydroxyl and phenol groups can undergo deprotonation. As phenolic end groups are produced during the depolymerization of PC, the phenoxide species act as strong nucleophiles, further accelerating the breakdown of remaining carbonate bonds through an autocatalytic effect. This likely speeds up the depolymerization of PC, making it happen faster than Tritan™, which does not generate phenolic groups and only has hydroxyl groups present.

A.2.3. Bisphenol-A depolymerization of PET and PC

We attributed a visual difference in the polymers depolymerized with EG and BPA to swelling and dissolution. **Figure A.4** demonstrates how PC experienced swelling and dissolution from EG and BPA. **Figure A.4 (a)** shows a visual representation of the diffusion of the solvent into the PC flake. **Figure A.4 (b)** shows the change in the PC flakes with depolymerization time with BPA. Visually, it appeared that the PC flakes became thinned with reaction time. To verify

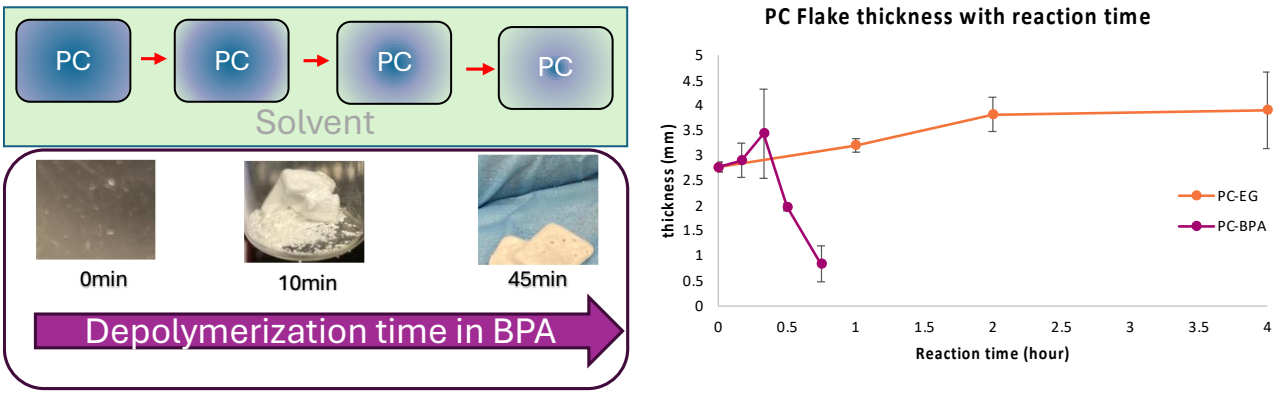

Figure A.4 Demonstrates the diffusion of the solvent into the polymer flakes. (a) It is a visual signal of solvent (EG or BPA) slowly diffusing into the polymer flake. (b) It shows a visual change in PC flakes with depolymerization time in BPA. (c) shows a graph of PC flake thickness vs reaction time in EG (orange) and BPA (purple).

this, we measured the thickness of the PC flakes. **Figure A.4 (c)** shows the change in PC flake thickness with reaction time when depolymerized in BPA (purple line) or EG (orange line). PC flakes depolymerized in BPA increased in thickness initially, then decreased in thickness well below the original thickness of the PC flake. However, the PC flakes depolymerized in EG slowly increased in thickness with reaction time and never decreased despite reacting four times as long as the reactions utilizing BPA.

When depolymerizing both polymers with BPA, we isolated flakes that were BPA insoluble and powder that was BPA soluble but methanol insoluble. The molecular weights of both fractions were calculated using SEC GPC, shown in **Figure A.5. Figure A.5 (a)** shows the change in M_n (dark green), M_w (green), and Đ (purple) of PET that is BPA insoluble as a change in reaction time; it also shows the change in M_n (dark orange), M_w (orange), and Đ (blue) of PET that is BPA soluble as a change in reaction time. The Đ of the BPA soluble and insoluble PET oligomers increased with reaction time, which was not observed when depolymerizing PET with EG. Surprisingly, we could isolate PET oligomers of substantial molecular weight that were BPA soluble, which we did not observe when depolymerizing PET with EG. The molecular weight of both the soluble and insoluble fractions decreased with reaction time. However, the BPA soluble fraction of the PET oligomers decreases in molecular weight faster than the BPA insoluble fraction, as the soluble fraction is in the same phase as BPA. PET depolymerized in BPA takes a shorter amount of time than PET depolymerized in EG, as the yield of PET oligomers isolated during depolymerization with BPA in both the soluble and insoluble fractions decreases with reaction time, as shown in **Figure 3.9.**

Figure A.5 (b) shows the change in M_n (dark purple), M_w (light purple), and Đ (pink-orange line) of PC that is BPA insoluble as a change in reaction time; it also shows the change in

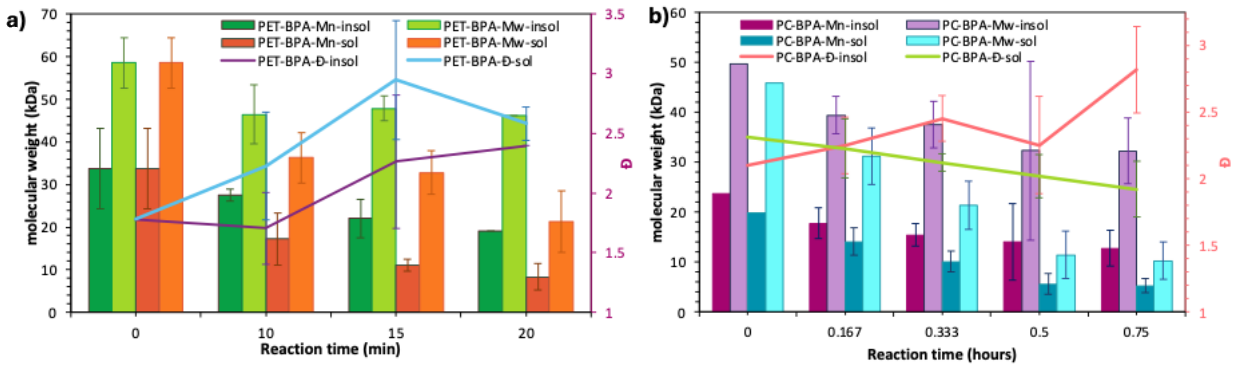

Figure A.5 PET and PC depolymerized in BPA. **(a)** shows the change in molecular weight of the insoluble (M_n dark orange, M_w orange) and soluble (M_n dark green, M_w green) fractions of PET with reaction time and the change in dispersity of the insoluble (purple) and soluble fraction (blue). **(b)** shows the change in molecular weight of the insoluble (M_n dark purple, M_w purple) and soluble (M_n dark blue, M_w blue) fractions of PC with reaction time and the change in dispersity of the insoluble (orange) and soluble fraction (green).

M_n (dark blue), M_w (light blue), and Đ (green line) of PC that is BPA soluble as a change in reaction time. The Đ of the BPA insoluble PC oligomers continually increased with reaction time, which was not observed when depolymerizing PET with EG. However, the BPA-soluble PC oligomers decrease Đ with reaction time, as observed when depolymerizing PC with EG. We expect the reactions of depolymerizing polymers with EG to react faster than those with BPA, as BPA is a poorer nucleophile than EG because BPA has a lower pKa.[28] Again, we could isolate PC oligomers of substantial molecular weight that were BPA soluble, which we did not observe when depolymerizing PC with EG. The molecular weight of both the soluble and insoluble fractions decreased with reaction time. However, the BPA soluble fraction of the PC oligomers decreases in molecular weight faster than the BPA insoluble fraction, as the soluble fraction is in the same phase as BPA.

Figure A.6 shows PET and PC's normalized swelling per polymer flake in BPA. **Figure 3.4** demonstrates that our amorphous polymer (PC) swells with more EG than our semicrystalline polymer (PET), which is not unexpected.[29] **Figure A.6** shows the change in normalized swelling for PET (green line) and PC (pink line) versus the square root of time (minutes). The swelling experiments utilizing BPA were substantially shorter than those utilizing EG as both polymers started to dissolve in BPA faster than in EG. Also, the BPA swelling experiments observed a higher percentage of swelling per polymer flake for both polymers than those using EG. Unexpectantly, this time, the amorphous polymer swells with less solvent than our semicrystalline polymer.

Figure A.7 shows the DSC of PET in varying conditions to understand why semicrystalline PET swells similarly or more than amorphous PC with BPA. When PET is depolymerized (dark blue) or swelled (light blue) with EG, the percent crystallinity increases

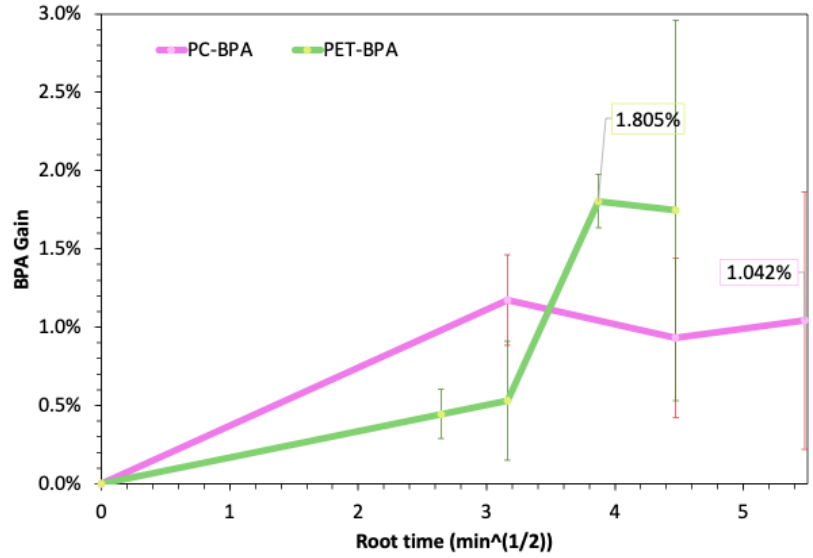

Figure A.6 demonstrates the normalized swelling of BPA into PET (green) and PC (pink)

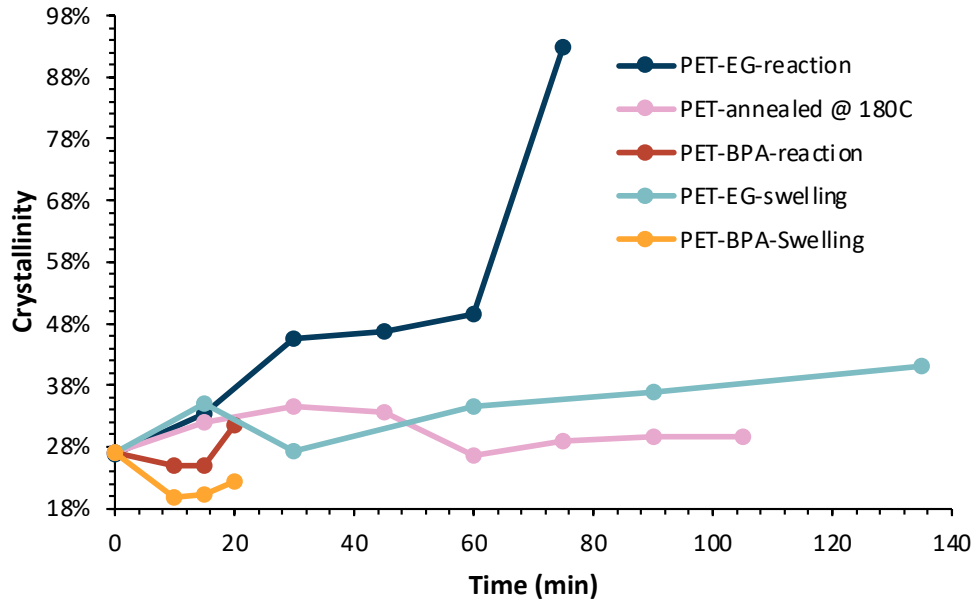

Figure A.7 shows the change in percent crystallinity of PET under different conditions (Depolymerized with EG (dark blue), swelled with EG (light blue), annealed at reaction temperature (pink), depolymerized with BPA (red), swelled with BPA (orange) with time.

with time, though the depolymerization mechanism enhances the increase in crystallinity with reaction time. PET annealed at the reaction temperature under vacuum (pink) increases in crystallinity similarly to PET swelled with EG. However, PET depolymerized (red) or swelled (orange) with BPA decreases in crystallinity initially. PET depolymerized with BPA decreases and then increases crystallinity, again demonstrating that the mechanism of the depolymerization aids in crystal growth. However, PET swelled with BPA decreases in crystallinity as it is hypothesized that BPA disturbs or dissolves the PET crystals, making PET more amorphous and able to swell similarly to PC, as shown in **Figure A.6**.

Figure A.8 shows the FTIR spectra of the PET and PC BPA soluble and BPA insoluble fractions to further understand the swelling of the polymer flakes. The FTIR spectra of BPA (left top) have a distinct hydroxyl peak (3500 cm^{-1}), which was used as a reference in the scans of our polymers, as BPA has a similar chemical structure to PC except for the hydroxyl peak. FTIR was taken of the polymer flakes and powder to observe BPA swelling into the flakes and ensure that the powder was polymer and not undissolved BPA. Both polymer powders (PC red middle and PET red bottom spectra) show no indication of the hydroxyl peak in BPA, indicating that these BPA-insoluble powders were polymer. Both polymer flakes (PC pink middle and PET green bottom spectra) have a distinct hydroxyl peak at 3500 cm-1, demonstrating that BPA had diffused into the polymer flakes.

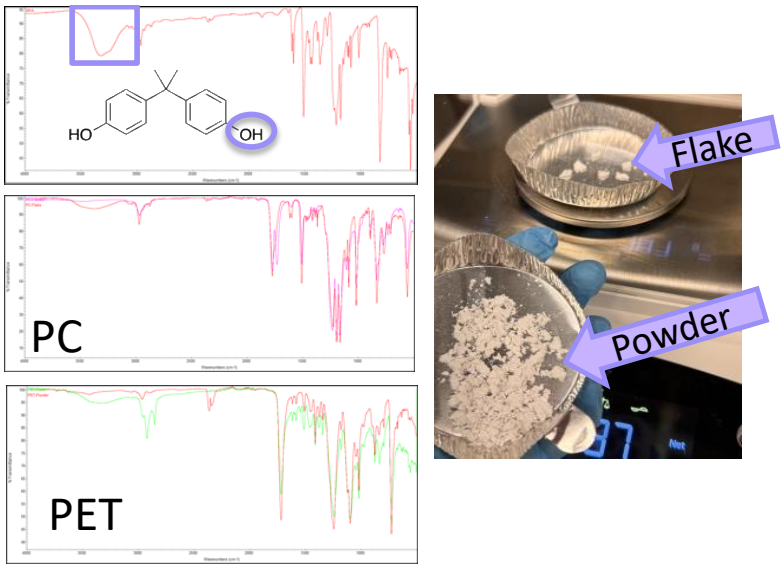

Figure A.8 shows the FTIR spectra for BPA, PET, and PC. The top left in red shows the FTIR of BPA with the alcohol peak highlighted in a purple square. The Middle FTIR spectra show the PC powder in red and the flake in pink. The bottom spectra show FTIR of PET powder in red and PET flakes in green. The right side of the image also shows the visual difference in the polymer flakes and the polymer powder.

References

(1) Liu, Y.; Yin, L.; Zhao, H.; Song, G.; Tang, F.; Wang, L.; Shao, H.; Zhang, Y. Lamellar and fibrillar structure evolution of poly(ethylene terephthalate) fiber in thermal annealing. *Polymer* **2016**, *105*, 157-166. DOI: https://doi.org/10.1016/j.polymer.2016.10.031.

(2) Chen, Z.; Jenkins, M. J.; Hay, J. N. Annealing of poly (ethylene terephthalate). *Eur. Polym. J.* **2014**, *50*, 235-242. DOI: 10.1016/j.eurpolymj.2013.11.004.

(3) Bhagia, S.; Bornani, K.; Ozcan, S.; Ragauskas, A. J. Terephthalic Acid Copolyesters Containing Tetramethylcyclobutanediol for High-Performance Plastics. *ChemistryOpen* **2021**, *10* (8), 830-841. DOI: 10.1002/open.202100171.

(4) Holdsworth, P. J.; Turner-Jones, A. The melting behaviour of heat crystallized poly(ethylene terephthalate). *Polymer* **1971**, *12* (3), 195-208. DOI: https://doi.org/10.1016/0032-3861(71)90045-0.

(5) Blaine, R. L. *Determination of Polymer Crystallinity by DSC*; TA Instruments, https://www.tainstruments.com/pdf/literature/TA123new.pdf.

(6) Blaine, R. L. *THERMAL APPLICATIONS NOTE*; TA Instrument, https://www.tainstruments.com/pdf/literature/TN048.pdf.

(7) Najmi, S.; Vance, B. C.; Selvam, E.; Huang, D.; Vlachos, D. G. Controlling PET oligomers vs monomers via microwave-induced heating and swelling. *Chem. Eng. J.* **2023**, *471*, 144712. DOI: https://doi.org/10.1016/j.cej.2023.144712.

(8) Zhou, X.; Wang, J.; Nie, J.; Du, B. Poly(N-isopropylacrylamide)-based ionic hydrogels: synthesis, swelling properties, interfacial adsorption and release of dyes. *Polym. J.* **2016**, *48* (4), 431-438. DOI: 10.1038/pj.2015.123.

(9) Jehanno, C.; Demarteau, J.; Mantione, D.; Arno, M. C.; Ruipérez, F.; Hedrick, J. L.; Dove, A. P.; Sardon, H. Selective Chemical Upcycling of Mixed Plastics Guided by a Thermally Stable Organocatalyst. *Angew. Chem. Int. Ed.* **2021**, *60* (12), 6710-6717. DOI: 10.1002/anie.202014860.

(10) Jehanno, C.; Flores, I.; Dove, A. P.; Müller, A. J.; Ruipérez, F.; Sardon, H. Organocatalysed depolymerisation of PET in a fully sustainable cycle using thermally stable protic ionic salt. *Green Chemistry* **2018**, *20* (6), 1205-1212. DOI: 10.1039/c7gc03396f.

(11) Jin, L.; Wu, Y.; Kim, C.-K.; Xue, Y. Theoretical study on the aminolysis of ester catalyzed by TBD: Hydrogen bonding or covalent bonding of the catalyst? *Journal of Molecular Structure: THEOCHEM* **2010**, *942* (1-3), 137-144. DOI: 10.1016/j.theochem.2009.12.012.

(12) Hong, M.; Chen, J.; Chen, E. Y. X. Polymerization of Polar Monomers Mediated by Main-Group Lewis Acid–Base Pairs. *Chem. Rev.* **2018**, *118* (20), 10551-10616. DOI: 10.1021/acs.chemrev.8b00352.

(13) Kaiho, S.; Hmayed, A. A. R.; Delle Chiaie, K. R.; Worch, J. C.; Dove, A. P. Designing Thermally Stable Organocatalysts for Poly(ethylene terephthalate) Synthesis: Toward a One-Pot, Closed-Loop Chemical Recycling System for PET. *Macromolecules* **2022**, *55* (23), 10628-10639. DOI: 10.1021/acs.macromol.2c01410.

(14) Grabowski, S. J. Hydrogen Bond and Other Lewis Acid–Lewis Base Interactions as Preliminary Stages of Chemical Reactions. *Molecules* **2020**, *25* (20), 4668. DOI: 10.3390/molecules25204668.

(15) Olazabal, I.; Luna, E.; De Meester, S.; Jehanno, C.; Sardon, H. Upcycling of BPA-PC into trimethylene carbonate by solvent assisted organocatalysed depolymerisation. *Polymer Chemistry* **2023**, *14* (19), 2299-2307. DOI: 10.1039/d3py00441d.

(16) Kim, J.; Gracz, H. S.; Roberts, G. W.; Kiserow, D. J. Spectroscopic analysis of poly(bisphenol A carbonate) using high resolution 13C and 1H NMR. *Polymer* **2008**, *49* (2), 394-404. DOI: 10.1016/j.polymer.2007.11.046.

(17) Falkenstein, P.; Gräsing, D.; Bielytskyi, P.; Zimmermann, W.; Matysik, J.; Wei, R.; Song, C. UV Pretreatment Impairs the Enzymatic Degradation of Polyethylene Terephthalate. *Frontiers in microbiology*. **2020**, *11*. DOI: 10.3389/fmicb.2020.00689.

(18) Kamps, J. H.; Hoeks, T.; Kung, E.; Lens, J. P.; McCloskey, P. J.; Noordover, B. A. J.; Heuts, J. P. A. Activated carbonates: enabling the synthesis of differentiated polycarbonate resins via melt transcarbonation. *Polymer Chemistry* **2016**, *7* (33), 5294-5303. DOI: 10.1039/c6py00925e.

(19) Maia, J.; Cruz, J. M.; Sendón, R.; Bustos, J.; Cirugeda, M. E.; Sanchez, J. J.; Paseiro, P. Effect of amines in the release of bisphenol A from polycarbonate baby bottles. *Food Research International* **2010**, *43* (5), 1283-1288. DOI: 10.1016/j.foodres.2010.03.014.

(20) Kim, J. G.; Lee, G. S.; Lee, A. Triazabicyclodecene: A versatile catalyst for polymer synthesis. *Journal of Polymer Science* **2024**, *62* (1), 42-91. DOI: 10.1002/pol.20230643.

(21) Onida, K.; Fayad, M.; Norsic, S.; Boyron, O.; Duguet, N. Chemical upcycling of poly(bisphenol A carbonate) to vinylene carbonates through organocatalysis. *Green Chemistry* **2023**, *25* (11), 4282-4291. DOI: 10.1039/d2gc04413g.

(22) Simón, L.; Goodman, J. M. The Mechanism of TBD-Catalyzed Ring-Opening Polymerization of Cyclic Esters. *The Journal of Organic Chemistry* **2007**, *72* (25), 9656-9662. DOI: 10.1021/jo702088c.

(23) Lamparelli, D. H.; Villar-Yanez, A.; Dittrich, L.; Rintjema, J.; Bravo, F.; Bo, C.; Kleij, A. W. Bicyclic Guanidine Promoted Mechanistically Divergent Depolymerization and Recycling of a Biobased Polycarbonate. *Angew. Chem. Int. Ed.* **2023**, *62* (51). DOI: 10.1002/anie.202314659.

(24) Tang, X. C.; Pikal, M. J.; Taylor, L. S. *Pharm. Res.* **2002**, *19* (4), 484-490. DOI: 10.1023/a:1015199713635.

(25) Lee, H. Effects of temperature, salt concentration, and the protonation state on the dynamics and hydrogen-bond interactions of polyelectrolyte multilayers on lipid membranes. *Physical Chemistry Chemical Physics* **2016**, *18* (9), 6691-6700. DOI: 10.1039/c5cp08039h.

(26) Gupta, M.; Svendsen, H. F. Theoretical Study of Temperature dependent Enthalpy of Absorption, Heat Capacity, and Entropy changes for Protonation of Amines and Amino Acid Solvents. *Energy Procedia* **2014**, *63*, 1099-1105. DOI: 10.1016/j.egypro.2014.11.118.

(27) Reisinger, D.; Kriehuber, M. U.; Bender, M.; Bautista-Anguís, D.; Rieger, B.; Schlögl, S. Thermally Latent Bases in Dynamic Covalent Polymer Networks and their Emerging Applications. *Adv. Mater.* **2023**, *35* (24), 2300830. DOI: 10.1002/adma.202300830.

(28) Dave Evans, D. H. R. *pKa's of Inorganic and Oxo-Acids*. ACS Organic Division, 2024. https://organicchemistrydata.org/hansreich/resources/pka/pka_data/evans_pKa_table.pdf (accessed 2024.

(29) Miller-Chou, B. A.; Koenig, J. L. A review of polymer dissolution. *Prog. Polym. Sci.* **2003**, *28* (8), 1223-1270. DOI: 10.1016/s0079-6700(03)00045-5.

Appendix B: Supporting Information for Chapter IV

B.1. Methods

B.1.1. Differential Scanning Calorimetry (DSC)

The Differential Scanning Calorimetry (DSC) Q200 curves of the depolymerization product (3-7 mg) were measured in a Hermetic aluminum pan. In the DSC run, the sample was equilibrated at 50 °C before being heated to 280 °C for Polyethylene Terephthalate (PET) with a ramp of 10 °C/min. PET was heated to 280 °C as literature has shown PET melts at 260 °C.[1, 2] This ramp rate was chosen to inhibit recrystallization during scanning.[3] Enthalpies of melting of the PET samples were determined by measuring the heat flow associated with the melting of PET from the first cycle.[4] The percent crystallinity of each sample was calculated by dividing the enthalpy of the melting of a PET sample by the enthalpy of 100% crystalline PET (140 J/g).[5]

B.1.2. Normalized Swelling

Half a gram of polymer PET was placed in a 20 mL vial with EG, stir bar, and sealed with septa in a 1:35 molar ratio of polymer to solvent. Samples were mixed and heated in a 180 °C oil bath for various times (30, 60, 90, and 135 minutes) following the swelling procedure from Najmi.[6] Swelling times are not as long as previously reported by Najmi to prevent the dissolution of the polymer into the solvent. After a specific time, the solvent was decanted hot from the vial and rinsed with DI water for 15 minutes. Then, the water was decanted, rinsed again for another 15 minutes, and repeated. The samples were heated at 75 °C for 72 hours to evaporate off the remaining water before being weighed. The normalized swelling was calculated using **Equation B.1**, where m_f is the final mass and m_i is the initial mass. **Equation B.1** uses the swelling ratio equation to obtain the percent swelling.[6, 7] Measurements were stopped when the polymer started to dissolve, demonstrated by a significant decrease in the normalized swelling.

Equation B.1 $$\boldsymbol{Swelling}\ [\%] = \frac{m_f - m_i}{m_i} * \mathbf{100}$$

B.2. Results and Discussion

B.2.1. Small Angle X-Ray Scattering (SAXS)

The PET flakes were also scattered using small angle x-ray scattering, and the scattering curves were analyzed using the 1D correlation function (**Equation B.2**) to find the lamellae thickness and the crystalline phase thickness during annealing and depolymerization post annealing, as shown in **Figure B.1**.[8-10]

Equation B.2 $$\boldsymbol{K(z)} = \frac{\int \mathbf{4\pi q^2} * \boldsymbol{I(q)} * \mathbf{cos}(\boldsymbol{q} * \boldsymbol{z}) \boldsymbol{dq}}{\int_0^{\infty} \boldsymbol{I(q)} * \boldsymbol{q^2 dq}}$$

Though there is little change in the lamellae with annealing, there appears to be some level of orientation in the material, as shown in **Figure B.1 (a)**. Though this was not a controlled variable in this study, it was seen in scattering that the lamellae and crystalline unit cells were oriented along the bottle, this orientation appeared to be altered due to depolymerization. The plastic was cut into square pieces, and orientation of which was not tracked. This wouldn't have been a problem; however, the lamellae appear to be oriented along the bottle, likely due to the manufacturing process. The scattering of the data was oriented such that the angle with the most intense scattering was artificially aligned with the orientation of a piece scattered with known orientation relative to the bottle. The intensity around the azimuthal [Intensity vs. angle graphs] was tracked and alignment factors were calculated. The alignment factor (**Equation B.3**) was defined by Walker and Wagner[11] as:

Equation B.3 $$\boldsymbol{Alignment\ Factor(AF)} = \frac{\int_0^{2\pi} \boldsymbol{I(q, \psi)} * \boldsymbol{cos}(\mathbf{2}\boldsymbol{\psi}) \boldsymbol{d\psi}}{\int_0^{2\pi} \boldsymbol{I(q, \psi)} \boldsymbol{d\psi}}$$

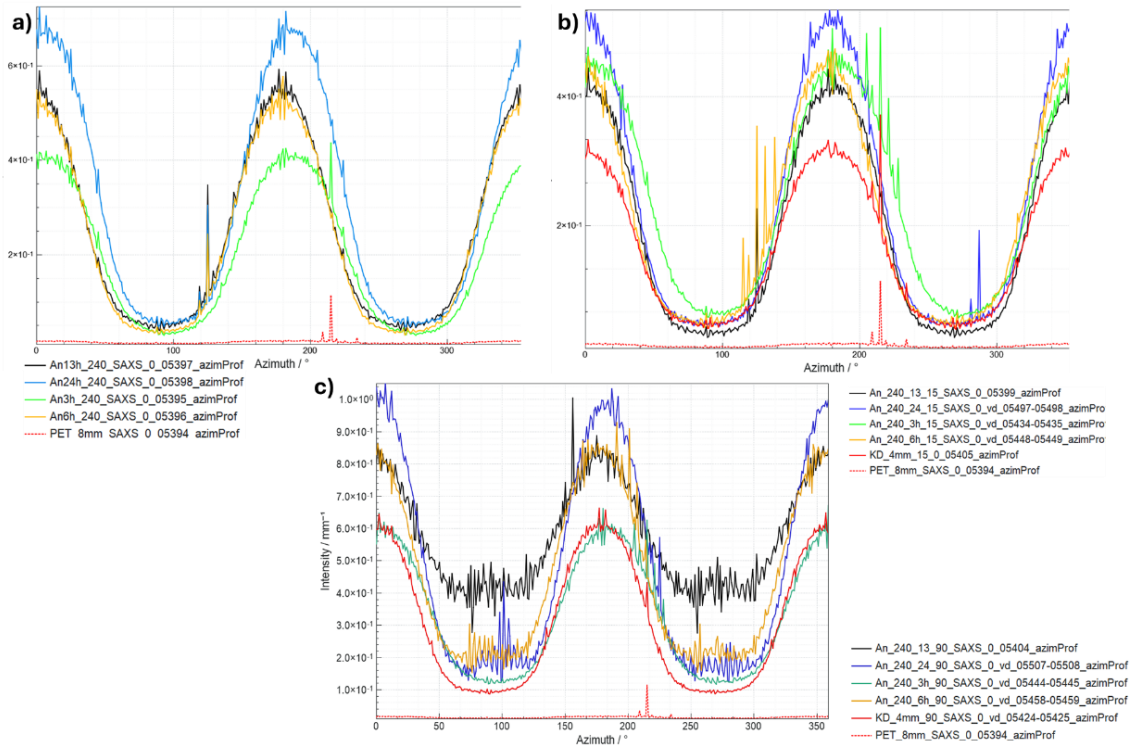

Figure B.1 SAXS of annealed PET before and after depolymerization. **(a)** compares PET annealed for 0-24 hours. **(b)** shows scattering of pre-depolymerization annealed PET for 0-24 hours depolymerized for 15 minutes **(c)** shows scattering of pre-depolymerization annealed PET for 0-24 hours depolymerized for 90 minutes.

Where $I(q,\psi)$ is the intensity around the azimuthal angle (ψ). The results were that annealing the sample at any amount does increase orientation significantly, but additional annealing does not impact alignment significantly. This may be because this was not a controlled variable in this study, and the artificial alignment may have skewed the results. **Figure B.1 (b) and (c)** show the scattering of PET annealed for varying amounts of time before being depolymerized for 15 and 90 minutes respectively. We observed that the depolymerization process impacts our unannealed PET's orientation similarly to how annealing PET for extended periods of time near the T_m impacts orientation.

B.2.2. Analysis of Starting Material (Annealed PET)

To further understand if crystalline perfection is occurring, by the slight decrease in crystalline domain size during annealing, as depicted in **Figure 4.2 (b),** we looked back at the melting curve via DSC of our annealed PET. Crystal perfection has been previously linked to an increase of T_m and a decrease of the crystalline domain, demonstrating modifications of the immediate amorphous phase that create a smaller entropy during melting and, therefore, increase the T_m.[12] **Figure B.2** illustrates the DSC curve of PET with changing annealing time, 0 hours (green; unannealed), 3 hours (brown), 6 hours (blue), 13 hours (red), and 24 hours (yellow). The 3-hour sample has a second melting curve of 230 °C, which is below the onset of the melting curve of our 0-hour PET (240 °C). Literature previously shows a secondary peak can appear in DSC after heat treatment with increasing crystallization time above certain temperatures. That secondary peak can go from lower to higher temperatures, and at the same time, the initial peak will decrease in size and disappear with increasing crystallization time.[3, 13] **Figure 4.3**

demonstrates that after annealing PET for over 3 hours, the secondary peak increases in temperature, merging with our initial peak, and further increasing the melting temperature to 250 °C. The secondary peak increasing in temperature and merging with the initial peak demonstrates smaller or imperfect crystals growing to a similar size and strain effect to the original crystals. **Figure B.2** demonstrates an increase in the onset melting temperature of PET with increased annealing, from 240 °C (for the unannealed sample) to ~250 °C (for the samples annealed for 6+ hours). This combined with the decrease in the crystalline phase could demonstrate the modifications in the immediate amorphous phase, and therefore demonstrate crystalline perfection.

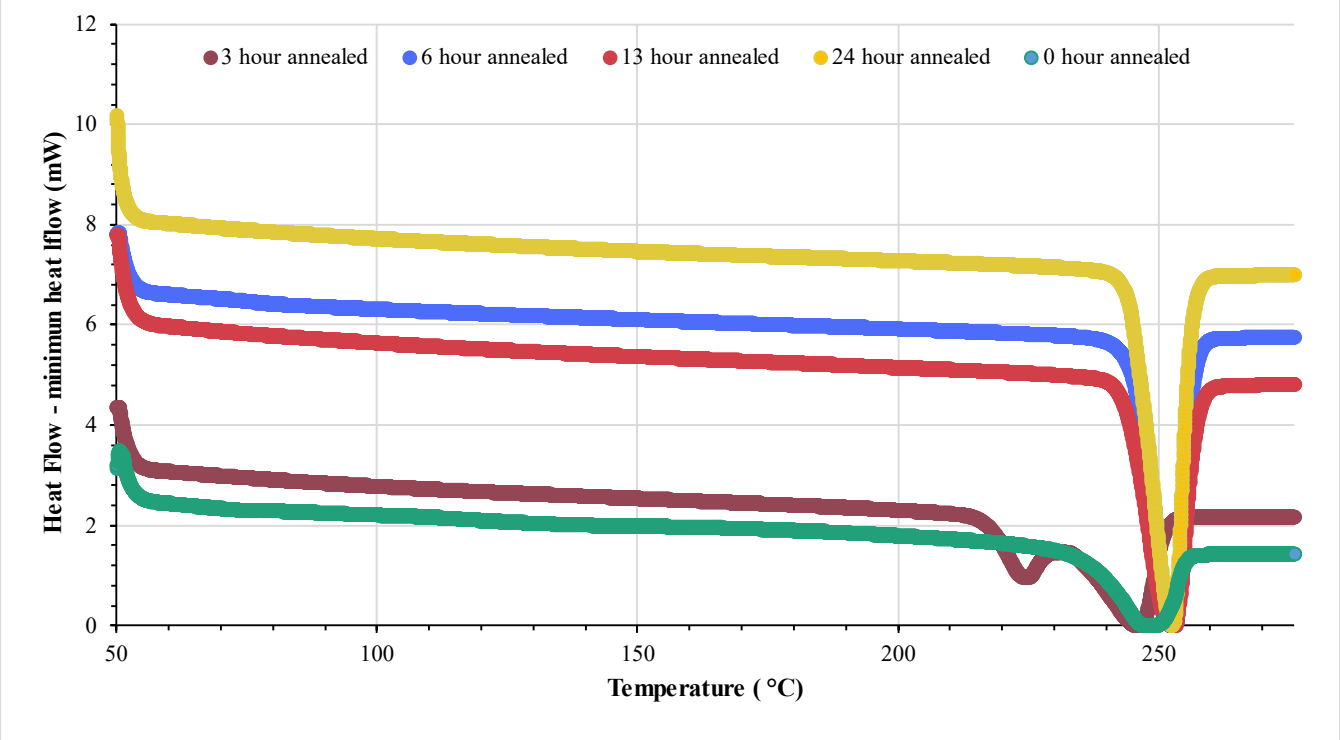

Figure B.2 DSC Q2000 curves of PET with changing Annealing time (0 hours green (unannealed), 3 hours purple, 6 hours blue, 13 hours red, and 24 hours yellow). Exo up

To understand how the M_w of PET increases with further annealing, as seen in **Figure 4.2** (c), the average number of hydroxyl end groups per chain was calculated. As previous work shows when M_n values from GPC and NMR are compared, the average number of hydroxyl end groups per chain can be found when those values (M_n from NMR and GPC) are the same. **Figure B.3** demonstrates that the number of hydroxyl groups decreases with continued annealing past 3 hours, showing a condensation/transesterification reaction causing our increase in M_w; further esterification has been previously demonstrated when annealing PET but has not been previously linked to how it impacts molecular weight.[12] End group analysis in **Figure B.3** shows PET annealed for 13 and 24 hours has ~1 hydroxyl group per chain. We hypothesize our M_w increases with increased annealing time because the reactive tie chains from annealing react with the immediate amorphous phase and undergo transesterification, causing a decrease in the average number of hydroxyl end groups per chain. [12, 14] As M_w is more affected than M_n by higher molecular weight chains, our hydroxyl end groups reacting with ester groups within the PET backbone to link those chains would increase our M_w.

Figure B.4 shows the percent swelling of EG into the PET flakes that were pre-swell annealed for varying amounts of time (0 hour green, 3 hour purple, 6 hour blue, 13 hour red, and 24 hour yellow). The unannealed sample (0 hour green) swelled with the most EG initially (15 minutes into the experiment). **Figure 4.2 (a)** demonstrated that our unannealed sample is the least crystalline sample, so it should swell the least as it is the most amorphous sample.[15] Our PET pre-swell annealed for 3 and 6 hours swell initially the same, as well as PET pre-swell annealed for 13 and 24 hours as they have similar bulk crystallinities to each other, shown in **Figure 4.2 (a)**. After 45 minutes of swelling generally all the PET samples start to decrease in percent swelling as the PET flakes begin to dissolve.

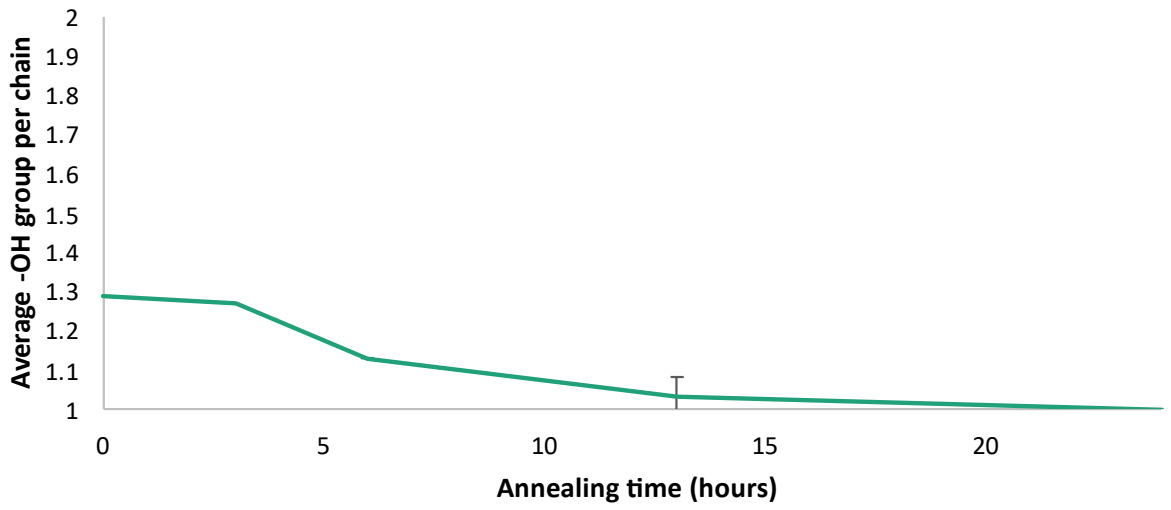

Figure B.3 Average number of hydroxyl end groups per chain changes with annealing time. The number of hydroxyl end groups per chain was determined by comparing M_n from NMR and SEC-GPC.

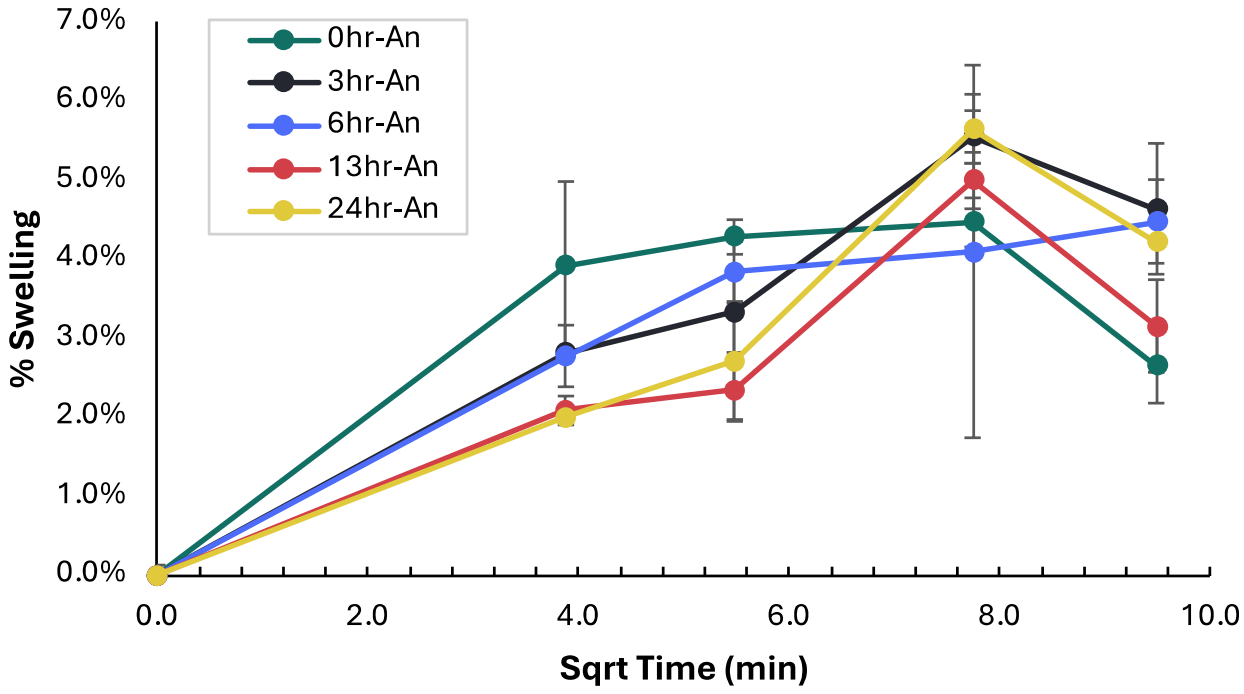

Figure B.4 Swelling of EG into PET that is annealed for varying amounts of time (0 hour green, 3 hour purple, 6 hour blue, 13 hour red, and 24 hour yellow).

B.2.3. DSC of PET Annealed or Swelled at Reaction Temperature

Figure B.5 shows the heat flow of PET annealed for a variety of time at 180 °C (0 minutes green, 15 minutes brown, 30 minutes navy, 45 minutes purple, 60 minutes blue-green, 75 minutes red, 90 minutes pink, and 105 minutes light blue). PET has a distinct melting curve starting at 240 °C, which follows the literature, as shown in **Figure B.5 (a)**. [1, 2] **Figure B.5 (b)** shows a DSC curve between 150-220 °C to better see the new melting curve appearing at 180 °C, the annealing temperature. Previous studies have shown that annealing below well below the melting temperature can nucleate new weak crystals that will melt at the annealing temperature. Annealing at 180 °C has demonstrated an increase in crystallinity, but not the same way demonstrated from annealing at 240 °C or our depolymerization. **Figure B.5** demonstrates that after annealing PET at 180 °C for over 105 minutes, the initial peak disappears as the secondary peak increases at 180 °C. The increasing melting peak at 180 °C while annealing at 180 °C demonstrates a melting and recrystallization of smaller PET crystals that will melt at their annealing temperature, as demonstrated in **Figure B.5 (b)**. YaoPeng Zhang previously saw a change in crystallinity from annealing at 125 °C, so our PET annealed at 180 °C experiencing a change in crystallinity is unsurprising.[1] We see that with increasing annealing time there is an increase in the secondary peak melting temperature, shown in **Figure B.5 (b)**. This increase in melting temperature of the secondary peak is unsurprising and similar to what we observed in **Figure B.2**.

Figure B.6 shows the DSC curve for PET from our swelling experiments (heated at 180 °C in EG) for varying amounts of time (0 minute red, 15 minute green, 30 minute brown, 60 minute blue, 90 minute purple, and 135 minute light blue.) The swelling data shown in **Figure B.4** stops at 60 minutes as the PET flake starts to dissolve. However, looking at the DSC curves

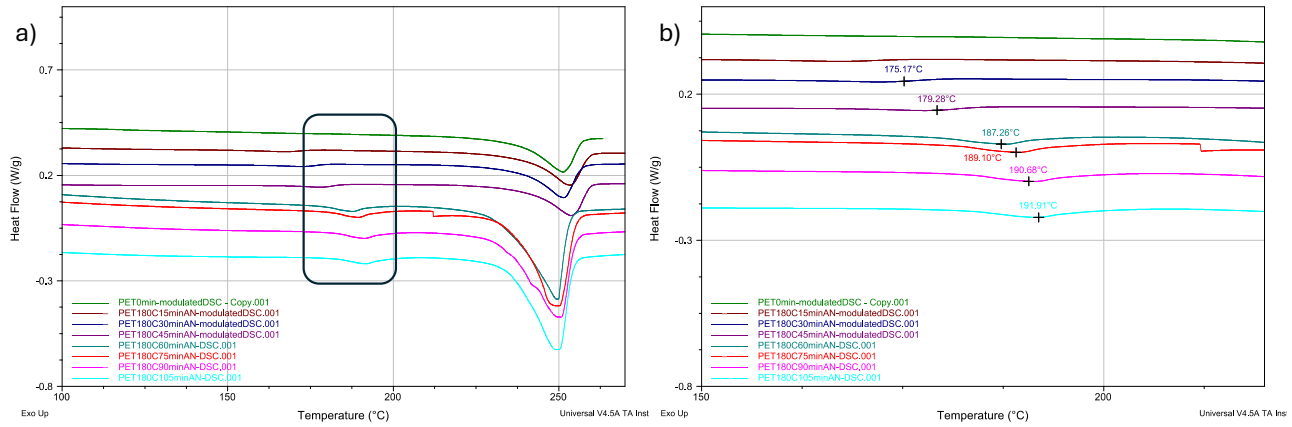

Figure B.5 Differential Scanning Calorimetry of PET annealed at 180 °C for varying times

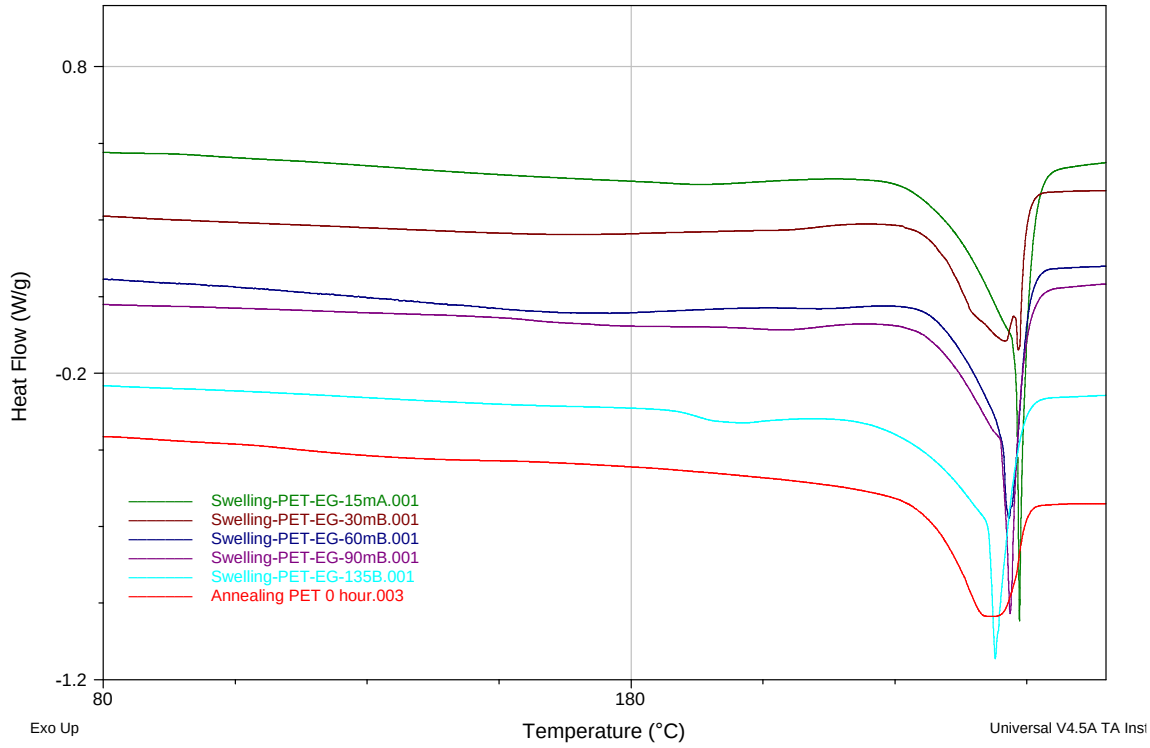

Figure B.6 Differential Scanning Calorimetry of PET swelled at 180 °C for varying times

of PET swelled over a 135 minute period, we see that the melting temperature increases with swelling time and that our melting curve becomes more narrow, demonstrating more similarly sized crystals. Therefore, it is the mechanism of the reaction (EG swelling into PET) that causes the change in crystallinity that is similar to the change in crystallinity observed when annealing near the T_m.

B.2.4. Change in Crystallinity from Annealing to Depolymerization

We hypothesize annealing only affects percent change in M_w at 15 minutes into the reaction because annealed starting material has more chemically reactive tie chains. To further this idea, swelling experiments were run on the annealed and unannealed starting material. **Figure B.4** shows that increased annealing time decreases initial swelling of EG into the polymer flake, demonstrating that the percent change in M_w is dependent on the reactivity of tie chains, as our 13 and 24 hour samples that change in percent M_w the most have swollen with the least amount of EG. Another contributing factor could be crystallinity or crystal size. To further understand their impact, DSC and SAXS was run on our annealed depolymerized samples shown in **Figure B.7**. **Figure B.7 (a)** illustrates how our PET flakes annealed before depolymerization (0 hour green, 3 hours purple, 6 hours blue, 13 hours red, and 24 hours yellow) change in bulk crystallinity via DSC with reaction time. Generally, annealing between 3-24 hours allows for the isolation of higher crystalline oligomers compared to the 0h annealed sample for any reaction time. To account for crystallinity changes that could occur during depolymerization because of the reaction temperature, PET was annealed at 180 °C (light green). PET annealed at the reaction temperature increases in percent crystallinity before decreasing after 60 minutes of annealing, showing an overall minimal increase in bulk crystallinity. **Figure B.7 (b) and (c)** demonstrate how our PET flakes annealed before depolymerization (0 hour green, 3 hours purple, 6 hours

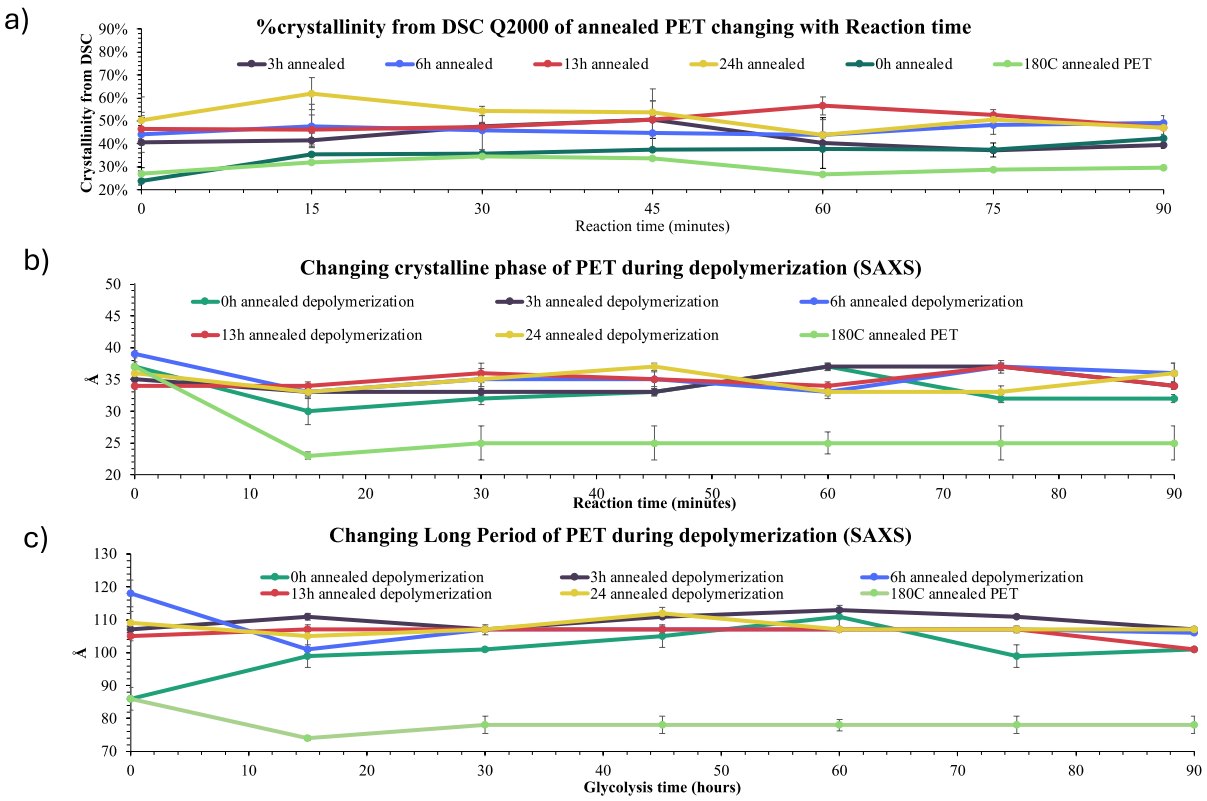

Figure B.7 Crystallinity of annealed and non-annealed PET are changing with glycolysis. PET was annealed for 0 hours (green; unannealed), 3 hours (purple), 6 hours (blue), 13 hours (red), and 24 hours (yellow) before depolymerization. **(A)** Percent Crystallinity from DSC vs reaction time. **(B)** Crystalline phase from SAXS vs reaction time. **(C)** Long phase from SAXS vs reaction time.

blue, 13 hours red, and 24 hours yellow) change in crystal size and long period, respectively, with reaction time via SAXS. Generally, **Figure B.7 (b)** shows our 3-24 hour annealed samples do not change crystal size throughout the depolymerization reaction. However, our unannealed sample decreases in crystal size in the first 15 minutes of the reaction. Then, crystal size increases like previously seen during the annealing of PET, potentially demonstrating crystal perfection during depolymerization. **Figure B.7 (c)** shows that the long period of our annealed samples does not change with reaction time, but our unannealed samples increase in the long period, similar to our annealed samples. While the size of the crystal phase could limit the reaction rate or oligomers obtained, this limitation was prevented as our non-annealed PET undergoes crystal perfection to similar sizes as our annealed samples during the reaction and similar stretching of amorphous tie chains by increasing the long period, this limitation was prevented. Since this was not demonstrated when annealing PET at the reaction temperature (light green line) as a decrease in crystal size occurred, we interpret our data to say that the reaction mechanism (swell of EG into the polymer flake) prevents crystal perfection that produces smaller crystal sizes. Observing DSC of PET annealed at the reaction temperature in **Figure B.7** we once again see smaller/weaker crystals that melt at 180 °C. To understand how the swell of EG into the polymer flake might affect crystallinity we ran DSC of PET from our swelling experiments and saw that our bulk crystallinity increased with swelling time and no small crystals were produced, as shown in the DSC curve of **Figure B.6**. The reaction mechanism of EG swelling the PET flake during depolymerization increases the abundance of similarly sized crystals despite the reaction temperature being well below the T_m. The increase in bulk crystallinity, increased abundance of similarly sized crystals, and increase in the long period could be the cause of PET oligomers being a similar molecular weight after 15 minutes of

glycolysis despite changing the pre-depolymerization annealing time. We hypothesize EG prefers to chain scission extended tie chains over bulk un-oriented amorphous polymer, so the PET oligomers at any glycolysis time are of similar molecular weight between pre-depolymerization annealing time, as all annealed and unannealed samples have amorphous tie chains stretched to similar lengths during the depolymerization. This preference for breaking extended tie-chains over bulk amorphous polymer has been demonstrated before with the depolymerization of PET with amine vapor.[16]

References

(1) Liu, Y.; Yin, L.; Zhao, H.; Song, G.; Tang, F.; Wang, L.; Shao, H.; Zhang, Y. Lamellar and fibrillar structure evolution of poly(ethylene terephthalate) fiber in thermal annealing. *Polymer* **2016**, *105*, 157-166. DOI: https://doi.org/10.1016/j.polymer.2016.10.031.

(2) Chen, Z.; Jenkins, M. J.; Hay, J. N. Annealing of poly (ethylene terephthalate). *Eur. Polym. J.* **2014**, *50*, 235-242. DOI: 10.1016/j.eurpolymj.2013.11.004.

(3) Holdsworth, P. J.; Turner-Jones, A. The melting behaviour of heat crystallized poly(ethylene terephthalate). *Polymer* **1971**, *12* (3), 195-208. DOI: https://doi.org/10.1016/0032-3861(71)90045-0.

(4) Blaine, R. L. *Determination of Polymer Crystallinity by DSC*; TA Instruments, https://www.tainstruments.com/pdf/literature/TA123new.pdf.

(5) Blaine, R. L. *THERMAL APPLICATIONS NOTE*; TA Instrument, https://www.tainstruments.com/pdf/literature/TN048.pdf.

(6) Najmi, S.; Vance, B. C.; Selvam, E.; Huang, D.; Vlachos, D. G. Controlling PET oligomers vs monomers via microwave-induced heating and swelling. *Chem. Eng. J.* **2023**, *471*, 144712. DOI: https://doi.org/10.1016/j.cej.2023.144712.

(7) Zhou, X.; Wang, J.; Nie, J.; Du, B. Poly(N-isopropylacrylamide)-based ionic hydrogels: synthesis, swelling properties, interfacial adsorption and release of dyes. *Polym. J.* **2016**, *48* (4), 431-438. DOI: 10.1038/pj.2015.123.

(8) Strobl, G. R.; Schneider, M. Direct evaluation of the electron density correlation function of partially crystalline polymers. *Journal of Polymer Science: Polymer Physics Edition* **1980**, *18* (6), 1343-1359. DOI: 10.1002/pol.1980.180180614.

(9) Xenocs. *XSACT: X-ray Scattering Analysis and Calculation Tool. SAXS & WAXS Data Analysis Software*. https://www.xenocs.com/saxs-products/xsact-software/. (accessed.

(10) Tencé-Girault, S. L., S.; Bunau, O.; Dang, P.; Bargain, F. . Simultaneous SAXS-WAXS Experiments on Semi-Crystalline Polymers: Example of PA11 and Its Brill Transition. . *Crystals* **2019**, *9*.

(11) Walker, L. M.; Wagner, N. J. SANS Analysis of the Molecular Order in Poly(γ-benzyl <scp>l</scp>-glutamate)/Deuterated Dimethylformamide (PBLG/d-DMF) under Shear and during Relaxation. *Macromolecules* **1996**, *29* (6), 2298-2301. DOI: 10.1021/ma951127p.

(12) Wang, Z. G.; Hsiao, B. S.; Sauer, B. B.; Kampert, W. G. The nature of secondary crystallization in poly(ethylene terephthalate). *Polymer* **1999**, *40* (16), 4615-4627. DOI: https://doi.org/10.1016/S0032-3861(99)00067-1.

(13) Ronkay, F.; Molnár, B.; Nagy, D.; Szarka, G.; Iván, B.; Kristály, F.; Mertinger, V.; Bocz, K. Melting temperature versus crystallinity: new way for identification and analysis of multiple endotherms of poly(ethylene terephthalate). *Journal of Polymer Research* **2020**, *27* (12). DOI: 10.1007/s10965-020-02327-7.

(14) Wunderlich, B. The Annealing of Crystals. In *Macromolecular Physics: Volume 2 Crystal Nucleation, Growth, Annealing*, Academic Press, 1976; pp 348-435.

(15) Miller-Chou, B. A.; Koenig, J. L. A review of polymer dissolution. *Prog. Polym. Sci.* **2003**, *28* (8), 1223-1270. DOI: 10.1016/s0079-6700(03)00045-5.

(16) Rabiei, N.; Kish, M. H. Aminolysis of polyesters for cracking and structure clarifying: A review. *Polym. Adv. Technol.* **2022**, *33* (12), 3903-3919. DOI: 10.1002/pat.5837.

VITA

Shelby Rebecca Watson-Sanders was raised in Asheville, North Carolina, and graduated from Enka High School in the spring of 2017. That fall, she began her studies at Western Carolina University, where she earned a B.S. in Chemistry in 2020. During her undergraduate years, Shelby studied Chinese in China and Taiwan through both the U.S.-China Rising Star Program and the U.S. State Department Critical Language Scholarship.

Shelby continued her education at the University of Tennessee, Knoxville, where she is currently completing her Ph.D. in polymer chemistry under the mentorship of Professor Mark Dadmun. Her research has led to multiple peer-reviewed publications, national conference presentations, and the mentorship of undergraduate researchers. Beyond the lab, Shelby has been actively involved in leadership and service, serving two terms as secretary for the Association of Chemistry Graduate Students, and contributing as social chair and historian to foster a collaborative and inclusive student community. She has also served as secretary for the East Tennessee Section of the American Chemical Society and earned a Certificate from the Center for the Integration of Research, Teaching, and Learning, as well as the State Department Critical Language Scholarship Refresh program.

Outside of academia, Shelby enjoys crafting, homesteading, playing with her cats, and continuing her study of the Chinese language.